Aalborg Universitet

AALBORG UNIVERSITY
DENMARK

Modeling and Analysis for Integration of Multi-Energy Systems

Zeng, Qing

Publication date:
2018

Document Version
Publisher's PDF, also known as Version of record

Link to publication from Aalborg University

Citation for published version (APA):
Zeng, Q. (2018). *Modeling and Analysis for Integration of Multi-Energy Systems*. Aalborg Universitetsforlag. Ph.d.-serien for Det Ingeniør- og Naturvidenskabelige Fakultet, Aalborg Universitet

General rights
Copyright and moral rights for the publications made accessible in the public portal are retained by the authors and/or other copyright owners and it is a condition of accessing publications that users recognise and abide by the legal requirements associated with these rights.

? Users may download and print one copy of any publication from the public portal for the purpose of private study or research.
? You may not further distribute the material or use it for any profit-making activity or commercial gain
? You may freely distribute the URL identifying the publication in the public portal ?

Take down policy
If you believe that this document breaches copyright please contact us at vbn@aub.aau.dk providing details, and we will remove access to the work immediately and investigate your claim.

Downloaded from vbn.aau.dk on: December 27, 2020

MODELING AND ANALYSIS FOR INTEGRATION OF MULTI-ENERGY SYSTEMS

BY
QING ZENG

DISSERTATION SUBMITTED 2018

AALBORG UNIVERSITY
DENMARK

MODELING AND ANALYSIS FOR INTEGRATION OF MULTI-ENERGY SYSTEMS

by

Qing Zeng

AALBORG UNIVERSITY
DENMARK

Ph.D. Dissertation

.

Dissertation submitted:	March 15, 2018
PhD supervisor:	Prof. Zhe Chen, Aalborg University
Assistant PhD supervisor:	Assistant Prof. Jiakun Fang, Aalborg University
PhD committee:	Professor Claus Leth Bak (Chairman) Aalborg University
	Professor Eduard Muljadi Auburn University
	Professor Jerry Jinyue Yan Royal Institute of Technology and Mälardalen University
PhD Series:	Faculty of Engineering and Science, Aalborg University
Department:	Department of Energy Technology

ISSN (online): 2446-1636
ISBN (online): 978-87-7210-175-0

Published by:
Aalborg University Press
Langagervej 2
DK – 9220 Aalborg Ø
Phone: +45 99407140
aauf@forlag.aau.dk
forlag.aau.dk

© Copyright: Qing Zeng

Printed in Denmark by Rosendahls, 2018

CV

Qing Zeng was born in China. He received B.Sc. degrees in thermal energy and power engineering from Huazhong University of Science and Technology (HUST), China, in 2007, and received M.Sc. degree in engineering mechanics from Tsinghua University, China, in 2011.

He is currently a Ph.D. fellow at the Department of Energy Technology, Aalborg University, Aalborg, Denmark. His research interests include energy management systems, energy systems integration and electricity markets.

ENGLISH SUMMARY

The public awareness of climate change and fossil fuel depletion promotes the deployment of renewable energy sources. Multi-energy system provides an opportunity to improve the economic and environmental performance of energy use. Recently, the interdependency between the natural gas system, electric power system, and district heating system is enhanced by the use of gas-fired power generators, heat pumps, combined heat and power units, and power-to-gas units. Thus, the integration of multi-energy system is currently receiving increasing attention.

This Ph.D. project aims at promoting the coordination of various energy resources to accommodate the fluctuated renewables and to shape an efficient and low-cost energy system. We study the integration of multi-energy system in terms of three aspects: energy flow model, network expansion planning, and operation strategy. Thus, the contributions of this project include three parts:

- Energy flow model of multi-energy systems. A steady-state flow model is developed to describe the electricity, natural gas, and district heating systems. Then a unified energy flow solution is proposed to analyze the energy distribution in the integrated energy system. The per-unit system is proposed to improve the computational efficiency.

- Optimal joint operation of multi-energy systems. A coordinated optimization model is developed to jointly operate the integrated energy systems with the aims of maximizing efficiency and minimizing cost. Since weather-dependent renewable sources are considered, the model is improved as a two-stage stochastic programming problem. It allows the optimal scheduling of reserves to facilitate real-time adjustment decisions, which results in minimum cost while integrating the highest level of renewable energy.

- Co-expansion planning of multi-energy systems. A bi-level programming structure is developed to optimize the investment and operation cost of the integrated energy systems. The upper level aims at minimizing the expansion plan and determining the network topology. The lower level is formulated as an optimal economic dispatch under the operational constraints given by the upper-level decision. A hybrid algorithm is presented to solve this bi-level programming.

DANSK RESUME

Den offentlige bevidsthed om klimaændringer, udslip af fossile brændstoffer og bæredygtig energipolitik fremmer udbredelsen af vedvarende energikilder. Integrationen af multi-energisystemer giver mulighed for at forbedre den økonomiske og miljømæssige udnyttelse af energiforbruget på grund af optimal koordinering mellem forskellige energisystemer som el, gas, varme, køling, transport og så videre. For nylig er indbyrdes afhængighed mellem elsystemet, naturgasystemet og fjernvarmesystemet forbedret ved udbredt anvendelse af gasfibreffektgeneratorer, varmepumper, kombinerede varme- og kraftaggregater og kraft-til-gas-enheder. Integrationen af gas, fjernvarme og elektriske systemer får således øget opmærksomhed.

Dette ph.d.-projekt sigter mod at fremme koordineringen af forskellige energiressourcer for at imødekomme de svingede vedvarende energikilder og forme et effektivt og lavpris energisystem. Vi studerer integrationen af gas, fjernvarme og elektriske systemer med hensyn til fire aspekter: energimængde model, netværksudvidelsesplanlægning, driftsstrategi, energimarked. Projektets bidrag omfatter således fire dele:

• Energi flow model af multi-energisystemer. For det første er der udviklet en ensartet model til at beskrive den konstante strøm af de integrerede gas-, fjernvarme- og elforsyningssystemer.

• Fælles drift af multi-energisystemerne. En koordineret optimeringsmodel er udviklet til i fællesskab at drive de integrerede energisystemer med det formål at maksimere effektiviteten og minimere omkostningerne. Da vejrafhængige vedvarende kilder overvejes (fx vindkraft), forbedres modellen som et to-trins stokastisk programmeringsproblem. Det første trin repræsenterer planlægningsbeslutninger forud for realtidsoperation til forskellige vindkraftscenarier, mens anden fase repræsenterer driftstimer i realtid.

• Samudvidelsesplanlægning af multi-energisystemerne.En programmeringsstruktur på to niveauer er udviklet for at minimere både investerings- og driftsomkostningerne for de integrerede energisystemer. Det øverste niveau optimerer ekspansionsplanen og bestemmer netværkstopologien samt genereringskapaciteten, mens lavere niveau formuleres som en optimal økonomisk forsendelse under de operationelle begrænsninger, der er givet af beslutningen på øverste niveau.

ACKNOWLEDGMENTS

The Ph.D. project, entitled “MODELING AND ANALYSIS FOR INTEGRATION OF MULTI-ENERGY SYSTEMS” is carried out from October 2014 to April 2018, under the supervision of Professor Zhe Chen and Assistant Professor Jiakun Fang. This Ph.D. study is financially supported by ForskEL project (HIGHE2014-1-12220) and ForskEL project (SEMI2017-07-878043). I would like to express my gratitude to them, and to John K Pedersen, Tina Larsen, Corina Gregersen, Claus Leth Bak and Helene Ulrich Pedersen from AAU for their help which smoothed the study here.

Grateful thanks should be given to my supervisor Professor Zhe Chen. Thanks for providing me the precious opportunity and great environment to pursue my Ph.D. degree here. Your constructive advice, suggestive discussions, and patient corrections not only contribute to this work but also have a deep influence on my future career. Sincere thanks to my co-supervisor, Assistant Professor Jiakun Fang, for his inspired suggestions and invaluable help to both the research and the future career.

At the same time, I would like to thank Professor Antonio J. Conejo from Ohio State University. When I studied abroad at Ohio State University, Professor Antonio J. Conejo provides me great help on academic discussion and paper writing which are very helpful for my research.

Thanks are also given to Dr. Baohua Zhang, Professor Jinghua Li for the great cooperation in publishing papers. Then I want to thank some researchers in our department for their help in the academic area. Dr. Dong Liu, Dr. Yanbo Wang, Dr. Rui Hu, Dr. Rongwu Zhu, Assistant Prof. Chi Su, Dr. Nan Qin are thanked here. All your help enriched my Ph.D. research.

Special thanks to my parents who spare no effort to support me. Finally but significantly, I would like to thank all my best friends here. All your names are written in my heart. I will cherish the golden time here in my life.

Qing Zeng January 2018 Aalborg

TABLE OF CONTENTS

LIST OF ACRONYMS

CPG	Coal-fired power generation
GPG	Gas-fired power generation
P2G	Power to gas
DHS	District heating system
EPS	Electric power system
NGS	Natural gas system
GT	Gas Terminal
GS	Gas storage
GC	Gas compressor
WC	Wind curtailment
WF	Wind farm
UE	Unserved electricity

TABLE OF FIGURES

CHAPTER 1. INTRODUCTION

Electric power system (EPS), natural gas system (NGS), district heating system (DHS) are essential infrastructures that supply electricity, gas, and heating to the modern society. The system planning and operation strategy plays a critical role in the security and economy of the future energy distribution systems with multiple energy carriers. Energy load flow studies are fundamental for the study of planning and operation of multi-energy systems (MES). This chapter provides a brief introduction to the basic framework as well as the studied contents concerned in the whole thesis.

Firstly, the background of this Ph.D. project is presented to introduce the motivations of this study. Secondly, the research problems are formulated according to the project objectives. Then, the state-of-the-art of the research problems is investigated. The contributions are concluded afterward. Finally, the thesis outline and the list of publications related to this thesis are presented.

1.1. BACKGROUND AND MOTIVATIONS

Nowadays, district heating, renewable, and natural gas supply are increasingly important in the global goal of greenhouse gas emission reduction [1], [2]. Meanwhile, with the development and application of gas-fired power generation (GPG) [3], power to gas (P2G) technology [4], heat pump (HP) [5] and combined heat and power (CHP) units [6], The interdependence and coupling are increasingly enhanced between the EPS, DHS, and NGS, which is explained in detail as follows.

Firstly, the rapid growth of intermittent renewables requires a backup capacity to provide the peaking shaving for a power system [7]. Due to the strong ability of peak regulation, GPG plays a critical role in the growing share of intermittent renewable [2]. In recent years, renewable energy is developed rapidly, as the public pay more attention to the global warming and fossil fuel depletion. Taking the development of Danish wind power, for example, the wind power in Danish electricity supply has maintained a sustained, rapid upward trend, as shown in Figure 1-1. By the end of 2017, the capacity of Danish wind power has been up to 5300MW [8]. The wind power supplied 43.6% of electricity consumption of Denmark in 2017 [8]. Furthermore, a political agreement has been put forward that there should be a 100% renewable energy world at Denmark in 2050 [9], which has been further detailed in [10]-[12]. Also, the technical routine on developing the distributed renewable sources has been investigated in [13]. However, the unpredictable nature of the renewable source increases the difficulty in balancing

energy supply and consumption [14]. Thus, the flexibility is needed to accommodate the increasing share of renewables in the power generation. It is considered that GPG has strong ability of peak regulation which can respond quickly to fluctuations. So GPGs play a vital role in providing backup to the rapid development of renewable sources [2].

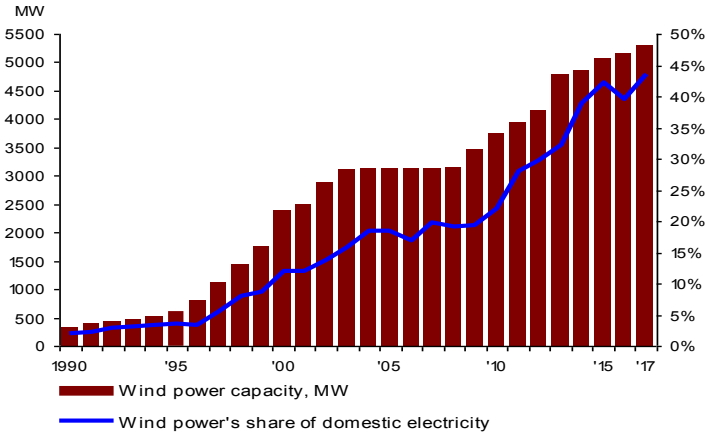

Figure 1-1 Wind power's share of electricity supply in Denmark.

Secondly, P2G technology displays the potential for converting excess electrical power to gas [15]. Nowadays, there is still lack of utility-scale electrical energy storage technology with good techno-economic feasibilities [16]–[18]. For instance, the super-capacitor energy storage (SCES), battery energy storage (BES) [19] and the flywheel energy storage (FES) [20] have been piloted, but most have been built in distribution networks for peak load shaving; the superconducting magnetic energy storage (SMES) is featured with its fast response [17], but with huge investment on the cryogenic systems and superconducting coils; the pumped-storage hydroelectricity (PSH) [22] and compressed air energy storage (CAES) [21] have large-scale energy capacities, but both of them have critical requirements to the geographical locations. Under this circumstance, encouragingly, P2G provides an opportunity to store surplus renewables in the NGS with a large scale and long duration way[23].

Thirdly, DHS can play the role as a manageable load [24]. Such integration of gas, heating, and electricity presents the good potential to deal with renewable power fluctuation, to maximize the utilization of renewable energy, to supply electric, heating and gas load reliably. The analysis on the North European Power System showed that the there are various benefits from the integration of heat and wind, including the reduction of wind power curtailment, regulation of power price, and a

decrease of fuel oil consumption [25]. Also, by the coordination of large-scale wind power and the heat pumps in New York State, the utilization of wind-generated electricity was significantly increased [26]. Hence, the techniques of combining electrical and heat systems have a big potential to play the role as a manageable load.

In summary, NGS plays a vital role in providing flexibility to the EPS to accommodate the rapid development of renewable resources. P2G technology displays the potential for converting excess electrical power to gas. DHS can play the role as a manageable load. Thus, the DHS, EPS, and NGS are becoming increasingly interconnected and interdependent [27]. The integration of multi-energy systems (MES) shows a better technical, economic and environmental performance than the traditional independent energy systems at both the operational and the planning level [28]. Meanwhile, the extensive development of CHP, GPG, HP and P2G can also enhance the synergies of the multiple energy carriers, as shown in Figure 1-2. Finally, energy systems integration, a renovation of existing energy systems to ensure the optimal interoperability among electricity, natural gas, heating, transportation, etc., has drawn broad interests.

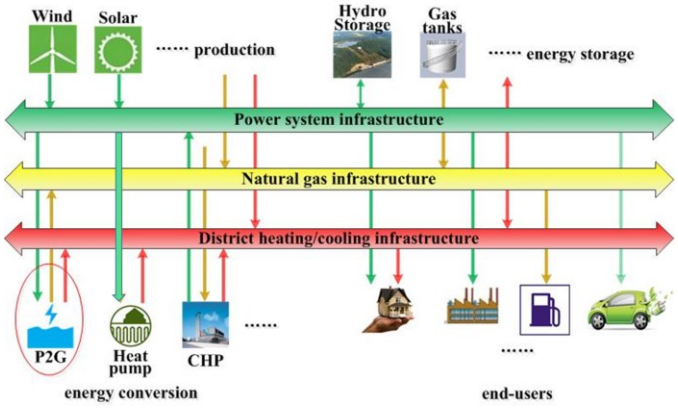

Figure 1-2 The schematic of research objects for the multiple energy systems.

1.2. RESEARCH OBJECTIVES

The core objective of this thesis is to provide comprehensive solutions to the system planning and operation strategy of the future energy distribution systems with multiple energy carriers. The research objective will be completed by achieving the following four particular research targets:

- To develop a general mathematical model of MES in a unified formulation.

- To assess the interaction among gas, heating and electric systems considering wind fluctuation in the electric power system.
- To explore an optimization model to jointly operate MES considering the impact of wind power uncertainty.
- To help the planner with decision support on expansion planning of the future MESs.

These research targets help to address the following questions: How to analyze the energy flow distribution of MES? How to operate these energy conversion facilities? When and how much energy should be transferred from one energy carrier to another? How to optimally site and size the facilities, such as Gas-fired Power Generation (GPG) and P2G station in the integrated energy system? How to develop advanced optimization techniques, especially considering the interactive nonlinear constraints? Therefore, to address the system design and operation strategy problems of the integrated energy systems, this project focused on the further development of problem formulations and mathematical methodologies for the harmonized integration of MES.

1.3. STATE OF THE ART

Traditionally, energy carriers such as EPS, DHS and NGS were mostly operated independently [27]. The modeling and optimization have been widely studied for individual energy carrier (Natural gas network [28]–[30], district heating network [31], [32], electricity network [33]–[35]). However, the individual analysis has been incompatible with the ongoing reconstruction of the energy systems, like the DHS, EPS, NGS are becoming increasingly interdependent [36]. In the past decade, the combined modeling and optimization of multiple energy carriers have been carried out from the following aspects [37]–[40]: the efficiency of different systems, the correct sizing, the operation cost and the availability of different energy networks, etc.

Recently, the research in the integrated analysis of MES has been developed in terms of technological and economic aspects [41]. The optimization models are developed for the combined electricity-gas systems to analyze the coupled network behavior [42]. Additionally, [43] proposes market models for analyzing the phenomenon that a single entity would play as a gas buyer and an electricity producer. [44] proposes a security model to analyze the interdependencies between EPS and NGS. It shows that the integrated model is user-friendly and quite effective in analyzing the interactions between EPS and NGS.

For these reasons, numerous efforts have been centered on the joint operation of the MES [45]. In these researchers, [46]–[49] studies the impact of NGS on the security and economic dispatch of EPS：[46] shows that the NGS has a definite impact on the electricity price. [47] demonstrates that the gas allocation affects the security of the EPS. In [46], [47], the security-constrained unit commitment (SCUC) model is developed by incorporating gas fuel allocation. However, the network constraints of NGS are ignored. Further, the coordinated operation of multiple carriers considering detailed network constraints has also been presented, e.g., in [50]–[52]. However, these researchers do not take into account the increasing deployment of renewable sources, especially in power systems, which introduces significant uncertainties. Therefore, it is necessary to develop a novel decision model for the joint operation of power, gas, and district heating systems under the uncertainties.

In addition to the joint operation, some research efforts have been devoted to the expansion planning of the MES. In [53], a detailed gas flow model is combined with the power flow model for investigating the expansion planning of the integrated gas-power network. [54] proposes a mixed-integer linear optimization problem for the long-term multi-stage expansion planning of the combined EPS and NGS. Further, a holistic approach is proposed to investigate the effect of high penetration of GPGs on the multi-energy networks [55]. [56] carries out expansion planning on integrated energy systems by considering the energy reliability and CO_2 emission reduction. However, there are few works considering the long-term planning of P2G and GPG in the integrated MES [45].

1.4. CONTRIBUTIONS

The harmonized integration of GNS, DHS, and EPS is comprehensively studied in this Ph.D. project. The contribution of this research consists of developing a series of algorithms and models for joint operation and planning problems of MES. Specifically, the technical results are highlighted with three main achievements:

1. Energy flow model for the integrated energy system:

Chapter 2 proposes the steady-state analysis on the integrated MES. The computational efficiency is enhanced by conducting a unified unit system on simplification of the mathematical description. Case studies are carried out to demonstrate the efficiency and feasibility of the proposed method. It is shown that the harmonized integration utilizes the flexibilities from heating and gas systems to help power systems to accommodate renewables. One journal paper and one conference paper published based on this work.

2. Multi-time period optimization method for the integrated energy system

Following the work of Chapter 2, the optimal operation of the integrated energy systems is further developed as a multi-time-period optimization problem by taking the weather-dependent renewable sources into account. A two-stage stochastic programming problem is formulated. The first stage represents scheduling decisions prior to real-time operation for different wind power scenarios, while the second stage represents real-time operating actions. Detailed contents are presented in Chapter 3. Two journal paper and three conference paper have been published according to the results.

3. Multi-objective optimization method for network design and expansion

The coordinated expansion planning is proposed for the combined gas-power systems. A bi-level multi-stage programming problem is established for minimization of the total operational and investment costs. We develop a hybrid algorithm by combining a modified binary particle swarm optimization method with an interior point method, which presents high computational efficiency in finding the optimized solution. Detailed contents are reported in Chapter 4. One journal paper and one conference paper published based on the work.

1.5. THESIS OUTLINE

According to the requirements and regulations of the graduate school, this Ph.D. thesis is documented as ***a collection of papers***, including a summary report and a collection of the published or submitted papers. In the thesis, research work is briefly summarized according to the contributions. The relevant papers are attached at last, and the papers are listed in Section 1.6. The thesis contains fives chapters and it is organized as follows:

Chapter 1 introduces the background and motivation of the Ph.D. project. The objectives and state-of-the-art, contributions are presented.

Chapter 2 presents the energy flow models for both the NGS and DHS based on detailed formulations of the mass flow and thermal balance. A unified model is developed to describe the energy flow of MES. Papers related to this chapter are J1.

Chapter 3 addresses the joint operation of the MESs under uncertainty. A two-stage stochastic programming problem is formulated to allow the optimal scheduling of reserves to facilitate real-time adjustment decisions. Case studies have been carried out to demonstrate the effectiveness of the proposed approach. Papers related to this chapter are J3, and C1, C2, C3.

Chapter 4 focuses on the co-expansion planning of the MESs. A bi-level multi-stage programming structure is developed to minimize both the operation and investment cost of the MESs. Case studies are carried out on the western Danish electricity and gas system. Papers related to this chapter are J2 and C4.

Chapter 5 gives the conclusions and future perspectives of this research project.

1.6. LIST OF PUBLICATIONS

A list of publications is given below. There are five journal papers and six conference papers related to the thesis, which have been published or under review.

Journal papers:

1. Q. Zeng, J. Fang, J. Li, and Z. Chen, "Steady-state analysis of the integrated natural gas and electric power system with bi-directional energy conversion," Appl. Energy, vol. 184, pp. 1483–1492, Dec. 2016.
2. Q. Zeng, B. Zhang, J. Fang, and Z. Chen, "A bi-level programming for multistage co-expansion planning of the integrated gas and electricity system," Appl. Energy, vol. 200, pp. 192–203, Aug. 2017.
3. J. Li, J. Fang, Q. Zeng, and Z. Chen, "Optimal operation of the integrated electrical and heating systems to accommodate the intermittent renewable sources," Appl. Energy, vol. 167, pp. 244–254, Apr. 2016.

Conference papers:

1. Q. Zeng, A. J. Conejo, Z. Chen, and J. Fang, "A Two-stage Stochastic Programming Approach for Operating Multi-energy Systems," in the first IEEE Conference on Energy Internet and Energy System Integration, 2017. In press.
2. Q. Zeng, J. Fang, B. Zhang, and Z. Chen, "The coordinated operation of electricity, gas and district heating systems," in the Applied Energy Symposium and Forum, REM2017: Renewable Energy Integration with Mini/Microgrid. In press.
3. Q. Zeng, B. Zhang, J. Fang, and Z. Chen, "Coordinated Operation of the Electricity and Natural Gas Systems with Bi-directional Energy Conversion," *Energy Procedia*, vol. 105, pp. 492–497, May 2017.
4. Q. Zeng, J. Fang, Z. Chen, J. Li, and B. Zhang, "A multistage coordinative optimization for sitting and sizing P2G plants in an integrated electricity and natural gas system," in 2016 IEEE International Energy Conference (ENERGYCON), 2016, pp. 1–6.

CHAPTER 2. STEADY-STATE ANALYSIS OF THE MULTI-ENERGY SYSTEMS

This chapter focuses on the steady-state analysis of the multi-energy systems. Firstly, the steady-state models are developed to describe the EPS, DHS, NGS, respectively. Then the solution technique is proposed to analyze the energy distribution in the combined electricity-gas system. After that, case studies are proposed to validate the feasibility and efficiency of the proposed method and results are analyzed. At last, the conclusions are drawn.

2.1. STEADY STATE MODELLING OF ELECTRIC POWER SYSTEM

2.1.1. AC POWER FLOW

The power-flow study aims at obtaining the voltage magnitudes and angles in the EPS with given load, generators' active, and reactive power output, etc [57]. The problem is formulated as shown below.

$$V_i = |V_i| \angle \theta_i = |V_i| \left(\cos \theta_i + j \sin \theta_i \right) \tag{2.1}$$

$$Y_{ij} = |Y_{ij}| \angle \theta_{ij} = |Y_{ij}| \left(\cos \theta_{ij} + j \sin \theta_{ij} \right) = G_{ij} + jB_{ij} \tag{1.2}$$

$$P_i = |V_i| \sum_{j=1}^{N} |V_j| \left(G_{ij} \cos \theta_{ij} + B_{ij} \sin \theta_{ij} \right) \tag{1.3}$$

$$Q_i = |V_i| \sum_{j=1}^{N} |V_j| \left(G_{ij} \sin \theta_{ij} - B_{ij} \cos \theta_{ij} \right) \tag{1.4}$$

where θ is the angle of voltage and $\theta_{ij} = \theta_i - \theta_j$. G_{ij} and B_{ij} represent electrical conductance and electrical susceptance, respectively.

The nodal power balance equations are given as:

$$\Delta P_i = P_{\mathrm{g},i} - P_{\mathrm{d},i} - |V_i| \sum_{j=1}^{N} |V_j| \left(G_{ij} \cos \theta_{ij} + B_{ij} \sin \theta_{ij} \right) = 0 \tag{1.5}$$

$$\Delta Q_i = Q_{\mathrm{g},i} - Q_{\mathrm{d},i} - |V_i| \sum_{j=1}^{N} |V_j| \left(G_{ij} \sin\theta_{ij} - B_{ij} \cos\theta_{ij} \right) = 0 \tag{1.6}$$

where $P_{\mathrm{g},i}$ and $P_{\mathrm{d},i}$ are the power generation and consumption at bus *i*, respectively.

2.1.2. DC POWER FLOW

As can be seen from above description, AC power flow model is non-linear. In some cases, the DC power-flow model is used instead, which is a linearization of AC power flow, based on the following assumptions [58].

1. The reactive power flow is significantly smaller than the real power flow. Hence the reactive power balance, indicated by the equation (1.4), can be ignored.

2. Line resistance is much smaller than the reactance; the conductance can be ignored. This assumption implies that grid losses are neglected.

$$G_{ij} = 0 \tag{1.7}$$

3. When calculated in terms of per unit, the amplitudes of different buses are close enough to 1.0.

$$|V_i| \approx |V_j| \approx 1 \tag{1.8}$$

4. The difference between the voltage angles across the line is small. This assumption results in linearization of the sine and cosine terms in the AC power flow equations.

$$\sin\theta_{ij} \approx \theta_{ij} \tag{1.9}$$

$$\cos\theta_{ij} \approx 1 \tag{1.10}$$

Hence, the AC power flow model can be simplified to the DC power flow equation.

$$P_{ij} = B_{ij}(\theta_i - \theta_j) \tag{1.11}$$

2.2. STEADY STATE MODELLING OF NATURAL GAS SYSTEM

2.2.1. GAS FLOW IN THE NATURAL GAS SYSTEM

The steady-state energy flow of the NGS is analyzed by solving the gas flow equations as follows [27],

$$\prod_k - \prod_m = R_{km} G_{\mathrm{gas},\,km}^2 \tag{1.12}$$

where $G_{\text{gas},km}$ is the standard pipeline gas flow rate; $\prod_k = p_k^2$, $\prod_m = p_m^2$ where p_m and p_k represent gas pressure at the node of both ends of the pipeline. $R_{km} = 1/C_{km}^2$, R_{km} represents the hydraulic resistance coefficient of the gas pipeline, similar to the line impedance of the power transmission lines [27]. C_{km} represents the physical characteristics of each gas pipeline, which can be written as below [27]:

$$C_{km} = C\left(\frac{T_{\text{b}}}{p_{\text{b}}}\right) D_{km}^{2.5} \left(\frac{1}{L_{km}\gamma_{\text{G}} T_{\text{a},km} Z_{\text{a}} f_{km}}\right)^{0.5} E_{\text{p},km} \tag{1.13}$$

where C_{km} $\left(\text{m}^3/\text{h}\right)/\text{kPa}$ denotes the overall transmission coefficient; C is a constant; $E_{\text{p},km}$ is the pipeline efficiency; T_{b} is the gas temperature at base condition; p_{b} is gas pressure at base condition in kPa; D_{km} is the inside diameter of pipe in meter; L_{km} is the length of pipe in kilometers; γ_{G} is the specific gravity of natural gas; Z_{a} is the average compressibility factor of the natural gas; $T_{\text{a},km}$ is average absolute temperature in the pipeline; the friction factor f_{km} is determined by the characteristics of gas pipe [59]. Thus, given the pipeline parameters and gas compositions, the overall transmission coefficient C_{km} can be determined accordingly [27].

Let $G_{\text{s},k}$ and $G_{\text{d},k}$ denote the gas supply and gas demand at node k; the nodal gas balance equations are given as

$$\Delta G_k = G_{\text{s},k} - G_{\text{d},k} - \sum_{m \in k} G_{\text{gas},km} = 0 \tag{1.14}$$

2.2.2. GAS COMPRESSOR

The gas compressor (GC) increases gas pressure by reducing gas volume. The brake horsepower (BHP) of the GC can be calculated by the equation (1.15).

$$\text{BHP}_{km} = K_{\text{GC}} Z_{\text{a}} G_{\text{GC},km} \left[\frac{T_s}{E_{\text{c}}\eta_{\text{c}}}\right]\left[\frac{c_k}{c_k - 1}\right]\left[(CR)^{\frac{c_k - 1}{c_k}} - 1\right] \tag{1.15}$$

where CR represents compression ratio, which is the ratio of discharge pressure to the suction pressure [60].

$$CR = \frac{p_m}{p_k} = \left(\frac{\prod_m}{\prod_k} \right)^{0.5} \tag{1.16}$$

where K_{GC} is a constant; E_{c} and η_{c} represent compressors' parasitic efficiency and compression efficiency, respectively; T_s is the suction temperature of the compressor; c_k is specific heat ratio for the natural gas.

2.2.3. GAS LINEPACK

The gas linepack is the amount of gas stored in the gas pipeline [61]. The initial linepack value is proportional to the average gas pressure over that pipeline [61][62].

$$LP_{km}^{0} = k_{\mathrm{LP},km} \cdot \overline{p_{km}} \tag{1.17}$$

The constant $k_{\mathrm{LP},km}$ is given by [45]:

$$k_{\mathrm{LP},km} = c_{\mathrm{LP},km} \frac{T_{st}}{p_{st}} \frac{1}{Z_{\mathrm{a}} \cdot T_{km}} D_{km}^{2} L_{km} \tag{1.18}$$

where T_{st} and p_{st} represent the temperature and gas pressure at standard conditions, respectively; T_{km} represents the gas temperature at pipe km. The average gas pressure $\overline{p_{km}}$ is given by [62]:

$$\overline{p_{km}} = \frac{2}{3} \left(p_k + p_m - \frac{p_k p_m}{p_k + p_m} \right) \tag{1.19}$$

The NGS is subject to the mass balance constraints so that the linepack can be calculated by the difference between the injection and withdrawal of the natural gas in the pipeline [56], [63]:

$$LP_{km}(t) = LP_{km}^{0} + \sum_{h=1}^{t} \left[P_{\mathrm{in},km}^{\mathrm{LP}}(h) - P_{\mathrm{with},km}^{\mathrm{LP}}(h) \right] \tag{1.20}$$

Need to be reminded that the linepack should be refilled after usage, so after n^{T} time, the linepack should be the same with an initial value.

$$\left| LP_{km}^{n^{\mathrm{T}}} - LP_{km}^{0} \right| = 0 \tag{1.21}$$

2.3. STEADY STATE MODELLING OF DISTRICT HEATING SYSTEM

DHS mainly includes a heat source, pipe network and heat consumer as shown in Figure 2-1. Heat energy is generated by the heating station, transferred by the hot water, exchanged by the heat exchanger.

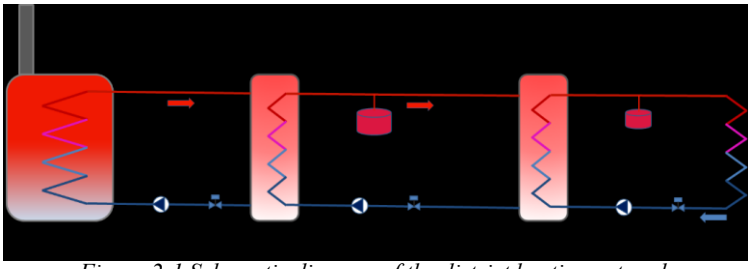

Figure 2-1 Schematic diagram of the district heating network

2.3.1. WATER FLOW IN THE DISTRICT HEATING SYSTEM

The steady-state modeling of the DHS is formulated by the nodal mass balance and water flow equations as follows.

$$p_{n,t} - p_{m,t} = \mu_{nm} \left(m_{nm,t} \right)^2 \tag{1.22}$$

$$\sum_{h \in \Omega_n^{\mathrm{HS}}} m_{h,t}^{\mathrm{HS}} + \sum_{s \in \Omega_n^{\mathrm{ST}}} \left(m_{s,t}^{\mathrm{ST,in}} - m_{s,t}^{\mathrm{ST,with}} \right) - \sum_{l \in \Omega_n^{\mathrm{HL}}} m_{l,t}^{\mathrm{HL}} = \sum_{m \in \Lambda_n} m_{nm,t}, \tag{1.23}$$

where $p_{n,t}, p_{m,t}$ represent the water pressure at the node n and m , $m_{nm,t}$ is water pipeline flow, μ_{nm} represents the hydraulic resistance coefficient of the pipeline *nm*. $m_{h,t}^{\mathrm{HS}}$, $m_{s,t}^{\mathrm{ST,in}}$, $m_{s,t}^{\mathrm{ST,with}}$, $m_{l,t}^{\mathrm{HL}}$ are the water mass flow rate of heat source, inlet of heat storage, outlet of heat storage (HS) and heat load in the period, respectively.

2.3.2. WATER PUMP

As pressure loss is created in the process of water transmission, water pump should be used to drive the water flow. The power consumption in the pump is related to the mass flow rate and the pressure difference [64], which can be calculated by

$$D_{p,t}^{\mathrm{WP}} = \frac{m_{p,t} \cdot \left(p_{n,t}^{\mathrm{out}} - p_{n,t}^{\mathrm{in}} \right)}{\eta_p^{\mathrm{WP}} \rho^{\mathrm{W}}} \tag{1.24}$$

where $D_{p,t}^{\mathrm{WP}}$ is the power consumption of water pumps, $m_{p,t}$ is water flow through the pump, $p_{n,t}^{\mathrm{out}}$ and $p_{n,t}^{\mathrm{in}}$ represent water pressure at the inlet and outlet of water

pump, respectively. η_p^{WP} is the efficiency of the water pump in heat station and ρ^{W} is water density.

2.3.3. WATER TEMPERATURE

In the district heating network, water works as a medium. Heat is a quantity of energy which may be transferred between two systems, while the water temperature is a measure of energy. Therefore, water temperature is a vital state parameter in district heating network. Heat loss is considered in this model occurs since there is a large difference between the water temperature and its ambient temperature, [64] as shown below:

$$\tau_{m,t}^{\mathrm{out}} - \tau^{\mathrm{am}} = \left(\tau_{n,t}^{\mathrm{in}} - \tau^{\mathrm{am}}\right) \times \lambda_{nm} \tag{1.25}$$

where $\tau_{n,t}^{\mathrm{in}}$ and $\tau_{m,t}^{\mathrm{out}}$ represent the inlet temperature and outlet temperature of pipe nm. τ^{am} is the ambient temperature, λ_{nm} represents heat loss coefficient.

Due to the energy exchange when two water streams are meet, the nodal temperature of the mixed water is given as

$$\tau_{n,t}^{\mathrm{mix}} \sum_{m \in \Lambda_n} m_{mn,t} = \sum_{j \in i} \left(m_{mn,t} \cdot \tau_{n,t}^{\mathrm{out}}\right) \tag{1.26}$$

where $m_{mn,t}$ is water pipeline flow from m to n, $\tau_{n,t}^{\mathrm{mix}}$ is the mixed temperature.

2.3.4. HEAT EXCHANGER

In the district heating system, heat transfer from heat sources to heat loads is accomplished through heat exchanger.

$$H_{h,t}^{\mathrm{HE}} = c \cdot m_{h,t}^{\mathrm{HE}} \cdot \left(\tau_{h,t}^{\mathrm{in}} - \tau_{h,t}^{\mathrm{out}}\right) \tag{1.27}$$

where $m_{h,t}^{\mathrm{HE}}$ represents mass flow rate through the heat exchanger. $\tau_{h,t}^{\mathrm{in}}$ and $\tau_{h,t}^{\mathrm{out}}$ represent inlet temperature and outlet temperature of the heat exchanger. c represents specific heat capacity. $H_{h,t}^{\mathrm{HE}}$ represents the amount of heat exchange via heat exchanger. A positive value represents releasing heat to heat load. A negative value represents absorbing heat from heat source.

2.4. THE ENERGY CONVERSION FACILITIES

2.4.1. GAS-FIRED POWER GENERATION

For the GPG, the power plant efficiency is a critical factor which is related to its heat rate (HR) shown as [66]:

$$\eta_{\mathrm{GPG}} = \frac{3600}{HR} \tag{1.28}$$

The relationship between the NGS and power generation is formulated by the heat rate curve [27]:

$$HR = \alpha + \beta P_{\mathrm{g,GPG}} + \gamma P_{\mathrm{g,GPG}}^2 \tag{1.29}$$

where the coefficients α, β, γ define the energy efficiency of the power generation process. $G_{\mathrm{d,GPG}}\left(\mathrm{m}^3/\mathrm{h}\right)$ represents the gas consumption, which can be approximated by[27]:

$$G_{\mathrm{d,GPG}} = \frac{HR \cdot P_{\mathrm{g,GPG}}}{\mathrm{LHV}} \tag{1.30}$$

The gas consumption in GPG can also be calculated by [27]:

$$G_{\mathrm{d,GPG}} = \left(\frac{3600}{\eta_{\mathrm{GPG}}\mathrm{LHV}}\right) P_{\mathrm{g,GPG}} \tag{1.31}$$

2.4.2. POWER TO GAS

Since methane is the main component of gas, the objective production of P2G is methane in this work. There are two steps for P2G to produce methane [67]: electrolysis and methanation.

Electrolysis is decomposition of water into oxygen and hydrogen by consuming electricity. The chemical reaction [67] of electrolysis is given as

$$2\,\mathrm{H_2O\,(l)} \longleftrightarrow 2\,\mathrm{H_2(g)} + \mathrm{O_2\,(g)} \quad \Delta\mathrm{H} = +571.6\,\mathrm{kJ} \tag{1.32}$$

Methanation is the conversion of CO_2 to methane through hydrogenation. [27]. This process can be given as:

$$\mathrm{CO_2(g)} + 2\,\mathrm{H_2(g)} \longleftrightarrow \mathrm{CH_4(g)} + \mathrm{O_2(g)} \quad \Delta\mathrm{H} = +318.7\,\mathrm{kJ} \tag{1.33}$$

Then the overall process in the P2G can be summarized as

$$CO_2(g)+2H_2O(l)\longleftrightarrow CH_4(g)+2O_2(g)\ \ \Delta H=+890.3kJ \tag{1.34}$$

In practice, the energy conversion efficiency of P2G (η_{P2G}) should be considered. Thus, the relationship between the gas production $G_{s,P2G}$ and the power consumption $P_{d,P2G}$ can be given as

$$\eta_{P2G}=\frac{\left(G_{s,P2G}/3600\right)\cdot \mathrm{LHV}}{P_{d,P2G}}\times 100\% \tag{1.35}$$

where $G_{s,P2G}$ represents gas production of the P2G in m^3/h, which can be given as

$$G_{s,P2G}=\left(\frac{3600\eta_{P2G}}{\mathrm{LHV}}\right)\times P_{d,P2G} \tag{1.36}$$

The equation can be rewritten by a simplified form as shown below:

$$G_{s,P2G}=C_{P2G}P_{d,P2G} \tag{1.37}$$

where C_{P2G} denotes the energy conversion coefficient of the P2G system, the value of C_{P2G} is in proportion to the energy efficiency of the P2G system.

$$C_{P2G}=\frac{3600\eta_{P2G}}{\mathrm{LHV}} \tag{1.38}$$

2.4.3. COMBINED HEAT AND POWER

The interfaces among the electricity, natural gas, and district heating systems are constrained by the energy conversion relationships of the CHP (1.39)-(1.40). The gas-fired CHP is an energy efficient technology that generates electricity by consuming natural gas and captures the heat that would otherwise be wasted. The relationship between the heat production and electricity generation is given by (1.39) , and the gas consumption is given by (1.40).

$$H_{i,t}^{CHP}=P_{i,t}^{CHP}\cdot\left(1-\eta_{i,t}^{e}-\eta_{i,t}^{l}\right)/\eta_{i}^{e}\times K^{e} \tag{1.39}$$

$$D_{i,t}^{CHP}=P_{i,t}^{CHP}/\eta_{i}^{e} \tag{1.40}$$

where $H_{i,t}^{CHP}$, $P_{i,t}^{CHP}$ and $D_{i,t}^{CHP}$ represent heat supply, power production and gas consumption in CHP unit, respectively. η_{i}^{e} $\eta_{i,t}^{l}$ and K^{e} represent generating

coefficient, heat loss coefficient and heat exchange coefficient of CHP unit, respectively.

2.5. A UNIFIED GAS AND POWER FLOW SOLUTION

This section gives an example of the integrated NGS-EPS to analyze the steady state energy flow of the MES. Since the model of the integrated gas-electricity system consists of a set of nonlinear equations[27], Newton-Raphson method is selected to solve this problem.

Newton-Raphson method is a popular linearization technology which can be given by the Taylor series expansion [34] as

$$F(X) = -J \times \Delta X \tag{1.41}$$

where X represents all the unknown variables, which is considered as a point that closes to the exact solution. $F(X)$ represents the mismatches, as shown below:

$$X = \begin{bmatrix} \theta & |V| & P_{\mathrm{GPG}} & P_{\mathrm{P2G}} & P_{\mathrm{GC}} & \prod & G_{\mathrm{gas}} \end{bmatrix}^{\mathrm{T}} \tag{1.42}$$

$$F(X) = \begin{bmatrix} \Delta P & \Delta Q & \Delta \prod & \Delta G & \Delta P_{\mathrm{GC}} \end{bmatrix}^{\mathrm{T}} \tag{1.43}$$

The Jacobian matrix (J) is the matrix of all first-order partial derivatives:

$$J = \begin{bmatrix} \frac{\partial \Delta P}{\partial \theta} & \frac{\partial \Delta P}{\partial |V|} & \frac{\partial \Delta P}{\partial P_{\mathrm{GPG}}} & \frac{\partial \Delta P}{\partial P_{\mathrm{P2G}}} & \frac{\partial \Delta P}{\partial P_{\mathrm{GC}}} & 0 & 0 \\ \frac{\partial \Delta Q}{\partial \theta} & \frac{\partial \Delta Q}{\partial |V|} & 0 & 0 & 0 & 0 & 0 \\ 0 & 0 & 0 & 0 & 0 & \frac{\partial \Delta \prod}{\partial \prod} & \frac{\partial \Delta \prod}{\partial G_{\mathrm{gas}}} \\ 0 & 0 & \frac{\partial \Delta G}{\partial P_{\mathrm{GPG}}} & \frac{\partial \Delta G}{\partial P_{\mathrm{P2G}}} & \frac{\partial \Delta G}{\partial P_{\mathrm{GC}}} & \frac{\partial \Delta G}{\partial \prod} & \frac{\partial \Delta G}{\partial G_{\mathrm{gas}}} \\ 0 & 0 & 0 & 0 & \frac{\partial \Delta P_{\mathrm{GC}}}{\partial P_{\mathrm{GC}}} & \frac{\partial \Delta P_{\mathrm{GC}}}{\partial \prod} & \frac{\partial \Delta P_{\mathrm{GC}}}{\partial G_{\mathrm{gas}}} \end{bmatrix} \tag{1.44}$$

Thus, the correction can be derived to determine the corrections in unknown variables.

$$\Delta X = -J^{-1} F(X) \tag{1.45}$$

If the corrections exceed the specified tolerance, we move on to the next iteration $(k+1)$ with the new corrected value of variables based on:

$$X^{k+1} = X^k + \Delta X \tag{1.46}$$

Then solve the nonlinear equations $F(X^{k+1})$ using the most recent values X^{k+1}. The process continues until a sufficiently accurate value is reached.

2.6. CASE STUDY

The convergence of the proposed method has been demonstrated by carrying out simulations under differing initial values, and simulation results are shown in Table 2-1,

Table 2-2 and

Table 2-3 [27]. Two types of cases have been carried out for comparison study [27]: Case 1) we consider that the unit of voltage, power flow, gas flow and gas pressure are kV, MW, m^3/h and kPa, respectively; Case 2) we convert the unit of the natural gas to the power unit as MW.

Finally, the base value of voltage, gas pressure and power are 110kV, 10 bar and 100MW for the per-unit system, respectively.

2.6.1. STRUCTURE OF THE INTEGRATED GAS AND ELECTRICITY SYSTEM

Case studies have been carried on a combined 7-node natural gas and IEEE-9 test system as shown in Figure 2-2.

Table 2-2 gives the parameters of this combined gas-electricity system [27]: the impedance of power transmission lines, the hydraulic resistance coefficient of gas pipeline, the energy efficiency of GPG and P2G [35].

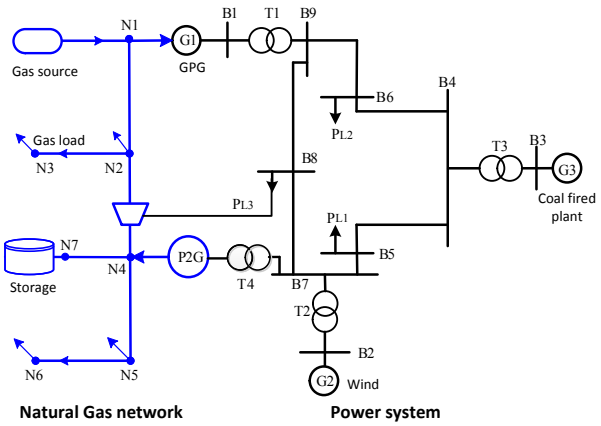

Figure 2-2 Structure of an integrated gas and electricity system

2.6.2. INITIALIZATION AND COMPARISON

Newton-Raphson method starts with initial guesses of all variables [68]. In this study, the "flat start" is used, i.e., all the initial variables are set as zero [27]. The simulation results are illustrated in the following tables: Table 2-1 summarizes the results for the natural gas network [27].

Table 2-2 and

Table 2-3 give the gas pipeline's parameters and the data of electric network, respectively[27]. It shows that simulation results of Case 2 with the unified solution agree well with the results in Case 1. Thus, the per-unit system is feasible.

Table 2-1 The nodal parameters of the natural gas network

No.	Case 1			Case 2		
	Gas supply (m^3/h)	Gas demand (m^3/h)	Gas pressure (kPa)	Gas supply (p.u.)	Gas demand (p.u.)	Gas pressure (p.u.)
1	60000	12012.09	969.98	6.210	1.243	0.97
2	0	10000	500	0	1.035	0.50
3	0	12000	438.63	0	1.242	0.44

4	10012.1	0	1000	1.036	0	1
5	0	20000	860.69	0	2.070	0.86
6	0	16000	814.86	0	1.656	0.81
7	0	0	1000	0	0	1

Table 2-2 The branch parameters of the natural gas network

Branch	**From**	**To**	**Case 1**		**Case 2**	
			$R_{km}\left(\mathrm{kPa}^2/(\mathrm{m}^3/\mathrm{h})^2\right)$	$G_{km}\ \left(\mathrm{m}^3/\mathrm{h}\right)$	$Z_{km}\left(\mathrm{p.u.}\right)$	$S_{km}\left(\mathrm{p.u.}\right)$
1	6	1	0.0003	47987.9	0.0280	4.967
2	1	2	0.0004	12000	0.0373	1.242
3	2	3	0	25987.9	0.0000	2.689
4	4	3	0.00025	0	0.0233	0
5	5	4	0.0002	36000	0.0187	3.726
6	6	5	0.0003	16000	0.0280	1.656

Table 2-3 The electric parameters of power system

Bus	**Case 1**				**Case 2**			
	$\lvert V_i\rvert(\mathrm{kV})$	$\theta_i\left(rad\right)$	$P_g\left(\mathrm{MW}\right)$	$P_d\left(\mathrm{MW}\right)$	$\lvert V_i\rvert(\mathrm{p.u.})$	$\theta_i\left(\mathrm{p.u.}\right)$	$P_g\left(\mathrm{p.u.}\right)$	$P_d\left(\mathrm{p.u.}\right)$
1	112.97	-0.054	99.5	0	1.027	-0.054	0.995	0
2	109.89	-0.112	90	0	0.999	-0.112	0.9	0.000
3	111.32	-0.075	160	0.6	1.012	-0.075	1.6	0.006
4	112.75	-0.031	0	0	1.025	-0.031	0	0
5	111.32	-0.056	0	125	1.012	-0.056	0	1.250
6	113.41	0.033	0	90	1.031	0.033	0	0.900
7	112.75	0.022	0	129.5	1.025	0.022	0	1.295
8	112.75	0.121	0	0	1.025	0.121	0	0.000
9	114.4	0.000	0	0	1.040	0.000	0	0.000

2.6.3. THE EFFECT OF POWER DEMAND AND WIND POWER ON THE INTEGRATED GAS AND POWER SYSTEM

This section focuses on the effect of power load and wind power on the energy conversion systems, i.e., P2G and GPG. The time series of electricity loads are injected into the power system at bus 5 and 6.The wind power is given as a time-series injecting electrical power at bus 2, and The operational data for Danish power system in 2014 from Energinet.dk [27] is adopted in this study.

Figure 2-3 shows the effect of the electricity demand and wind power on the output of P2G. When the wind power output is higher, and the electricity demand is lower, there is much higher gas production at the P2G unit. These results indicate the energy storage property of P2G. The surplus electricity power can be converted to gas fuel and stored in the gas storage and natural gas networks [27]. Thus, P2G technology has the potential of providing the flexibility to an energy system with the rapid increasing renewable energy.

Figure 2-4 illustrates the effect of the wind power and electricity demand on the output of GPG. It shows that the generation of GPG decreases with the wind power's output and increases with power load. When there is lower wind power and a higher power load, the GPG will increase its production to meet the power demand. This demonstrates that GPG has the ability of peak regulation.

Figure 2-5 shows the impact of wind power and electricity demand on the reducing ratio of the total energy loss. It should be noted that the reducing ratio of the total energy loss is defined as the quotient of the decrease of the total energy loss and the total energy loss generated in the system without P2G [27]. It can be seen from Figure 2-5 that the reducing ratio of the total energy loss increases with the output of wind power and decreases with power demand, which indicates that the MES has a more significant reduction on the power loss when there is a larger output of wind power and lower power demand [27].

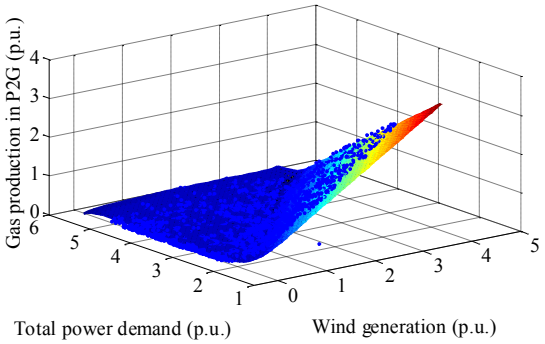

Figure 2-3 The effect of the wind power and power demand on the output of P2G

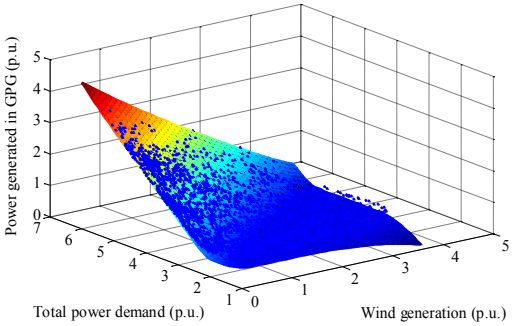

Figure 2-4 The effect of the wind power and power demand on the output of GPG

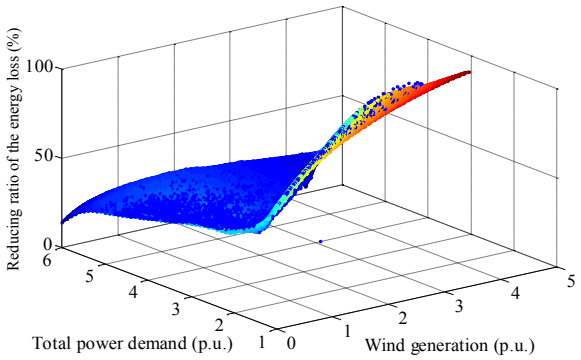

Figure 2-5 The reducing ratio of energy loss in the integrated energy system

2.7. SUMMARY

In this chapter, the steady state energy flow models are developed for the electric power, natural gas, and district heating systems. A unified solution is proposed to solve the combined energy flow equations. A per-unit system is adopted for simplifying the energy flow model and improving the computational efficiency. Case studies are carried out on a test system to demonstrate the applicability of the proposed method. Later, data on wind power and electricity loads are inputted to study the mitigation effect of GPG and P2G on the integrated gas and power systems. Simulation results demonstrate the capabilities of GPG and P2G for peak regulation. It also shows that implementing P2G in an MES can reduce energy losses.

The technical details are presented in J1.

CHAPTER 3. JOINT OPERATION OF THE MULTI-ENERGY SYSTEMS

Based on the energy flow models built in Chapter 2, the coordinated optimization model is developed to jointly operate the integrated energy systems with the aims of maximizing efficiency and minimizing cost. Two optimal operation models are developed. The one is optimal energy flow model for the combined energy system. Another one is the two-stage stochastic programming problem, which allows the optimal scheduling of the reserves to facilitate real-time adjustment decisions while integrating the highest level of renewable energy.

3.1. OPTIMAL ENERGY FLOW MODEL FOR INTEGRATED POWER AND HEATING SYSTEM

This section investigates the interaction of the heating system with the power system in district areas. An optimization problem is developed to solve the optimal energy dispatch of the combined power-heating system. So that the power and heat demand could be met simultaneously at the lowest operating cost. Furthermore, the best location is decided to link the electricity-heating system by considering the energy transmission loss.

3.1.1. MATHEMATICAL FORMULATIONS

The objective is to minimize the total operation costs F^{Total} consisting of electrical and heating system throughout the whole operational horizons [69]:

$$F^{\mathrm{Total}} = \sum\sum \qquad \sum\sum \tag{2.1}$$

where $P_{s,t}^{\mathrm{G}}$ is power generation, $H_{s,t}^{\mathrm{P}}$ is heat production, a is cost coefficient. t_{num} and represent the operational horizons and the number of sources, respectively.

The objective function is subjected to the operational constraints of DHS, EPS and the interfaces between DHS and EPS. Moreover, the power flow and mass flow equations are modeled as equality constraints which are detailed in Chapter 2. The operational limits are categorized in the following [69]: 1) the operational constraints consist of the flow capacities of the water pipes and the flow capacities of the electricity lines; 2) the nodal operational constraints including within the reasonable range of voltages and temperatures; 3) the facilities such as heat exchangers, generators should be within their capacities. Full content is published on Applied Energy, refer to [69] for details. The formulated optimization problem is

nonlinear programming. Hence, we propose a decomposition-coordination algorithm to solve the optimization problem [69].

3.1.2. OPTIMAL OUTPUT OF THE ENERGY SOURCES

Figure 3-1 gives a test integrated electrical and heating system. The excess wind power can be converted to heat and stored in HS[69]. Figure 3-2 shows the optimal hourly-dispatch of electricity and heat sources throughout 24 hours [69]: 1) Figure 3-2(a) shows that the valley periods of DHS are the peak periods of EPS. Figure 3-2(b) shows that the EPS consumes all the wind power during the peak periods (9th~23rd) of the EPS. Hence, there is no heat production from wind power during the 9th ~ 23rd time periods as shown in Figure 3-2(c). However, during the low load periods 1st ~ 8th, the surplus wind power is converted into heat, which helps to reduce the wind curtailment. Also, Figure 3-2(b) shows that the electricity productions of G1 and G2 are smooth and steady. Thus, the joint operation of the electricity-heating system helps to buffer the production and demand variation. Finally, Figure 3-2(d) shows the operational process of the heat storage. The HS charges at time periods (3, 5 and 7) to cut down the wind curtailment and discharges at time periods (4, 6 and 8) to supply the heat load [69].

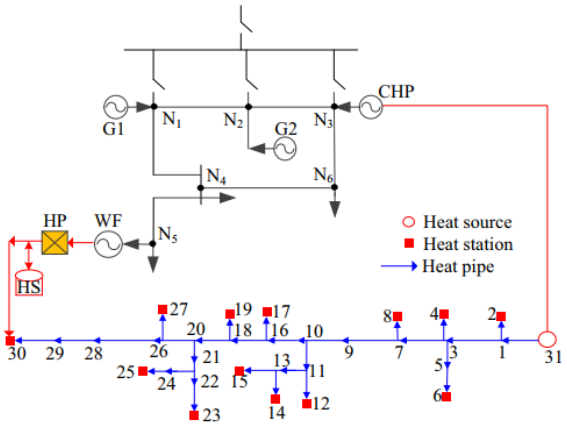

Figure 3-1 Studied case of the integrated electrical and heating systems.

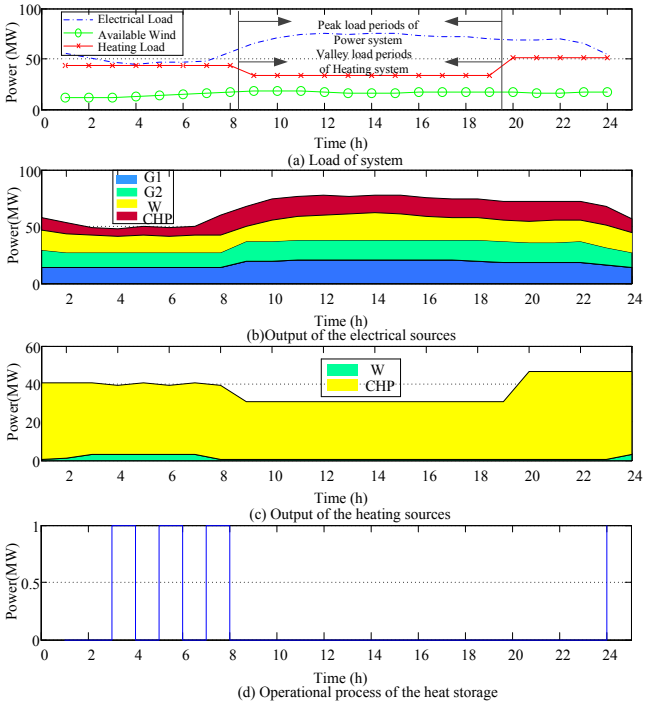

Figure 3-2 Optimal dispatch of sources in electrical and heating systems.

3.1.3. COMPARISON BETWEEN INDIVIDUAL-OPERATION AND COORDINATED-OPERATION

This section conducts comparative studies between the separated operation (I-operation) and combined operation (Co-operation). Simulation results include the minimum heat requirement from the heat source, wind curtailment, and heat loss [69].

Figure 3-3 compares the results of wind power curtailment. Because the power loads are high during the periods of 9th~23th, there is no wind curtailment for both operation approaches. During the low-load periods of 2nd ~8th, there are wind curtailments for both of the Co-operation and I-operation. However, the wind curtailment by using I-operation is much higher than that of Co-operation during the periods of 2nd ~ 8th [69].

Figure 3-4 compares the heat production from the heat sources. It shows that the heat requirements from heat sources are lower by using Co-operation. The total heat requirements throughout 24 hours are 873 MWh and 987 MWh for Co-operation and I-operation, respectively. The total heat requirements for I-operation is 11.55%

higher than that in Co-operation since more wind power is used to produce heat in Co-operation case [69].

Figure 3-5 compares the simulation results of heat loss. It shows that the heat loss is reduced by using Co-operation mode compared to I-operation. The sum of heat loss throughout 24 hours is 9.54 MW and 13.03 MW for Co-operation and I-operation, respectively. The heat loss in I-operation is 26.8% higher than that in Co-operation [69].

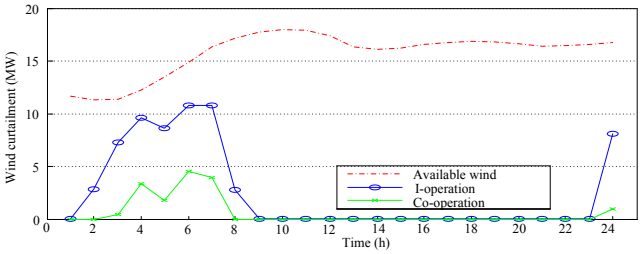

Figure 3-3 Comparisons of the wind curtailment with Co-operation and I-operation.

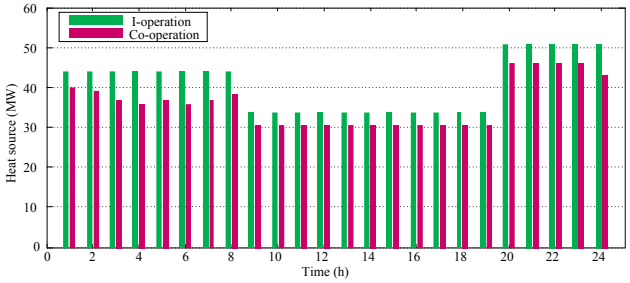

Figure 3-4 Comparisons of the requirement of the source with Co-operation and I-operation.

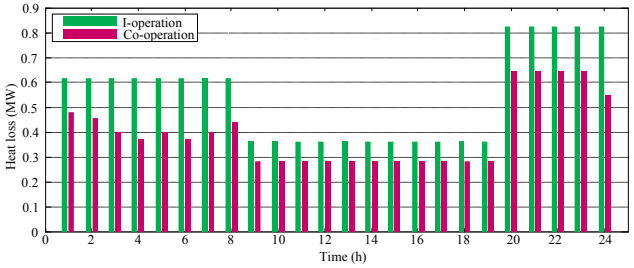

Figure 3-5 Comparisons of the heat loss with Co-operation and I-operation.

3.2. JOINT OPERATION OF GAS, HEATING AND ELECTRICITY SYSTEMS UNDER UNCERTAINTY

In addition to the deterministic case for the integrated energy systems, this section presents the optimization model for the joint operation of the gas, electricity, and district heating systems with the aims of minimizing the cost. Since weather-dependent electricity sources are considered (e.g., wind power), the model is formulated as a two-stage stochastic programming problem. The first stage represents scheduling decisions prior to real-time operation for different wind power scenarios, while the second stage represents real-time operating actions. The model is illustrated using the energy system of a city that includes a gas subsystem, electricity subsystem and a district heating subsystem.

3.2.1. MATHEMATICAL FORMULATIONS

$$
\begin{aligned}
\min_{\Xi} \sum_{t=1}^{n^{\mathrm{T}}} \Bigg\{ & \sum_{j=1}^{n^{\mathrm{CHP}}} \left(c_j^{\mathrm{CHP,P}} P_{j,t}^{\mathrm{CHP}} + c_j^{\mathrm{CHP,H}} H_{j,t}^{\mathrm{CHP}} \right) + \sum_{i=1}^{n^{\mathrm{CFP}}} c_i^{\mathrm{CFP}} P_{i,t}^{\mathrm{CFP}} \\
& + \sum_{f=1}^{n^{\mathrm{WF}}} c_f^{\mathrm{WF}} W_{f,t}^{\mathrm{S}} + \sum_{w=1}^{n^{\mathrm{GW}}} c_w^{\mathrm{GW}} Q_{w,t}^{\mathrm{GW}} + \sum_{k=1}^{n^{\mathrm{P2G}}} \left(c_k^{\mathrm{P2G,Q}} Q_{k,t}^{\mathrm{P2G}} + c_k^{\mathrm{P2G,H}} H_{k,t}^{\mathrm{P2G}} \right) \\
& + \sum_{s=1}^{n^{\mathrm{GS}}} \left(c_s^{\mathrm{GS,in}} Q_{s,t}^{\mathrm{GS,in}} + c_s^{\mathrm{GS,out}} Q_{s,t}^{\mathrm{GS,out}} \right) + \sum_{h=1}^{n^{\mathrm{HS}}} \left(c_h^{\mathrm{HS,in}} H_{h,t}^{\mathrm{HS,in}} + c_h^{\mathrm{HS,out}} H_{h,t}^{\mathrm{HS,out}} \right) \Bigg\} \\
+ \sum_{\omega \in \Phi} \pi_\omega \sum_{t=1}^{n^{\mathrm{T}}} \Bigg\{ & \sum_{j=1}^{n^{\mathrm{CHP}}} \left[c_j^{\mathrm{CHP,P}} \left(PR_{j,\omega,t}^{\mathrm{CHP,U}} - PR_{j,\omega,t}^{\mathrm{CHP,D}} \right) + c_j^{\mathrm{CHP,H}} \left(H_{j,\omega,t}^{\mathrm{CHP}} - H_{j,t}^{\mathrm{CHP}} \right) \right] \\
& + \sum_{i=1}^{n^{\mathrm{CFP}}} c_i^{\mathrm{CFP}} \left(PR_{i,\omega,t}^{\mathrm{CFP,U}} - PR_{i,\omega,t}^{\mathrm{CFP,D}} \right) + \sum_{w=1}^{n^{\mathrm{GW}}} c_w^{\mathrm{GW}} \left(Q_{w,\omega,t}^{\mathrm{GW}} - Q_{w,t}^{\mathrm{GW}} \right) \\
& + \sum_{k=1}^{n^{\mathrm{P2G}}} \left[c_k^{\mathrm{P2G,Q}} \left(QR_{k,\omega,t}^{\mathrm{P2G,U}} - QR_{k,\omega,t}^{\mathrm{P2G,D}} \right) + c_k^{\mathrm{P2G,H}} \left(H_{k,\omega,t}^{\mathrm{P2G}} - H_{k,t}^{\mathrm{P2G}} \right) \right] \\
& + \sum_{s=1}^{n^{\mathrm{GS}}} \left[c_s^{\mathrm{GS,in}} \left(Q_{s,\omega,t}^{\mathrm{GS,in}} - Q_{s,t}^{\mathrm{GS,in}} \right) + c_s^{\mathrm{GS,with}} \left(Q_{s,\omega,t}^{\mathrm{GS,out}} - Q_{s,t}^{\mathrm{GS,out}} \right) \right] \\
& + \sum_{h=1}^{n^{\mathrm{HS}}} \left[c_h^{\mathrm{HS,in}} \left(H_{h,\omega,t}^{\mathrm{HS,in}} - H_{h,t}^{\mathrm{HS,in}} \right) + c_h^{\mathrm{HS,out}} \left(H_{h,\omega,t}^{\mathrm{HS,out}} - H_{h,t}^{\mathrm{HS,out}} \right) \right] \\
& + \sum_{f=1}^{n^{\mathrm{WF}}} c_f^{\mathrm{WF}} \left(W_{f,\omega,t} - W_{f,\omega,t}^{\mathrm{spill}} - W_{f,t}^{\mathrm{S}} \right) + \sum_{d=1}^{n^{\mathrm{ED}}} V_d^{\mathrm{LOL}} D_{d,\omega,t}^{\mathrm{ED,shed}} \Bigg\}
\end{aligned}
\tag{2.2}
$$

The objective function (2.2) minimizes the total expected operation costs, which consist of two parts: the day-ahead scheduling cost and the expected cost of the anticipated balancing actions during the real-time operation.

This objective function (2.2) consists of several terms. The first term represents the operation cost of scheduling CHP units to produce electricity and heat. For the gas-

fired CHP units, the operation cost does not include the fuel cost as it is computed as a part of the total gas supply cost. The second and third terms represent the operation cost of scheduling coal-fired power (CFP) units and wind farms (WF) to produce electricity, respectively. The fourth term represents the cost of gas supply scheduling of gas wells (GW). The fifth term represents the operation cost of scheduling P2G units to produce gas and heat. The sixth term represents the cost of gas output and gas input of gas storage in the scheduling stage. The seventh term represents the operational cost of heat output and heat input in the HS in the scheduling stage. The eighth to fourteenth terms represent the expected balancing cost of operating the CHP, CFP, GW, P2G, GS, HS and wind farms of the integrated system in real-time operation. The fifteenth term represents the cost of any load that must be shed in real-time operation.

This objective function subjects to both the scheduling constraints and the real-time operation constraints. Each set of constraints is divided into four categories, which are the electricity, gas, district heating, and the linking constraints. Also, the model has been simplified by making some assumptions:

1) For the electricity system, the DC power flow model is used. Power losses are ignored.

2) For the gas network, we assume that all nodal gas pressures are within normal ranges. Nodal gas flow balances, the facility capacities and the pipeline transmission limits are considered in the gas network constraints.

3) For the district heating network, we assume that the water temperature and the water pressure are within normal ranges. The nodal heat flow balance, heat supply capacities and heat transmission limits are considered in the heat network constraints.

4) Upward and downward reserves for CFP, CHP, and P2G units are scheduled to compensate high/low wind power production.

5) For simplicity, the gas flow rates and heat flow rates are converted to power units, and the per-unit system is used.

3.2.2. DAY-AHEAD SCHEDULING OF THE ENERGY SOURCES

The optimal scheduling strategy of the MES is analyzed throughout a 24-hour time horizon. The test system considered is shown in Figure 3-6. Figure 3-7 shows the optimal schedule of the EPS. It should be noted that the total power consumption consists of both power load and power consumption in the P2G unit. It can be observed in Figure 3-7 that the generation of the CFP unit is smooth. Conversely, the gas-fired CHP unit plays a critical role regarding peak regulation. On the gas system side, Figure 3-8 illustrates the gas injections and consumptions. Since there is wind power surplus in the scheduling stage, the excess electricity is converted into gas and heat by the P2G unit, which reduces wind power curtailment. Note that gas supply is flat from the gas well. The difference between gas supply from gas sources and gas consumption is balanced by the gas linepack and storage. At the district

heating system side, Figure 3-9 illustrates the heat supplies and consumptions. The difference between heat supply and heat consumption is balanced by the heat storage.

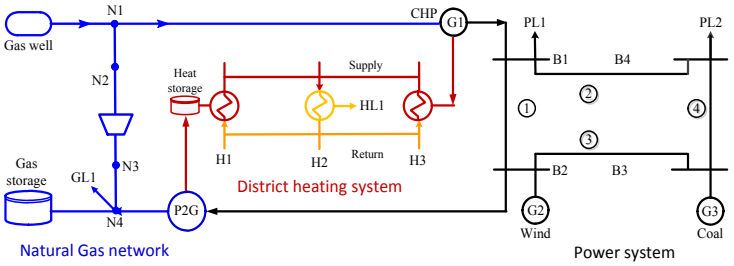

Figure 3-6 The Structure of integrated electricity, natural gas and district heating system.

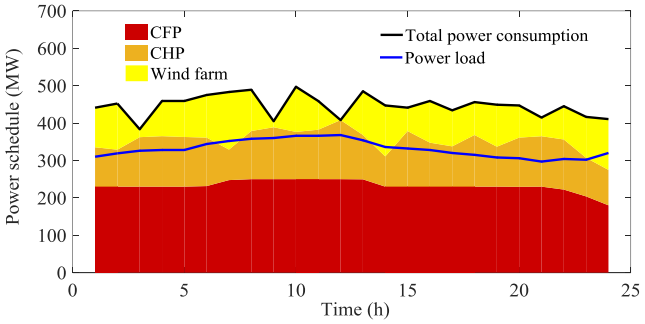

Figure 3-7 Optimal schedule of sources in the electrical system

.

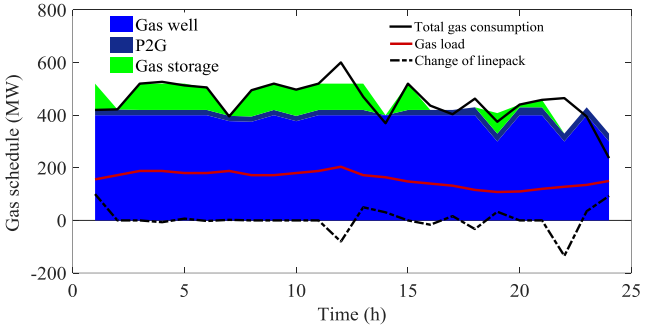

Figure 3-8 Optimal schedule of sources in the gas system.

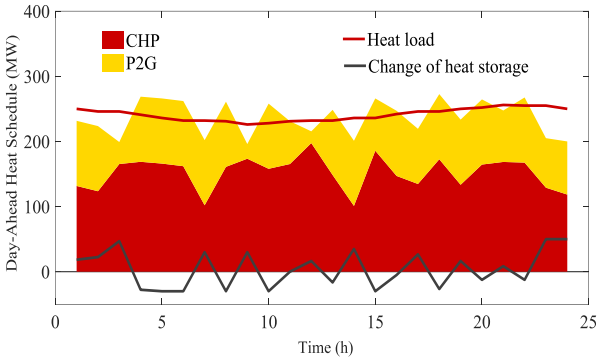

Figure 3-9 Optimal schedule of sources in the district heating system.

3.2.3. REAL-TIME ADJUSTMENT OF ENERGY SOURCES

Figure 3-10 provides the deployment of downward and upward reserve adjustments in the EPS to account for wind variability. A positive value represents an upward reserve adjustment and a negative one a downward reserve adjustment. For scenario "high wind", the downward reserves of units CPG and CHP is deployed to accommodate high wind power production in most of the periods. For scenario "low wind", the upward reserve of unit CPG is deployed in most of the periods.

Figure 3-11 provides the deployment of downward and upward reserve in NGS to account for wind variability. For scenario "low wind", the downward reserve of the P2G unit is deployed in most of the periods as there is no surplus electricity, while the gas supply is increased from the gas well to satisfy the gas demand.

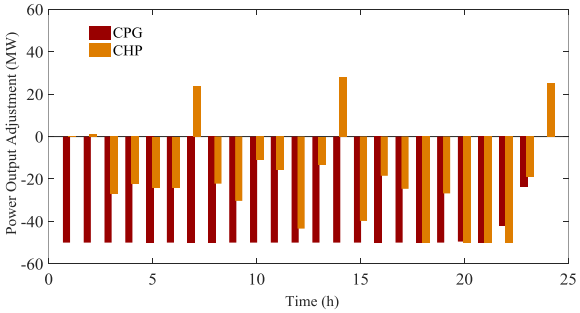

(a) High wind

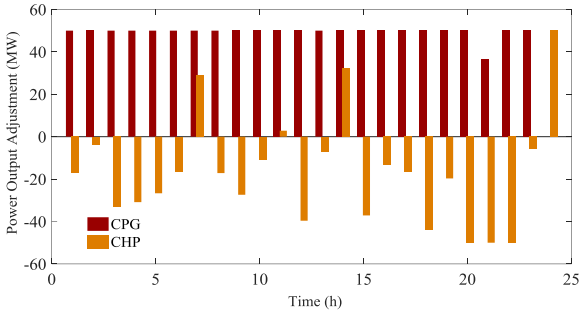

(b) Low wind

Figure 3-10 Optimal adjustment of sources in the electricity system.

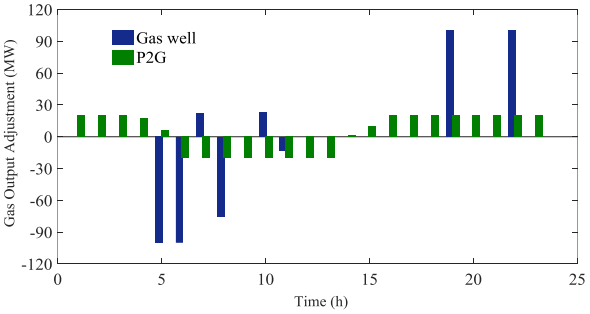

(a) High wind

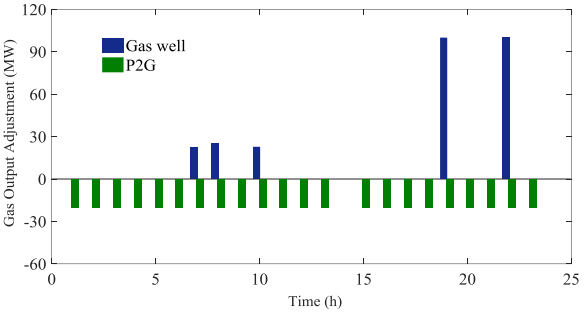

(b) Low wind

Figure 3-11 Optimal adjustment of sources in the gas system.

To assess the computational efficiency of the proposed method, we have run problems with 50 scenarios using CPLEX under GAMS. The CPU core used for the simulations clocks at 2.7 GHz. Available RAM is 8 GB. The solution time is 1.64 seconds for this case with 50 wind power scenarios.

3.2.4. THE IMPACT OF THE UNCERTAINTY ON THE TOTAL SYSTEM OPERATION COST

In order to evaluate the impact of wind power uncertainty on the expected operating costs of the entire system, case studies are carried out on a variety of scenarios. Table 3-1 consists of the total costs, energy production costs and reserve capacity costs. We compare the cost breakdown under four different scenarios, namely:

Case a) No uncertainty: Wind power generation is completely known in advance, and it is consistent with its expected value.

Case b) No wind production: There is no wind farm in the system. Thus, all the loads are completely provided by thermal power plants.

Case c) Uncertain wind power: We consider the uncertainty of wind power. The result can be obtained by solving the two-stage stochastic programming problem.

Case d) Network congestion: Reduce the capacity of a single transmission line from 200 MW to 40 MW. Wind power generation is the same as case 3).

Table 3-1 Comparison of the expected cost breakdown

Case	a	b	c	d
Energy cost	398650	455735	401740	424864
Reserve cost	0	0	31206	25812
Total cost	**398650**	**455735**	**432946**	**450676**

It is clear that wind power has a significant effect on the energy production cost by comparing cases (a) or (c) with case (b). It shows that the expected cost of (a) is significantly less than (c). The reason is that some costs are spent on reserve capacity to accommodate the uncertainty of wind power production.

Case (d) emphasizes the effect of line capacity on the total cost. When a single transmission line has a lower capacity in the system, part of the wind power may be curtailed and the electricity system will not fully benefit from the no-cost wind power generation. Further, the cost of the system will have a bigger growth in the case of defects, such as outrage on lines.

3.3. SUMMARY

The developed model reported in this Chapter allows jointly operating the electricity, gas, and district heating systems of a city to achieve an efficient and economic

performance. This joint operation scheme for all subsystems (electricity, gas and district heating) is clearly better than the independent operation of each of these subsystems. The considered two-stage stochastic formulation allows the optimal scheduling of reserves to facilitate real-time adjustment decisions, which results in minimum cost while integrating the highest level of wind energy. The required computational time is small and clearly compatible with operational requirements. The papers related to this chapter are J3 and C1, C2, C3.

CHAPTER 4. CO-EXPANSION PLANNING OF THE MULTI-ENERGY SYSTEMS

This chapter deals with the co-expansion planning of the multi-energy systems. We develop a bi-level multi-stage programming problem to minimize the total investment and operating costs. The upper level focuses on the system expansion planning, while the lower level focuses on the optimal operation of gas and electricity facilities. To solve this problem, a hybrid algorithm is proposed by combining the Binary Particle Swarm Optimization (BPSO) and Interior Point Method (IPM). Examples have been studied on western Danish gas and power transmission networks.

4.1. FORMULATION OF BI-LEVEL PROGRAMMING ON THE CO-EXPANSION PLANNING

The upper-level subproblems aim at minimizing the total investment cost, while lower level subproblems try to optimize network operations [45]. Both problems are interactive. Reducing investment in capacity expansion results in higher operating costs. On the contrary, obtaining lower operating costs requires more investment in expanding electricity networks [45].

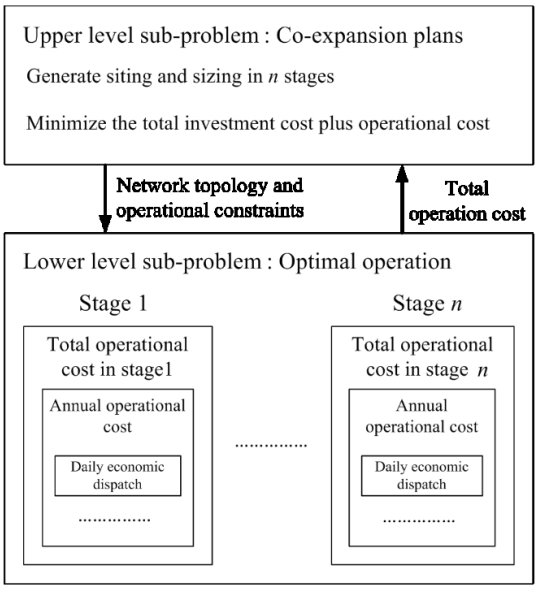

Figure 4-1 Framework of bi-level programming on co-expansion planning

The upper-level subproblem decides the expansion plan of the integrated energy system, which consists of the siting and sizing of the facilities, such as generators, lines and pipes, etc. [45]. The objective can be given as

$$OF = \sum_{y=1}^{Y} \frac{1}{(1+r)^{y-1}} \left(F_{\text{investment}}(y) + F_{\text{operation}}(y) \right) \tag{3.1}$$

where the symbol Y is the planning time horizon, $F_{\text{investment}}$ is the investment cost, $F_{\text{operation}}$ is the operational cost. The investment objective function is subjected to the following constraints [45]:

1) Avoiding remove the expanded generators within the planning horizon.
2) Due to the limited floor space, the maximum expansion capacity should be limited to facilities.
3) The total annual investment should be limited to meet the financial budget.

In the lower level subproblem, the economic dispatch is carried out to minimize the operational cost of the planned network and the plants. The annual operating costs $F_{\text{operation}}(y)$ is translated into the sum of the operating costs of that year [45]:

$$F_{\text{operation}}(y) = \sum_{d=1}^{D_y} F_{\text{operation}}(d) \tag{3.2}$$

where D_y is the time horizon for that year.

The objective subjects to the following constraints:

1) For the power system, the operation should meet the transmission capacities, power flow balance, network constraints and generator capacities.
2) For the gas network, the operation should subject to the gas flow balance constraints and the operational limits of the facilities, such as the gas compressor, gas terminal, and gas storage, etc.

4.2. SOLUTION METHODOLOGY

The bi-level optimization problem can be summarized as shown below [45].

$$\begin{aligned} \min \quad & \sum_{y=1}^{Y} \frac{1}{(1+r)^{y-1}} \left(F_{\text{investment}}(y) + F_{\text{operation}}(y) \right) \\ \text{s.t.} \quad & \begin{cases} \text{Planning constraints} \\ \text{Operational constraints} \end{cases} \end{aligned} \tag{3.3}$$

where $F_{\text{operation}}(y) = \sum_{d=1}^{D_y} F_{\text{operation}}(d)$. Moreover, is implicitly defined by

$$\begin{aligned} &\min \ F_{\text{operation}}(d) \\ &\text{s.t.} \ \begin{cases} \text{Power system constraints} \\ \text{Gas system constrains} \\ \text{Linkages} \end{cases} \end{aligned} \tag{3.4}$$

It is a bi-level mixed-integer non-linear programming. A hybrid algorithm that integrates the BPSO and IPM is proposed to solve this problem [45]. A BPSO is used [70] to solve the co-expansion plan problems in the upper level. For lower-level, IPM is used to solve the optimization sub-problems. Figure 4-2 shows a detailed flowchart for using the hybrid algorithm to solve the bi-level mixed-integer non-linear programming. The steps for applying the hybrid algorithm to bi-level programming are shown below:

1. Randomly initialize a set of particles at random positions and velocities to provide network topology and operational constraints.

2. Calculate lower-level operating costs based on the network topology and operating limits provided by the upper-level.

3. Calculate the fitness function of the upper-level, including the operating and investment costs.

4. Update the local optimal position and the global optimum solution.

5. Calculate the particle speed in the next step and update the position of particles.

6. Obtain the optimal solution from PSO if the total cost is not changed for several iterations. Otherwise, back to step 2.

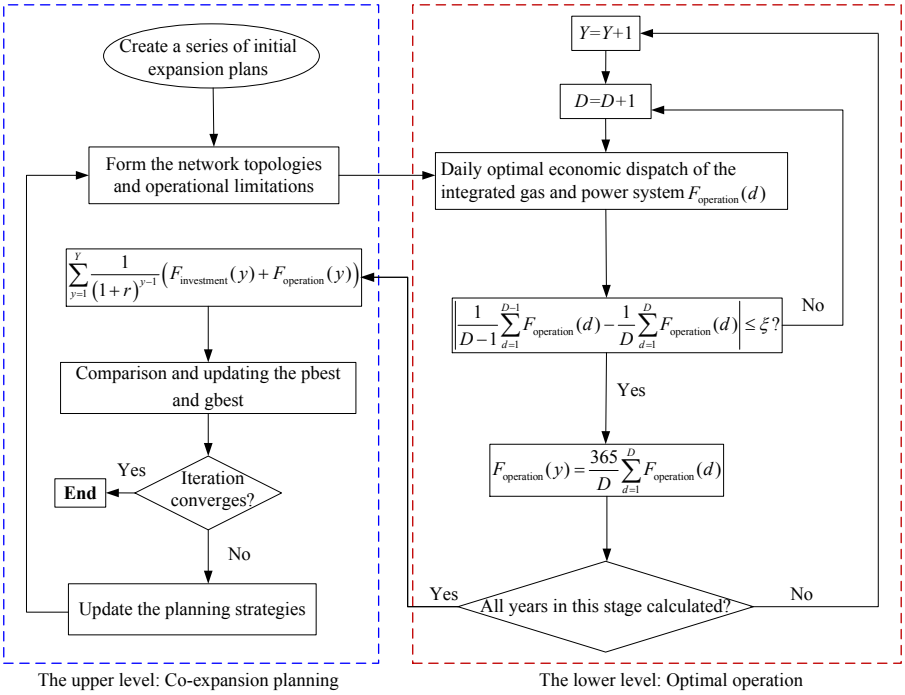

Figure 4-2 Flowchart of solving bi-level programming with the hybrid algorithm

4.3. CASE STUDY

As shown in Figure 4-3, case studies are carried out on the in western Danish natural gas and power transmission networks. System parameters are obtained from Energinet.dk, a Danish operator of electricity and natural gas transmission systems [71], [72].

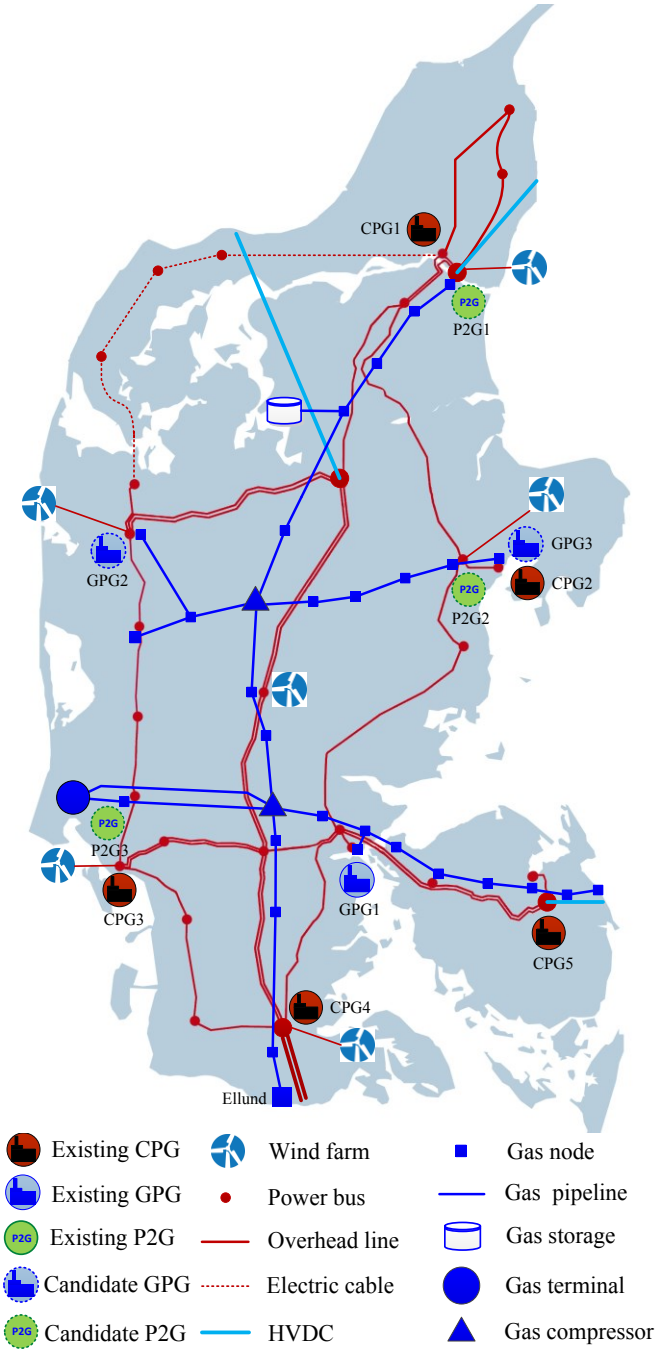

Figure 4-3 The natural gas and electricity transmission system in western Denmark.

4.3.1. SCENARIO FORECAST AND THE INVESTMENT COSTS

The planning period is nine years (2016-2024) and consists of 3 stages. The detailed forecast shown in Table 4-1 is obtained from Energinet.dk.

Table 4-1 The Energinet.dk's forecast of the planning horizon (2016–2024)

Year	Coal price	Gas price	CO_2 price	Electricity prices	Electricity load	Wind capacity	Percentage of wind
	€/MWh	€/MWh	€/ton	€/MWh	GWh	MW	%
2016	8.1	21.3	7.3	30	20737	5041	41
2017	8.8	22.9	8.8	29.1	20959	5191	43
2018	9.6	24.8	10.8	36.3	21208	5341	45
2019	10.5	26.9	13.5	43.6	21384	5541	48
2020	11.5	28.9	16.8	50.9	21552	6341	58
2021	11.6	29.4	18.1	51.3	21841	6591	61
2022	11.7	29.7	19.5	53.2	22205	6841	64
2023	11.7	30.1	20.7	53.7	22512	6891	66
2024	11.8	30.4	22	54.3	22866	6941	66

This table includes the average price of electricity, fuel, carbon dioxide emissions, as well as the future expansion of Danish electricity consumption and wind power generation capacity. From a consumer's perspective, Denmark's electricity consumption growth is small [71]. From 2016 to 2024, the average annual growth rate is about 1%. From a power generation perspective, it is estimated by Energinet.dk that there will be 6941 MW wind power capacity in the Danish power system, generating 66% of the total electricity consumption by 2024. It will increase by approximately 3.5% per year since 2016 [72].

4.3.2. THE MULTISTAGE EVOLUTION OF THE CAPACITIES FOR P2G, GPG, AND CPG

Three scenarios were studied to validate the proposed method. Assume that the annual growth rates of wind power generation for scenarios 1, 2 and 3 are 2%, 3.5% and 5%, respectively. The simulation was performed on a computer with 3.06 GHz CPU/8GB RAM, the number of iterations and the particle size were set to 50 and 250, respectively.

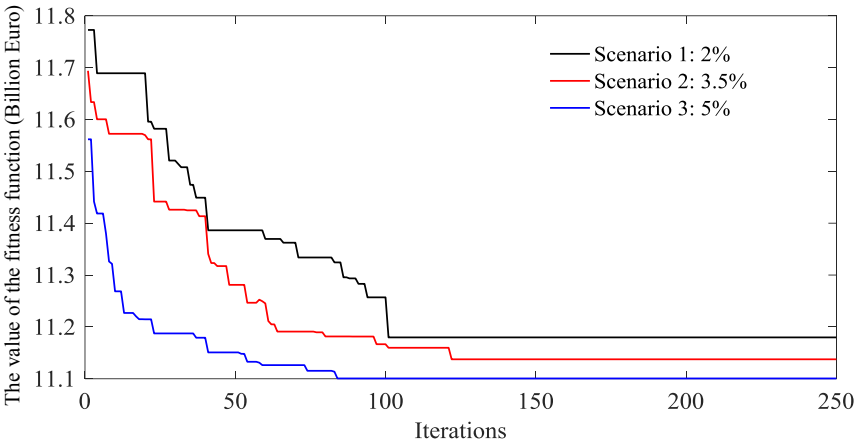

Figure 4-4 shows the iterative process of BPSO for the three scenarios. It shows that less than 150 steps are required before convergence, and the calculation times for options 1, 2 and 3 are 1054, 1205 and 1146 minutes, respectively. The simulation results are shown in Table 4-2. When the amount of wind power is increased, the operating cost is reduced due to the reduction in the consumption of natural gas and other fuels. However, more GPG and P2G investment costs are needed to ensure a safe energy supply [45].

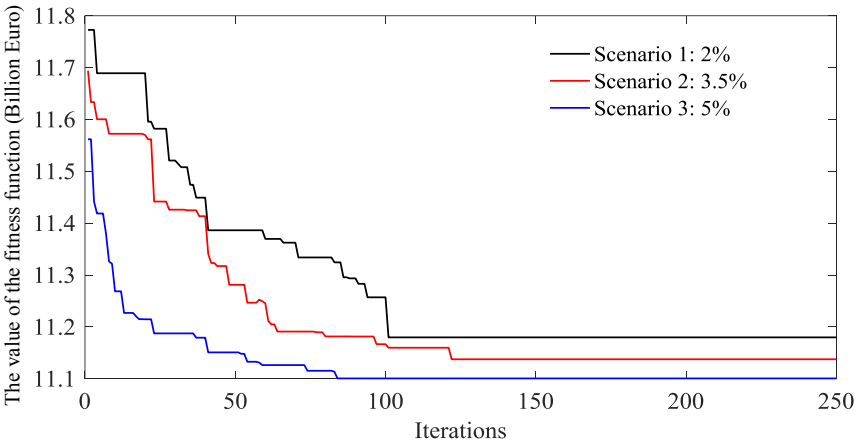

Figure 4-4 Optimization process of the proposed method

Figure 4-5 shows the multi-stage evolution of the energy mix. The capacity of CPG decreases with wind penetration level, while the capacity of GPG and P2G increases with wind penetration level. For Scenario 1, the CPG's capacity was reduced from 2685 MW to 2181 MW, while GPG's capacity was increased from 400 MW to 505 MW, and a 208 MW P2G plant was planned [45]. For Scenario 2, the capacity of the CPG was reduced from 2695 MW to 2029 MW, and in this case, the newly installed

capacity is 140 MW (from 400 MW to 540 MW) for GPG and the newly planned capacity is 295 MW for P2G [45]. Scenario 3 shows that the CPG's capacity will be shrunk to 1885 MW. In this case, it plans to expand 166 MW for GPG and 351 MW for P2G. As shown in the comparison of the three scenarios, the higher growth rate of wind power leads to more CPG closures and faster growth of GPG and P2G [45].

Table 4-2 Total expansion and operation cost in billions of Euro

Scenario no.	Iteration steps	Initial fitness	Optimal total	Investment cost	Operation cost
Scenario 1	101	11.78	11.18	0.17	11.01
Scenario 2	119	11.69	11.14	0.23	10.91
Scenario 3	82	11.56	11.10	0.24	10.86

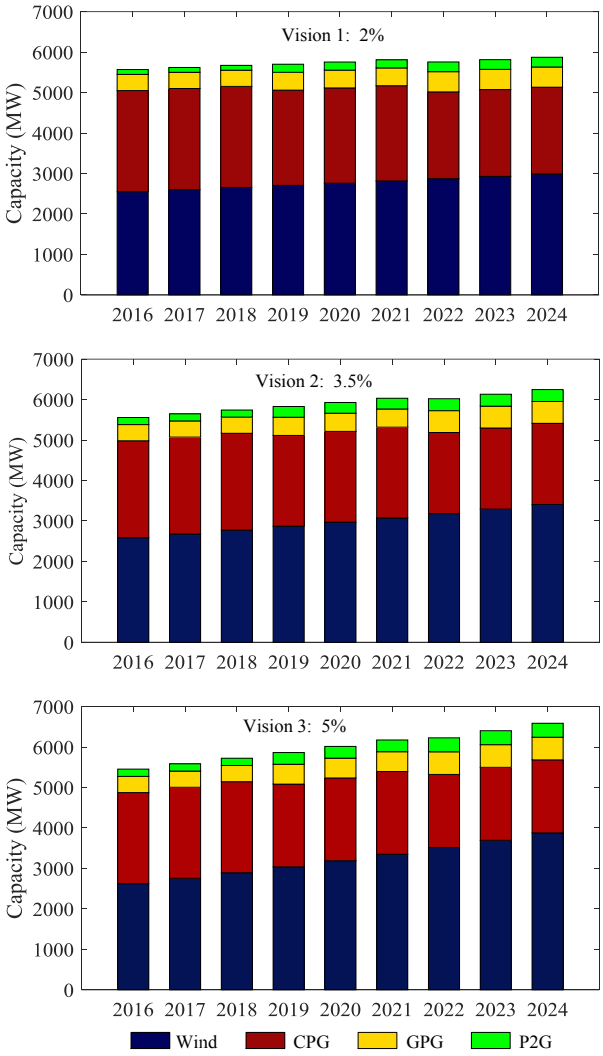

Figure 4-5 Evolution of the installed generation from 2016 to 2024 for three scenarios

4.3.3. THE DAILY OPTIMAL OPERATION OF THE INTEGRATED GAS AND ELECTRICITY SYSTEM

This section illustrates the daily operation of the combined GNS-EPS. Figure 4-6 shows the daily economic dispatch of the EPS with high wind power. It shows that all the wind power is supplied to meet the power load during the peak periods (7:00 AM~13:00 PM, 17:00 PM~18:00 PM) [45]. Meanwhile, both GPG and CPG raise

their outputs to balance the electricity demand. On the contrary, there is excess wind power during the midnight (12:00 PM~6:00 AM) which is converted into gas fuel by P2G. However, due to the limited available capacity of P2G, there is still wind curtailment in this period. It should be noted that the total electricity demand consists of both the nodal electricity demand and electricity consumption in P2G [45].

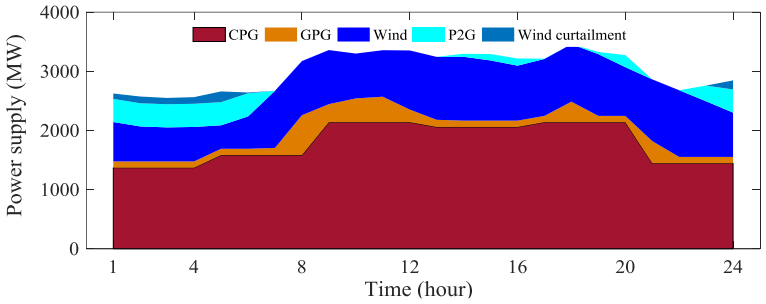

Figure 4-6 Daily economic dispatch at power system side

Figure 4-7 illustrates the daily economic dispatch of the gas facilities. This shows that the gas dispatch at the gas storage and gas terminal seems to be flat. The gas linepack balances the gas supply and gas demand. It can be seen that the linepack is consumed during the day and recovered at midnight. During the peak natural gas demand time (e.g. 8:00AM~13:00 PM), the natural gas demand from GPG continues to increase, resulting in rapid consumption of linepack. It shows that the sufficient linepack plays a critical role in balancing gas production and consumption [45].

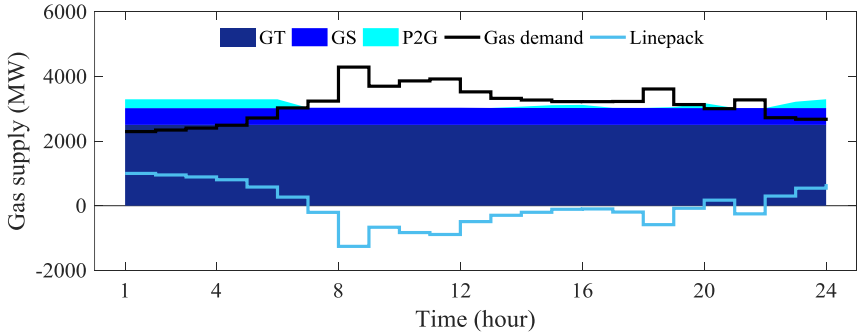

Figure 4-7 Optimized gas supply in the natural gas system Summary.

4.4. SUMMARY

For the integrated gas-power systems, a multi-stage expansion planning model was developed to optimize the investment and operating costs. A bi-level framework was constructed to achieve a good balance between investment and operating costs. A hybrid algorithm is proposed to solve the bi-level programming problem by combining improved BPSO and IPM. Case studies have been carried out on the western Danish natural gas and electricity transmission network to verify the effectiveness of the method. To overcome the challenges posed by changes in the energy mix, GPG and P2G are recommended to enhance the synergy between NGS and EPS. Simulation results show that P2G helps to reduce the operation cost for the lower wind curtailment and fewer carbon emissions.

The papers related to this chapter are J2 and C4.

CHAPTER 5. CONCLUSIONS FUTURE PERSPECTIVES

This thesis aims at developing strategies, models, and methods to optimize the planning and operation of the integrated power, gas and heating systems to improve the overall efficiency and sustainability of the energy system. The main aspects include models of energy sources and energy networks, energy flow modeling, network expansion planning and optimal operation strategies.

The energy flow model is developed in Chapter 2 to describe the gas, district heating, and electric power systems. Then a unified energy flow solution is proposed to analyze the energy distribution in the MES.

The coordinated optimization model is developed in Chapter 3 to jointly operate the integrated energy systems with the aims of maximizing efficiency and minimizing cost. The fluctuating wind power is considered with the two-stage stochastic programming.

The bi-level programming is formulated in Chapter 4 to minimize the total investment cost and operating cost. A hybrid algorithm combining the Binary Particle Swarm Optimization (BPSO) and Interior Point Method (IPM) is proposed to solve this problem.

All the proposed models and methods are tested under different scenarios. After analysis the simulation results, we can get the following conclusions:

1. The gas, electricity, and district heating systems interact with each other, and the coordinated operation and planning can help to improve the overall efficiency and sustainability.

2. P2G and GPG can help to enhance the synergies between the gas and power systems, to utilize the compressibility of the natural gas as the flexibility resources in power system.

3. P2G helps to reduce operation cost by lower the wind curtailment, fuel consumption, and carbon emission. All the power loss, BHP and the total energy loss can be reduced by using P2G in the integrated energy system.

4. Planning results suggest that enhancing the synergies between gas and power system using GPG and P2G helps to overcome the challenges brought by the change in the energy mix, and potentially contribute to the renewable targets.

5. The two-stage stochastic formulation allows the optimal scheduling of reserves to facilitate real-time adjustment decisions under uncertainties, which results in minimum cost while integrating the highest level of wind energy.

With the promising simulation results of this research, the proposed operation and planning frameworks have the potential to solve other system operation and planning problems of multi-energy systems. In the future, the following works can be expected.

1. Improvement on the energy flow model. The dynamic energy flow model can be formulated to analysis the MES by considering the different response times of the district heating, gas and power systems.

2. Coordinate the demand responses across multiple energy systems. Recently, demand response becomes the major flexibility source in the electrical distribution system. Part of the heating demand can be met without reducing the comfort level.

3. The multi-time period optimization problem can be formulated for the optimal management of the flexible sources in the integrated energy systems.

LITERATURE LIST

[1] A. Gebremedhin, "Optimal utilisation of heat demand in district heating system—A case study," *Renew. Sustain. Energy Rev.*, vol. 30, no. Supplement C, pp. 230–236, Feb. 2014.

[2] Massachusetts Institute of Technology, *The future of Natural Gas an interdisciplinary MIT study.* [Cambridge, Mass.]: Massachusetts Institute of Technology, 2011.

[3] M. A. Gonzalez-Salazar, T. Kirsten, and L. Prchlik, "Review of the operational flexibility and emissions of gas- and coal-fired power plants in a future with growing renewables," *Renew. Sustain. Energy Rev.*, vol. 82, no. Part 1, pp. 1497–1513, Feb. 2018.

[4] M. Götz *et al.*, "Renewable Power-to-Gas: A technological and economic review," *Renew. Energy*, vol. 85, pp. 1371–1390, Jan. 2016.

[5] H. Averfalk, P. Ingvarsson, U. Persson, M. Gong, and S. Werner, "Large heat pumps in Swedish district heating systems," *Renew. Sustain. Energy Rev.*, vol. 79, no. Supplement C, pp. 1275–1284, Nov. 2017.

[6] B. Yan, S. Xue, Y. Li, J. Duan, and M. Zeng, "Gas-fired combined cooling, heating and power (CCHP) in Beijing: A techno-economic analysis," *Renew. Sustain. Energy Rev.*, vol. 63, no. Supplement C, pp. 118–131, Sep. 2016.

[7] H. Chen, T. N. Cong, W. Yang, C. Tan, Y. Li, and Y. Ding, "Progress in electrical energy storage system: A critical review," *Prog. Nat. Sci.*, vol. 19, no. 3, pp. 291–312, Mar. 2009.

[8] J. N. Rasmussen, "Vindmøller slog rekord i 2014," *Energinet.dk*, 06-Jan-2015.

[9] B. V. Mathiesen, H. Lund, and D. Connolly, "Limiting biomass consumption for heating in 100% renewable energy systems," *Energy*, vol. 48, no. 1, pp. 160–168, Dec. 2012.

[10] D. Connolly, H. Lund, B. V. Mathiesen, and M. Leahy, "The first step towards a 100% renewable energy-system for Ireland," *Appl. Energy*, vol. 88, no. 2, pp. 502–507, Feb. 2011.

[11] B. V. Mathiesen *et al.*, "Smart Energy Systems for coherent 100% renewable energy and transport solutions," *Appl. Energy*, 2014.

[12] "CEESA: 100% Renewable Energy Scenarios for Denmark to 2050 (2012) | EnergyPLAN." .

[13] H. Lund *et al.*, "4th Generation District Heating (4GDH): Integrating smart thermal grids into future sustainable energy systems," *Energy*, vol. 68, pp. 1–11, Apr. 2014.

[14] G. Gahleitner, "Hydrogen from renewable electricity: An international review of power-to-gas pilot plants for stationary applications," *Int. J. Hydrog. Energy*, vol. 38, no. 5, pp. 2039–2061, Feb. 2013.

[15] S. Schiebahn, T. Grube, M. Robinius, V. Tietze, B. Kumar, and D. Stolten, "Power to gas: Technological overview, systems analysis and economic

assessment for a case study in Germany," *Int. J. Hydrog. Energy*, vol. 40, no. 12, pp. 4285–4294, Apr. 2015.

[16] X. Luo, J. Wang, M. Dooner, and J. Clarke, "Overview of current development in electrical energy storage technologies and the application potential in power system operation," *Appl. Energy*, vol. 137, pp. 511–536, Jan. 2015.

[17] M. H. Ali, B. Wu, and R. A. Dougal, "An Overview of SMES Applications in Power and Energy Systems," *IEEE Trans. Sustain. Energy*, vol. 1, no. 1, pp. 38–47, Apr. 2010.

[18] D. Connolly, *An investigation into the energy storage technologies available, for the integration of alternative generation techniques*. Department of Physics, University of Limerick, 2007.

[19] T. Shimizu and C. Underwood, "Super-capacitor energy storage for micro-satellites: Feasibility and potential mission applications," *Acta Astronaut.*, vol. 85, no. Supplement C, pp. 138–154, Apr. 2013.

[20] S. M. Mousavi G, F. Faraji, A. Majazi, and K. Al-Haddad, "A comprehensive review of Flywheel Energy Storage System technology," *Renew. Sustain. Energy Rev.*, vol. 67, no. Supplement C, pp. 477–490, Jan. 2017.

[21] M. Budt, D. Wolf, R. Span, and J. Yan, "A review on compressed air energy storage: Basic principles, past milestones and recent developments," *Appl. Energy*, vol. 170, no. Supplement C, pp. 250–268, May 2016.

[22] I. Kougias and S. Szabó, "Pumped hydroelectric storage utilization assessment: Forerunner of renewable energy integration or Trojan horse?," *Energy*, vol. 140, no. Part 1, pp. 318–329, Dec. 2017.

[23] M. Jentsch, T. Trost, and M. Sterner, "Optimal Use of Power-to-Gas Energy Storage Systems in an 85% Renewable Energy Scenario," *Energy Procedia*, vol. 46, pp. 254–261, 2014.

[24] B. Bach, J. Werling, T. Ommen, M. Münster, J. M. Morales, and B. Elmegaard, "Integration of large-scale heat pumps in the district heating systems of Greater Copenhagen," *Energy*, vol. 107, no. Supplement C, pp. 321–334, Jul. 2016.

[25] P. Meibom, J. Kiviluoma, R. Barth, H. Brand, C. Weber, and H. V. Larsen, "Value of electric heat boilers and heat pumps for wind power integration," *Wind Energy*, vol. 10, no. 4, pp. 321–337, Jul. 2007.

[26] M. Waite and V. Modi, "Potential for increased wind-generated electricity utilization using heat pumps in urban areas," *Appl. Energy*, vol. 135, pp. 634–642, Dec. 2014.

[27] Q. Zeng, J. Fang, J. Li, and Z. Chen, "Steady-state analysis of the integrated natural gas and electric power system with bi-directional energy conversion," *Appl. Energy*, vol. 184, pp. 1483–1492, Dec. 2016.

[28] P. Wong and R. Larson, "Optimization of natural-gas pipeline systems via dynamic programming," *IEEE Trans. Autom. Control*, vol. 13, no. 5, pp. 475–481, Oct. 1968.

[29] A. A. Jamshidifar, “Optimization of natural gas transmission network using genetic algorithm,” in *2011 11th International Conference on Intelligent Systems Design and Applications (ISDA)*, 2011, pp. 295–300.
[30] A. Osiadacz, *Simulation and analysis of gas networks*. Gulf Pub. Co., 1987.
[31] A. Benonysson, B. Bøhm, and H. F. Ravn, “Operational optimization in a district heating system,” *Energy Convers. Manag.*, vol. 36, no. 5, pp. 297–314, May 1995.
[32] D. K. Baker and S. A. Sherif, “Heat Transfer Optimization of a District Heating System Using Search Methods,” *Int. J. Energy Res.*, vol. 21, no. 3, pp. 233–252, Mar. 1997.
[33] J. Carpentier, “Optimal power flows,” *Int. J. Electr. Power Energy Syst.*, vol. 1, no. 1, pp. 3–15, Apr. 1979.
[34] A. R. Bergen and V. Vittal, *Power systems analysis*, 2nd ed. Upper Saddle River, NJ: Prentice Hall, 2000.
[35] A. J. Wood and B. F. Wollenberg, *Power generation, operation, and control*. Beijing: Tsinghua University Press, 2003.
[36] A. Martinez-Mares and C. R. Fuerte-Esquivel, “A Unified Gas and Power Flow Analysis in Natural Gas and Electricity Coupled Networks,” *IEEE Trans. Power Syst.*, vol. 27, no. 4, pp. 2156–2166, Nov. 2012.
[37] E. Fabrizio, V. Corrado, and M. Filippi, “A model to design and optimize multi-energy systems in buildings at the design concept stage,” *Renew. Energy*, vol. 35, no. 3, pp. 644–655, Mar. 2010.
[38] S. An, Q. Li, and T. W. Gedra, “Natural gas and electricity optimal power flow,” in *Transmission and Distribution Conference and Exposition, 2003 IEEE PES*, 2003, vol. 1, p. 138–143 Vol.1.
[39] M. Geidl and G. Andersson, “A modeling and optimization approach for multiple energy carrier power flow,” in *Power Tech, 2005 IEEE Russia*, 2005, pp. 1–7.
[40] J. Söderman and F. Pettersson, “Structural and operational optimisation of distributed energy systems,” *Appl. Therm. Eng.*, vol. 26, no. 13, pp. 1400–1408, Sep. 2006.
[41] P. Mancarella, “MES (multi-energy systems): An overview of concepts and evaluation models,” *Energy*, vol. 65, pp. 1–17, Feb. 2014.
[42] A. Martinez-Mares and C. R. Fuerte-Esquivel, “Integrated energy flow analysis in natural gas and electricity coupled systems,” in *North American Power Symposium (NAPS), 2011*, 2011, pp. 1–7.
[43] P. Duenas, J. Barquin, and J. Reneses, “Strategic Management of Multi-Year Natural Gas Contracts in Electricity Markets,” *IEEE Trans. Power Syst.*, vol. 27, no. 2, pp. 771–779, May 2012.
[44] B. C. Erdener, K. A. Pambour, R. B. Lavin, and B. Dengiz, “An integrated simulation model for analysing electricity and gas systems,” *Int. J. Electr. Power Energy Syst.*, vol. 61, pp. 410–420, Oct. 2014.

[45] Q. Zeng, B. Zhang, J. Fang, and Z. Chen, "A bi-level programming for multistage co-expansion planning of the integrated gas and electricity system," *Appl. Energy*, vol. 200, pp. 192–203, Aug. 2017.

[46] M. Shahidehpour, Y. Fu, and T. Wiedman, "Impact of Natural Gas Infrastructure on Electric Power Systems," *Proc. IEEE*, vol. 93, no. 5, pp. 1042–1056, May 2005.

[47] T. Li, M. Eremia, and M. Shahidehpour, "Interdependency of Natural Gas Network and Power System Security," *IEEE Trans. Power Syst.*, vol. 23, no. 4, pp. 1817–1824, Nov. 2008.

[48] C. Liu, M. Shahidehpour, Y. Fu, and Z. Li, "Security-Constrained Unit Commitment With Natural Gas Transmission Constraints," *IEEE Trans. Power Syst.*, vol. 24, no. 3, pp. 1523–1536, Aug. 2009.

[49] C. M. Correa-Posada and P. Sánchez-Martin, "Security-constrained optimal power and natural-gas flow," *IEEE Trans. Power Syst.*, vol. 29, no. 4, pp. 1780–1787, 2014.

[50] S. Hecq, Y. Bouffioulx, P. Doulliez, and P. Saintes, "The integrated planning of the natural gas and electricity systems under market conditions," in *Power Tech Proceedings, 2001 IEEE Porto*, 2001, vol. 1, p. 5 pp. vol.1-pp.

[51] B. H. Bakken and A. T. Holen, "Energy service systems: integrated planning case studies," in *IEEE Power Engineering Society General Meeting, 2004*, 2004, p. 2068–2073 Vol.2.

[52] C. Unsihuay, J. W. M. Lima, and A. C. Z. de Souza, "Modeling the Integrated Natural Gas and Electricity Optimal Power Flow," in *IEEE Power Engineering Society General Meeting, 2007*, 2007, pp. 1–7.

[53] M. Chaudry, N. Jenkins, M. Qadrdan, and J. Wu, "Combined gas and electricity network expansion planning," *Appl. Energy*, vol. 113, pp. 1171–1187, Jan. 2014.

[54] C. Unsihuay-Vila, J. W. Marangon-Lima, A. C. Z. de Souza, I. J. Perez-Arriaga, and P. P. Balestrassi, "A Model to Long-Term, Multiarea, Multistage, and Integrated Expansion Planning of Electricity and Natural Gas Systems," *IEEE Trans. Power Syst.*, vol. 25, no. 2, pp. 1154–1168, May 2010.

[55] C. A. Saldarriaga, R. A. Hincapie, and H. Salazar, "A Holistic Approach for Planning Natural Gas and Electricity Distribution Networks," *IEEE Trans. Power Syst.*, vol. 28, no. 4, pp. 4052–4063, Nov. 2013.

[56] J. Qiu, Z. Y. Dong, J. H. Zhao, K. Meng, Y. Zheng, and D. J. Hill, "Low Carbon Oriented Expansion Planning of Integrated Gas and Power Systems," *IEEE Trans. Power Syst.*, vol. 30, no. 2, pp. 1035–1046, Mar. 2015.

[57] J. Grainger and J. Stevenson William, *Power System Analysis*. New York: McGraw–Hill, 1994.

[58] D. V. Hertem, J. Verboomen, K. Purchala, R. Belmans, and W. L. Kling, "Usefulness of DC power flow for active power flow analysis with flow controlling devices," in *The 8th IEE International Conference on AC and DC Power Transmission*, 2006, pp. 58–62.

[59] E. S. Menon, *Gas Pipeline Hydraulics*, 1 edition. Boca Raton, FL: CRC Press, 2005.
[60] S. Mokhatab, W. A. Poe, and J. G. Speight, *Handbook of Natural Gas Transmission and Processing*. Burlington, MA, USA: Gulf Publishing Company, 2006.
[61] A. Kabirian and M. R. Hemmati, "A strategic planning model for natural gas transmission networks," *Energy Policy*, vol. 35, no. 11, pp. 5656–5670, Nov. 2007.
[62] R. G. B. I. LIBERALIZED, "GAS BALANCING AND LINE-PACK FLEXIBILITY," European University Institute, 2012.
[63] M. Chaudry, N. Jenkins, and G. Strbac, "Multi-time period combined gas and electricity network optimisation," *Electr. Power Syst. Res.*, vol. 78, no. 7, pp. 1265–1279, Jul. 2008.
[64] Z. Li, W. Wu, M. Shahidehpour, J. Wang, and B. Zhang, "Combined Heat and Power Dispatch Considering Pipeline Energy Storage of District Heating Network," *IEEE Trans. Sustain. Energy*, vol. PP, no. 99, pp. 1–11, 2015.
[65] A. L. Sheldrake, *Handbook of Electrical Engineering: For Practitioners in the Oil, Gas and Petrochemical Industry*, 1 edition. Chichester, West Sussex, England ; Hoboken, NJ, USA: Wiley, 2002.
[66] J. M. Beér, "High efficiency electric power generation: The environmental role," *Prog. Energy Combust. Sci.*, vol. 33, no. 2, pp. 107–134, 2007.
[67] L. Grond, P. Schulze, and J. Holstein, "Systems Analyses Power to Gas: A Technology Review," Groningen, Jun. 2013.
[68] A. Constantinides and N. Mostoufi, *Numerical Methods for Chemical Engineers with MATLAB Applications*. Upper Saddle River, N.J: Prentice Hall, 1999.
[69] J. Li, J. Fang, Q. Zeng, and Z. Chen, "Optimal operation of the integrated electrical and heating systems to accommodate the intermittent renewable sources," *Appl. Energy*, vol. 167, pp. 244–254, Apr. 2016.
[70] J. Zhang, Y. Liu, D. Tian, and J. Yan, "Optimal power dispatch in wind farm based on reduced blade damage and generator losses," *Renew. Sustain. Energy Rev.*, vol. 44, pp. 64–77, Apr. 2015.
[71] "Download data about the Danish electricity system in 2020." [Online]. Available: http://www.energinet.dk/EN/El/Nyheder/Sider/Nu-kan-du-downloade-data-om-det-danske-elsystem-i-2020.aspx. [Accessed: 06-Apr-2017].
[72] Energinet.dk, "System Plan 2015：Electricity and Gas in Denmark," Nov. 2015.

SELECTED PUBLICATIONS

Publication **J1**

Paper title:

Steady-state analysis of the integrated natural gas and electric power system with bi-directional energy conversion

Publication outlet:

Applied Energy

List of authors:

Qing Zeng, Jiakun Fang, Jinghua Li, Zhe Chen

DOI: 10.1016/j.apenergy.2016.05.060
Copyright © 2017 Copyright Clearance Center, Inc. All Rights Reserved. Privacy statement. Terms and Conditions.

Applied Energy 184 (2016) 1483–1492

Contents lists available at ScienceDirect

Applied Energy

journal homepage: www.elsevier.com/locate/apenergy

Steady-state analysis of the integrated natural gas and electric power system with bi-directional energy conversion

Qing Zeng [a], Jiakun Fang [a,*], Jinghua Li [a,b], Zhe Chen [a]

[a] Department of Energy Technology, Aalborg University, Aalborg DK9220, Denmark
[b] School of Electrical Engineering, Guangxi University, Nanning 530004, China

HIGHLIGHTS

- The integrated gas and electrical system with bi-directional energy conversion is formulated.
- The unified unit system is proposed to enhance the computational efficiency.
- Numerical simulations are carried out to validate the proposed method.
- Transmission loss reduction and increasing renewable integration by P2G.

ARTICLE INFO

Article history:
Received 23 November 2015
Received in revised form 21 March 2016
Accepted 7 May 2016
Available online 18 May 2016

Keywords:
Natural gas system
Power system
Integrated gas and power system
Power to gas
Newton–Raphson method

ABSTRACT

Nowadays, the electric power system and natural gas network are becoming increasingly coupled and interdependent. A harmonized integration of natural gas and electricity network with bi-directional energy conversion is expected to accommodate high penetration levels of renewables in terms of system flexibility. This work focuses on the steady-state analysis of the integrated natural gas and electric power system with bi-directional energy conversion. A unified energy flow formulation is developed to describe the nodal balance and branch flow in both systems and it is solved with the Newton–Raphson method. Both the unification of units and the per-unit system are proposed to simplify the system description and to enhance the computation efficiency. The applicability of the proposed method is demonstrated by analyzing an IEEE-9 test system integrated with a 7-node natural gas network. Later, time series of wind power and power load are used to investigate the mitigation effect of the integrated energy system. At last, the effect of wind power and power demand on the output of Power to Gas (P2G) and gas-fired power generation (GPG) has also been investigated.

© 2016 Elsevier Ltd. All rights reserved.

1. Introduction

Due to the broad public attention of the climate change and fossil resource depletion, renewable sources such as wind and solar are developed rapidly in recent years. Taking Denmark for example, by the end of 2014, the wind power capacity in Denmark has reached 4855 MW. Furthermore, a long-term goal has been put forwarded by a political agreement in Denmark that a 100% renewable energy should be implemented in 2050 [1]. The design of the future 100% renewable energy systems has also been documented in general terms in [2,3]. Though the renewable has been developed in recent years with great potential, its intermittent and unpredictable nature raises the difficulty to balance the energy production and consumption [4]. Existing options to accommodate the renewables include: increasing deployment of the fast-ramping sources such as pumped hydro power plants [5] and electrical energy storages [6,7], coordinating wind and solar across wide spatial diversities [8], optimal managing the demands to meet the renewable generation profiles [9,10].

Natural gas is another environmentally-friendly energy source in accommodating the intermittent renewable energy. Firstly, natural gas-fired power generation (GPG) plays a critical role in peak regulation in the absence of hydropower, because it can respond rapidly to changes in demand and supply [11]. So the natural gas network becomes increasingly important for providing backup to the growing supplies of intermittent renewable energy. Secondly, the P2G technology provides an opportunity to convert surplus renewables to a gas fuel. It shows a big potential to store renewables in the natural gas network in large-scale and long duration way [12]. It works by using the surplus wind power or other renewable sources to produce gas fuel that can be stored in the

* Corresponding author.
E-mail address: jfa@et.aau.dk (J. Fang).

http://dx.doi.org/10.1016/j.apenergy.2016.05.060
0306-2619/© 2016 Elsevier Ltd. All rights reserved.

Nomenclature

Indices

s, d, g	supply, demand, generation
GPG, P2G, GC	gas-fired power generation, power to gas, gas compressor

Parameter

C	constant
CR	compression ratio
C_{GPG}	the proportional relationship of energy conversion from gas to power in GPG, $m^3/MW\,h$
C_{P2G}	the energy conversion from electricity to the natural gas in P2G system, $m^3/MW\,h$
C_{km}	the overall transmission coefficient for an individual pipeline, $(m^3/h)/kPa$
c_k	specific heat ratio for the natural gas
D_{km}, L_{km}	the inside diameter of pipe in meter, the pipe length in km
$E_{p,km}$	the pipeline efficiency, a decimal value no larger than 1.0
E_c	compressors parasitic efficiency, 0.99 for centrifugal units
f_{km}	the friction factor
G_{ij}, B_{ij}, Y	electrical conductance, electrical susceptance, line admittance matrix
G_k, $G_{s,k}$, $G_{d,k}$	the gas flow, the gas supply, the gas demand at node k, m^3/h
HR	the heat rate, MJ/MW h
J	Jacobian matrix of partial derivatives
K_{GC}	constant of compressor
LHV	lower heating value, MJ/m^3
p_b	gas pressure at base condition, kPa
$P_{g,i}$, $P_{d,i}$	the active power generated of bus i, the active power demand of bus i, MW
$Q_{g,i}$, $Q_{d,i}$	the reactive power generated of bus i, the reactive power demand of bus i, MVar
R_{km}	$R_{km} = 1/C_{km}^2$, the hydraulic resistance coefficient of the pipeline, $kPa^2/(m^3/h)^2$
$S_{s,k}$, $S_{d,k}$	gas supply and demand at node k, MW
T_s	suction temperature of compressor, R
T_b	gas temperature at base condition, K (273+ °C)
$T_{a,km}$	average absolute temperature of pipeline, K (273 +°C)
V, Y	bus voltage, nodal admittances matrix
Z_{km}	the resistance coefficient of the pipeline, $kPa^2/(MW)^2$
Z_a	average compressibility factor
γ_G	the natural gas specific gravity, dimensionless
η_c, η_{GPG}, η_{P2G}	compression efficiency, the energy efficiency of GPG, the energy efficiency of P2G

Variables

BHP_{km}	brake horsepower consumed by the gas compressor, horsepower
$G_{d,GPG}$, $G_{s,P2G}$	gas consumption in GPG, gas generation in P2G, m^3/h
$P_{d,P2G}$, $P_{GC,km}$, $P_{g,GPG}$	power consumed by P2G system, by gas compressor, power generated by GPG, MW
$G_{gas,km}$	standard gas flow rate in the pipeline, measured at base temperature and pressure, m^3/h
$G_{GC,km}$	natural gas flow in the compressor, m^3/h
p_m, p_k	the Nodal gas pressure at both ends of the pipeline, kPa
Π_k, Π_m	$\Pi_k = p_k^2$, $\Pi_m = p_m^2$, kPa^2
$S_{gas,km}$	gas flow rate in the pipeline from the node k to m, measured in MW
$S_{d,GPG}$, $S_{g,P2G}$	gas consumption in GPG, gas generation in P2G, MW
$\|V\|$, θ	magnitude of voltage, angle of voltage

existing natural gas networks, and the stored energy can then be injected back into electricity system through GPG when needed. Thus, the electric power system and natural gas network are becoming increasingly coupled and interdependent. The extensive development and application of GPG and P2G will significantly enhance the interaction between the gas and electrical systems.

While extensive studies have been conducted in natural gas and electric power systems individually, a coordinated analysis of the integrated gas and electric power system is still insufficient [13]. The state of the art reviews on the integrated natural gas and power system can be found in [14,15]. Literatures on this topic can be classified into two general perspectives: the economic perspective and the technical perspective. The economic or market perspective mainly aims at the interaction of the pricing mechanisms between different systems [16,17]. Building a feasible economic model is an important step in economic assessment. However, the influence of the technical constraints is often overlooked or given in a simplified way. For example, the network constraints are often neglected in such studies. The technical perspective focuses on the secure and efficient operation and planning of the integrated energy systems [15]. Different approaches have been proposed in terms of the time horizon. A multi-time period combined gas and electricity network optimization model was developed in [18], which takes into account the varying nature of gas flows, network support facilities. Qiu et al. [19] proposed a multi-stage co-planning model to identify the optimal co-expansion plan in the integrated energy systems. The reliability is another important issue of the integrated energy systems [20]. It aims at analyzing the interdependence of the integrated electricity and gas system under abnormal conditions, such as cascading failures propagating from one system to another [21].

In these studies mentioned above, the GPG has been widely considered as the single-directional linkage between the natural gas and electricity networks. However, P2G, which enables bi-directional energy conversion, has only recently appeared in the investigation of the integrated natural gas and electric power system. Qadrdan et al. [22] investigated the impacts and benefits of employing P2G in the integrated operation of the electricity and gas networks. It showed that the introduction of P2G not only reduced the wind curtailment but also improved the optimal dispatch for electricity and gas. To further analyze the steady state energy flow in the integrated energy system with bi-directional energy conversion, a comprehensive method is needed including both P2G and GPG. The main objective of this paper is to provide a unified formulation for the steady state analysis of the integrated energy system with bi-directional energy conversion. A set of nonlinear equations representing the gas and power systems are obtained based on the nodal balance of the gas and power flows, respectively. The integrated formulation of the natural gas and electric power system is obtained by combining the stated flow models through links of the gas compressor, P2G and gas-fired power plants. A case study has been conducted to demonstrate the feasibility of the proposed approach on the IEEE-9 test system connected with a 7-node natural gas network. The effect of the fluctuant power supply and power demand on the integrated natural gas and electric power system has been studied with historical

data. The effect of wind power and power demand on the output of the GPG and P2G has also been investigated. The major contributions of this work are:

- A harmonized integration of natural gas and electric power system with bi-directional energy conversion is formulated, including the gas compressors, the power-to-gas and the gas-fired power plants.
- Both the unification of units and the per-unit system are proposed to simplify the system description and to enhance the computational efficiency.
- Numerical simulations are carried out to validate and demonstrate the feasibility, efficiency and accuracy of the proposed method and results are analyzed.

The remainder of the paper is organized as follows: Section 2 introduces the formulation of the integrated gas and power system; Section 3 presents a unified gas and power flow solution for analyzing the steady-state energy distribution; Section 4 illustrates a verification of the unified solution for the integrated system; Finally, case studies are described in Section 5, and the conclusion is provided in Section 6.

2. Modeling of the integrated gas and power system

2.1. Power flow in the electric power system

Power flow studies are of great importance in planning and operation of power systems. The goal of a power-flow study is to obtain voltage angle and magnitude information for each bus in a power system for specified load and generator power and voltage conditions [23]. The problem can be formulated as follows. The bus voltage V and nodal admittances matrix Y of the system are given in polar coordinates by

$$V_i = |V_i|\angle\theta_i = |V_i|(\cos\theta_i + j\sin\theta_i) \tag{1}$$

$$Y_{ij} = |Y_{ij}|\angle\theta_{ij} = |Y_{ij}|(\cos\theta_{ij} + j\sin\theta_{ij}) = G_{ij} + jB_{ij} \tag{2}$$

Then the real power and reactive power injection at different buses are given by

$$P_i = |V_i|\sum_{j=1}^{N}|V_j|(G_{ij}\cos\theta_{ij} + B_{ij}\sin\theta_{ij}) \tag{3}$$

$$Q_i = |V_i|\sum_{j=1}^{N}|V_j|(G_{ij}\sin\theta_{ij} - B_{ij}\cos\theta_{ij}) \tag{4}$$

where $\theta_{ij} = \theta_i - \theta_j$. Eqs. (3) and (4) constitute the polar form of the power flow equations. The net active power P_i and reactive power Q_i entering bus i are calculated. Let $P_{g,i}$ and $P_{d,i}$ denote the power generation and consumption at bus i. Then the nodal power balance equations are given as

$$\Delta P_i = P_{g,i} - P_{d,i} - |V_i|\sum_{j=1}^{N}|V_j|(G_{ij}\cos\theta_{ij} + B_{ij}\sin\theta_{ij}) \tag{5}$$

$$\Delta Q_i = Q_{g,i} - Q_{d,i} - |V_i|\sum_{j=1}^{N}|V_j|(G_{ij}\sin\theta_{ij} - B_{ij}\cos\theta_{ij}) \tag{6}$$

2.2. Wind power output

For each wind-power unit, the active power for a variable speed wind turbine ($P_{g,var}$) is calculated based on [24]

$$P_{g,var}(v) = \begin{cases} 0 & \text{if } v < V_{ci} \text{ or } v > V_{co} \\ a + bv^3 & \text{if } V_{ci} \leqslant v \leqslant V_r \\ P_r & \text{if } V_r \leqslant v \leqslant V_{co} \end{cases} \tag{7}$$

where $P_{g,var}(v)$ is the wind power for a variable speed wind turbine at wind speed v. P_r is the rated power output of the wind-power unit., V_{ci}, V_r and V_{co} are the cut-in, rated and cut-out wind speeds, respectively. The coefficient a is the bias value, and b is the gradient value.

2.3. Gas flow in the natural gas system

The steady-state modelling of the natural gas system is formulated by the gas flow equations, compression power calculation and nodal mass balance. In this work, the elevation deviation in the gas pipelines is neglected. Besides, the assumption of isothermal flow is good enough for most practical purposes, since the gas temperature reaches constant values in long transmission lines [25]. Therefore, the temperature deviation in the gas pipelines is neglected in this work. We concentrate on the steady-state isothermal flow of gas in pipelines. With these assumptions, the flow equations and nodal balance equations can be formulated as follows.

2.3.1. Pipeline flow equation

For the steady-state isothermal flow in a gas pipeline, the flow rate is related to the pressure drop. Based on the assumptions that there is no elevation change in the pipeline, and the condition of flow is isothermal [25], the pipeline flow equation is expressed by

$$G_{gas,km} = C\left(\frac{T_b}{p_b}\right)D_{km}^{2.5}\left(\frac{p_k^2 - p_m^2}{L_{km}\gamma_G T_{a,km} Z_a f_{km}}\right)^{0.5} E_{p,km} \tag{8}$$

In the flow equation, the friction factor f_{km} is determined by different formulas based on different flow regimes. Note that in high-pressure gas transmission pipelines with high flow rates, only two types of flow regimes are observed: partially turbulent flow and fully turbulent flow [26]. Under this situation, f_{km} is given in SI units as

$$f_{km} = \frac{0.009407}{\sqrt[3]{D_{km}}} \tag{9}$$

where the friction factor f_{km} is determined only by the pipe diameter as mentioned above.

The physical characteristics of each pipeline with fixed gas composition in Eq. (8) can be summarized by a single constant C_{km} [27]:

$$C_{km} = C\left(\frac{T_b}{p_b}\right)D_{km}^{2.5}\left(\frac{1}{L_{km}\gamma_G T_{a,km} Z_a f_{km}}\right)^{0.5} E_{p,km} \tag{10}$$

And then a more compact form of Eq. (8) depicting the gas flow from node k to m can be given as

$$\Pi_k - \Pi_m = R_{km} G_{gas,km}^2 \tag{11}$$

where $\Pi_k = p_k^2$, $\Pi_m = p_m^2$ and $R_{km} = 1/C_{km}^2$, R_{km} represents the hydraulic resistance coefficient of the pipeline whose meaning is similar to the line impedance of the power system.

2.3.2. Compression power calculation

The brake horsepower of the gas compressor is related to the compression ratio (CR) and gas flow rate from the compressor. Compression ratio (CR) is the ratio of absolute discharge pressure to the absolute suction pressure [28].

$$CR = \frac{p_m}{p_k} = \left(\frac{\Pi_m}{\Pi_k}\right)^{0.5} \tag{12}$$

$$\mathrm{BHP}_{km} = K_{GC} Z_a G_{GC,km} \left[\frac{T_s}{E_c \eta_c}\right] \left[\frac{c_k}{c_k - 1}\right] \left[\left(\frac{p_m}{p_k}\right)^{\frac{c_k - 1}{c_k}} - 1\right] \tag{13}$$

$$\mathrm{BHP}_{km} = K_{GC} Z_a G_{GC,km} \left[\frac{T_s}{E_c \eta_c}\right] \left[\frac{c_k}{c_k - 1}\right] \left[\left(\frac{\Pi_m}{\Pi_k}\right)^{\frac{c_k - 1}{2c_k}} - 1\right] \tag{14}$$

where K_{GC} is a constant, the value depends on the units of the $G_{GC,km}$ in the equation, for MMscfd, the value of K_{GC} is 0.0854; It should be mentioned that 1 MMscfd of gas flow at 15 °C equals 1177 m^3/h in flow rate. So the value of K_{GC} is 7.26×10^{-5} if the unit of $G_{GC,km}$ is given as m^3/h.

2.3.3. Nodal gas balance equation

The nodal gas balance equations simply indicate that the sum of the inflows and outflows at the node should be zero:

$$G_{s,k} - G_{d,k} - \sum_{m \in k} G_{gas,km} = 0 \tag{15}$$

Considering a natural gas network consisting of N nodes and M branches, a reference node is pre-set with given nodal pressure. The unknown variables include $(N-1)$ nodal pressures and M pipeline flow rates.

2.4. Integrated natural gas and power flow formulation

The energy conversion between the gas and electric power system primarily takes place in the GPG units and P2G.

2.4.1. Gas-fired power generation

For the Gas-fired power generation, heat rate (HR) is a term used to indicate the power plant efficiency, which is the ratio of heat given up by the natural gas, regarding its lower heating value (LHV), to the power available at the GPG [29]. It has the SI unit of MJ/MW h. Therefore, a lower heat rate gives higher energy efficiency. And the relationship between the heat rate and efficiency can be found in [30] as

$$\eta_{GPG} = \frac{3600}{HR} \tag{16}$$

The relationship between the power generation and the natural gas network is mathematically formulated by the heat rate curve,

$$HR = \alpha + \beta P_{g,GPG} + \gamma P_{g,GPG}^2 \tag{17}$$

where the coefficients α, β, γ define the efficiency in this energy conversion process.

Then the gas consumption, $G_{d,GPG}$ (m^3/h), can be calculated approximately from

$$G_{d,GPG} = \frac{HR \cdot P_{g,GPG}}{\mathrm{LHV}} \tag{18}$$

The gas flow required for the energy demanded can also be computed by the following equation if the power plant efficiency is known.

$$G_{d,GPG} = \left(\frac{3600}{\eta_{GPG} \mathrm{LHV}}\right) P_{g,GPG} \tag{19}$$

where LHV represents the lower heating value of the natural gas, the value is from 35.40 to 39.12 MJ/m^3 [31]. An average value of 37.26 MJ/m^3 is used in this paper.

2.4.2. Power to gas

Power to gas (P2G) system can produce hydrogen, and the produced hydrogen can also be injected into the gas network. But the amount of hydrogen to be fed into the gas system is limited since there are still many impacts and uncertainties on injecting hydrogen into the gas system. Firstly, blending hydrogen into natural gas pipeline reduces the thermal energy due to the lower energy density of the hydrogen gas. Secondly, blending hydrogen gas gives bad effects on pipe material including embrittlement, which decreases material strength. Thirdly, the leakage rate of hydrogen is greater than methane since hydrogen is a much smaller molecule, a large leakage of hydrogen may also cause economic and safety concerns [32]. Besides, blending hydrogen in gas network gives adverse effects on the gas appliance, such as burners, boilers or gas engines. Therefore, there are still many mandatory restrictions for injecting hydrogen into gas network. For example, the maximum level of hydrogen content that is allowed in the UK is 0.1% (by volume) [22]. Considering the main composition of natural gas is methane, the target product of P2G is methane in this paper. Thus, the production chain of P2G consists of two steps: electrolysis and methanation. Electrolysis is a process of using electricity to split water into hydrogen and oxygen. The chemical reaction [33] in the electrolyzer is elaborated by

$$2H_2O(l) \leftrightarrow 2H_2(g) + O_2(g) \quad \Delta H = +571.6\ \mathrm{kJ} \tag{20}$$

Methanation is the synthesis of hydrogen and carbon dioxide to methane. This process is based on the Sabatier reaction

$$CO_2(g) + 2H_2(g) \leftrightarrow CH_4(g) + O_2(g) \quad \Delta H = +318.7\ \mathrm{kJ} \tag{21}$$

The methane is then compressed, metered and injected into the natural gas system. Combine both of the reaction (20) and (21), an overall reaction P2G can be given as

$$CO_2(g) + 2H_2O(l) \leftrightarrow CH_4(g) + 2O_2(g) \quad \Delta H = +890.3\ \mathrm{kJ} \tag{22}$$

From the overall Eq. (22), theoretically, with every 890.3 kJ of energy consumed, 1 mol of CO_2 can be turned into 1 mol of methane. In practice, the energy conversion efficiency (η_{P2G}) should also be considered. In this work, η_{P2G} is defined as the ratio of the absorbed energy density by the produced gas to the power consumed by P2G, per unit volume of gas produced. The same as GPG, the energy density of natural gas is given regarding its lower heating value (LHV). Thereby the energy conversion relationship between the gas generation rate $G_{s,P2G}$ and the consumed power $P_{d,P2G}$ can be given as

$$\eta_{P2G} = \frac{(G_{s,P2G}/3600) \cdot \mathrm{LHV}}{P_{d,P2G}} \times 100\% \tag{23}$$

where $G_{s,P2G}$ is gas generation rate of the P2G system, m^3/h, which can be calculated from

$$G_{s,P2G} = \left(\frac{3600 \eta_{P2G}}{\mathrm{LHV}}\right) \times P_{d,P2G} \tag{24}$$

The physical characteristics of each P2G system in Eq. (24) can be expressed by a single constant C_{P2G} given by

$$C_{P2G} = \frac{3600 \eta_{P2G}}{\mathrm{LHV}} \tag{25}$$

This leads to a simpler equation for the P2G system,

$$G_{s,P2G} = C_{P2G} P_{d,P2G} \tag{26}$$

where C_{P2G} denotes the energy conversion from electricity to the natural gas in P2G system, the value of C_{P2G} is in proportion to the energy efficiency of the P2G system.

This is a simplified model for showing the relationship between the amount of used electricity and the amount of gas production in P2G. In this model, the amount of used electricity is determined by the amount of gas production and the efficiency of the P2G system, which is similar to the model in [22].

3. A unified gas and power flow solution

The integrated natural gas and electric power system is composed of a gas network and a power grid. The formulation of the integrated natural gas and electricity infrastructures is obtained by combining the stated flow models. The bi-directional energy flow is formed by considering the links between both infrastructures via the gas compressor, GPG and P2G. For simplification of analysis, the unit of the gas flow rate is converted to power unit as MW and then per-unit conversion is carried out in the integrated system. Finally, a unified modelling and solution framework is described to solve the coupled gas and power flow equations.

3.1. Unification of units and the per-unit system

The integrated gas and power system is composed of a gas network and a power system. For simplification of analysis in the integrated energy system, the unit of the gas flow rate is converted to power unit as MW by introducing the energy density of natural gas. For natural gases, the energy density is its lower heating value (LHV) in MJ/m^3. Thus, the novel gas flow rate (S_{gas}) can be calculated by

$$S_{\text{gas}} = \frac{G_{\text{gas}} \times \text{LHV}}{3600} \tag{27}$$

where S_{gas} is the converted form of gas flow rate in MW.

Thus, Eq. (11) can be rewritten as

$$\Pi_k - \Pi_m = Z_{km} S_{\text{gas},km}^2 \tag{28}$$

where Z_{km} in kPa^2/(MW)^2 represents the resistance coefficient of the pipeline whose meaning is similar to the line impedance of the power system.

Accordingly, Eqs. (15), (19) and (24) can be rewritten as the following equations.

$$\Delta S_k = S_{s,k} - S_{d,k} - \sum_{m \in k} S_{\text{gas},km} \tag{29}$$

$$S_{d,\text{GPG}} = \frac{P_{g,\text{GPG}}}{\eta_{\text{GPG}}} \tag{30}$$

$$S_{g,\text{P2G}} = \eta_{\text{P2G}} P_{d,\text{P2G}} \tag{31}$$

The unit of BHP is also converted to the power unit (MW), it is known that one horsepower equals to 745.7 Watts. Thus, the converted form of power consumption in compressor can be given as

$$P_{\text{GC},km} = 745.7 \times 10^{-6} \times \text{BHP}_{km} \tag{32}$$

$$P_{\text{GC},km} = K'_{\text{GC}} Z_a S_{\text{gas},km} \left[\frac{T_s}{E_c \eta_c}\right] \left[\frac{c_k}{c_k - 1}\right] \left[\left(\frac{\Pi_m}{\Pi_k}\right)^{\frac{c_k - 1}{2c_k}} - 1\right] \tag{33}$$

where K'_{GC} is a constant, the value depends on the units of the $S_{\text{gas},km}$ in the equation. If the unit of $S_{\text{gas},km}$ is given as MW, and the energy density of natural gas is set as 37.26 MJ/m^3, the value of K'_{GC} is 5.23×10^{-6}.

Thereby, both of gas flow and power flow are measured by MW in this paper.

Furthermore, for simplicity, a per-unit system is applied to describe the integrated gas and power system which is widely adopted in the power systems analysis. In this paper, we consider that the base value of voltage is 110 kV, the base value of gas pressure is 1 MPa and the base value of power is 100 MW. Then the rest of the units can be derived from the independent based values. Finally, all the related coefficients are adjusted to meet the per-unit system accordingly.

3.2. Unified gas and power flow solution

In order to analyze the steady state energy distribution in the integrated energy system, the integrated energy flow is formed by gathering the stated flow models of both natural gas and electric power system. A set of nonlinear equations representing the gas and power systems are obtained based on the nodal balance of gas and power flows, respectively.

$$\Delta P_i = P_{g,i} - P_{d,i} - |V_i| \sum_{j=1}^{N} |V_j| (G_{ij} \cos\theta_{ij} + B_{ij} \sin\theta_{ij}) \tag{5}$$

$$\Delta Q_i = Q_{g,i} - Q_{d,i} - |V_i| \sum_{j=1}^{N} |V_j| (G_{ij} \sin\theta_{ij} - B_{ij} \cos\theta_{ij}) \tag{6}$$

$$\Delta\Pi_{km} = \Pi_k - \Pi_m - Z_{km} S_{\text{gas},km}^2 \tag{34}$$

$$\Delta S_k = S_{k,s} - S_{k,d} - \sum_{m \in k} S_{\text{gas},km} \tag{35}$$

$$\Delta P_{\text{GC}} = P_{\text{GC}} - K'_{\text{GC}} Z_a S_{\text{gas},km} \left[\frac{T_s}{E_c \eta_c}\right] \left[\frac{c_k}{c_k - 1}\right] \left[\left(\frac{\Pi_m}{\Pi_k}\right)^{\frac{c_k - 1}{2c_k}} - 1\right] \tag{36}$$

The Newton–Raphson method is popular for solving the nonlinear equations. Concretely, consider a point X close to the exact solution, the linearization of all the nonlinear equations at X can be given by the Taylor series expansion [34] as

$$F(X) = -J \times \Delta X \tag{37}$$

The above equation forms the basis for the iterative procedure to calculate the solution. Where X represents all the unknown variables and $F(X)$ represents all of the mismatches, thus

$$X = [\,\theta \quad |V| \quad P_{\text{GPG}} \quad P_{\text{P2G}} \quad P_{\text{GC}} \quad \Pi \quad S_{\text{gas}}\,]^{\text{T}} \tag{38}$$

$$F(X) = [\,\Delta P \quad \Delta Q \quad \Delta\Pi \quad \Delta S \quad \Delta P_{\text{GC}}]^{\text{T}} \tag{39}$$

and J is a Jacobian matrix of partial derivatives which is given by

$$J = \begin{bmatrix} \frac{\partial\Delta P}{\partial\theta} & \frac{\partial\Delta P}{\partial|V|} & \frac{\partial\Delta P}{\partial P_{\text{GPG}}} & \frac{\partial\Delta P}{\partial P_{\text{P2G}}} & \frac{\partial\Delta P}{\partial P_{\text{GC}}} & 0 & 0 \\ \frac{\partial\Delta Q}{\partial\theta} & \frac{\partial\Delta Q}{\partial|V|} & 0 & 0 & 0 & 0 & 0 \\ 0 & 0 & 0 & 0 & 0 & \frac{\partial\Delta\Pi}{\partial\Pi} & \frac{\partial\Delta\Pi}{\partial S_{\text{gas}}} \\ 0 & 0 & \frac{\partial\Delta S}{\partial P_{\text{GPG}}} & \frac{\partial\Delta S}{\partial P_{\text{P2G}}} & \frac{\partial\Delta S}{\partial P_{\text{GC}}} & \frac{\partial\Delta S}{\partial\Pi} & \frac{\partial\Delta S}{\partial S_{\text{gas}}} \\ 0 & 0 & 0 & 0 & \frac{\partial\Delta P_{\text{GC}}}{\partial P_{\text{GC}}} & \frac{\partial\Delta P_{\text{GC}}}{\partial\Pi} & \frac{\partial\Delta P_{\text{GC}}}{\partial S_{\text{gas}}} \end{bmatrix} \tag{40}$$

According to the practical operation situation of the power system and gas network, every parameter has an available solution domain that provides a setting range of the initial values. In the available solution domain, the convergence of Newton–Raphson method has been verified in this work by comparing various calculation results under differing initial iterative values.

4. Numerical verification of the unified solution

In this section, we establish several cases to verify our proposed unified modelling and solution. The convergence of Newton–Raphson method has been verified in this work by comparing various calculation results under differing initial iterative values. The simulation results are summarized in Tables 1–4.

Cases for comparison: (1) In Case 1, the unit of the gas network has not been converted to the power unit, we consider that the unit of gas flow rate is m^3/h and the unit of gas pressure is kPa; the unit for voltage is kV, and the unit of power is MW. (2) Case 2 is a per-unit system, the unit of the gas flow rate is converted to power unit

Table 1
The nodal parameters of natural gas network.

No.	Case 1			Case 2		
	Gas supply (m^3/h)	Gas demand (m^3/h)	Gas pressure (kPa)	Gas supply (p.u.)	Gas demand (p.u.)	Gas pressure (p.u.)
1	60,000	12012.09	969.98	6.210	1.243	0.97
2	0	10,000	500	0	1.035	0.50
3	0	12,000	438.63	0	1.242	0.44
4	10012.1	0	1000	1.036	0	1
5	0	20,000	860.69	0	2.070	0.86
6	0	16,000	814.86	0	1.656	0.81
7	0	0	1000	0	0	1

as MW. Furthermore, in the per-unit system, the base value of voltage is 110 kV, the base value of gas pressure is 1 MPa, and the base value of power is 100 MW.

4.1. The structure of the integrated gas and electricity system

An IEEE-9 test system combined with a 7-node natural gas network is applied to illustrate the proposed approach as shown in Fig. 1. The 7-node gas network is not a real gas network, but a simplified version of a gas system. It is composed of six pipelines and seven nodes. The node of N7 is connected with gas storage which is considered the reference node where the nodal pressure is specified as 1 MPa shown in Table 1. Its parameters are taken from the real gas system as shown in Table 2. On the other hand, the electricity infrastructure has three generators at B1, B2 and B3, and has three load buses at B5, B6 and B8. B1 is defined as a gas-fired generator that is connected to N1. B2 and B3 are set as a wind farm and a coal-fired power plant, respectively. Finally, there are three links between the 7-nodes gas network and IEEE-9 system, which are gas-fired generator, gas compressor and P2G. There are four kinds of parameters in this integrated system: the pipeline's hydraulic resistance coefficient given in Table 2; the impedance of the transmission lines in electricity system; the energy efficiency of GPG which is given as 0.8 in this case study; the last one is the energy efficiency of P2G, which is expected in the region of 55–80% [35]. In this study, the energy efficiency of P2G is set as 0.8.

4.2. Initialization and comparison

Newton–Raphson method begins with initial guesses of all unknown variables (such as voltage magnitudes and angles at load buses and voltage angles at generator buses, nodal pressures at the gas network, and pipeline flow rates). It is common to use a "flat start" in which all pipeline flow rates, nodal pressures and voltage angles are set to zero. The initial guesses of the unknown voltage magnitudes are set as 1. The pre-set tolerance is 10^{-10}. The detailed simulation results are summarized in Tables 1–4.

Table 1 summarizes the results for the natural gas network associated with the natural gas source, gas demanded by the gas-fired plant, gas supplied by P2G, as well as the nodal pressures. Table 2 summarizes the pipeline's parameters and gas flow rates. The data of electric network are summarized in Table 3, which includes active power supplies, active power demands, voltage magnitudes, as well as voltage phase angles. The comparison results indicate that the calculation of the unified solution in Case 2 agreed well with that in Case 1. Thus, the testing results prove that this unified solution with the per-unit system is feasible and sufficiently accurate.

Furthermore, Table 4 gives the comparison of calculation results in terms of power loss (*PL*), energy loss (*EL*) and power consumption in the gas compressor (BHP or P_{GC}) under differing initial iterative values. It shows that all the calculations can converge to a stable value even though the initial value of all the unknown voltage magnitude $|V_i|$ vary from 1 to 4. This illustrates that the Newton–Raphson method has good convergence when used in the integrated gas and power system. Further, the iteration in Case 2 is faster than the iteration in Case 1 as shown in Table 4. This indicates that the unified solution with the per-unit system has a better computational efficiency. It also helps to extend this method to the real-word implementations.

5. Numerical simulations

5.1. The mitigation effect of the integrated natural gas and electricity system

5.1.1. The mismatch of wind power and power demand

In order to investigate the impact of the fluctuant power supply and demand on the integrated natural gas and electricity system, a stochastic data of wind power and power demand is injected into the electric network. The data of wind power and power demand is obtained from Energinet.dk, the power transmission system operator in Denmark. These data measured with a time interval of one hour. The data in the first two weeks of January 2014 is adopted in this study. Fig. 2 shows the time series of the wind power and power load. It shows that the overall power demand is usually lower during the night hours while the wind blows. And there are peak demands in the morning and later in the evening. Compared with the electricity demand, the output of wind power is more unpredictable and intermittent. It shows that sometimes the fluctuation of wind power has a reverse trend to electricity

Table 2
The branch parameters of natural gas network.

Branch	From	To	Case 1		Case 2	
			R_{km}(kPa^2/(m^3/h)^2)	G_{km}(m^3/h)	Z_{km}(p.u.)	S_{km}(p.u.)
1	6	1	0.0003	47987.9	0.0280	4.967
2	1	2	0.0004	12,000	0.0373	1.242
3	2	3	0	25987.9	0.0000	2.689
4	4	3	0.00025	0	0.0233	0
5	5	4	0.0002	36,000	0.0187	3.726
6	6	5	0.0003	16,000	0.0280	1.656

Table 3
The electric parameters of power system.

Bus	Case 1				Case 2			
	$\|V_i\|$(kV)	$\theta_i(rad)$	P_g(MW)	P_d(MW)	$\|V_i\|$(p.u.)	θ_i(p.u.)	P_g(p.u.)	P_d(p.u.)
1	112.97	−0.054	99.5	0	1.027	−0.054	0.995	0
2	109.89	−0.112	90	0	0.999	−0.112	0.9	0.000
3	111.32	−0.075	160	0.6	1.012	−0.075	1.6	0.006
4	112.75	−0.031	0	0	1.025	−0.031	0	0
5	111.32	−0.056	0	125	1.012	−0.056	0	1.250
6	113.41	0.033	0	90	1.031	0.033	0	0.900
7	112.75	0.022	0	129.5	1.025	0.022	0	1.295
8	112.75	0.121	0	0	1.025	0.121	0	0.000
9	114.4	0.000	0	0	1.040	0.000	0	0.000

Table 4
The comparison of calculation results under differing initial iterative values.

Case 1					Case 2				
Initial values of all $\|V_i\|$(kV)	Iterations (times)	*PL* (MW)	BHP (Horsepower)	*EL* (MW)	Initial values of all $\|V_i\|$(p.u.)	Iterations (Times)	*PL* (p.u.)	P_{GC} (p.u.)	*EL* (p.u.)
110	11	4.33	847.1	55.64	1	6	0.043	0.0064	0.556
220	12	4.33	847.1	55.64	2	8	0.043	0.0064	0.556
330	16	4.33	847.1	55.64	3	9	0.043	0.0064	0.556
440	14	4.33	847.1	55.64	4	10	0.043	0.0064	0.556

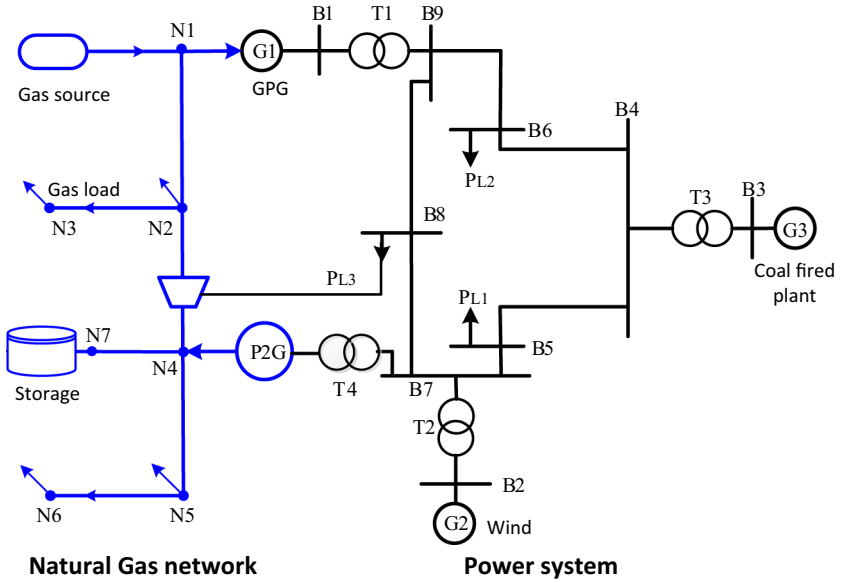

Fig. 1. Structure of an integrated gas and electricity system.

demand. Thus, a backup capacity such as GPG is required to provide peak regulation, while a large scale storage technology such as P2G is increasingly needed to store the surplus wind power to accommodate the growing supplies of intermittent renewable energy.

5.1.2. The mitigation effect of using P2G in the integrated system

In order to investigate the mitigation effect of using P2G in the integrated natural gas and electric power system, the comparison of the integrated energy system with P2G and without P2G is carried out in the context of power loss, power consumption in the gas compressor and the total energy loss as shown in Figs. 3–5. The total energy loss is defined as the difference between the total energy supply in the integrated system and the total energy demand. Similar to voltage in the power system, the nodal gas pressure is a vital factor for the security operation of the gas network, the effect of P2G on the nodal gas pressure is another issue investigated as shown in Fig. 6.

The stochastic wind power is injected into the electric power system through B2, and the time-series of power load is distributed to B5 and B6 in the power system. The gas demand in the gas network is also set as a time series which is obtained from Energinet.dk. It should be noted that the gas injection from the gas source is generally assumed to be a flat profile which means it is a constant injection rate. We set the gas injection rate from the gas source as 4 p.u. in this study. Thereby the fluctuation of the gas demand will be balanced by the linepack of the gas network. To be specific, the change of gas load will result in linepack variation. Especially, in the peak hour, the increased gas demand from GPG will lead to a rapid linepack reduction, which brings a great challenge to the linepack maintenance. Thus, a sufficient linepack is critical for the reliability of gas supply. The effect of using P2G on the variation of linepack is shown in Fig. 7.

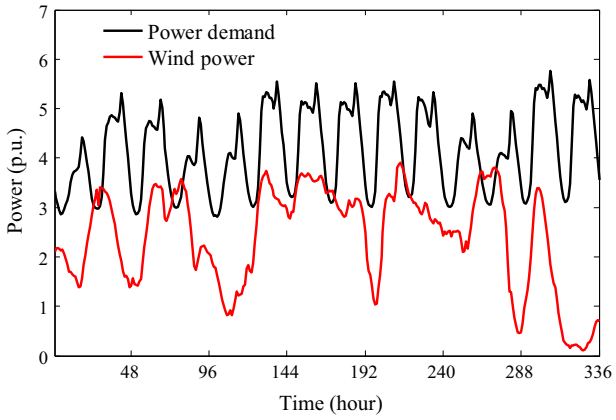

Fig. 2. The fluctuation of wind power and power demand.

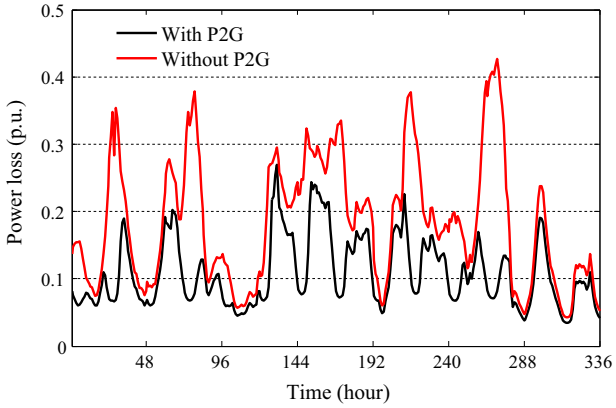

Fig. 3. Comparing the power loss in the integrated system with P2G versus without P2G.

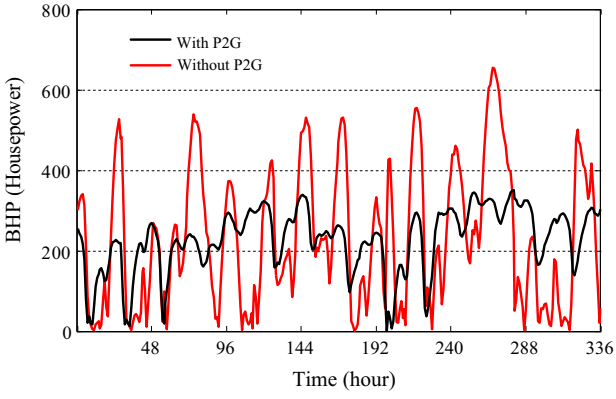

Fig. 4. Comparing the brake horsepower in the integrated system with P2G versus without P2G.

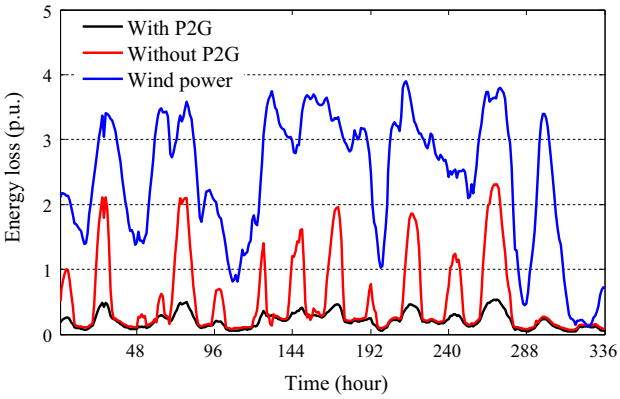

Fig. 5. Comparing the total energy loss in the integrated system with P2G versus without P2G.

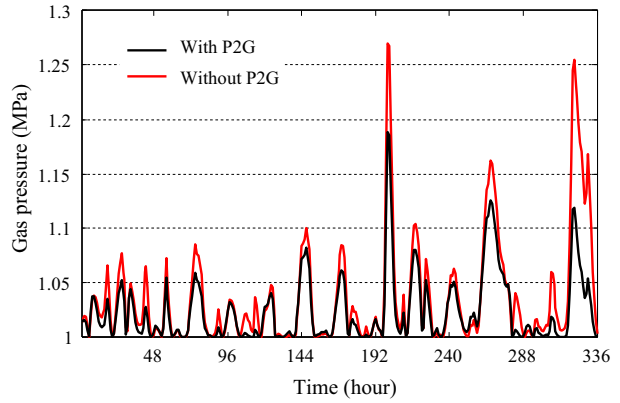

Fig. 6. Comparing the fluctuation of the nodal gas pressure in the integrated system with P2G versus without P2G.

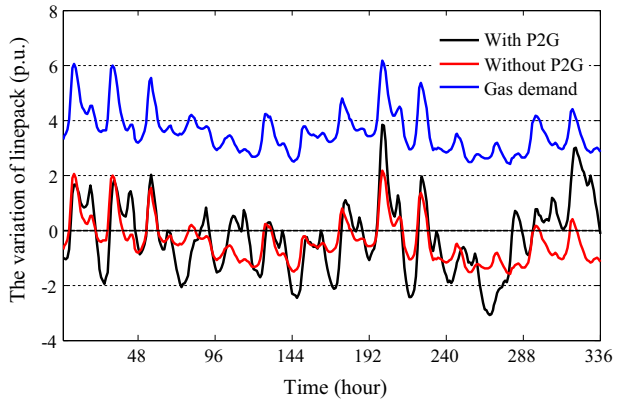

Fig. 7. Comparing the variation of linepack in the integrated system with P2G versus without P2G.

The power loss in the power system is illustrated in Fig. 3. It shows that power loss can be reduced by the integration of P2G in the coupled natural gas and power system. Without P2G, the power loss fluctuates significantly from 0.05 p.u. to 0.43 p.u. The total power loss accounts for 5.6% of the total power demand. While, in the integrated systems with P2G, the power loss is reduced, it just fluctuates between 0.04 and 0.28 p.u. Within the given time horizon, 27.5% total power loss is reduced by using P2G. The reason is that the P2G, located at B7, can help with the local balance of the wind power. Part of the surplus wind power produced at B2 can be consumed by P2G at B7 so that it would not need to transmit long distances to other buses such as B6. Thus, from the perspective of reducing power loss, it is preferred to locate P2G near a wind farm.

Similar to the power system, there is energy loss in the transmission of natural gas. The transmission loss in the natural gas network is mainly consumed by the gas compressor. Fig. 4 shows the brake horsepower (BHP) in the gas compressor. Compared with the integrated system without P2G, the BHP fluctuation is dampened when P2G is introduced to the integrated energy system. Without P2G, the BHP fluctuates significantly from 0 to 660 horsepower.

Whereas in the integrated systems with P2G, the BHP is decreased, it just fluctuates between 0 and 340 horsepower. As some gas fuel can be produced by P2G and then injected into the gas network from N4, the local gas consumption can be balanced by gas supplies from P2G, which helps to reduce the natural gas flow in the compressor. From Eq. (13), it is seen that BHP is proportional to the gas flow rate in the compressor. That's why P2G has mitigation effect on the BHP.

Fig. 5 shows the comparison of the total energy loss that is defined as the difference between the total energy generation in the integrated system and the total energy demand. It should be mentioned that the wind generation is taken into account. It is seen that when there is a lower penetration level of wind power, there is not much difference in the total energy loss between the integrated systems with P2G and without P2G. But the difference increases with the penetration level of wind power. The reason is that without P2G, surplus wind power is curtailed when there is a high penetration level of wind power but low power demand. Whereas, as a part of surplus wind power can be converted to gas fuel by using P2G, the wind curtailment is decreased, and the total energy loss can also be reduced. Further analysis shows that the total energy loss in the given horizon is reduced 62 percent by using P2G if the wind curtailment is regarded as a part of the total energy loss.

The effect of using P2G on the natural gas network is another issue of concern. The simulation results of the nodal gas pressure at N4 and the linepack of the gas network are illustrated in Figs. 6 and 7, respectively.

Just like the voltage stability, which is an important factor on the reliability of electric power system, the nodal gas pressure is a vital factor for the security operation of the gas network. Fig. 6 shows the fluctuation of the gas pressure at N4. It can be seen that the gas pressure fluctuation is dampened when P2G is introduced to the integrated gas and power system. In this figure, the gas pressure fluctuates within a range of 1–1.27 MPa if the integrated system is operated without P2G. When the integrated system is operated with P2G, it is limited in a narrower range between 1 MPa and 1.18 MPa. This indicates that the integrated gas and electricity system with GPG and P2G has more flexibility to help accommodate the fluctuation of the power system. It can preserve high stabilization in the gas network when a sufficient linepack is considered in the operational process.

It should be noted that the gas injection from the gas source are assumed to be flat which means the gas supply is at a constant rate. So linepack plays an important role in providing flexibility to meet the load fluctuation. When the gas demand exceeds gas supply, it is consumed. When there is more gas injection than gas demand, it is replenished. Fig. 7 shows the variation of linepack. It should be mentioned that the linepack is consumed when the variation value is positive, and the linepack is replenished when the variation value is a minus. It can be seen that the variation of linepack constantly changes with gas demand. And linepack plays a more critical role in the integrated system with P2G. From Fig. 7, the variation of the integrated system with P2G is larger than that without P2G. The reason is that the surplus wind power can be converted to gas fuel through the using of P2G, which can increase the replenishing speed of the linepack, accordingly it makes a more rapid variation on the linepack. It also illustrates that the linepack plays a more important role in the integrated system with P2G than that without P2G.

5.2. The effect of the wind power and power demand on the integrated gas and power system

The fluctuation and mismatch of wind power and power demand have been described above. We also concern the effect of wind power and power demand on the energy converters (P2G and GPG). In order to investigate the effect of wind power and power demand on P2G and GPG, a time series of wind power is injected into the electric network through bus 2, and the load at bus 5 and 6 are also set as a stochastic time-series. One year's data of 2014 is adopted in this study that is obtained from Energinet.dk.

Fig. 8 shows the relationship of the wind power, power demand and the output of P2G. It's clear that there is much higher gas produced by P2G when the power consumption is lower and the penetration of wind power is higher. Which can be attributed to the energy storage property of P2G: when the production of wind power increases, the surplus electricity power will be used to produce gas fuel that can be stored in the existing natural gas networks and the stored energy can then be injected back into electricity system through GPG. This indicates that the P2G technology has a potential to provide flexibility to the growing intermittent renewable energy.

The effect of the wind power and power demand on the output of gas-fired power plant is shown in Fig. 9. As we can see, the electricity generation in GPG increases with power demand and decreases with the wind power. When there is lower in wind power supply and higher in power consumption, the GPG will increase electricity production to meet the power balance. This result provides a clear exhibit of the ability of peak regulation of the gas-fired power generation. Thus, the required flexibility to meet the fluctuation of power load and renewables can be managed by the GPG.

Fig. 10 shows the relationship among the wind power, power demand and the reducing ratio of the total energy loss, where the reducing ratio of the total energy loss is defined as the decrease of the total energy loss by using integrated energy system with P2G divided by the total energy loss generated in the system without P2G. As we can see, this reducing ratio of the total energy loss

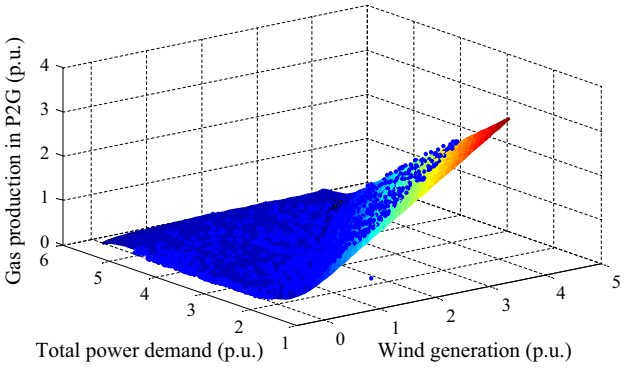

Fig. 8. The effect of the wind power and power demand on the output of P2G.

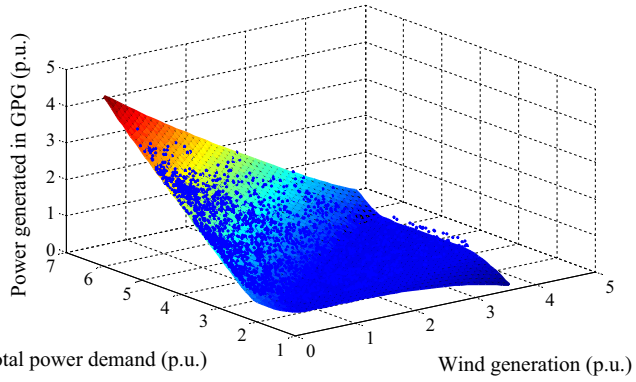

Fig. 9. The effect of the wind power and power demand on the output of gas-fired power plant.

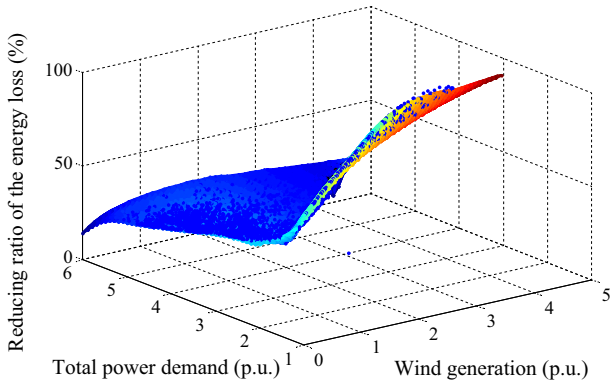

Fig. 10. The reducing ratio of energy loss in the integrated energy system.

increases with wind power and decreases with power demand, which indicates that the integrated energy system has a more notable influence on reducing the power loss when there is a larger output of wind power and lower power demand.

6. Conclusion

In this paper, a harmonized integration of natural gas and electric power system with bi-directional energy conversion is formulated as a set of non-linear equations. And a unified modelling and solution framework is developed to solve the coupled gas and power flow equations. The unification of units and per-unit system are proposed to simplify the system description and to enhance the computation efficiency. Case studies on an IEEE-9 test system combined with a 7-node natural gas network are carried out to demonstrate the applicability of the proposed approach. The testing results indicate that this unified solution with the per-unit system is feasible and sufficiently accurate. Furthermore, the unified solution with the per-unit system has a better computational efficiency. After that, time series of wind power and power load are introduced to investigate the mitigation effect of using P2G in the integrated natural gas and electric power system. Simulation results show that all the power loss, BHP and the total energy loss can be reduced by using P2G in the integrated energy system. It also indicates that the integrated gas and power system with P2G can maintain a stable level due to its network flexibility. Besides, a sufficient line-pack is more critical for the integrated energy system with P2G. At last, the effect of wind power and power demand on the output of the P2G and GPG is also investigated, the result provides an exhibit of the ability of peak regulation of GPG and P2G.

Acknowledgments

This study is a part of the research project supported by the ForskEL project Harmonized Integration of Gas, District Heating and Electric Systems (HIGHE863107).

References

[1] Mathiesen BV, Lund H, Connolly D. Limiting biomass consumption for heating in 100% renewable energy systems. Energy 2012;48:160–8.
[2] Mathiesen BV, Lund H, Connolly D, Wenzel H, Østergaard PA, Möller B, et al. Smart energy systems for coherent 100% renewable energy and transport solutions. Appl Energy 2015;145:139–54.
[3] Connolly D, Lund H, Mathiesen BV, Leahy M. The first step towards a 100% renewable energy-system for Ireland. Appl Energy 2011;88:502–7.
[4] Gahleitner G. Hydrogen from renewable electricity: an international review of power-to-gas pilot plants for stationary applications. Int J Hydrog Energy 2013;38:2039–61.
[5] Beevers D, Branchini L, Orlandini V, De Pascale A, Perez-Blanco H. Pumped hydro storage plants with improved operational flexibility using constant speed Francis runners. Appl Energy 2015;137:629–37.
[6] Luo X, Wang J, Dooner M, Clarke J. Overview of current development in electrical energy storage technologies and the application potential in power system operation. Appl Energy 2015;137:511–36.
[7] Cutter E, Haley B, Hargreaves J, Williams J. Utility scale energy storage and the need for flexible capacity metrics. Appl Energy 2014;124:274–82.
[8] Bhandari B, Lee K-T, Lee CS, Song C-K, Maskey RK, Ahn S-H. A novel off-grid hybrid power system comprised of solar photovoltaic, wind, and hydro energy sources. Appl Energy 2014;133:236–42.
[9] Neves D, Pina A, Silva CA. Demand response modeling: a comparison between tools. Appl Energy 2015;146:288–97.
[10] Dupont B, Dietrich K, De Jonghe C, Ramos A, Belmans R. Impact of residential demand response on power system operation: a Belgian case study. Appl Energy 2014;122:1–10.
[11] Massachusetts Institute of Technology. The future of natural gas an interdisciplinary MIT study. Cambridge (Mass.): Massachusetts Institute of Technology; 2011.
[12] Jentsch M, Trost T, Sterner M. Optimal use of power-to-gas energy storage systems in an 85% renewable energy scenario. Energy Proc 2014;46:254–61.
[13] Erdener BC, Pambour KA, Lavin RB, Dengiz B. An integrated simulation model for analysing electricity and gas systems. Int J Electr Power Energy Syst 2014;61:410–20.
[14] Mancarella P. MES (multi-energy systems): an overview of concepts and evaluation models. Energy 2014;65:1–17.
[15] Ouyang M. Review on modeling and simulation of interdependent critical infrastructure systems. Reliab Eng Syst Saf 2014;121:43–60.
[16] Lienert M, Lochner S. The importance of market interdependencies in modeling energy systems – the case of the European electricity generation market. Int J Electr Power Energy Syst 2012;34:99–113.
[17] Duenas P, Barquin J, Reneses J. Strategic management of multi-year natural gas contracts in electricity markets. IEEE Trans Power Syst 2012;27:771–9.
[18] Chaudry M, Jenkins N, Strbac G. Multi-time period combined gas and electricity network optimisation. Electr Power Syst Res 2008;78:1265–79.
[19] Qiu J, Dong ZY, Zhao JH, Xu Y, Zheng Y, Li C, et al. Multi-stage flexible expansion co-planning under uncertainties in a combined electricity and gas market. IEEE Trans Power Syst 2015;30:2119–29.
[20] Quan H, Srinivasan D, Khosravi A. Incorporating wind power forecast uncertainties into stochastic unit commitment using neural network-based prediction intervals. IEEE Trans Neural Netw Learn Syst 2015;26:2123–35.
[21] Hernandez-Fajardo I, Dueñas-Osorio L. Probabilistic study of cascading failures in complex interdependent lifeline systems. Reliab Eng Syst Saf 2013;111:260–72.
[22] Qadrdan M, Abeysekera M, Chaudry M, Wu J, Jenkins N. Role of power-to-gas in an integrated gas and electricity system in Great Britain. Int J Hydrog Energy 2015;40:5763–75.
[23] Grainger J, William Stevenson J. Power system analysis. New York: McGraw-Hill; 1994.
[24] Zhao M, Chen Z, Blaabjerg F. Probabilistic capacity of a grid connected wind farm based on optimization method. Renew Energy 2006;31:2171–87.
[25] Menon ES. Gas pipeline hydraulics. 1st ed. Boca Raton (FL): CRC Press; 2005.
[26] Bagajewicz M, Valtinson G. Computation of natural gas pipeline hydraulics. Ind Eng Chem Res 2014;53:10707–20.
[27] Martinez-Mares A, Fuerte-Esquivel CR. A unified gas and power flow analysis in natural gas and electricity coupled networks. IEEE Trans Power Syst 2012;27:2156–66.
[28] Mokhatab S, Poe WA, Speight JG. Handbook of natural gas transmission and processing. Burlington (MA, USA): Gulf Publishing Company; 2006.
[29] Sheldrake AL. Handbook of electrical engineering: for practitioners in the oil, gas and petrochemical industry. 1st ed. Chichester (West Sussex, England); Hoboken (NJ, USA): Wiley; 2002.
[30] Beér JM. High efficiency electric power generation: the environmental role. Prog Energy Combust Sci 2007;33:107–34.
[31] Shahidehpour M, Fu Y, Wiedman T. Impact of natural gas infrastructure on electric power systems. Proc IEEE 2005;93:1042–56.
[32] Bhuiyan FA, Yazdani A. Reliability assessment of a wind-power system with integrated energy storage. IET Renew Power Gener 2010;4:211–20.
[33] Grond L, Schulze P, Holstein J. Systems analyses power to gas: a technology review. Groningen; 2013.
[34] Bergen AR, Vittal V. Power systems analysis. 2nd ed. Upper Saddle River (NJ): Prentice Hall; 2000.
[35] Ahern EP, Deane P, Persson T, Gallachóir BÓ, Murphy JD. A perspective on the potential role of renewable gas in a smart energy island system. Renew Energy 2015;78:648–56.

Publication **J2**

Paper title:

A bi-level programming for multistage co-expansion planning of the integrated gas and electricity system

Publication outlet:

Applied Energy

List of authors:

Qing Zeng, Baohua Zhang, Jiakun Fang, Zhe Chen

DOI:1016/j.apenergy.2017.05.022.
Copyright © 2017 Copyright Clearance Center, Inc. All Rights Reserved. Privacy statement. Terms and Conditions.

Applied Energy 200 (2017) 192–203

Contents lists available at ScienceDirect

Applied Energy

journal homepage: www.elsevier.com/locate/apenergy

A bi-level programming for multistage co-expansion planning of the integrated gas and electricity system

Qing Zeng, Baohua Zhang, Jiakun Fang *, Zhe Chen

Department of Energy Technology, Aalborg University, Aalborg DK9220, Denmark

HIGHLIGHTS

- Coordinated expansion planning of the integrated power and gas system is studied.
- A bi-level framework to minimize the investment plus operational cost is built.
- Bi-directional energy conversions between power and gas systems are considered.
- Hybrid approach combining the heuristic and analytical optimization is proposed.
- Case studies on the practical western Danish energy system are conducted.

ARTICLE INFO

Article history:
Received 23 January 2017
Received in revised form 15 April 2017
Accepted 3 May 2017
Available online 15 May 2017

Keywords:
Bi-level programming
Co-expansion planning
Power to gas
Integrated gas and electricity system

ABSTRACT

This paper focuses on the coordinated expansion planning of the integrated natural gas and electrical power systems with bi-directional energy conversion. Both the Gas-fired Power Generations (GPGs) and Power-to-Gas stations (P2Gs) are considered as the linkages between the natural gas and electric power systems. The system operation is optimized and embedded in the planning horizon. A bi-level multi-stage programming problem is formulated to minimize the investment cost plus the operational cost. The upper-level optimizes the expansion plan and determines the network topology as well as the generation capacities, while the lower-level is formulated as an optimal economic dispatch under the operational constraints given by the upper-level decision. To solve the bi-level multi-stage programming problem, a hybrid algorithm is proposed combining the modified binary particle swarm optimization (BPSO) and the interior point method (IPM). The BPSO is used for the upper-level sub-problem, and the IPM is adopted for the lower-level sub-problem. Numerical case studies have been carried out on the practical gas and electricity transmission network in western Denmark. Simulation results demonstrate the effectiveness of the proposed approach.

© 2017 Elsevier Ltd. All rights reserved.

1. Introduction

The integration of multi-energy systems (MES) presents the opportunity to improve the efficiency and sustainability of the energy utilization as it can optimally interact with each other among different energy systems such as electricity, gas, heating, cooling and transport [1]. Among all the energy systems, the natural gas system and electrical power system are the most common options for bulk energy transmission over thousands of kilometers. Also, the interdependency between the electricity power and natural gas systems are dramatically increasing in recent years [2]. First, natural gas (NG) becomes one of the important energy sources in the world. It accounts for 25% of the world's primary energy production, and it is still expected to grow at a rate of 2.9–3.2% per year until 2030 [3]. Second, Gas-fired power generation (GPG) provides a linkage between natural gas and power systems [4]. As the GPG has the fast response capability, low fuel cost and low environmental emission, it currently plays an important role in ensuring security in power systems with high wind power penetrations [5], which results in an increasingly close coupling between the natural gas and electrical power systems [4,6]. Third, the emerging Power to Gas (P2G) technology enables the reverse energy conversion from the electricity system to the natural gas network, and the converted gas fuel can be used later for electricity production [7]. It might be one of the most promising energy storage technologies in the mid-term [8,9]. The P2G not only helps avoid the curtailment of renewables in the electrical power system

* Corresponding author.
E-mail address: jfa@et.aau.dk (J. Fang).

http://dx.doi.org/10.1016/j.apenergy.2017.05.022
0306-2619/© 2017 Elsevier Ltd. All rights reserved.

Nomenclature

Parameter

A	the present value of annuity factor
a, b, c	first, second, and third order coefficient of the utility function for the generator
B	electrical susceptance
c_k	specific heat ratio for the natural gas
C	the equivalent annual cost for the expansion planning component
d	day
e	acceleration coefficient
E	compressors parasitic efficiency, 0.99 for centrifugal units
f	random numbers in (0,1) interval
g_{id}^k	the individual optimum's positions of ith-particle in dth-dimension and the kth-iteration
g_{gd}^k	the global optimum's positions in dth-dimension and the kth-iteration
HR	heat rate
K	constant of compressor
L	length in km
N	the total number of a certain facility
r	the discount rate in %
t	time, h
T	suction temperature of compressor, °R
w	the inertia weight
y	year
Y	the planning horizon
Z_a	average compressibility factor
Z_{ij}	the resistance coefficient of the pipeline, kPa/(MW)^2
α, β, γ	first, second, and third order coefficient of the heat rate curve
η	efficiency, %
τ	the lifespan of the component
γ	the equivalent annual cost for the reduced capacity
ϕ	the equivalent annual cost for the new selected location
σ	the penalty factor
ε	CO_2 emission coefficient
ψ	the price in Euro
ξ	the compression ratio

Variables

EC	expanded capacity, MW
LP	the amount of linepack storage, MW
p	the gas pressure, kPa
P	electrical power or gas flow, MW
RC	reduced capacity, MW
S	gas flow rate in the pipeline, MW
β	the binary decision variable which represents the state on/off (1/0) of candidate component
θ	voltage phase angle
v_{id}^k	the velocity of ith-particle in dth-dimension and the kth-iteration
x_{id}^k	the positions of ith-particle in dth-dimension and the kth-iteration

Indices and subscripts

con, gen, sup, load	consumption, generation, supply, load
CPG, GPG, P2G	coal-fired power generation, Gas-fired power generation, Power to Gas
carbon	carbon emission
GT, GS, GC	Gas Terminal, Gas storage, Gas compressor
i,j	index of nodes, pipes or units
t	index of time
$\bar{}$, $\underline{}$	the upper limit, the lower limit

Abbreviations

elec, gas	electricity system, gas network
UE, WC, W, D	unserved electricity, Wind curtailment, Wind power, Demand
with, inject	withdrawal, injection

but also helps couple the natural gas and power systems with bi-directional energy conversion [4]. Thus, the harmonized integration of natural gas and power system can optimally utilize the flexibility provided by the gas network to improve the sustainability, reliability, and efficiency of energy utilization [10].

Due to these benefits, significant efforts have been devoted to the coordinated operation of the integrated gas and power systems. In the early research, the impact of the interdependency of natural gas and power systems on power security and economic dispatch are investigated in [11–14]: [11] demonstrates that the natural gas supply has a serious impact on the power security and the electricity price [12] also shows that the daily natural gas allocation can impact the security and economics of the power systems. In [11,12], the natural gas network is incorporated in the security-constrained unit commitment (SCUC) by various fuel constraints. However, the network constraints are neglected in these studies. In [13], an integrated model for SCUC is proposed by taking into consideration both the power transmission constraints and the natural gas transmission constraints [14] proposes a mixed-integer linear programming (MILP) security-constrained optimal power and gas flow under $N-1$ contingencies.

In recent years, with the increasing deployment of renewables and energy demands, it is of great importance to consider uncertainties regarding supply, demand and infrastructure for both electricity system and natural gas network. The stochastic programming is generally used to handle uncertainties. In [15], stochastic programming is adopted in the optimization model to deal with wind power uncertainty, in which a large number of wind forecast scenarios are generated and a scenario reduction algorithm is applied [16] applies stochastic optimization to the unit commitment problem with a number of wind power scenarios. And [17] proposed a coordinated stochastic model to consider the impact of the system uncertainties. Stochastic optimization generally requires the probability distribution of renewables or demands, but it is hard to know in reality. The robust optimization is another effective method which is widely used to deal with the problem of uncertainty. A robust optimization approach is proposed in [18] to deal with the scheduling of quick start units considering natural gas transmission constraints [19] proposed a two-stage robust optimization method to make unit commitment decisions under different uncertainty sets. As the robust optimization finds the optimal solution for the worst case scenario which happens at a very low probability, it is always considered too conservative especially in cases where uncertain parameters have a large range of variability [20]. Currently, the interval optimization method is considered as an alternative for addressing the uncertainty problems due to its good computational performance. In [2], an interval optimization framework is introduced to address

wind power uncertainty for the operating strategy of the integrated gas and electricity system.

In addition to the coordinated operation, the expansion planning in the natural gas and power system can be harmonized so that more mutual benefits can be obtained. The aim of the co-expansion planning for the integrated natural gas and power system is to determine the location, capacity and installation time for the new components or capacity expansion for the lines in both systems together in a harmonized way. In [21], a DC power flow model and a detailed gas network model are used for the combined gas and electricity network expansion planning. A mixed-integer linear optimization problem is formulated in [22] for the long-term, multi-area, and multi-stage expansion planning of integrated electricity and natural gas systems. Further, the energy networks are taken into account in [23]. The holistic approach is proposed that plans both generation capacity expansion and the line capacity expansion to accommodate high penetration of natural gas-fueled distributed generation. Later work [24] considers the uncertainties of the renewable generation and demand using stochastic optimization approaches [25] aims at both the reliability of energy supply and CO_2 emission reduction. In this work, the timeline mismatch between gas and electricity market is also considered by simulating the daily linepack variations [26] proposes a multi-stage integrated expansion planning model and applied to the real-world system.

In most of the previous research, the GPG has been widely considered as the linkage between the electricity network and gas network [6]. But P2G has only recently appeared in the investigation of the integrated natural gas and electric power system [4,10,27]. In [28], the P2G is included in the candidate planning facility to convert the surplus renewable energy to gas and store in the natural gas network. It shows that P2G technology implementation makes it possible to increase the supply security for the chosen region. However, there is still few report focus on the medium or long term planning of P2G and GPG in the integrated energy system to meet the rapid growth of renewables. Nowadays, the annual energy consumptions in some countries are not expected to grow in the future, but the dramatical change in energy mix challenges the co-expansion planning of the integrated energy system. For the case in Denmark, the gas consumption in Denmark will drop in the following years. Meanwhile, the increase in Danish electricity consumption will decrease to approximate 0 percent from 2020 to 2035 [29]. On the other hand, wind power produced 39% electricity consumption in 2014 [30]. Moreover, Energinet.dk, the Danish transmission system operator for both electricity and natural gas, has an ambitious goal to increase the share of electricity production from wind to 58% by 2020 and 66% by 2024 [29].

Therefore, the focus of our work is to improve system flexibility for accommodating the intermittent renewable energy by the expansion planning of P2G and GPG. A multi-stage co-expansion planning for the integrated gas and electricity system is investigated in this paper. Both the GPG and P2G are considered as the linkages between the natural gas and electric power system with bi-directional energy conversion. The mutual impact between the system expansion planning and the operation is considered. More specifically, less investment in the capacity expansion means a stricter operational constraint which may lead to a higher operational cost. In contrast, a lower operational cost requires a more relax operational condition so that more investment should be devoted to building larger generation sites or more transmission lines. Thus, the motivation of combining the expansion planning and the optimal operation is to achieve the feasibility and economics at the same time. The objective is to minimize the total investment plus the operational cost across the planning horizon. Network constraints and operation limits such as gas pressure constraints, gas transmission limits, nodal gas balance, nodal power balance, power transmission capacities and the generator capacities are considered in both gas and power systems. A bi-level programming structure is built to divide the optimization into two sub-problems. To solve this bi-level programming, a hybrid algorithm is presented which includes the modified binary particle swarm optimization (BPSO) and the interior point method (IPM). Case studies on the Danish gas and power transmission systems are conducted. The capacity expansion of gas pipelines or power transmission lines is not included in this study since the electricity and gas demand will not increase significantly in the planning horizon [29].

The remainder of the paper is organized as follows. Section 2 presents the model of the energy flow in the integrated gas and power systems. The formulation of the co-planning model is described in Section 3. Section 4 describes the solution methodology which is applied to solve the optimization problem. Section 5 presents the numerical results. Finally, Section 6 gives the conclusion of this work.

2. Modeling of the integrated gas and electricity system

The integrated gas and electricity system is mainly composed of gas network, power grid, and the links between the gas network and power system, such as GPG and P2G, etc. To analyze the steady state energy distribution in the integrated energy system, the integrated energy flow is formulated by gathering the steady-state flow models of both systems. In this paper, gas flow and gas load are measured by MW for the unification of the units with the power system. Moreover, the per-unit system is proposed to simplify the description of the integrated system and to enhance the computational efficiency. Specifically, the base value of gas pressure is 1 MPa, the base value of power is 100 MW, and the base value of voltage is 110 kV.

2.1. The energy flow in the natural gas system

The load flow in the power system is well-documented. It builds the relationship between the power transfer and the bus voltages. Similarly, the natural gas system follows the simple principle that the gas flows from nodes with higher pressure to lower pressure. In the isothermal gas pipeline, the flow rate is determined by the pressure drop:

$$p_i^2 - p_j^2 = Z_{ij}(S_{ij})^2 \tag{1}$$

The transportation of gas is subject to the law of mass conservation. Therefore, nodal balance is enforced by Eq. (2), which indicates that the gas inflows at each node (gas supply, gas withdrawal from linepack, gas inflow from pipe) are balanced with gas outflows (gas consumption, gas injection to linepack, gas outflow from pipe).

$$\sum_{m\in\Omega_i} P^{\text{gas}}_{\text{sup},m} - \sum_{n\in\Omega_i} P^{\text{gas}}_{\text{con},n} + \sum_{j\in\Omega_i} P^{\text{LP}}_{\text{with},ij} - \sum_{j\in\Omega_i} P^{\text{LP}}_{\text{in},ij} - \sum_{j\in\Omega_i} S_{ij} = 0 \tag{2}$$

2.2. Energy conversion between the gas and power systems

The energy can be converted between the gas and electricity systems via the GPG, P2G and gas compressors (GC). GPG burns natural gas to produce electricity. The relationship between the power generation and the natural gas consumption is mathematically formulated by the heat rate (HR) curve

$$HR = \alpha + \beta P^{\text{elec}}_{\text{GPG,gen}} + \gamma (P^{\text{elec}}_{\text{GPG,gen}})^2 \tag{3}$$

Then the gas consumption of GPG $P^{gas}_{GPG,con}$ can be calculated approximately from

$$P^{gas}_{GPG,con} = HR \cdot P^{elec}_{GPG,gen} \tag{4}$$

P2G is the emerging technology in recent years, which consumes electricity to produce gas. The energy conversion relationship between the gas generation rate $P^{gas}_{P2G,gen}$ and the consumed power $P^{elec}_{P2G,con}$ is related to the energy conversion efficient η_{P2G} [10], which can be given as

$$P^{gas}_{P2G,gen} = \eta_{P2G} P^{elec}_{P2G,con} \tag{5}$$

where η_{P2G} denotes the energy conversion efficiency in the P2G system. Note that the efficiency of the P2G plant is around 55–80% according to the state-of-the-art technology [31]. Due to the limited efficiency of the P2G plants, they should be carefully operated to avoid reducing the overall efficiency of the integrated energy systems.

Gas compressors (GC) can consume either gas or electricity to increase the gas pressure. The energy consumed by GC depends on the gas flow rate through GC and the compression ratio of GC [32].

$$P_{GC} = K_{GC} Z_a S_{GC} \left[\frac{T}{E_{GC}\eta_{GC}}\right]\left[\frac{c_k}{c_k - 1}\right]\left[\left(\frac{p^{out}}{p^{in}}\right)^{\frac{c_k-1}{c_k}} - 1\right] \tag{6}$$

2.3. Gas linepack

In the natural gas system, linepack plays a major role in balancing the gas production and consumption. The linepack is the total amount of gas present in the gas pipeline and is proportional to the average pressure over that pipeline [33]. Thus the initial linepack value can be determined by Eq. (7) [34].

$$LP^0_{ij} = k_{LP,ij} \cdot \overline{p_{ij}} \tag{7}$$

The constant $k_{LP,ij}$ depends on the geometrical volume of the pipeline, the referenced standard conditions and the factor $c_{LP,ij}$, which is given by

$$k_{LP,ij} = c_{LP,ij} \frac{T_{st}}{p_{st}} \frac{1}{Z_a \cdot T} D^2_{ij} L_{ij} \tag{8}$$

The average pressure is calculated according to Eq. (9) [34]:

$$\overline{p_{ij}} = \frac{2}{3}\left(p_i + p_j - \frac{p_i p_j}{p_i + p_j}\right) \tag{9}$$

In dynamic situations, the gas system is also subject to a temporal balance by means of line-pack balance based on the law of mass conservation, linepack can be determined by the accumulated difference between the injection and withdrawal of the gas flows in the pipeline [25,35]

$$LP_{ij}(t) = LP^0_{ij} + \sum_{h=1}^{t}\left[P^{LP}_{in,ij}(h) - P^{LP}_{with,ij}(h)\right] \tag{10}$$

It should be noted that the linepack storage should be restored after usage. In this work, the linepack is recovered every 24 h at the beginning of each day.

3. Formulation of bi-level programming on the co-expansion planning

In this section, a bi-level programming problem is formulated for the co-expansion planning. As shown in Fig. 1, the bi-level programming seeks for the optimal trade-off between the investment on the newly built facilities and the system operational cost. The upper-level sub-problem minimizes the investment while avoiding the significant increase of the operation cost. Given the system topology and capacities of the facilities determined by the upper-level sub-problem, the lower-level sub-problem optimize the system operation and feedback the minimum operation cost to the upper-level sub-problem. The flow equations and energy conversion relationships in the previous section are also embedded in the operational constraints.

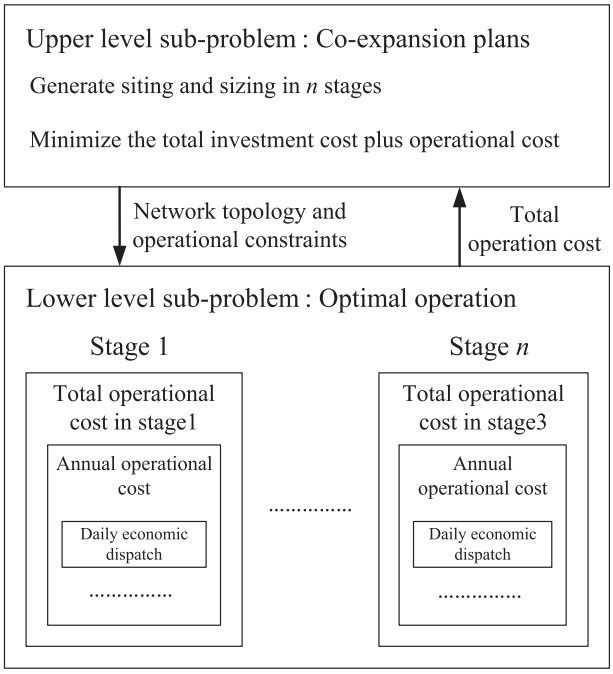

Fig. 1. Framework of bi-level programming on co-expansion planning.

Two sub-problems are interdependent and mutually influenced. Less investment in the capacity expansion means a stricter operational constraint which may lead to a higher operational cost. In contrast, a lower operational cost requires a more relax operational condition so that more investment should be devoted to building larger generation sites or more transmission lines. Therefore, the ultimate decision of the bi-level programming is the result of the gaming between the planning level and the operation level. The specific formulation of both sub-problems is introduced in the next sub-sections respectively.

3.1. The upper-level expansion planning sub-problem

The upper-level sub-problem is to determine the optimal expansion plan, including the optimal location and size of the newly installed facilities such as P2Gs and GPGs in each year across the planning horizon. Besides, a potential capacity expansion for the existing infrastructures such as generation sites and lines and pipes are also determined in this sub-problem. The objective can be given as

$$OF = \sum_{y=1}^{Y} \frac{1}{(1+r)^{y-1}}\left(F_{investment}(y) + F_{operation}(y)\right) \tag{11}$$

where $F_{investment}$ and $F_{operation}$ represents the investment cost and operational cost, respectively. $F_{investment}$ is the present value of the equivalent annual investment cost, which is given as

$$F_{\text{investment}}(y) = \sum_{i=1}^{N_{\text{P2G}}} \phi_{\text{CO}_2,i}(\beta_{\text{P2G},i,y} - \beta_{\text{P2G},i,y-1}) L_{\text{CO}_2,i} + \sum_{i=1}^{N_{\text{P2G}}} \phi_{\text{P2G},i}(\beta_{\text{P2G},i,y} - \beta_{\text{P2G},i,y-1}) + \sum_{i=1}^{N_{\text{P2G}}} C_{\text{P2G},i}\beta_{\text{P2G},i,y} EC_{\text{P2G},i,y} + \sum_{i=1}^{N_{\text{GPG}}} \phi_{\text{GPG},i}(\beta_{\text{GPG},i,y} - \beta_{\text{GPG},i,y-1}) + \sum_{i=1}^{N_{\text{GPG}}} C_{\text{GPG},i}\beta_{\text{GPG},i,y} EC_{\text{GPG},i,y} + \sum_{i=1}^{N_{\text{CPG}}} \phi_{\text{CPG},i}(\beta_{\text{CPG},i,y} - \beta_{\text{CPG},i,y-1}) + \sum_{i=1}^{N_{\text{CPG}}} C_{\text{CPG},i}\beta_{\text{CPG},i,y} EC_{\text{CPG},i,y} + \sum_{i=1}^{N_{\text{GPG}}} \gamma_{\text{GPG},i} RC_{\text{GPG},i,y} + \sum_{i=1}^{N_{\text{CPG}}} \gamma_{\text{CPG},i} RC_{\text{CPG},i,y} \quad (12)$$

The first term represents the investment on new pipelines to connect the new P2Gs and CPGs for the CO_2 transportation. The investment in the new plant is divided into two parts: the fixed installation cost wherever there exists no such plant before, and the sizing cost proportional to the capacity. The fixed installation cost makes the existing location as a preferred choice which helps to improve the sustainability of the existed location. The second to seventh terms are the fixed installation cost and the sizing cost for different plants including P2G, GPG, and CPG. The eighth and ninth terms give the nominal cost on shutting down the existed CPG and GPG.

In this optimal co-expansion plan, in the upper-level sub-problem, the decision on whether to install the new facilities are represented by binary variable β. $\beta = 1$ means to install and 0 means not to install. The subscription y is the year that new plant should be ready to commission. And the bus is represented by the subscription i and capacity of the plant is designed as EC.

The investment is annualized. c, γ, ϕ are the equivalent annual costs, which are calculated by dividing the investment cost by the present value of annuity factor $A_{\tau,r}$.

$$A_{\tau,r} = \frac{1}{r} - \frac{1}{r(1+r)^{\tau}} \quad (13)$$

The upper-level co-expansion planning sub-problem is subjected to the following constraints. First, the sustainability of the investment is guaranteed by avoiding to remove the selected sites within the planning horizon. Second, maximum expansion capacity of the individual plant should be limited due to the limited floor space. Third, the total investment in each year should be capped for financial budget considerations.

3.2. The lower-level of optimal operation

To obtain the operational cost $F_{\text{operation}}(y)$ in the upper-level sub-problem, the lower-level sub-problem optimizes the operation of the GPGs, P2Gs, CPGs, etc. to minimize the operational cost with the planned network and the plants. First, the yearly operational cost $F_{\text{operation}}(y)$ is transformed to the sum of the daily optimal operation costs $F_{\text{operation}}(d)$ in that year.

$$F_{\text{operation}}(y) = \sum_{d=1}^{D_y} F_{\text{operation}}(d) \quad (14)$$

where D_y is the time horizon of that year.

The optimization goal is to find the set of decision variables that allows the minimization of the objective throughout the whole operational horizons. The identified decision variables consist of the unit output, the gas supply, the wind curtailment, the expected unserved electric load.

$$F_{\text{operation}}(d) = \sum_{t=1}^{T_d}\sum_{i=1}^{N_{\text{P2G}}} (a_{1i}P_{\text{P2G},i,t}^2 + b_{1i}P_{\text{P2G},i,t} + c_{1i}) + \sum_{t=1}^{T_d}\sum_{i=1}^{N_{\text{GPG}}} (a_{2i}P_{\text{GPG},i,t}^2 + b_{2i}P_{\text{GPG},i,t} + c_{2i}) + \sum_{t=1}^{T_d}\sum_{i=1}^{N_{\text{CPG}}} (a_{3i}P_{\text{CPG},i,t}^2 + b_{3i}P_{\text{CPG},i,t} + c_{3i}) + \sum_{t=1}^{T_d}\sum_{i=1}^{N_{\text{wind}}} \sigma_{\text{WC},i}P_{\text{WC},i,t}^2 + \sum_{t=1}^{T_d}\sum_{i=1}^{N_{\text{D}}} \sigma_{\text{UE},i}P_{\text{UE},i,t} + \sum_{t=1}^{T_d}\sum_{i=1}^{N_{\text{GT}}} (\psi_{\text{GT},i}P_{\text{GT},i,t}) + \sum_{t=1}^{T_d}\sum_{i=1}^{N_{\text{GS}}} (\psi_{\text{with},i}P_{\text{GS},i,t}^{\text{with}} + \psi_{\text{in},i}P_{\text{GS},i,t}^{\text{in}}) + \sum_{t=1}^{T_d}\sum_{i=1}^{N_{\text{GPG}}} \psi_{\text{carbon}}\varepsilon_{\text{GPG},i}P_{\text{GPG},i,t} + \sum_{t=1}^{T_d}\sum_{i=1}^{N_{\text{CPG}}} \psi_{\text{carbon}}\varepsilon_{\text{CPG},i}P_{\text{CPG},i,t} - \sum_{t=1}^{T_d}\sum_{i=1}^{N_{\text{P2G}}} \psi_{\text{carbon}}\varepsilon_{\text{P2G},i}P_{\text{P2G},i,t} \quad (15)$$

The first three terms represent the operational cost of P2G, GPG, and CPG, respectively. Penalties are set for the wind curtailment [36,37] and unsupplied energy demand, indicated by the fourth and fifth term, respectively. The sixth term is the cost of gas supply from the gas terminal. The seventh express the operational cost of gas withdraw and gas inject in the gas storage. The eighth and ninth terms represent carbon emission cost of GPG and CPG. Finally, the tenth term expresses reward on using P2G to reduce CO_2 emission.

In addition to the objective function, following constraints are considered from both power system side and gas system side.

3.2.1. The operational constraints of the power systems

The operational constraints from power system side consist of network constraints, power transmission capacities, and the generator capacities. First, the dc power flow is used in the network constraint together with the nodal power balance.

$$P_{ij,t} = B_{ij}\theta_{ij,t}, \quad (\forall i,j \in N, t \in T_D) \quad (16)$$

$$|P_{ij,t}| \leqslant \overline{P_{ij}}, \quad (\forall i,j \in N, t \in T_D) \quad (17)$$

$$P_{\text{sup},i,t}^{\text{elec}} - (P_{\text{load},i,t}^{\text{elec}} - P_{\text{UE},i,t}^{\text{elec}}) = \sum_{j \in i} P_{ij,t}, \quad (\forall i,j \in N, t \in T_D) \quad (18)$$

where $P_{\text{sup},i,t}^{\text{elec}}$ includes the power supply from GPG and CPG ($P_{\text{GPG},i,t}$, $P_{\text{CPG},i,t}$), it also includes the power supply from the wind farm and the amount of wind curtailment $P_{\text{WC},i,t}$. The unserved electricity demand $P_{\text{UE},i,t}^{\text{elec}}$ and wind curtailment $P_{\text{WC},i,t}$ should be no larger than the power demand and available wind power, respectively.

$$0 \leqslant P_{\text{UE},i,t}^{\text{elec}} \leqslant P_{\text{load},i,t}, \quad (\forall i \in N, t \in T_D) \quad (19)$$

$$0 \leqslant P_{\text{WC},i,t} \leqslant \overline{P_{\text{W},i,t}}, (\forall i \in N_{\text{W}}, t \in T_D) \quad (20)$$

Except for the wind farms, other generation sites are subject to their minimum and maximum outputs and the ramping capabilities.

$$\underline{P_i} \leqslant P_{\text{sup},i,t}^{\text{elec}} \leqslant \overline{P_i}, \quad (\forall i \in N, t \in T_D) \quad (21)$$

$$|P^{\text{elec}}_{\text{sup},i,t} - P^{\text{elec}}_{\text{sup},i,t-1}| \leqslant P^{\text{ramp}}_{i}, \quad (\forall i \in N, t \in T_D) \tag{22}$$

The capacities and the ramping capabilities of the generators are determined by the upper-level expansion planning.

3.2.2. Constraints in the natural gas system

In the natural gas system, the network constraints include the pipeline flow Eq. (1) and the nodal gas balance Eq. (2). In the gas network, the mass flow rate and the pressure should be within the capacity of the pipeline.

$$-\overline{S_{ij}} \leqslant S_{ij,t} \leqslant \overline{S_{ij}}, \quad (\forall i,j \in N, t \in T_D) \tag{23}$$

$$\underline{p_i} \leqslant p_{i,t} \leqslant \overline{p_i}, \quad (\forall i \in N, t \in T_D) \tag{24}$$

Moreover, the facilities, including the gas terminal, gas storage, gas compression station, etc. are subject to their operational limits.

$$\underline{P_{\text{GT},i}} \leqslant P_{\text{GT},i,t} \leqslant \overline{P_{\text{GT},i}}, \quad (\forall i \in N_{\text{GT}}, t \in T_D) \tag{25}$$

$$0 \leqslant P_{\text{GS},i,t} \leqslant \overline{P_{\text{GS},i}}, \quad (\forall i \in N_{\text{GS}}, t \in T_D) \tag{26}$$

$$0 \leqslant P^{\text{in}}_{\text{GS},i,t} \leqslant \overline{P^{\text{in}}_{\text{GS},i}}, \quad (\forall i \in N_{\text{GS}}, t \in T_D) \tag{27}$$

$$0 \leqslant P^{\text{with}}_{\text{GS},i,t} \leqslant \overline{P^{\text{with}}_{\text{GS},i}}, \quad (\forall i \in N_{\text{GS}}, t \in T_D) \tag{28}$$

$$1 < \frac{p^{\text{out}}_{i,t}}{p^{\text{in}}_{i,t}} < \overline{\xi_i}, \quad (\forall i \in N_{\text{GC}}, t \in T_D) \tag{29}$$

$$P_{\text{GC},i,t} \leqslant \overline{P_{\text{GC},i}}, \quad (\forall i \in N_{\text{GC}}, t \in T_D) \tag{30}$$

The linepack storage should be limited in the safe operational region and restored at the beginning of each day.

$$LP_{i,end} = LP_{i,0}, \quad (\forall i \in N_{\text{LP}}, t \in T_D) \tag{31}$$

$$\underline{LP_i} \leqslant LP_{i,t} \leqslant \overline{LP_i}, \quad (\forall i \in N_{\text{LP}}, t \in T_D) \tag{32}$$

3.2.3. The operational constraints of the interfaces between gas and power network

Besides the network constraints and the operational limits for the facilities in the individual gas and power systems, the interfaces between the gas and power networks including GPG and P2G should be operated under their capacities. Moreover, the energy conversion relationship between the gas and power follows (3), (4) and (5).

4. Solution methodology

Combining the objective and constraints in both power and gas systems, the bi-level programming problem formulated in the previous sections is summarized as follows.

$$\begin{aligned} &\min \sum_{y=1}^{Y} \frac{1}{(1+r)^{y-1}} \left(F_{\text{investment}}(y) + F_{\text{operation}}(y)\right) \\ &\text{s.t.} \quad (1)-(10), (12)-(32) \end{aligned} \tag{33}$$

where $F_{\text{operation}}(y) = \sum_{d=1}^{D_y} F_{\text{operation}}(d)$. And $F_{\text{operation}}(d)$ is implicitly defined by

$$\begin{aligned} &\min \quad F_{\text{operation}}(d) \\ &\text{s.t.} \quad \begin{cases} \text{Power system constraints}: (16)-(22) \\ \text{Gas system constrains}: (1)-(2), (7)-(10), (23)-(32) \\ \text{Linkages}: (3)-(6) \end{cases} \end{aligned} \tag{34}$$

This formulated problem is bi-level nonlinear programming with integer decision variables, which is difficult to find the global optimal solution. In this work, a hybrid algorithm is presented integrating the binary particle swarm optimization (BPSO) and the interior point method (IPM). The upper-level co-expansion planning sub-problem is solved heuristically using the improved BPSO [38]. And for the lower-level optimal operation sub-problem, IPM is used to obtain the optimal daily economic dispatch. Monte-Carlo simulation samples the days randomly to get the approximated total operational cost for the whole year. The upper-level and lower-level problems are solved iteratively to reach the coordination.

The BPSO used in this paper is derived from the basic particle swarm optimization algorithms [39,40]. Each particle updates the speed and position of itself on the basis of individual optimum value and global optimum value, which can be described by the following equations:

$$v^{k+1}_{id} = w v^{k}_{id} + e_1 f_1 (g^{k}_{id} - x^{k}_{id}) + e_2 f_2 (g^{k}_{gd} - x^{k}_{id}) \tag{35}$$

$$w = w_{\max} - (w_{\max} - w_{\min}) \times (k/K)^2 \tag{36}$$

$$x^{k+1}_{id} = v^{k+1}_{id} + x^{k}_{id} \tag{37}$$

When the binary decision variables are introduced, the position x^k_{id} is updated using

$$x^{k}_{id} = \begin{cases} 1 & f < s(v^{k}_{id}) \\ 0 & others \end{cases} \tag{38}$$

where $s(v^k_{id})$ is a sigmoid function calculated by

$$s(v^{k}_{id}) = 1/(1 + \exp(-v^{k}_{id})) \tag{39}$$

In update strategy (39), when the velocity of the particle approaches zero, the variation probability of the position becomes very large, this induces a high diversity of the population. Thus the overall detective ability could be improved. However, it may reduce the local search ability. Therefore, the improved BPSO is used in this paper, which increased the local search ability by updating the particle position using the following equations [38]:

$$v^{k}_{id} < 0, \quad x^{k}_{id} = \begin{cases} 0 & f \leqslant s(v^{k}_{id}) \\ x^{k}_{id} & others \end{cases} \tag{40}$$

$$v^{k}_{id} > 0, \quad x^{k}_{id} = \begin{cases} 1 & f \leqslant s(v^{k}_{id}) \\ x^{k}_{id} & others \end{cases} \tag{41}$$

where $s(v^k_{id})$ is the probabilistic mapping function after revision calculated by

$$s(v^{k}_{id}) = \begin{cases} 1 - 2/(1 + \exp(-v^{k}_{id})) & v^{k}_{id} \leqslant 0 \\ 2/(1 + \exp(-v^{k}_{id})) - 1 & v^{k}_{id} > 0 \end{cases} \tag{42}$$

Compared with traditional BPSO, the improved BPSO has the greater searching ability and faster convergence ability; therefore it is adopted in this paper to solve the mix-integer nonlinear programming problem at upper-level co-expansion planning.

The steps of the hybrid algorithm applied to the bi-level programming are as follows:

(1) A group of particles are initialized randomly by a heuristic rule, regarding random position and speed. All the particles provide the network topology and operational limitations.
(2) Based on the provided network topology and operational limitations on the upper level, the operational cost can be calculated on the lower level by using IPM.

(3) The investment cost can be easily calculated as it is the function of the decision variables of planning given by the position of the particles. Thus, the fitness function of the upper level can be calculated which is the sum of the total investment cost and the operational cost.
(4) After the fitness evaluation, the local optimum solution and the global optimum position can be updated. Calculate the particle's velocity in next step, and update the positions of the particles. The speed and position of the particles are determined from the probability point of view.
(5) If the lowest investment cost plus operational cost has not changed for several times or the iterations meet the maximum number, ends the PSO calculation. Otherwise, back to step 2.

Fig. 2 shows the detailed flowchart of solving bi-level programming with the hybrid algorithm.

5. Case study

The proposed bi-level programming for multi-stage co-expansion planning is validated by using the gas and electricity transmission network in western Denmark, as depicted in Fig. 3. The system parameters are obtained from the report [41,42] published Energinet.dk, the transmission system operator for electricity and natural gas in Denmark. The natural gas network is composed of one gas terminal, one gas storage, and two compressor stations. The injection capacity of the gas terminal located on the western coast is 60 GW h/day. And the nodal pressure is constantly at 80 bar. The storage capacity of the gas storage is 5600 GW h with the injection capacity 0.8 GW and the withdrawal capacity 1.2 GW. In the Danish gas system, the compressors are gas-driven, and the compression ratio is 2. The calorific value of the natural gas is 37.26 MJ/m^3.

In the power system, there are six wind farms, five central CPGs, and one GPG. The detailed operational data can be found in Table 1. Two candidate locations for GPGs and three candidate locations for P2Gs are selected as shown in Fig. 3. These 5 candidate locations are placed on the common nodes in the gas and power systems so that no more connection branches are needed.

5.1. Scenario forecast and the investment costs

The planning horizon is set nine years (2016–2024) in this paper and divided into 3 stages. The detailed forecast shown in Table 2 is also obtained from Energinet.dk [30].

In this table, the average prices for the fuels, electricity and CO_2 emission are illustrated as well as the future capacity expansion of electricity consumption and wind power in Denmark. From the consumers' side, Danish electricity consumption is growing slowly. The annual average increase is approximately 1% from 2016 to 2024. From the generation side, it has been estimated by Energinet.dk that 6941 MW wind power will be integrated into the Danish power system, producing 66% of total electricity by 2024, with the annual increase approximately 3.5% from 2016.

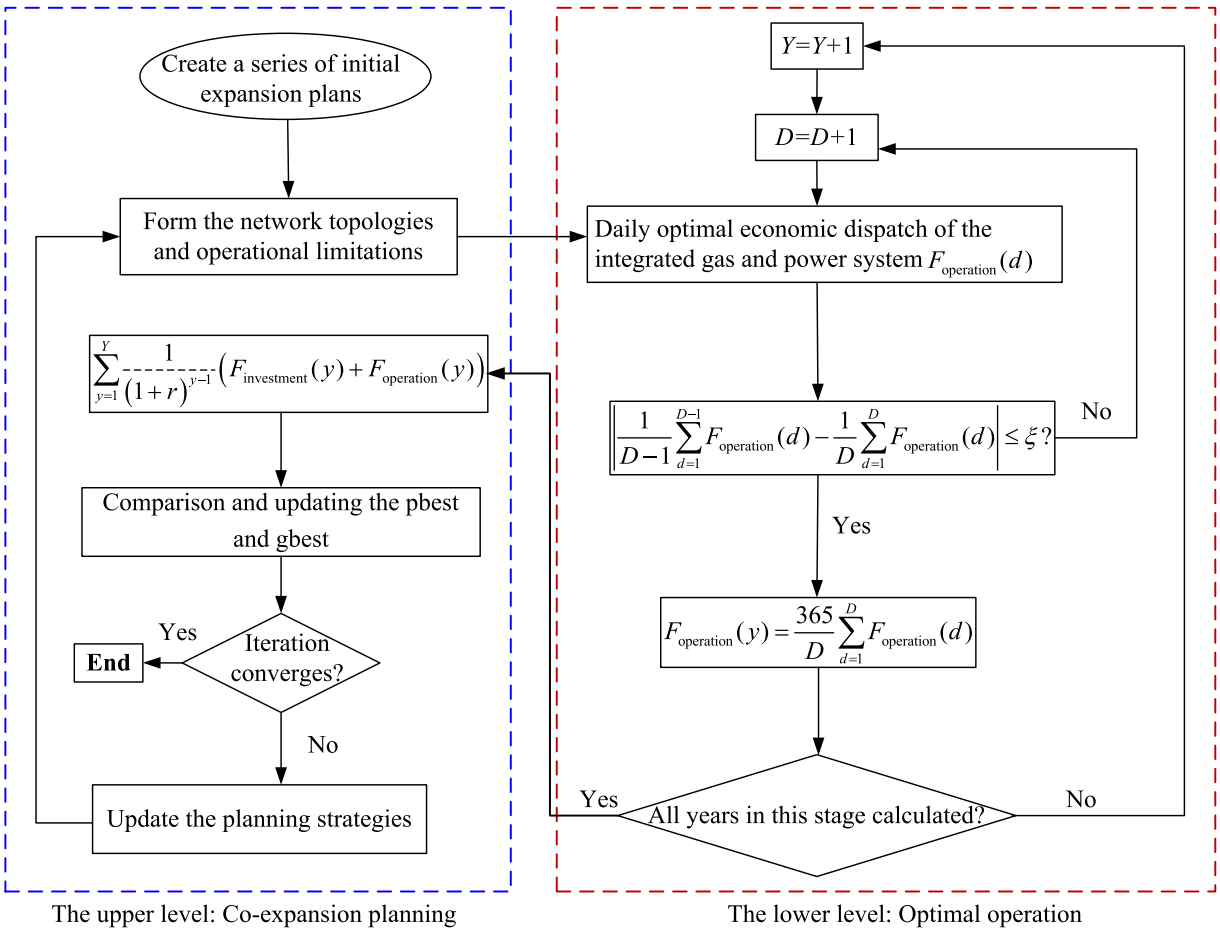

Fig. 2. Flowchart of solving bi-level programming with the hybrid algorithm.

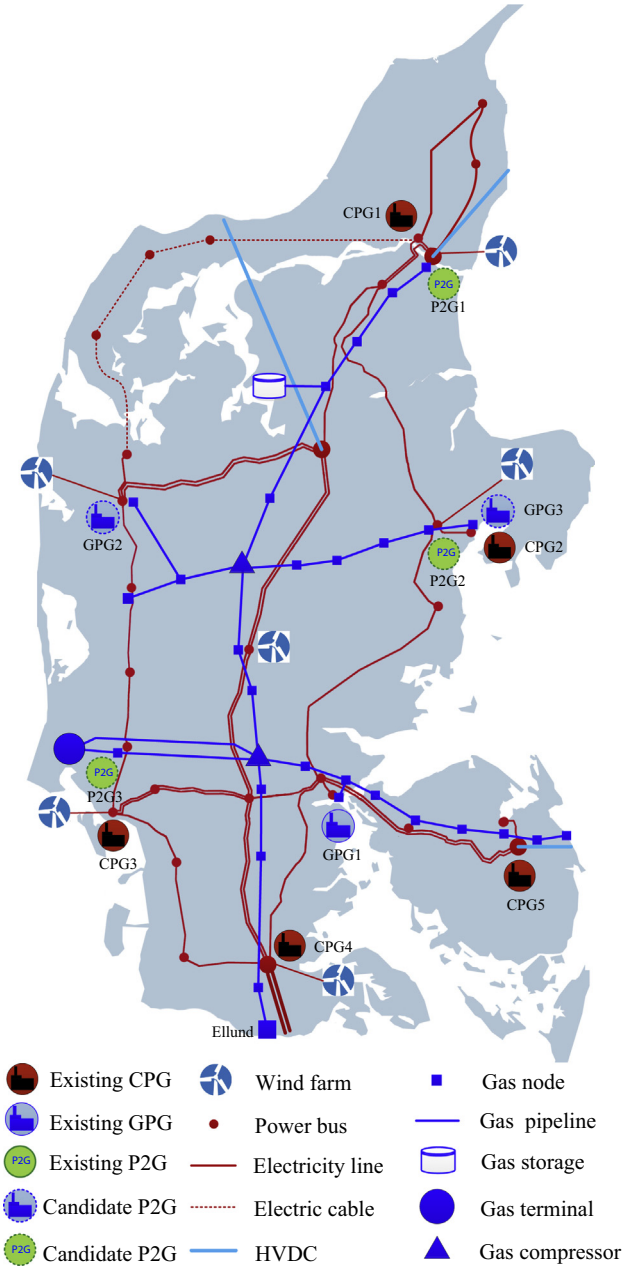

Fig. 3. The natural gas and electricity transmission system in western Denmark.

To evaluate the investment cost, this work assumes that it takes 0.27 million Euro and 0.13 million Euro fixed installation cost to set up a new P2G and GPG plant, respectively. For the existing facilities, the expansion cost is 2 million Euro/MW for P2G, 0.8 million Euro/MW for GPG and 1.5 million Euro/MW for CPG [28]. Besides, the nominal cost to shut down the existed CPG and GPG is 0.1 million Euro/MW. Further, a pipeline with a diameter of 100 mm (4 in.) is selected for the transportation of CO_2 gas from the central power plants to the P2G systems. Its investment cost is about 0.08 million Euro/km [28,43]. The lengths of the CO_2 pipelines are 10 km, 15 km, and 30 km for P2G1, P2G2, and P2G3, respectively. The lifespan is assumed to be 40 years for GPG and 30 years for P2G, and 40 years for CO_2 pipelines.

5.2. The multistage evolution of the capacities for P2G, GPG, and CPG

To validate the proposed approach, we carry out the case study on the western Danish electricity and natural gas system. Three different scenarios are studied. Scenario 1 assumes that the annual growth rate of the wind power production is 2%. In Scenario 2, 3.5% of annual growth is assumed and 5% for Scenario 3. The system planning horizon is nine years (2016–2024) consisting of 3 stages. The CPU core used for simulations is 3.06 GHz, the iteration times and particle sizes are set as 50 and 250. The iterative processes of the BPSO for the three scenarios are shown in Fig. 4. It takes less than 150 steps to update before convergence and the computation time are 1054, 1205 and 1146 min for Scenario 1, 2 and 3 respectively. It can be considered acceptable for the planning studies. Hence, the result indicates that the proposed method is applicable for the multi-stage expansion co-planning in a real application. The optimization results are shown in Table 3. When the wind power production is higher, the operational cost decreases since less fuel such as gas and coal is burned. However, more investment on the GPG and P2G is needed to ensure the secure energy supply.

The multi-stage evolution of the energy mix is shown in Fig. 5. It can be seen that the capacity of CPG decreases with the increase of the wind penetration level. Meanwhile, the capacities of both GPG and P2G increase at the same time. For scenario 1, the capacity of the CPG is shrunk from 2685 MW to 2181 MW, while the total capacity of GPG increased from 400 MW to 505 MW. 208 MW P2G plants are planned. For scenario 2, the capacity of the coal-fired power plant is reduced from 2695 MW to 2029 MW, while 140 MW GPG (increased from 400 MW to 540 MW) is newly installed. 295 MW P2G is planned in this scenario. Scenario 3 assumes 5% annual growth for the wind power production. The

Table 1
Operational parameters of CPG, GPG, and P2G in 2016.

Generator	Fuel cost			CO_2 emission (Ton/MW h)	$\overline{P}$ (MW)	$\underline{P}$ (MW)
	a (€/MW h^2)	b (€/MW h)	c (€)			
CPG1	0.0051	8.1	1000	1.05	410	250
CPG2	0.0035	8.1	1600	1.05	800	400
CPG3	0.0049	8.1	1000	1.05	400	240
CPG4	0.0041	8.1	1300	1.05	665	300
CPG5	0.0049	8.1	1000	1.05	410	240
GPG1	0.0021	21.3	600	0.65	400	100
GPG2	0.0021	21.3	600	0.65	–	–
GPG3	0.0021	21.3	600	0.65	–	–
P2G1	0.006	4.5	500	−0.16	–	–
P2G2	0.006	4.5	500	−0.16	–	–
P2G3	0.006	4.5	500	−0.16	–	–

Table 2
The Energinet.dk's forecast of the planning horizon (2016–2024).

Year	Coal price €/MW h	Gas price €/MW h	CO_2 price €/ton	Electricity prices €/MW h	Electricity load GW h	Wind capacity MW	Percentage of wind %
2016	8.1	21.3	7.3	30	20,737	5041	41
2017	8.8	22.9	8.8	29.1	20,959	5191	43
2018	9.6	24.8	10.8	36.3	21,208	5341	45
2019	10.5	26.9	13.5	43.6	21,384	5541	48
2020	11.5	28.9	16.8	50.9	21,552	6341	58
2021	11.6	29.4	18.1	51.3	21,841	6591	61
2022	11.7	29.7	19.5	53.2	22,205	6841	64
2023	11.7	30.1	20.7	53.7	22,512	6891	66
2024	11.8	30.4	22	54.3	22,866	6941	66

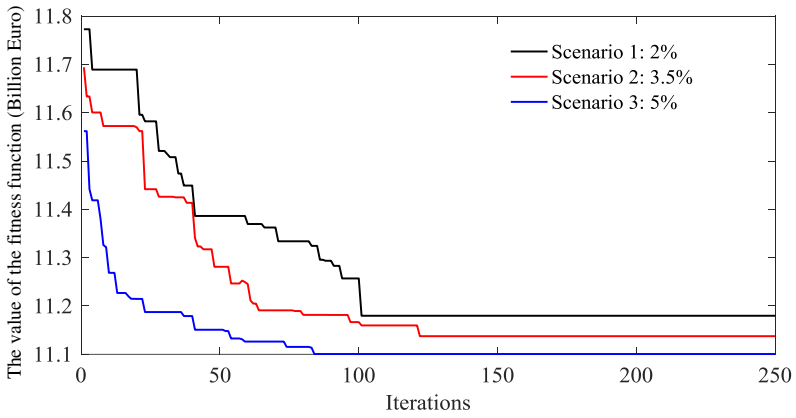

Fig. 4. Optimization process of the proposed method.

Table 3
Total expansion and operation cost in billions of Euro.

Scenario no.	Iteration steps before convergence	Initial fitness value	Optimal total cost	Investment cost	Operation cost
Scenario 1	101	11.78	11.18	0.17	11.01
Scenario 2	119	11.69	11.14	0.23	10.91
Scenario 3	82	11.56	11.10	0.24	10.86

capacity of CPG will be reduced to 1885 MW. Additional 166 MW GPG and 351 MW P2G are planned in Scenario 3. As can be seen from the comparison of 3 scenarios, the higher the growth rate of wind power can result in more CPG shut down, and faster growing capacities of GPG and P2G in coordination.

As shown in Fig. 3, the candidate locations for P2Gs are near the wind farms. So in this case study, P2Gs consumes the surplus wind power in all the three scenarios to reduce the fuel cost for electricity generation. The difference is that the lengths of the CO_2 pipelines are 10 km, 15 km, and 30 km for P2G1, P2G2, and P2G3, respectively. So the investment cost of P2G2 is larger than that of P2G1, and the investment cost of P2G3 is the highest if taking the cost of CO_2 pipelines into consideration. Table 4 illustrates the detailed capacity evolution at each candidate location. P2G1 is the preferred option among the 3 candidate locations. So the capacity of P2G1 grows faster than P2G2. P2G3 is only suggested in scenario 3 with the highest penetration of wind power. For CPGs and GPGs, it can be seen from Table 4 that with the wind power increases, the part of the units at CPG2 are suggested to be shut down and replaced by newly installed gas turbines installed at GPG3. GPG3 has a lower investment cost in comparison with GPG2 because GPG2 requires the fixed installation cost for the initial construction of a newly selected location. So the existing location GPG3 is a preferred choice to install new gas-fired power generators.

5.3. The daily optimal operation of the integrated gas and electricity system

In this subsection, the optimal operation strategy of the integrated gas and power system is investigated. Fig. 6 shows the optimal operation strategy of the power units in a typical day with high wind. During the peak load periods (7:00 AM ~ 13:00 PM, 17:00 PM ~ 18:00 PM), all the available wind power is utilized to supply the electrical load. Moreover, both the GPG and CPG increase their unit outputs to balance the power demand. During the midnight (12:00 PM ~ 6:00 AM), the excess wind power is converted into gas fuel by P2G. Due to the limitation of the available capacities of the P2G, there is still some wind curtailment in this period but reduced by using P2G. It should be mentioned that the total power load includes both the nodal power demand and electricity consumed by P2G.

At the gas system side, Fig. 7 illustrates the gas injections and consumptions. It shows that the gas supply from the gas terminal

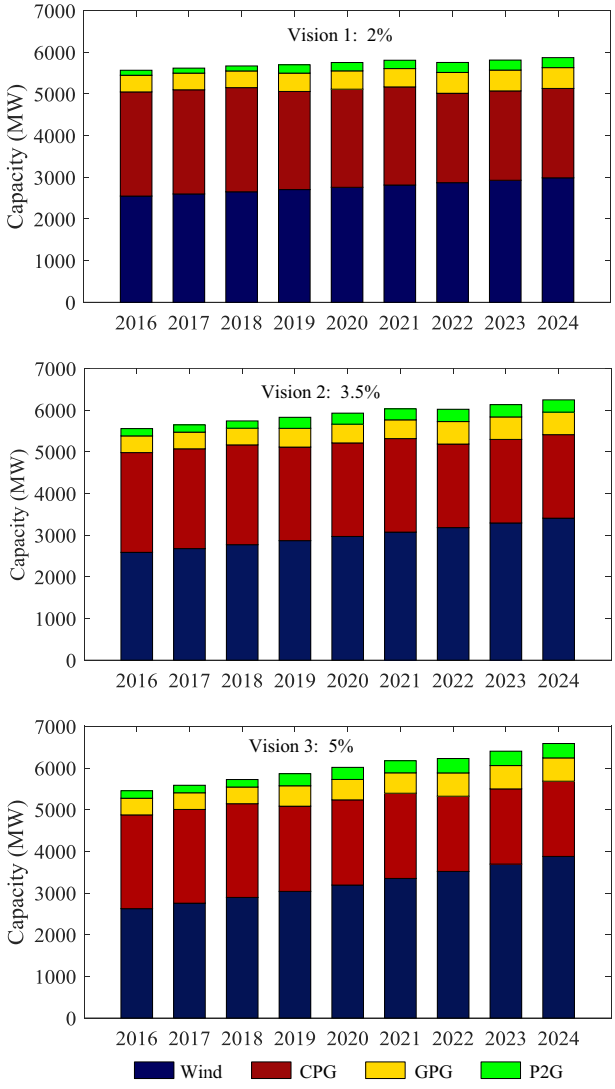

Fig. 5. Evolution of the installed generation from 2016 to 2024 for three scenarios.

and gas storage appears to be a constant value. Besides, P2G only converts the surplus wind power due to the efficiency considerations. The difference between the gas supply and consumption is balanced by the linepack. It can be seen that the linepack is consumed in the day and restored in the midnight. In the peak-gas-demand hour (e.g. 8:00 AM ~ 13:00 PM), the increasing gas

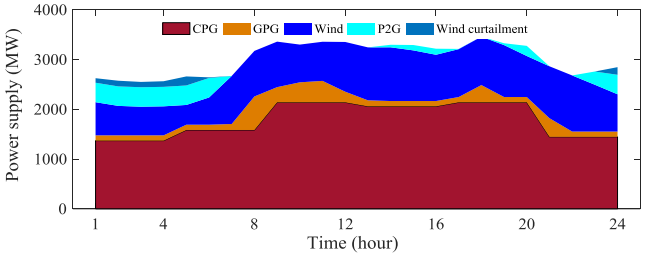

Fig. 6. Daily economic dispatch at power system side.

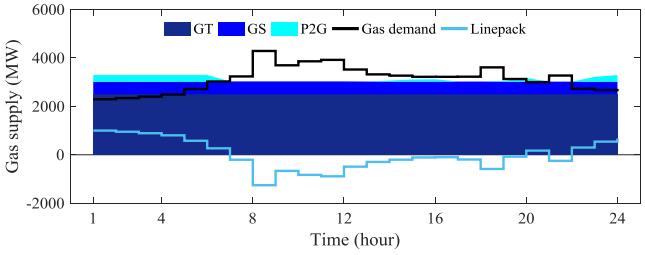

Fig. 7. Optimized gas supply in the natural gas system.

demand from GPG leads to a rapid linepack consumption. In the gas system, there are not as many regulation facilities as the power system. So the sufficient linepack storage plays an essential role in balancing gas production and consumption.

5.4. Comparison of the daily operation with and without P2Gs

To investigate the effect of P2G, 2 cases for the daily operation are compared under stage 2 from 2019 to 2021. In Case 1, total 265 MW P2G is installed while in Case 2 no P2G is installed. The comparison is carried out in a high-wind week from the following aspects: the wind curtailment, the gas supply, and the operational cost, as is shown in Fig. 8. Results show that as part of surplus wind power can be converted to gas fuel by using P2G, the wind curtailment can be reduced and less gas is consumed from the gas terminal and storage. Such benefits help to reduce the daily operational cost of Case 1.

6. Conclusion

This paper proposes a bi-level multi-stage co-expansion planning model for the integrated natural gas and electricity system to minimize the investments plus the operation cost. The main

Table 4
Detailed planning strategy in different sites.

Candidate location	Initial capacity	Scenario 1			Scenario 2			Scenario 3		
		Stage1	Stage2	Stage3	Stage1	Stage2	Stage3	Stage1	Stage2	Stage3
P2G1	0	91	91	121	100	140	170	78	162	162
P2G2	0	59	87	87	75	125	125	90	90	135
P2G3	0	0	0	0	0	0	0	54	54	54
GPG1	400	400	400	400	400	400	400	400	400	400
GPG2	0	0	0	0	0	0	0	0	0	0
GPG3	0	0	48	105	0	56	140	0	90	166
CPG1	410	410	410	410	410	410	410	410	410	410
CPG2	800	684	504	296	530	360	144	460	240	0
CPG3	400	400	400	400	400	400	400	400	400	400
CPG4	665	665	665	665	665	665	665	665	665	665
CPG5	410	410	410	410	410	410	410	410	410	410

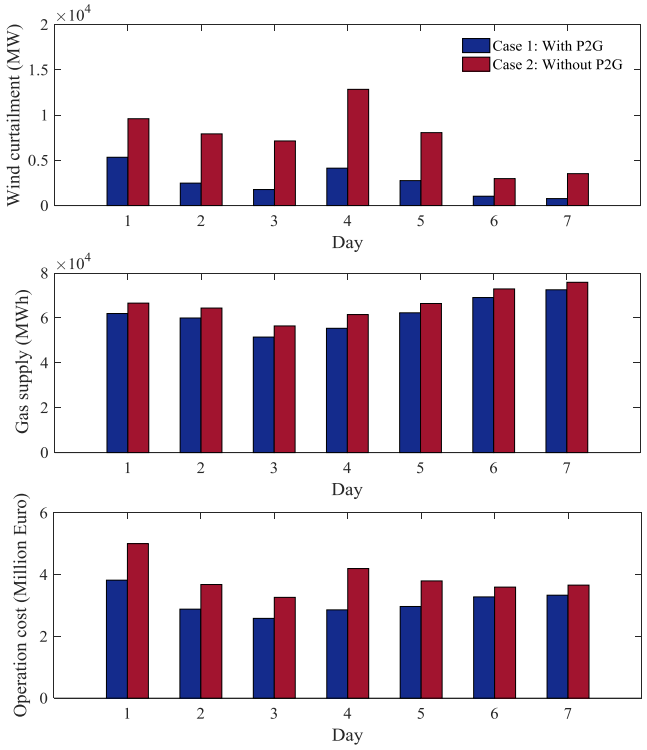

Fig. 8. Comparison of the daily operation between the integrated system with and without P2G.

contents and major contributions of the paper are summarized as follows:

- An integrated model is formulated to describe the combined natural gas and electricity energy system with bi-directional energy conversion. Both the P2G and the GPG are considered as the linkage between the electricity network and gas network.
- A bi-level programming framework is built to achieve the good balance between investment on the system expansion and the operational cost. The overall decision-making process is divided into two sub-problems: the upper-level optimizes the investment co-planning for the integrated system, while the lower-level optimizes the operation strategy under given constraints from upper-level sub-problem. The two sub-problems are solved iteratively.
- A hybrid algorithm is proposed to solve the bi-level programming problem combining the modified binary particle swarm optimization (BPSO) and the interior point method (IPM) for the upper-level and lower-level sub-problems, respectively.
- The proposed method is validated by case studies on the gas and electricity transmission network in western Denmark. The simulation result indicates the effectiveness of the proposed method.
- Through the analysis of the simulation results, it is suggested that enhancing the synergies between gas and power system using GPG and P2G helps to overcome the challenges brought by the change in the energy mix. The beneficial role of the P2G to improve wind power accommodation is also investigated. Simulation results show that P2G helps to reduce the operation cost by less wind curtailment, gas fuel consumption and carbon emission.

The proposed co-expansion planning model and the hybrid algorithm of this paper can be used to help system planner with decision support in the future integrated multi-energy systems.

Acknowledgments

This study is a part of the research project supported by the ForskEL project Harmonized Integration of Gas, District Heating and Electric Systems (HIGHE2014-1-12220).

References

[1] Mancarella P. MES (multi-energy systems): An overview of concepts and evaluation models. Energy 2014;65:1–17.
[2] Bai L, Li F, Cui H, Jiang T, Sun H, Zhu J. Interval optimization based operating strategy for gas-electricity integrated energy systems considering demand response and wind uncertainty. Appl Energy 2016;167:270–9.
[3] Üster H, Dilaveroğlu Ş. Optimization for design and operation of natural gas transmission networks. Appl Energy 2016;167:270–9.
[4] Li G, Zhang R, Jiang T, Chen H, Bai L, Li X. Security-constrained bi-level economic dispatch model for integrated natural gas and electricity systems considering wind power and power-to-gas process. Appl Energy 2016;194:696–704.
[5] Devlin J, Li K, Higgins P, Foley A. The importance of gas infrastructure in power systems with high wind power penetrations. Appl Energy 2016;167:294–304.
[6] Zheng JH, Wu QH, Jing ZX. Coordinated scheduling strategy to optimize conflicting benefits for daily operation of integrated electricity and gas networks. Appl Energy 2016;192:370–81.
[7] Jentsch M, Trost T, Sterner M. Optimal use of power-to-gas energy storage systems in an 85% renewable energy scenario. Energy Procedia 2014;46:254–61.
[8] Vandewalle J, Bruninx K, D'haeseleer W. Effects of large-scale power to gas conversion on the power, gas and carbon sectors and their interactions. Energy Convers Manage 2015;94:28–39.
[9] Bailera M, Lisbona P, Romeo LM, Espatolero S. Power to Gas–biomass oxycombustion hybrid system: energy integration and potential applications. Appl Energy 2016;167:221–9.
[10] Zeng Q, Fang J, Li J, Chen Z. Steady-state analysis of the integrated natural gas and electric power system with bi-directional energy conversion. Appl Energy 2016;184:1483–92.
[11] Shahidehpour M, Fu Y, Wiedman T. Impact of natural gas infrastructure on electric power systems. Proc IEEE 2005;93:1042–56.
[12] Li T, Eremia M, Shahidehpour M. Interdependency of natural gas network and power system security. IEEE Trans Power Syst 2008;23:1817–24.
[13] Liu C, Shahidehpour M, Fu Y, Li Z. Security-constrained unit commitment with natural gas transmission constraints. IEEE Trans Power Syst 2009;24:1523–36.
[14] Correa-Posada CM, Sánchez-Martin P. Security-constrained optimal power and natural-gas flow. IEEE Trans Power Syst 2014;29:1780–7.
[15] Qadrdan M, Wu J, Jenkins N, Ekanayake J. Operating strategies for a GB integrated gas and electricity network considering the uncertainty in wind power forecasts. IEEE Trans Sustain Energy 2014;5:128–38.
[16] Quan H, Srinivasan D, Khambadkone AM, Khosravi A. A computational framework for uncertainty integration in stochastic unit commitment with intermittent renewable energy sources. Appl Energy 2015;152:71–82.
[17] Zhang X, Shahidehpour M, Alabdulwahab A, Abusorrah A. Hourly electricity demand response in the stochastic day-ahead scheduling of coordinated electricity and natural gas networks. IEEE Trans Power Syst 2016;31:592–601.
[18] Liu C, Lee C, Shahidehpour M. Look ahead robust scheduling of wind-thermal system with considering natural gas congestion. IEEE Trans Power Syst 2015;30:544–5.
[19] An Y, Zeng B. Exploring the modeling capacity of two-stage robust optimization: variants of robust unit commitment model. IEEE Trans Power Syst 2015;30:109–22.
[20] Shapiro A, Tekaya W, Soares MP, da Costa JP. Worst-case-expectation approach to optimization under uncertainty. Oper Res 2013;61:1435–49.
[21] Chaudry M, Jenkins N, Qadrdan M, Wu J. Combined gas and electricity network expansion planning. Appl Energy 2014;113:1171–87.
[22] Unsihuay-Vila C, Marangon-Lima JW, de Souza ACZ, Perez-Arriaga IJ, Balestrassi PP. A model to long-term, multiarea, multistage, and integrated expansion planning of electricity and natural gas systems. IEEE Trans Power Syst 2010;25:1154–68.
[23] Saldarriaga CA, Hincapie RA, Salazar H. A holistic approach for planning natural gas and electricity distribution networks. IEEE Trans Power Syst 2013;28:4052–63.
[24] Saldarriaga CA, Hincapie RA, Salazar H. An integrated expansion planning model of electric and natural gas distribution systems considering demand uncertainty. 2015 IEEE Power Energy Soc. Gen. Meet. 2015:1–5.
[25] Qiu J, Dong ZY, Zhao JH, Meng K, Zheng Y, Hill DJ. Low carbon oriented expansion planning of integrated gas and power systems. IEEE Trans Power Syst 2015;30:1035–46.
[26] Barati F, Seifi H, Sepasian MS, Nateghi A, Shafie-khah M, Catalão JPS. Multi-period integrated framework of generation, transmission, and natural gas grid expansion planning for large-scale systems. IEEE Trans Power Syst 2015;30:2527–37.
[27] Qadrdan M, Abeysekera M, Chaudry M, Wu J, Jenkins N. Role of power-to-gas in an integrated gas and electricity system in Great Britain. Int J Hydrog Energy 2015;40:5763–75.

[28] Moskalenko N, Lombardi P, Komarnicki P. Multi-criteria optimization for determining installation locations for the power-to-gas technologies. 2014 IEEE PES Gen. Meet. Conf. Expo. 2014:1–5.
[29] Energinet.dk 2015Energinet.dk. Energinet dk's analysis assumptions 2015-2035. <https://www.energinet.dk/SiteCollectionDocuments/Danske%20dokumenter/El/Energinet.dk's%20analyseforuds%C3%A6tninger%202015-2035%20-%20ekstern%20version.docx%202516716_2_1.pdf>; 2015 [accessed 28.03.16].
[30] Rasmussen JN. Vindmøller slog rekord i; 2014.
[31] Ahern EP, Deane P, Persson T, Ó Gallachóir B, Murphy JD. A perspective on the potential role of renewable gas in a smart energy island system. Renew Energy 2015;78:648–56.
[32] Mokhatab S, Poe WA, Speight JG. Handbook of natural gas transmission and processing. Burlington, MA, USA: Gulf Publishing Company; 2006.
[33] Kabirian A, Hemmati MR. A strategic planning model for natural gas transmission networks. Energy Policy 2007;35:5656–70.
[34] Nico K. Gas balancing and line-pack flexibility. European University Institute; 2012.
[35] Chaudry M, Jenkins N, Strbac G. Multi-time period combined gas and electricity network optimisation. Electr Power Syst Res 2008;78:1265–79.
[36] Wu W, Chen J, Zhang B, Sun H. A robust wind power optimization method for look-ahead power dispatch. IEEE Trans Sustain Energy 2014;5:507–15.
[37] Li Z, Wu W, Zhang B, Wang B. Adjustable robust real-time power dispatch with large-scale wind power integration. IEEE Trans Sustain Energy 2015;6:357–68.
[38] Zhang J, Liu Y, Tian D, Yan J. Optimal power dispatch in wind farm based on reduced blade damage and generator losses. Renew Sustain Energy Rev 2015;44:64–77.
[39] Shi Y, Eberhart R. A modified particle swarm optimizer. IEEE Int. Conf. Evol. Comput. 1998:69–73.
[40] Shi Y, Eberhart RC. Empirical study of particle swarm optimization. Proc. 1999 Congr. Evol. Comput. 1999:1945–50.
[41] Energinet.dk. Download data about the Danish electricity system in 2020. <http://www.energinet.dk/EN/El/Nyheder/Sider/Nu-kan-du-downloade-data-om-det-danske-elsystem-i-2020.aspx>; 2016 [accessed 06.04.16].
[42] Energinet.dk. System Plan 2015: Electricity and Gas in Denmark. 2015. <http://energinet.dk/DA/OM-OS/Periodiske-rapporter/Sider/Systemplan.aspx; 2016 [accessed 06.04.16].
[43] Ai Qian, Fan Songli, Piao Longjian. Optimal scheduling strategy for virtual power plants based on credibility theory. Prot Control Modern Power Syst 2016;1(3):1–8. http://dx.doi.org/10.1186/s41601-016-0017-x.

Publication **J3**

Paper title:

Optimal operation of the integrated electrical and heating systems to accommodate the intermittent renewable sources

Publication outlet:

Applied energy

List of authors:

Jinghua Li, Jiakun Fang, Qing Zeng, Zhe Chen

DOI: 10.1016/j.apenergy.2015.10.054
Copyright © 2015 Copyright Clearance Center, Inc. All Rights Reserved. Privacy statement. Terms and Conditions.

Applied Energy 167 (2016) 244–254

Contents lists available at ScienceDirect

Applied Energy

journal homepage: www.elsevier.com/locate/apenergy

Optimal operation of the integrated electrical and heating systems to accommodate the intermittent renewable sources

Jinghua Li [a,b,*], Jiakun Fang [b], Qing Zeng [b], Zhe Chen [b]

[a] College of Electrical Engineering, Guangxi University, Nanning 530004, China
[b] Department of Energy Technology, Aalborg University, Aalborg DK9220, Denmark

HIGHLIGHTS

- The optimization problem of combing electricity and heat is formulated.
- An efficient algorithm is studied for solving the integrated problem.
- The amount of the energy conversion between electricity and heat is decided.
- The best node to join with the electrical system and heating system is chosen.
- Benefits of the integration of electricity and heat are discussed.

GRAPHICAL ABSTRACT

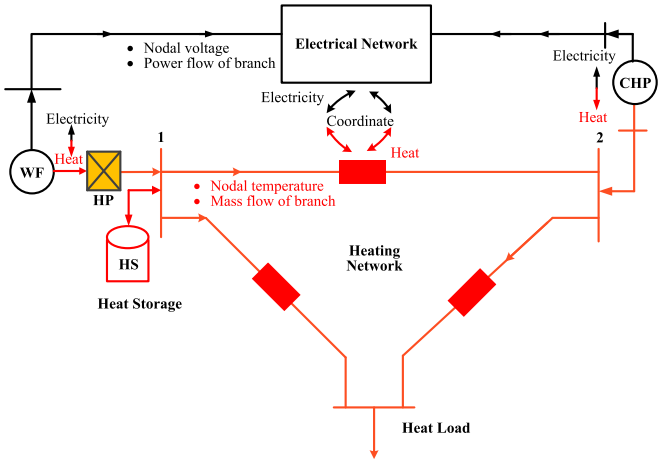

ARTICLE INFO

Article history:
Received 29 May 2015
Received in revised form 6 October 2015
Accepted 7 October 2015
Available online 26 October 2015

Keywords:
Integrated energy system
Combined electricity and heat
Intermittent renewable sources
Optimal operation of energy system
Decomposition–coordination algorithm

ABSTRACT

The integration of electrical and heating systems has great potential to enhance the flexibility of power systems to accommodate more renewable power such as the wind and solar. This study was to investigate an optimal way to integrate the energy of both systems in urban areas. The amount of energy conversion between the electrical system and heating system was optimally decided so that the demand within both systems could be met at the least operational cost. Besides, the best node to join with the electrical system and heating system was chosen by consideration of the energy transmission loss. The mathematical formulation of the optimization problem was detailed as a large-scale non-linear program (LSNLP) in this paper. A decomposition–coordination algorithm was proposed to solve this LSNLP. At last, a 6-bus electrical power system with 31-node heating transmission system was studied to demonstrate the effectiveness of the proposed solution. The results showed that coordinated optimization of the energy distribution have significant benefits for reducing wind curtailment, operation cost, and energy losses. The proposed model and methodology could help system operators with decision support in the emerging integrated energy systems.

© 2015 Elsevier Ltd. All rights reserved.

* Corresponding author at: College of Electrical Engineering, Guangxi University, Nanning 530004, China.
E-mail address: happyjinghua@163.com (J. Li).

http://dx.doi.org/10.1016/j.apenergy.2015.10.054
0306-2619/© 2015 Elsevier Ltd. All rights reserved.

Nomenclature

Heating system

Indices

T	heat system
CHP, HS, HP	combined heat and power plant, heat storage, heat pump

Parameters

B^{T}_{num}, N^{T}_{num}	number of branches and nodes
S^{Heat}_{num} , S^{CHP}_{num}, S^{HP}_{num}, S^{HS}_{num}	number of heat sources, CHP, HP, and HS
A, B	incidence matrix, circuit matrix
α	cost coefficient of thermal power
c	the specific heat capacity of water
γ, l	heat loss coefficient of the branch, length of the branch
R_1, R_2	resistance of channel and insulation material (m °C/W)
β	additional heat loss coefficient of pipe auxiliaries, valve, and compensator
L	heat load of node (kW)
BQ^{min}, BQ^{max}	minimum, maximum mass flow rate of branch (t/h)
$SP^{HP,min}$, $SP^{HP,max}$	minimum, maximum thermal power of HP (kW)
$SP^{CHP,min}$, $SP^{CHP,max}$	minimum, maximum thermal power of CHP (kW)
$SP^{HS,min}$, $SP^{HS,max}$	minimum, maximum thermal power of HS (kW)
t^{Back}, t^{min}, t^{max}, t_0	temperature of return water, minimum and maximum temperature of node, ambient environment temperature (°C)
$SQ^{HS,max}$, SQ^{HS}_0	the capacity of HS (MW h), initial heat of HS (MW h)
K^e, η^l, η^e	heating coefficient of bromine refrigerator, heat loss coefficient and generated coefficient of CHP

Variables

BQ	mass flow rate of branch (t/h)
NQ	mass flow rate of nodal load (t/h)
e	temperature drop coefficient of branch (°C/(t/h))
Δt, t	temperature drop of branch, temperature (°C)
SQ = [SQ^{HP}; SQ^{CHP}; SQ^{HS}]	mass flow rate of HP, CHP, HS (t/h)
SP = [SP^{HP}; SP^{CHP}; SP^{HS}]	thermal power of HP, CHP, HS (kW)
d^{ch}, d^{dis}	charging and discharging state of HS

Electrical system

Indices

E	electrical system
G, Q, CHP, W	traditional thermal generator, reactive power source, combined heat and power plant, wind power

Parameters

B^{E}_{num}, N^{E}_{num}	number of branches and nodes
S_{num}	number of power sources
P^{ramp}	maximum power of the generator ramping up or down during a time interval
P^{min}; P^{max}	minimum, maximum output of active power sources
Q^{min}, Q^{max}	minimum, maximum output of reactive power sources
U^{min}, U^{max}	minimum, maximum limits of nodal voltage
P^{min}_{ij} ,P^{max}_{ij}	minimum, maximum limits of line's transmission power
$P^{W,av}$	the available wind power of wind farm
η_{W-T}	the conversion efficiency from wind power to heat
a_0, a_1, a_2	the cost coefficients of G

Variables

U, θ	magnitude of voltage, angle of voltage
P, Q	active power, reactive power
$P^{W,cur}$	wind curtailment before converting to heat
$\widetilde{P}^{W,cur}$	wind curtailment after converting to heat

1. Introduction

The climate change, fossil resource depletion, policy incentives as well as higher public awareness in term of sustainability have promoted the deployment of renewable generations, typically wind power and photovoltaic [1]. However, the intermittent and unpredictable features of the renewable generations raise the challenge to the power system operators to balance energy production and consumption. To accommodate the continuously increasing renewable sources connected to the grids, there is an urgent need to either enhance the system flexibility or mitigate the variability. Traditionally, when being operated independently, the power systems can acquire flexibility only through those fast-ramping generators [2,3], power flow regulations, electrical energy storages [4], and manageable loads [5,6]. Alternatively, the coordination single or multiple renewable sources in a certain region has been proved to be an effective way to mitigate the renewable's variability [7–9]. And together with a better energy management strategy the requirements to the system flexibility could be further reduced while with the energy adequacy guaranteed [10].

In recent years, the emerging technologies enhanced the interdependency of different energy systems. Research investigations and industrial practices have demonstrated the integrated energy systems (IES) could coordinate energy production and consumption in a broader scope, and hence improve the overall efficiency and sustainability of the energy utilization [11]. The integrated energy system consists of the electrical system, natural gas system, district heating system and electrified transportation system. The electrified vehicle can act as both a manageable load [12] and an energy carrier [13] to support the energy system operation. The power-to-gas plants, together with the gas-fired turbines can improve the dispatching ability of the renewable generations via temporal and spatial shifting [14]. The energy in the district heating systems may come from electrical heat pumps, solar power and co-generation of electricity, all of which are associated with electrical systems, and hence draws broad interests.

Extensive work has been done in optimal integration of electrical and heating systems. At the device level, the thermoelectric generators have been well modeled and optimized via both theoretical and experimental studies [15,16]. Some of the work focuses on providing reliable and sustainable electricity and heat to the residential demands such as buildings and communities [17,18]. In [19], a mixed-integer linear programming model has been developed for the integrated plan and evaluation of distributed energy systems. The analogy between the electrical circuit and heat transfer networks has been studied in [20]. At the macro level, computer tools have been developed to simulate and analyze the future integrated energy systems [21]. Taking Energy Plan [22] for example, it has been used in various regions for decision support on their development strategies [23]. However, the topologies of the heat and electrical networks are usually neglected for brevity.

This work focuses on the coordination of electrical system and heating system in urban areas considering network topologies. The optimal operation of the integrated heating and power system is mathematically formulated as a scaled nonlinear optimization problem. The objective is to minimize the operational costs for both electrical and heating system while at the same time maximizes the renewable energy consumed. In the constraints, the branch flow and nodal flow balance in both systems are considered as equality constraints. The operational limitations such as bus voltages, nodal temperatures, generation capacities are formed as inequality constraints in this paper. After the optimization problem is formulated, a decomposition–coordination algorithm is proposed to handle its scale and nonlinearity. The proposed method decouples the optimization problem into two sub-problems and solves them respectively. The boundary constraints are set according to the physical interface between these two systems. The major contributions of this paper are as follows:

- The optimal energy sources distribution of both systems is investigated. The amount of energy conversion between the electrical power system and heating system was optimally decided so that the energy demand of both systems could be met at the least operational cost.
- A detailed optimization operational model considering network constraints has been proposed. Besides, the proposed model can be extended for siting the HP at least energy transmission loss.
- A decomposition–coordination algorithm is proposed to solve the large-scale nonlinear optimization problem in accordance to the properties of the physical system, which can greatly reduce the computational complexity.

The remainder of the paper is organized as follows: Section 2 introduces the general framework of the integrated electrical and heating systems; Section 3 presents the detailed mathematical formulation of the optimal operation problem; Section 4 describes a decomposition–coordination algorithm that is applied to solve the optimization problem; Section 5 is the case studies and the concluding remarks are provided in Section 6.

2. Integration of the electrical and heating systems

Electricity and heat are two important energy demands in the daily life. This paper investigates the integrated systems combining the electricity and heat so as to more effective energy usage. A studied system is shown in Fig. 1.

In Fig. 1, the studied system consists of combined heat and power (CHP), wind farm (WF), heat storage (HS), heat pump (HP), and traditional thermal generator (G):

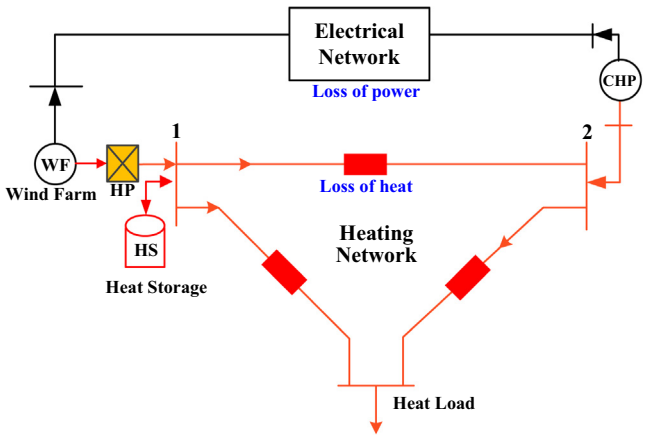

Fig. 1. The integrated system of electricity and heat.

- The CHP produce electricity and heat at the same time. It's an interface of the electrical and heating system. The demand of the heating system is mainly supplied by the CHP.
- The WF is directly connected with the electrical system and connected to the heating system via the HP. The excess wind power can be turned into thermal energy during the valley-electrical-load time periods to reduce the wind curtailment. In this sense, the heating system can be regarded as a large storage for the power system and the HP is used for energy conversion.
- The HS is also considered in this work to balance the heat inside the heating system. Usually, the heat can be stored when it is abundantly produced by the HP and CHP and released when heat demand is high. However, the heat in the HS is losing by time, so it is not suitable for storing the heat for long time.

Seen from above, by converting the excess wind power into the heating system, the curtailment of wind power can be reduced. Besides, by using wind power to supply heat demand, the fuel burned and the waste gas is reduced. However, the major operational challenge is that such integrated system is a closed loop operation system, as Fig. 1 shown. The challenges mainly embody in the following three aspects: (1) The production and consumption in both heating and electrical systems have to be balanced at any time; (2) The two sub-systems are interacted with the energy conversion devices, such as HP and CHP; (3) The capacities of the transmission lines and pipes limit the desired energy delivery.

Hence, the network topologies are needed to consider and those energy conversion devices are spatially and temporally coordinated so that the demand within both systems could be met at the lowest operational cost.

3. Mathematical formulations of the optimization problem

The optimization problem for the integrated electrical and heating systems is formulated in this section. The objective function is set as the operational cost. And the nodal energy flow equations are modeled as equality constraints. The operational limits of the both systems can be categorized as follows. First, the limits to the branches include flow capacities through the pipes and lines, the maximum temperature drop along with the pipeline. Second, the nodal operation limits keep the temperatures and voltages within a reasonable range to maintain the system security. Third, the devices such as G, CHP, WF, HS and HP should be within their capacities. The objective function and three categories of constraints are described in detail in following subsections.

3.1. The operational cost of the integrated electrical and heating system

The objective of the optimal operation is to minimize the total operation costs F^{Total} consisting of electrical system F^{E} and heating system F^{T} throughout the whole operational horizons (τ_{num}), as shown in (1). Eqs. (2) and (3) indicate the fuel cost for electricity and heat production, respectively. Wind power is considered as free so that it will be consumed as much as possible.

$$F^{\text{Total}} = F^{\text{E}} + F^{\text{T}} \tag{1}$$

$$F^{\text{E}} = \sum_{\tau=1}^{\tau_{\text{num}}} \sum_{s=1}^{S_{\text{num}}^{\text{G}}} a_{0,s} + a_{1,s} \times P_{s,\tau}^{\text{G}} + a_{2,s} \times \left(P_{s,\tau}^{\text{G}}\right)^2 \tag{2}$$

$$F^{\text{T}} = \sum_{\tau=1}^{\tau_{\text{num}}} \sum_{s=1}^{S_{\text{num}}^{\text{Heat}}} \alpha_s \times \text{SP}_{s,\tau} \tag{3}$$

The objective function is subjected to the following constraints.

3.2. The operational constraints of heating system

In the steady state, the mass flow balance at node i in the time period τ is formulated as (4) [24]. For each node, positive mass flow rate indicates the inflow and negative mass flow rate indicates the outflow. a_{ij} is the element of incidence matrix A. $SQ^{CHP}_{i,\tau}$, $SQ^{W}_{i,\tau}$, $SQ^{HS}_{i,\tau}$, $BQ_{i,\tau}$ are the mass flow rate of CHP, HP, HS, and pipe in time period τ, respectively. $NQ_{i,\tau}$ is the mass flow rate of heat load in the time period τ.

$$\sum_{j=1}^{B_{num}} a_{ij} \times BQ_{i,\tau} + SQ^{CHP}_{i,\tau} + SQ^{HP}_{i,\tau} + \left(T\_d^{dis}_{i,\tau} - T\_d^{ch}_{i,\tau}\right) \times SQ^{HS}_{i,\tau} - NQ_{i,\tau} = 0 \tag{4}$$

The conversional relationships between the mass flow rate (t/h) and thermal power (kW) are shown by (5) [25]. Eq. (5.a) is for the heat load and (5.b) is for the heat source. c is the specific heat capacity of water, 4.2 kJ kg^{-1} C^{-1}.

$$NQ_{i,\tau} \times \left(t_{i,\tau} - t^{Back}_{i,\tau}\right) \times c - 3.6 \times L_{i,\tau} = 0 \quad i = 1,2,\ldots,N^{T}_{num} \tag{5.a}$$

$$SQ_{i,\tau} \times \left(t_{i,\tau} - t^{Back}_{i,\tau}\right) \times c - 3.6 \times SP_{i,\tau} = 0 \quad i = 1,2,\ldots,S^{T}_{num} \tag{5.b}$$

In the heating system, the energy carrier could be both steam and liquid water. In this paper, only the heat water is considered for brevity. Eq. (6.a) interprets the temperature drop along with the pipeline. The temperature drop coefficient $e_{j,\tau}$ is determined by the mass flow rate of the branch $BQ_{j,\tau}$, the length of the branch l_j, and the heat loss coefficient of the branch γ_j, as shown in (6.b). The heat loss coefficient γ_j is determined by the temperatures of the water in pipe t_j, the ambient environment temperature t_0, the resistance of channel R_1, and the resistance of insulation material R_2, as shown in (6.c) [26].

$$\Delta t_{j,\tau} = e_{j,\tau} \times BQ_{j,\tau} \tag{6.a}$$

$$1000 \times c^{T} \times \left(BQ_{j,\tau}\right)^2 \times e_{j,\tau} - 3.6 \times \gamma_j \times (1+\beta) \times l_j = 0 \tag{6.b}$$

$$\gamma_j = \frac{t_j - t_0}{R_1 + R_2} \quad j = 1,2,\ldots,B^{T}_{num} \tag{6.c}$$

To simplify the problem, in this paper, the heat loss coefficient γ_j is approximate as a constant. γ_j is chosen according the temperatures of water and the ambient environment by the experience of operation.

Eq. (7) represents the operational limitations of the heating system including the nodal temperature, branch flow capacity, power of CHP, HP, and HS.

$$t^{min}_{i} \leqslant t_{i,\tau} \leqslant t^{max}_{i}, \quad i = 1,2,\ldots,N_{num} \tag{7.a}$$

$$BQ^{min}_{j} \leqslant BQ_{j,\tau} \leqslant BQ^{max}_{j}, \quad j = 1,2,\ldots,B_{num} \tag{7.b}$$

$$SP^{CHP,min}_{k} \leqslant SP^{CHP}_{k} \leqslant SP^{CHP,max}_{k}, \quad k = 1,2,\ldots,S^{CHP}_{num} \tag{7.c}$$

$$SP^{W,min}_{k} \leqslant SP^{W}_{k} \leqslant SP^{W,max}_{k}, \quad k = 1,2,\ldots,S^{W}_{num} \tag{7.d}$$

$$SP^{HS,min}_{k} \leqslant SP^{HS}_{k} \leqslant SP^{HS,max}_{k}, \quad k = 1,2,\ldots,S^{HS}_{num} \tag{7.e}$$

Eq. (8) represents the operational constraints of heat storage. Indicated by (8), the mass flow rate of the heat storage cannot exceed its capacity. Eq. (8.b) is the limitation of heat storage's state, which ensures that the charge state $d^{ch}_{i,\tau'}$ and the discharge state $d^{dis}_{i,\tau'}$ of the heat storage couldn't happen in the same time period.

$$0 \leqslant SQ^{HS}_{i,0} + \sum_{\tau'=1}^{\tau} (d^{ch}_{i,\tau'} - d^{dis}_{i,\tau'}) \times SQ^{HS}_{i,\tau'} \leqslant SQ^{HS,max}_{i} \tag{8.a}$$

$$d^{dis}_{i,\tau'} + d^{ch}_{i,\tau'} \leqslant 1 \quad \left(d^{dis}_{i,\tau'}, d^{ch}_{i,\tau'} = 0 \text{ or } 1\right) \tag{8.b}$$

3.3. The operational constraints of electrical system

The electrical system constraints include active and reactive power balance, nodal voltage, the capacity of traditional generators and lines, and the curtailment of wind power. The detail of each constraint is described as follow.

Nodal active and reactive power balance are considered in this paper, formulated as (9). In each node, the electrical power injection needs to be equal to power demand plus losses. Besides, the voltage of each node is limited by (10).

$$P^{G}_{i',\tau} + P^{W}_{i',\tau} + P^{CHP}_{i',\tau} - P^{Load}_{i',\tau} - U_{i',\tau} \sum_{j' \in i'} U_{j',\tau} (G_{i'j'} \cos\theta_{i'j',\tau} + B_{i'j'} \sin\theta_{i'j',\tau}) = 0 \tag{9.a}$$

$$Q^{G}_{i',\tau} - Q^{Load}_{i',\tau} + U_{i',\tau} \sum_{j' \in i'} U_{j',\tau} (G_{i'j'} \sin\theta_{i'j',\tau} + B_{i'j'} \cos\theta_{i'j',\tau}) = 0 \tag{9.b}$$

$$U^{min}_{i'} \leqslant U_{i',\tau} \leqslant U^{max}_{i'} \quad i' = 1,2,\ldots,N^{E}_{num} \tag{10}$$

In the electrical system, active power and reactive power of each source are restricted by the lower and upper bounds, including thermal generators, CHP, and wind farm. Also, the limitations of the ramping up/down power during each time interval are considered, as shown in (11).

$$P^{G,min}_{i'} \leqslant P^{G}_{i',\tau} \leqslant P^{G,max}_{i'}, \quad i' = 1,2,\ldots,S^{G}_{num} \tag{11.a}$$

$$|P^{G}_{i',\tau} - P^{G}_{i',\tau-1}| \leqslant P^{G,ramp}_{i'}, \quad i' = 1,2,\ldots,S^{G}_{num} \tag{11.b}$$

$$P^{CHP,min}_{i'} \leqslant P^{CHP}_{i',\tau} \leqslant P^{CHP,max}_{i'}, \quad i' = 1,2,\ldots,S^{CHP}_{num} \tag{11.c}$$

$$|P^{CHP}_{i',\tau} - P^{CHP}_{i',\tau-1}| \leqslant P^{CHP,ramp}_{i'}, \quad i' = 1,2,\ldots,S^{CHP}_{num} \tag{11.d}$$

$$0 \leqslant P^{W}_{i',\tau} \leqslant P^{W,av}_{i',\tau}, \quad i' = 1,2,\ldots,S^{W}_{num} \tag{11.e}$$

$$Q^{G,min}_{i'} \leqslant Q^{G}_{i',\tau} \leqslant Q^{G,max}_{i'}, \quad i' = 1,2,\ldots,S^{Q}_{num} \tag{11.f}$$

Here, we define the curtailment of wind power $P^{W,cur}_{i',\tau}$ equals to the available wind power $P^{W,av}_{i'}$ minus the wind power accommodate $P^{W}_{i',\tau}$, as shown in (12).

$$P^{W,cur}_{i',\tau} = P^{W,av}_{i'} - P^{W}_{i',\tau}, 0 \leqslant P^{W,cur}_{i',\tau} \leqslant P^{W,av}_{i'}, \ i' = 1,2,\ldots,S^{W}_{num} \tag{12}$$

Besides, the line transmission limits are considered, formulated as (13). The transfer power from i' to j' should not exceed the line transfer capacities for security consideration.

$$P^{min}_{i'j'} \leqslant (U_{i',\tau})^2 G_{i'j'} + U_{i',\tau} U_{j',\tau} (G_{i'j'} \cos\theta_{i'j',\tau} + B_{i'j'} \sin\theta_{i'j',\tau}) \leqslant P^{max}_{i'j'} \tag{13}$$

3.4. The constraints of the interfaces between electrical and heating system

- The conversional relationship of wind power, heat, and heat storage

To save the excess wind power during the valley load periods, the excess wind power is converted into heat. The obtained heat

can be stored in HS or directly injected into the heating system. Due to the limited capacities of HP and HS, may be not all the surplus wind power can be utilized and there is still wind curtailment $\tilde{P}^{W,Cur}_{i',\tau}$, shown as (14).

$$\eta_{W-T}\times\left(P^{W,Cur}_{i',\tau}-\tilde{P}^{W,Cur}_{i',\tau}\right)=d^{ch}_{i'}\times SP^{HS}_{i',\tau}+SP^{HP}_{i',\tau},\quad i'=1,2,\ldots,S^{W}_{num} \tag{14}$$

- The cogeneration of the heat and power (CHP)

The cogeneration unit can generate electricity and heat. The relationship between the output of electricity and heat is formulated as (15).

$$SP^{CHP}_{i',\tau}=P^{CHP}_{i',\tau}\times(1-\eta^{e}_{i',\tau}-\eta^{l}_{i'})/\eta^{e}_{i',\tau'}\times K^{e} \tag{15}$$

4. Decomposition–coordination algorithm for solving the problem

The mathematic formulation of the optimization problem introduced in the previous sections can be summarized as (16). It's a large-scale nonlinear program. Mathematically, it is very difficult to get the global optimal solution. To solve this problem, a decom position–coordination algorithm is proposed to get a sub-optimal solution. The basic idea of the methodology is to divide the optimization problem into two sub-optimizations and iteratively solve them to convergence to the optimal solution.

$$\begin{aligned}&\min\ (1)-(3)\\&s.t.\\&\begin{cases}\text{heating system constraints }(4)-(8)\\\text{electrical system constraints }(9)-(13)\\\text{interfaced constraints }(14)-(15)\end{cases}\end{aligned} \tag{16}$$

4.1. Decomposition of the problem

The formulations (16) can be written in a generalized form as (17).

$$\begin{aligned}&\sum_{\tau=1}^{\tau_{num}}\boldsymbol{f}_{\tau}\left(\boldsymbol{X}^{E}_{\tau},\boldsymbol{X}^{T}_{\tau}\right)\\&s.t.\ \boldsymbol{h}\left(\boldsymbol{X}^{E}_{\tau},\boldsymbol{X}^{T}_{\tau}\right)=\boldsymbol{0}\\&\quad\boldsymbol{g}(\boldsymbol{X}^{E}_{\tau},\boldsymbol{X}^{T}_{\tau})\leqslant\boldsymbol{0}\end{aligned} \tag{17}$$

In (17), the variables in optimization problem have been divided into 2 groups, $\boldsymbol{X}^{E}_{\tau}$ and $\boldsymbol{X}^{T}_{\tau}$ representing the variables in the electrical and heating system, respectively. For example, the mass flow rate of pipe BQ and nodal temperature t belong to $\boldsymbol{X}^{T}_{\tau}$; the active power of generator P and nodal voltage U belong to $\boldsymbol{X}^{E}_{\tau}$. $\boldsymbol{h}(\cdot)$ and $\boldsymbol{g}(\cdot)$ are the equality and inequality constraints, respectively.

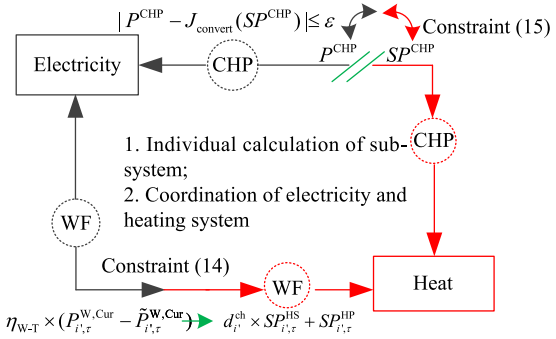

Fig. 2. Illustration of the decomposition–coordination method.

Let $\boldsymbol{X}^{E,B}$ and $\boldsymbol{X}^{T,B}$ denote the variables at the boundary of the electrical and heating system; $\boldsymbol{X}^{E,I}$ and $\boldsymbol{X}^{T,I}$ are the inner variables of the electrical and heating system. As Fig. 2 shows, heat generated by CHP ($SP^{CHP}_{i',\tau}$) and electricity generated by CHP ($P^{CHP}_{i',\tau}$), wind power curtailment ($P^{W,cur}_{i',\tau}$) and heat generated by wind power ($SP^{HP}_{i',\tau}$) are the boundary variables interacting between the electrical and heat system.

Choose the variables from the boundary variables to form the coordinated variables pairs, which are used for adjusting to satisfy interfaced constraints. The coordinated variables pairs are denoted as ($\boldsymbol{X}^{E,C}$, $\boldsymbol{X}^{T,C}$). We choose ($P^{CHP}_{i',\tau}$, $SP^{CHP}_{i',\tau}$) as the coordinated variables in this paper.

Based on the classification of the variables as described above, the problem (17) can be divided into two sub-problems, as shown in (18) and (19), representing the electrical and heating system respectively. The (20) is the boundary constraints denoted as $J_{convert}$, including conversional equations between boundary variables of the electrical and heating system. In the problem (16), (14) and (15) are the boundary constraints.

$$\begin{aligned}&\sum_{\tau=1}^{\tau_{num}}\boldsymbol{f}^{E}_{\tau}(\boldsymbol{X}^{E,I}_{\tau},\boldsymbol{X}^{E,B}_{\tau},\boldsymbol{X}^{E,C}_{\tau})\\&s.t.\ \boldsymbol{h}^{E}(\boldsymbol{X}^{E,I}_{\tau},\boldsymbol{X}^{E,B}_{\tau},\boldsymbol{X}^{E,C}_{\tau})=\boldsymbol{0}\\&\quad\boldsymbol{g}^{E}(\boldsymbol{X}^{E,I}_{\tau},\boldsymbol{X}^{E,B}_{\tau},\boldsymbol{X}^{E,C}_{\tau})\leqslant\boldsymbol{0}\end{aligned} \tag{18}$$

$$\begin{aligned}&\sum_{\tau=1}^{\tau_{num}}\boldsymbol{f}^{T}_{\tau}\left(\boldsymbol{X}^{T,I}_{\tau},\boldsymbol{X}^{T,B}_{\tau},\boldsymbol{X}^{T,C}_{\tau}\right)\\&s.t.\ \boldsymbol{h}^{T}\left(\boldsymbol{X}^{T,I}_{\tau},\boldsymbol{X}^{T,B}_{\tau},\boldsymbol{X}^{T,C}_{\tau}\right)=\boldsymbol{0}\\&\quad\boldsymbol{g}^{T}\left(\boldsymbol{X}^{T,I}_{\tau},\boldsymbol{X}^{T,B}_{\tau},\boldsymbol{X}^{T,C}_{\tau}\right)\leqslant\boldsymbol{0}\end{aligned} \tag{19}$$

$$\begin{cases}\boldsymbol{X}^{E,B}_{\tau}=J_{convert}\left(\boldsymbol{X}^{T,B}_{\tau}\right)\\\boldsymbol{X}^{E,C}_{\tau}=J_{convert}\left(\boldsymbol{X}^{T,C}_{\tau}\right)\end{cases} \tag{20}$$

4.2. Coordination of the sub-problems

After the decomposition of the problem, the sub-problems (18) and (19) are calculated individually, which greatly reduce the calculation scale. Next, by iteratively adjusting the coordinated variables from the results of sub-problems, the boundary constraints (20) will be satisfied. The procedures of the iterative coordination are as following.

Initialization: Let $k=0$, given initial value of the coordination variable in electrical system $\boldsymbol{X}^{E,C(k)}_{\tau}$;

Step 1: Substitute $\boldsymbol{X}^{E,C(k)}_{\tau}$ into (18) and solve it, then the value of the boundary variable in electrical system $\boldsymbol{X}^{E,B(k)}_{\tau}$ is obtained from the optimal solution of (18);

Step 2: Substitute $\boldsymbol{X}^{E,B(k)}_{\tau}$ and $\boldsymbol{X}^{E,C(k)}_{\tau}$ into (20), then boundary value in heating system $\boldsymbol{X}^{T,B(k)}_{\tau}$ and coordination value in heating system $\boldsymbol{X}^{T,C(k)}_{\tau}$ can be calculated;

Step 3: Substitute $\boldsymbol{X}^{T,B(k)}_{\tau}$ into (19) and solve it, then $\boldsymbol{X}^{T,C(k+1)}_{\tau}$ is obtained from the solution of (19);

Step 4: Calculate $|\boldsymbol{X}^{T,C(k+1)}_{\tau}-\boldsymbol{X}^{T,C(k)}_{\tau}|\leqslant\varepsilon$ to see if it is less than the pre-set threshold value ε. If yes, it means the boundary con-

strains (20) are satisfied, and then stop and output the results; else let $\boldsymbol{X}_{\tau}^{\mathrm{E,C}(k+1)} = J_{\mathrm{convert}}(\boldsymbol{X}_{\tau}^{\mathrm{T,C}(k+1)})$, $k = k + 1$ and turn to Step 1.

The above iterative steps can be explained by Fig. 2. At each iteration, the boundary constraint (14) is forced to satisfy by letting the heat $d_{i'}^{\mathrm{ch}} \times \mathrm{SP}_{i',\tau}^{\mathrm{HS}} + \mathrm{SP}_{i',\tau}^{\mathrm{HP}}$ equal to the $\eta_{\mathrm{W-T}} \times (P_{i',\tau}^{\mathrm{W,Cur}} - \widetilde{P}_{i',\tau}^{\mathrm{W,Cur}})$. And then adjust the coordination pairs $(P_{i',\tau}^{\mathrm{CHP}}, \mathrm{SP}_{i',\tau}^{\mathrm{CHP}})$ to satisfy boundary constraint (15). If the boundary constraint (15) is satisfied, that is $|P^{\mathrm{CHP}} - J_{\mathrm{convert}}(\mathrm{SP}^{\mathrm{CHP}})| \leqslant \varepsilon$, and then the iteration is end and output the optimum results. In this paper, ε is set to 10^{-5}.

The proposed algorithm divides the whole system into two sub-systems and optimizes both sub-systems iteratively. Mathematically, by doing so, a large optimization problem can be decoupled into small ones and solved respectively. This algorithm has the significant meaning with the increasing complexity of the modern energy systems. Meanwhile, though being decomposed, the two systems are actually interconnected by the interface constrains.

5. Numerical simulations

5.1. Description of the simulation system

A test case studied in this work is shown in Fig. 3. The heating system is from a city of China [27], including 30 pipes and 31 nodes. The surplus wind power can be converted to heat that is directly injected into the heating network or stored in heat storage. Generally, to reduce the heat loss, it is better to use the heat as soon as possible. The detailed parameters for the devices and network topologies are given in Tables A1–A8 in Appendix A, including electrical generator, CHP, HS, HP, wind power and electrical load, heat load, as well as electrical and heat network. The heat loss coefficient is set to 60 W/m in this case.

5.2. Simulation results

5.2.1. Iteration process by the decomposition–coordination algorithm

Fig. 4 illustrates the iteration process of the calculation in the 2nd time period. The iterative gap is measured by the difference of the CHP output in two sub-optimizations in the each iteration. Seen from Fig. 4(a), the iterative gap is less than the preset tolerance 10^{-5} after 15 iterations.

During the iteration process, the amount of energy conversion between the electrical system and heating system are optimized to satisfy the load. In Fig. 4(b), the heat produced by the wind

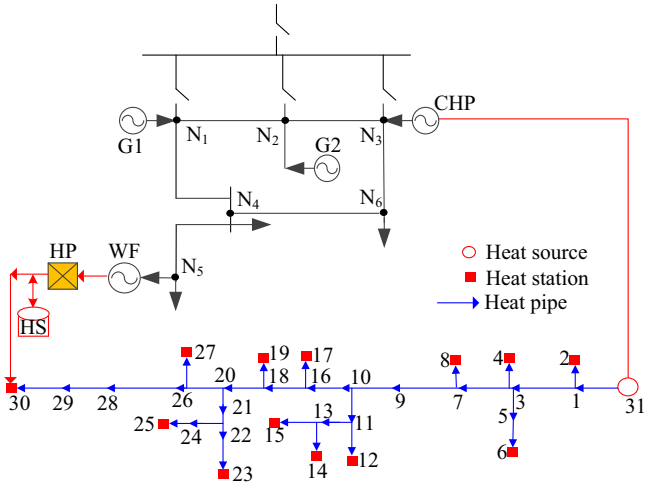

Fig. 3. Studied case of the integration of electrical and heating systems.

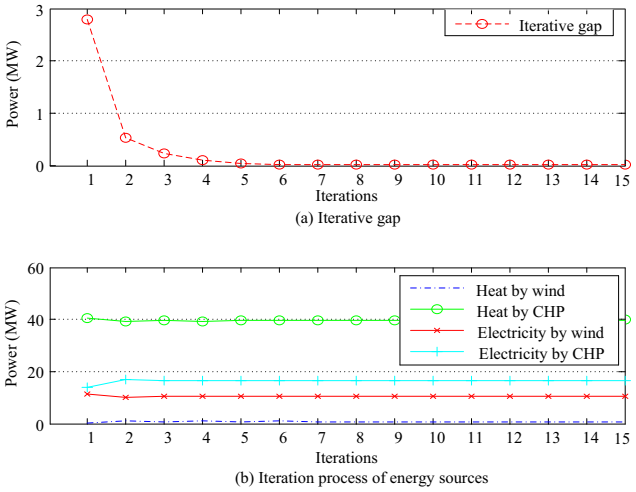

Fig. 4. Iteration process of the 2nd time period.

increases at the first iteration and then decreases to be stable after the 6th iteration. Correspondingly, the electricity from wind decreases at the first iteration and then increases to be stable. The heat produced by CHP decreases at the first iteration and then increases to be stable. The optimal amount of heat produced by the wind, heat produced by CHP, electricity produced by the wind, and electricity produced by CHP are obtained after 15 iterations.

5.2.2. Optimal output of the energy sources

Fig. 5 shows the optimal hourly output of electrical and heating power sources throughout the 24 time periods, at the lowest operational cost.

In Fig. 5(a), the peak load periods of the electrical system are the valley load periods of the heating system. As Fig. 5(b) showing,

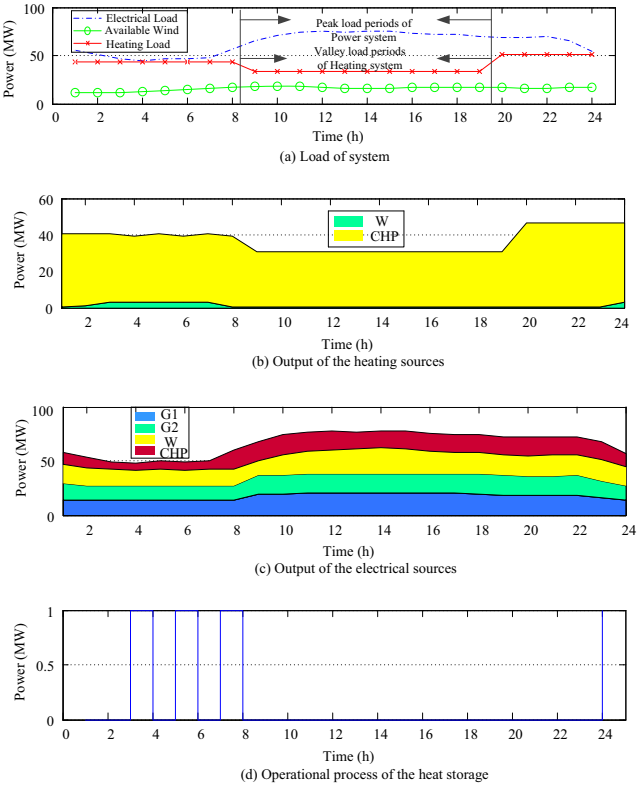

Fig. 5. Optimal dispatch of sources in electrical and heating systems.

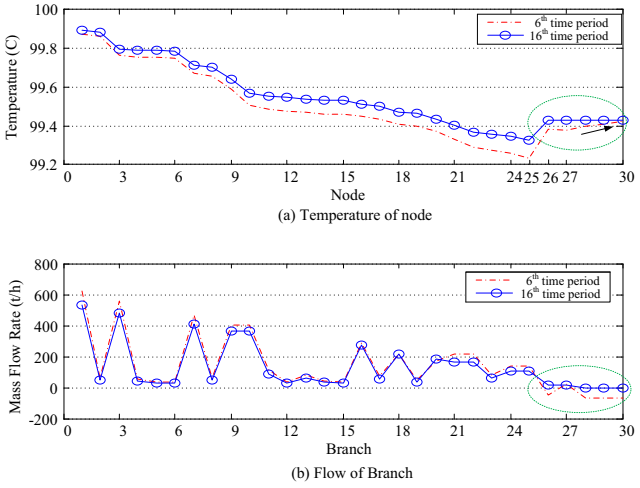

Fig. 6. Temperature drop along the pipes.

during the 9th–23rd time periods, there is no heat produced by wind power. However, during the periods 1st–8th, the load of the power system is low and the excess wind power is converted into heat, which reduces the wind power curtailment. Besides, it can be seen from Fig. 5(c) that the generation of G1 and G2 is flat. The heating system buffers the production and demand variation and helps to improve the operational efficiency of the thermal units. Fig. 5(d) is the operational process of the heat storage. The HS charges at 3, 5, 7 time periods to reduce the wind curtailment and discharges at 4, 6, 8 time periods to supply the heat load.

5.2.3. Energy distribution in heating network

To show the influence of wind power, Fig. 6 compares the energy distribution in the heating network with and without heat generated by wind power.

The curve of the 6th time period is the result with heat generated by wind power while the curve of 16th time period is the result without heat generated by wind power. Seen from Fig. 6 (a), the temperature is decreasing form Node 1 to Node 25 in the 6th and16th time period. The temperature of Node 26 is higher than Node 25, because Node 25 and Node 26 are not along the same transmissions direction. Compared with the 16th time period, in the 6th time period, the temperature from Node 26 to Node 30 is gradually increasing because there is heat by wind power

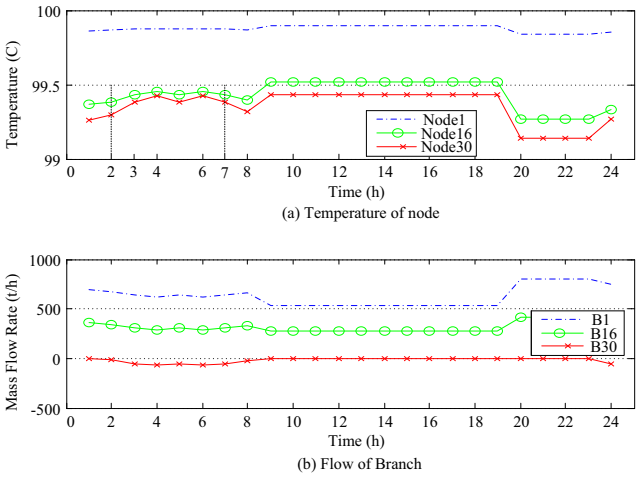

Fig. 7. Nodal temperature and branch's flow in heating system.

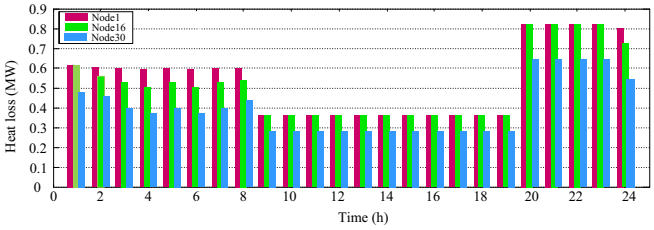

Fig. 8. Comparison of heat losses by connecting the wind power at different nodes.

injected into Node 30. Fig. 6(b) is the corresponding mass flow rate of the branches.

Fig. 7 shows the distribution of nodal temperature and branch flow in the heating system throughout the 24 time periods. For convenient explanation, we choose Node 1, Node 16, and Node 30; Branch 1, Branch 16, and Branch 30 for showing, which are the first node, middle node, and last node; first pipeline, middle pipeline, and last pipeline respectively. Seen from Fig. 7(a), the temperature of the first node is highest, the middle node is middle, and the last node is lowest. It means that the heat is losing during the process of transmission. Also in Fig. 7(a), we can see that during the periods 3rd–7th, the temperature of Node 30 is near Node 16. That is because during these time periods, there is heat produced by wind power injected into Node 30. Correspondingly, we can see from Fig. 7(b), the mass flow rate of the Branch 30 is negative because the heat flows from Node 30 to Node 29, while not the positive direction assumed from Node 29 to Node 30.

5.3. Optimal location of the HP in the heating system

In this section, we analyze the best node to locate the HP considering heat loss. The heat loss is different when the HP injected into different nodes, which gives the important information for choosing the best node to connect the HP with the heating system. In order to compare the heat loss by connecting the HP with different nodes, we have carried out the tests by connecting the HP at the begin (Node 1), middle (Node 16), and end (Node 30) of the heating system. Fig. 8 shows the corresponding heat loss.

Seen from Fig. 8, the heat loss is the least if we connect the HP at Node 30 of the heating system, where is the end of the heating network. It's because that there is a long pipe (pipe 28) near the end of the heating network. The length of pipe 28 is 2780 m. The heat supplied path from Node 1 or Node 16 to pipe 28 is far, which

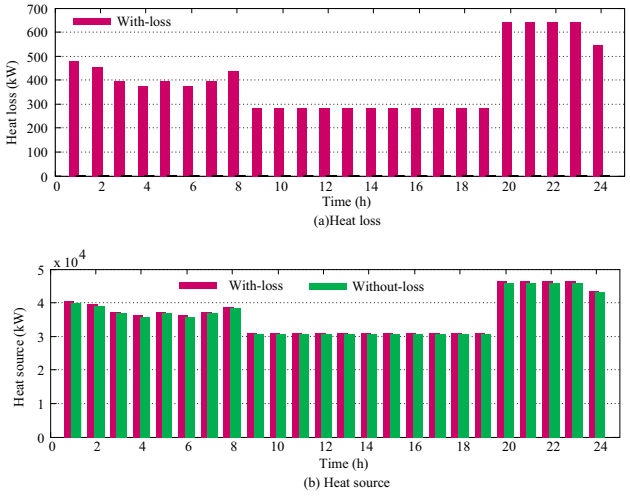

Fig. 9. Comparison results with and without consideration heating network loss.

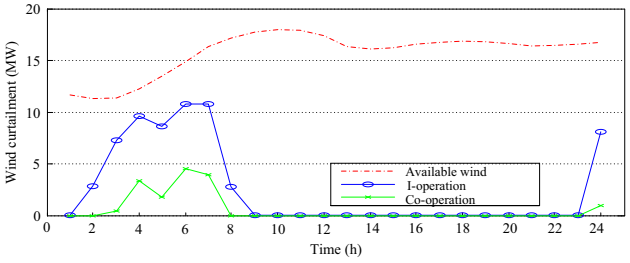

Fig. 10. Comparisons of the wind curtailment with Co-operation and I-operation.

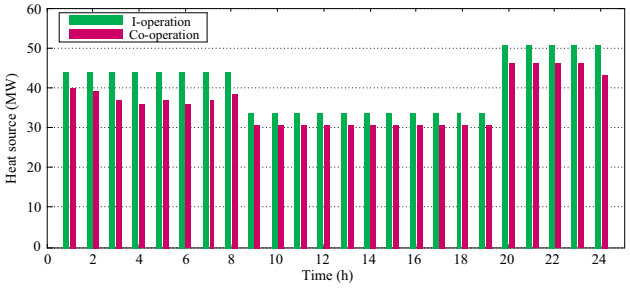

Fig. 11. Comparisons of the requirement of source with Co-operation and I-operation.

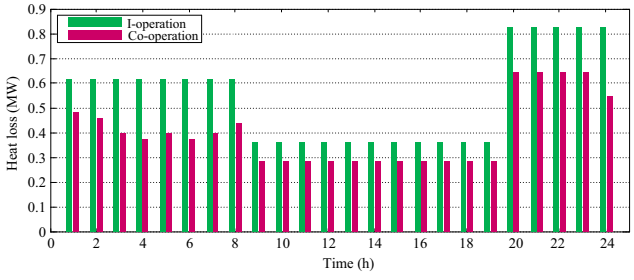

Fig. 12. Comparisons of the heat loss with Co-operation and I-operation.

causes the heat loss larger than the heat supplied from Node 30. Hence, based on the loss of network, we can choose the best place to connect the HP with the heating system is Node 30.

5.4. Comparative analysis with and without considering heating network loss

To show the significance of consideration of the energy transmission loss, the results with and without consideration of heat loss are compared. In Fig. 9(a), we show the comparative result

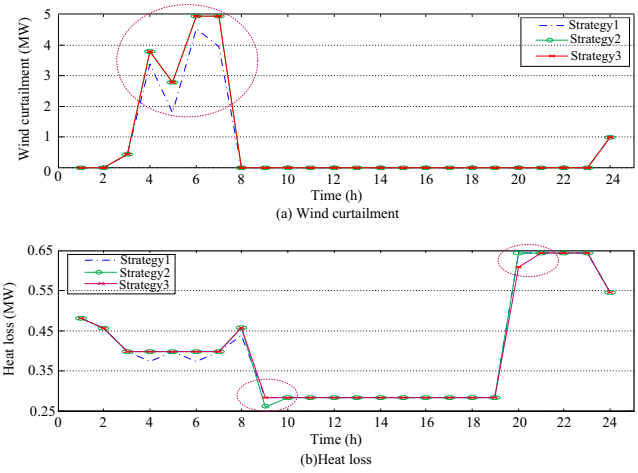

Fig. 14. Comparisons with different operational strategies.

Table A1
Parameters of electrical generator.

	Fuel cost			$\overline{T}^{on}$	$\overline{T}^{off}$	$\overline{P}$	$\overline{P}$	P^{climbe}
	c ($/MW h^2)	b ($/MW h)	c ($)	(h)	(h)	(MW)	(MW)	(MW)
F1	0.0533	11.669	2130	1	1	20	14	3
F2	0.0889	10.333	2000	1	1	18	12.6	3

of heat transmission loss. Without consideration of heat loss, the transmission loss is 0 throughout the 24 periods. So, if the heating network loss is not considered, we have no information to choose which node to connect HP with the heating system will result in less loss. Fig. 9(b) shows the output of heat sources with and without consideration heat transmission loss. Seen from Fig. 9(b), the output of heat source is less when the heat transmission loss is not considered, which may lead to the dispatch of the heat source is not enough for the heat load in the real time operation. Hence, it is necessary to consider the heating transmission loss, which is important for scheduling the heat sources and choosing the best place to connect HP with the heating system.

5.5. Comparative analysis of individual-operation and coordinated-operation

To verify the advantages of the integrated system of electricity and heat, comparative studies also have been conducted between individual operation (I-operation) and coordinated operation (Co-operation). Simulation results are shown and analyzed in this section, including curtailment of wind power, the minimum

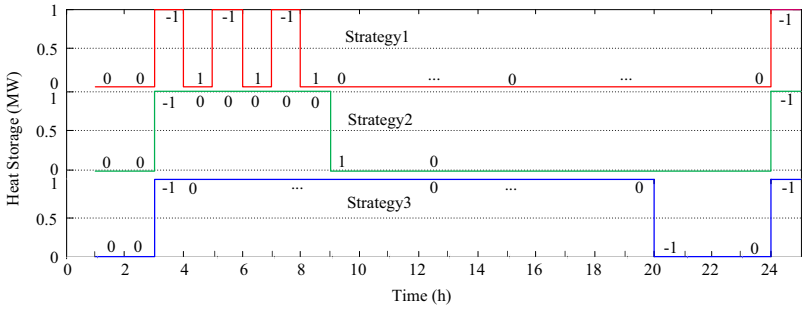

Fig. 13. The states of the heat storage in different operational strategies.

Table A2
Parameters of Combined Heat Power (CHP).

Number of CHP	$P^{CHP,max}$ (MW)	$P^{CHP,min}$ (MW)	$SP^{CHP,max}$ (MW)	$SP^{CHP,min}$ (MW)	K_e	η^e	η_l	c ($/MW h^2)	b ($/MW h)	c ($)	$\overline{T}^{on}$ (h)	$\overline{T}^{off}$ (h)	P^{climbe} (MW)
60	1	0	1.299	0	1.2	2.4	0.03	0.0741	10.833	2400	1	1	0.5

Table A3
Parameters of heat storage [28] and heat pump.

$SP^{HS,max}$ (MW)	$SP^{HS,min}$ (MW)	$SQ^{HS,max}$ (MW h)	SQ_0^{HS} (MWh)	$SP^{W,max}$ (MW)	$SP^{W,min}$ (MW)
1	0	1	0	3	0

requirement of heat source, and heat loss of the network. The 'I-operation' mode is conducted on the system shown in Fig. 3 by severing the connection between the heat and electrical system at Node 30.

5.5.1. Curtailment of wind power

Fig. 10 compares the results of wind power curtailment. See from Fig. 10, during the time periods of 9th–23rd, both operation ways have no wind curtailment. Because loads of electrical power system are high during these periods, and all the wind power has been used to balance the electrical power load. In the 2nd–8th time periods, the wind curtailment of Co-operation is much less than that of I-operation.

However, there is still wind curtailment of Co-operation, because the heat pump couldn't convert all the excess wind power to heat due to its power limitation. If the power of heat pump is large enough, the wind curtailment can be 0 in the Co-operation mode.

5.5.2. Minimum requirement of heat source

Fig. 11 compares the minimum requirements of the heat source. In Fig. 11, the requirements of the source of Co-operation way are less than the I-operation. The sum of the requirements of heat sources throughout 24 h is 873 MW in the mode of Co-operation, while 987 MW in the mode of I-operation, which is 11.55% higher than Co-operation.

5.5.3. Heat Loss of the network

Fig. 12 compares the heat loss of the heat network. In Fig. 12, the heat loss of Co-operation mode is less than which of I-operation. The sum of heat loss throughout 24 h is 9.54 MW in the mode of Co-operation, while 13.03 MW in the mode of I-operation, which is 26.8% higher than Co-operation.

5.5.4. Comparative analysis of different operational strategies of heat storage

To verify the operational strategy of heat storage in this paper (named as Strategy 1), we compare the results with other two operational strategies of heat storage. These two operational strategies are named as Strategy 2 and Strategy 3, respectively.

Table A5
Parameters of the bus load of electrical system.

Bus no	Ratio of the system load
4	0.2
5	0.4
6	0.4

Table A6
Parameters of the bus load of heat system.

Heat station	Node	Heat load (MW)		
		1–8 (h)	9–19 (h)	20–24 (h)
1	2	3.627	2.790	3.627
2	6	2.205	1.696	2.205
3	8	3.522	2.709	3.522
4	12	2.067	1.590	2.067
5	14	2.465	1.896	2.465
6	15	2.140	1.646	2.140
7	17	4.333	3.333	4.333
8	19	2.613	2.010	2.613
9	27	1.330	1.023	1.330
10	23	4.550	3.500	4.550
11	25	7.800	6.000	7.800
12	4	3.224	2.480	3.224
13	30	3.952	3.040	3.952

In Strategy 2, we let the heat storage charge when there is wind curtailment and discharge when there is no wind curtailment. In Strategy 3, we let the heat storage charge when there is wind curtailment and discharge when the heat load is in the peak time periods. In this simulation, the power of the heat storage is 1 MW and its capacity is 1 MW h. We assume that the initial heat of the storage is 0 MW and the heat storage can charge from 0 to its capacity in an hour. The storage period is 1 day (24 h).

The operational processes of the heat storage of the three strategies are shown in Fig. 13. In Fig. 13, the numbers marked on the curve are the state of the heat storage. 1 represents discharge, −1 represents charge, and 0 represents no action. Seen from Fig. 13, in Strategy 1, the heat storage charges to full in the front hour and discharge in the next hour during the 3rd–9th time periods. During 10th–23rd time periods, due to no wind curtailment (shown in Fig. 14(a)), the state of the heat storage is 0. The heat storage is charging in the 24 time periods that wind power is abundant. Different from Strategy 1, in Strategy 2, the heat storage charges only in the 3rd and discharges until the 9th time period, because there is wind curtailment in the 4th–8th time periods (Shown in Fig. 14 (a)). In Strategy 3, the storage charges to its capacity in the 3rd time periods and discharges in the peak load time period.

Table A4
Parameters of the wind power and electrical load (MW).

Time	1	2	3	4	5	6	7	8	9	10	11	12
Wind	11.7	11.3	11.3	12.3	13.5	14.9	16.4	17.2	17.7	18	17.9	17.4
Load	37	34	31	30	31.5	31	32	38	43.5	47.5	49.5	50
Time	13	14	15	16	17	18	19	20	21	22	23	24
Wind	16.3	16.1	16.2	16.6	16.8	16.9	16.8	16.6	16.4	16.5	16.6	16.8
Load	49.5	50	50	48.5	48	48	46.5	46	46	46.5	43.5	36

Table A7
Parameters of the branches of the electrical system.

No	From	To	R (p.u.)	X (p.u.)	B (p.u.)	$P_{i,j}^{max}$ (MW)	U^{max} (p.u.)	U^{min} (p.u.)	θ^{min} (deg)	θ^{max} (deg)
1	1	2	0.1	0.2	0.04	40	1.05	0.95	−360	360
2	1	4	0.05	0.2	0.04	60	1.05	0.95	−360	360
3	4	5	0.08	0.3	0.06	40	1.05	0.95	−360	360
4	2	3	0.05	0.25	0.06	40	1.05	0.95	−360	360
5	3	6	0.02	0.1	0.02	80	1.05	0.95	−360	360
6	4	6	0.2	0.4	0.08	100	1.05	0.95	−360	360

Table A8
Parameters of the branches of the heat system.

No	From	To	β	l_j (m)	t_i^{Back} (°C)	BQ_j^{min} (t/h)	BQ_j^{max} (t/h)	t_i^{min} (°C)	t_i^{max} (°C)
1	31	1	0.2	412	50	0	1000	95	100
2	1	2	0.2	259	50	0	1000	95	100
3	1	3	0.2	826	50	0	1000	95	100
4	3	4	0.2	90	50	0	1000	95	100
5	3	5	0.2	355	50	0	1000	95	100
6	5	6	0.2	203	50	0	1000	95	100
7	3	7	0.2	237	50	0	1000	95	100
8	7	8	0.2	90	50	0	1000	95	100
9	7	9	0.2	595	50	0	1000	95	100
10	9	10	0.2	265	50	0	1000	95	100
11	10	11	0.2	254	50	0	1000	95	100
12	11	12	0.2	249	50	0	1000	95	100
13	11	13	0.2	177	50	0	1000	95	100
14	13	14	0.2	74	50	0	1000	95	100
15	13	15	0.2	448.5	50	0	1000	95	100
16	10	16	0.2	233	50	0	1000	95	100
17	16	17	0.2	615	50	0	1000	95	100
18	16	18	0.2	180	50	0	1000	95	100
19	18	19	0.2	225	50	0	1000	95	100
20	18	20	0.2	316	50	0	1000	95	100
21	20	21	0.2	50	50	0	1000	95	100
22	21	22	0.2	249	50	0	1000	95	100
23	22	23	0.2	70	50	0	1000	95	100
24	22	24	0.2	403	50	0	1000	95	100
25	24	25	0.2	181	50	0	1000	95	100
26	20	26	0.2	530	50	0	1000	95	100
27	26	27	0.2	100	50	0	1000	95	100
28	26	28	0.2	2780	50	0	1000	95	100
29	28	29	0.2	330	50	0	1000	95	100
30	29	30	0.2	146	50	0	1000	95	100

To show the advantages of the Strategy 1, Fig. 14 compares the wind curtailment and heat loss of the three operational strategies. The wind curtailment of Strategy1 is the least in the 3rd–8th time periods because there is more wind power has been stored. Accordingly, the heat losses are the least of Strategy 1. It is because there is a lot of heat can be supplied from node 30 to its nearby load, the heat supplying path of which is much shorter than the heat supplied from node 1 to the node near 30. The results of the Strategy 2 and Strategy 3 are almost the same. Hence, the Strategy 1 has the best performance.

6. Conclusion

This paper investigates the optimal operation of the integrated electrical and heating system in urban areas. The optimal operation is mathematically formulated as a scaled nonlinear optimization problem considering the network constraints in both systems. By analyzing the network loss, the proposed model cannot be only used for optimizing operation strategies but also for best siting the electrical/heat storages and sources. The decomposition–coordination algorithm is proposed to solve the developed large-scale multi-stage optimization problem. Simulation results demonstrate the effectiveness of the proposed algorithm. Compared to the independent heating and electrical networks, the coordination can reduce the wind curtailment, fuel oil consumption, and heat losses. The model and method of this paper can be used to help system operators with decision support in the emerging integrated energy systems.

Acknowledgments

This work has been financially supported in part by the National Natural Science Foundation of China (NSFC 51377027) and by The National Basic Research Program of China (2013CB228205), and is carried out within the project of Development of a Secure, Economic and Environmentally-friendly Modern Power System (SEEFMPS) supported by the Danish Council for Strategic Research (DSF 09-067225).

Appendix A

See Tables A1–A8.

References

[1] Krause T, Andersson G, Frohlich K, Vaccaro A. Multiple-energy carriers: modeling of production, delivery, and consumption. Proc IEEE 2011;99(1):15–27.
[2] Roche R, Idoumghar L, Suryanarayanan S, Daggag M, Solacolu C, Miraoui A. A flexible and efficient multi-agent gas turbine power plant energy management system with economic and environmental constraints. Appl Energy 2013;101:644–54.
[3] Beevers D, Branchini L, Orlandini V, De Pascale A, Perez-Blanco H. Pumped hydro storage plants with improved operational flexibility using constant speed Francis runners. Appl Energy 2015;137:629–37.
[4] Cutter E, Haley B, Hargreaves J, Williams J. Utility scale energy storage and the need for flexible capacity metrics. Appl Energy 2014;124:274–82.
[5] Neves D, Pina A, Silva CA. Demand response modeling: a comparison between tools. Appl Energy 2015;146:288–97.
[6] Dupont B, Dietrich K, De Jonghe C, Ramos A, Belmans R. Impact of residential demand response on power system operation: a Belgian case study. Appl Energy 2014;122:1–10.
[7] Chong WT, Naghavi MS, Poh SC, Mahlia TMI, Pan KC. Techno-economic analysis of a wind–solar hybrid renewable energy system with rainwater collection feature for urban high-rise application. Appl Energy 2011;88(11):4067–77.
[8] Ma T, Yang HX, Lu L, Peng JQ. Technical feasibility study on a standalone hybrid solar-wind system with pumped hydro storage for a remote island in Hong Kong. Renew Energy 2014;69:7–15.
[9] Bhandari B, Lee KT, Lee CS, Song CK, Maskey RK, Ahn SH. A novel off-grid hybrid power system comprised of solar photovoltaic, wind, and hydro energy sources. Appl Energy 2014;133:236–42.
[10] Kroniger D, Madlener R. Hydrogen storage for wind parks: a real options evaluation for an optimal investment in more flexibility. Appl Energy 2014;136:931–46.
[11] Lee DH, Park SY, Hong JC, Choi SJ, Kim JW. Analysis of the energy and environmental effects of green car deployment by an integrating energy system model with a forecasting model. Appl Energy 2013;103:306–16.
[12] Kristoffersen TK, Capion K, Meibom P. Optimal charging of electric drive vehicles in a market environment. Appl Energy 2011;88(5):1940–8.
[13] Xi JQ, Li M, Xu M. Optimal energy management strategy for battery powered electric vehicles. Appl Energy 2014;134:332–41.
[14] Guandalini G, Campanari S, Romano MC. Power-to-gas plants and gas turbines for improved wind energy dispatchability: energy and economic assessment. Appl Energy 2015;147:117–30.
[15] Lombardi K, Ugursal VI, Beausoleil-Morrison I. Proposed improvements to a model for characterizing the electrical and thermal energy performance of Stirling engine micro-cogeneration devices based upon experimental observations. Appl Energy 2010;87(10):3271–82.

[16] Chen L, Lee JY. Effect of pulsed heat power on the thermal and electrical performances of a thermoelectric generator. Appl Energy 2015;150:138–49.
[17] Adam A, Fraga ES, Brett DJL. Options for residential building services design using fuel cell based micro-CHP and the potential for heat integration. Appl Energy 2015;138:685–94.
[18] Arsalis A, Kær SK, Nielsen MP. Modeling and optimization of a heat-pump-assisted high temperature proton exchange membrane fuel cell micro-combined-heat-and-power system for residential applications. Appl Energy 2015;147:569–81.
[19] Ren H, Gao W. A MILP model for integrated plan and evaluation of distributed energy systems. Appl Energy 2010;87(3):1001–14.
[20] Chen Q, Fu RH, Xu YC. Electrical circuit analogy for heat transfer analysis and optimization in heat exchanger networks. Appl Energy 2015;139:81–92.
[21] Connolly D, Lund H, Mathiesen BV, Leahy M. A review of computer tools for analysing the integration of renewable energy into various energy systems. Appl Energy 2010;87(4):1059–82.
[22] Lund H. Renewable energy systems. 2nd ed. Massachusetts: Academic Press; 2014.
[23] Mathiesen BV, Lund H, Karlsson K. 100% Renewable energy systems, climate mitigation and economic growth. Appl Energy 2011;88(2):488–501.
[24] Sivasakthivel T, Murugesan, Thomas HR. Optimization of operating parameters of ground source heat pump system for space heating and cooling by Taguchi method and utility concept. Appl Energy 2014;116:76–85.
[25] Vigants G, Blumberga D. Modelling of the district heating system's operation. Sci J Riga Techn Univ Environ Clim Technol 2011;6:132–7.
[26] Stubblefield MA, Pang SS, Cundy VA. Heat loss in insulated pipe – the influence of thermal contact resistance. A case study. Composites: Part B 1996;27B(1):85–93.
[27] Lu WR. Research on modelling method of thermodynamic calculation for heat-supply network [dissertation]. Master's thesis. North China Electric Power University; 2012.
[28] IEA-ETSAP and IRENA. Thermal energy storage – Technology Brief. 2012 Jan; WWW.etsap.org – WWW. Irena.org.

Publication **C1**

Paper title:

A Two-stage Stochastic Programming Approach for Operating Multi-energy Systems

Publication outlet:

First IEEE Conference on Energy Internet and Energy System Integration, 2017. In press.

List of authors:

Qing Zeng, Antonio J. Conejo, Zhe Chen, Jiakun Fang

A Two-stage Stochastic Programming Approach for Operating Multi-energy Systems

Qing Zeng, Jiakun Fang, Zhe Chen
Department of Energy Technology
Aalborg University
Aalborg, Denmark
qiz@et.aau.dk, jfa@et.aau.dk, zch@et.aau.dk

Antonio J. Conejo
Electrical and Computer Engineering Departments
The Ohio State University,
Columbus, USA
conejonavarro.1@osu.edu

***Abstract*—This paper provides a two-stage stochastic programming approach for joint operating multi-energy systems under uncertainty. Simulation is carried out in a test system to demonstrate the feasibility and efficiency of the proposed approach. The test energy system includes a gas subsystem with a gas source and a gas storage facility, and electricity subsystem that includes a coal-fired power plant, a combined heat and power unit and a power-to-gas facility, and a conventional district heating subsystem.**

Keywords— Multi-energy systems, power system, natural gas system, district heating system, stochastic programming.

I. INTRODUCTION

The integrated energy system, as a new type of regional energy system including multiple sub-systems such as electricity, gas, heating, and other energy supply systems is believed a promising solution to improve the efficiency and sustainability of the energy utilization.

As for the natural gas and power system, the gas linepack plays a crucial role in balancing supply and demand in most gas consuming [1]. The emerging power-to-gas (P2G) technologies can convert energy from electricity to natural gas [2], [3], which helps to accommodate the surplus wind and solar. Reference [4] proposes a steady-state model of the integrated natural gas and electric power system with bi-direction energy conversion, and [5] formulates a dynamic optimal energy flow model for the integrated gas and power systems.

For the integration of electrical and heating systems, some works focus on the clean energy supply for the residential demands such as buildings or communities [6]. Reference [7] proposes a coordinated planning model for the energy distribution of the integrated power and heating system. The district heating network is capable of bulk-volume heat storage, such as heat storage tanks [8], electric boilers [7] and heat pumps [9], which helps to increase the flexibility and reduce the wind curtailment.

Therefore, it illustrates that energy system integration brings potential to improve the overall efficiency and sustainability of the integrated energy systems. However, energy system integration also challenges system operation at the same time.

On the one hand, the complexity of the system increases when more subsystems are integrated and have different characteristics. On the other hand, the significant uncertainties are introduced to the power systems with the increasing deployment of renewable sources. There are various aspects of investigation on multi-energy systems involved, e.g. optimal operation with intermittent renewable sources [10], system expansion planning under different scenarios [11], and bidding strategies for large wind farms or energy storage plants [12], [13].

Though some works are reported in the energy system integration and related optimization tools applied, there is still an urgent need to address the uncertainty issue in the joint operation of electricity, gas and heating systems. So this paper addresses the coordinated operation of power, gas and district heating systems under uncertainty.

The remainder of the paper is organized as follows. Section II presents a two-stage stochastic programming model to describe the interaction between the day-ahead and the real-time operation of the integrated electricity, gas and heating system. Section III presents and analyzes a case study. Finally, Section IV gives conclusions.

II. MODEL FORMULATION

This section provides a detailed formulation of the proposed two-stage stochastic programming model. We first introduce the notation followed by the formulation of the model.

A. Notation

Sets and Indices

Φ	Set of scenarios
Ω_n^{ED}	Set of electricity demands at bus n
Ω_n^{GC}	Set of gas compressors at node n
Ω_n^{GD}	Set of gas demands at node n
Ω_n^{GS}	Set of gas storages at node n
Ω_n^{GW}	Set of gas source at node n
Λ^{EPS}	Set of buses in the electricity power system (EPS)
Λ^{NGS}	Set of nodes in the natural gas system (NGS)
Λ^{DHS}	Set of nodes in the district heating system (DHS)
Λ_n	Set of buses directly connected to bus n by transmission lines

978-1-5386-1427-3/17/$31.00 ©2017 IEEE

T Set of hours in the study horizon
Ξ Set of decision variables
REF Reference bus with phase angle fixed to 0

Constants

B_{nm} Susceptance of transmission line *n*-*m* [p.u.]
c_w^{GW} Marginal cost of the natural gas supplied from gas source *w* [$/MWh]
$c_s^{\mathrm{GS,in/out}}$ Marginal cost of gas input/output to/from gas storage *s* [$/MWh]
$c_j^{\mathrm{CHP,H/P}}$ Marginal cost of heat/power production from CHP unit *j* [$/MWh]
c_i^{CFP} Marginal cost of power production from CFP unit *i* [$/MWh]
$c_k^{\mathrm{P2G,H/P}}$ Marginal cost of heat/gas production from P2G unit *k* [$/MWh]
c_f^{WF} Marginal cost of power production from wind unit *f* [$/MWh]
$D_{d,t}^{\mathrm{ED}}$ Hour-*t* electricity demand at bus *d* [MW]
$D_{d,t}^{\mathrm{GD}}$ Hour-*t* gas demand at gas node *d* [MW]
$D_{d,t}^{\mathrm{HD}}$ Hour-*t* heat demand at heat node *d* [MW]
n^{T} Number of hours in the study horizon
$GS_s^{\mathrm{max/min}}$ Max/min gas stock in gas storage *s* [MWh]
$HS_h^{\mathrm{max/min}}$ Max/min heat reserve in heat storage *h* [MWh]
$H_h^{\mathrm{HS,in/out,max}}$ Heat input/output capacity of heat storage *h* [MW]
$H_j^{\mathrm{CHP,max/min}}$ Max/min heat supply level of CHP unit *j* [MW]
$H_k^{\mathrm{P2G,max/min}}$ Max/min heat supply level of P2G unit *k* [MW]
$H_{nm,t}^{\max}$ Capacity of heat transmission line *n*-*m* [MW]
$LP_l^{\mathrm{max/min}}$ Max/min gas linepack in pipeline *l* [MWh]
$P_i^{\mathrm{CFP,max/min}}$ Max/min power generation level of CFP unit *i* [MW]
$P_j^{\mathrm{CHP,max/min}}$ Max/min power generation level of CHP unit *j* [MW]
$P_{nm}^{\max}$ Capacity of transmission line *n*-*m* [MW]
$Q_w^{\mathrm{GW,max/min}}$ Max/min gas supply level of gas source *w* [MW]
$Q_k^{\mathrm{P2G,max/min}}$ Max/min gas generation level of P2G unit *k* [MW]
$Q_s^{\mathrm{GS,in/out,max}}$ Gas input/output capacity of gas storage *s* [MW]
$R_i^{\mathrm{CFP,U/D}}$ Maximum upward/downward reserve of CFP unit *i* [MW]
$R_j^{\mathrm{CHP,U/D}}$ Maximum upward/downward reserve of CHP unit *j* [MW]
RU_i^{CFP} Upward ramping limit of CFP unit *i* [MW/h]
RD_i^{CFP} Downward ramping limit of CFP unit *i* [MW/h]
RU_j^{CHP} Upward ramping limit of CHP unit *j* [MW/h]
RD_j^{CHP} Downward ramping limit of CHP unit *j* [MW/h]
$S_{nm}^{\max}$ Transmission capacity of gas pipeline *n*-*m* [MW]
V_d^{LOL} Electricity loss of load cost [$/MWh]
$W_f^{\max}$ Generating capacity of wind unit *f* [MW]
$W_{f\omega,t}$ Hour-*t* power supply from wind unit *f* [MW]
π_ω Probability of scenario ω
ε A pre-set small value
λ_g^{GC} Energy consumption coefficient of gas compressor *g*
η_j^{e} Generating coefficient of CHP unit *j*
η_j^{l} Heat loss coefficient of CHP unit *j*
K^e Heat exchange coefficient of CHP unit *j*
$\eta_k^{\mathrm{P2G,G/H}}$ Energy conversion efficiency from power to gas/heat at P2G unit *k*

Variables

$D_{j,t}^{\mathrm{CHP}}$ Hour-*t* gas consumption in CHP unit *j* [MW]
$D_{d,\omega,t}^{\mathrm{ED,shed}}$ Hour-*t* electricity load shed at node *d* in scenario ω [MW]
$D_{g,t}^{\mathrm{GC}}$ Gas consumption in gas compressor *g* [MW]
$D_{k,t}^{\mathrm{P2G}}$ Power consumption in P2G unit *k* [MW]
$GS_{s,t}$ Gas stocks in gas storage *s* [MWh]
$HS_{h,t}$ Heat stocks in heat storage *h* [MWh]
$H_{h,t}^{\mathrm{HS,in/out}}$ Heat input/ output of heat storage *h* [MW]
$H_{j,t}^{\mathrm{CHP}}$ Heat supply from CHP unit *j* [MW]
$H_{k,t}^{\mathrm{P2G}}$ Heat supply from P2G unit *k* [MW]
$LP_{l,t}$ Linepack stock in pipeline *l* [MW]
$P_{i,t}^{\mathrm{CHP}}$ Power production from CHP unit *i* [MW]
$PR_{i,\omega,t}^{\mathrm{CHP,U/D}}$ Upward/downward reserve of CHP unit *i* deployed in scenario ω of the operating stage [MW]
$P_{j,t}^{\mathrm{CHP}}$ Power supply from CHP unit *j* [MW]
$PR_{j,\omega,t}^{\mathrm{CHP,U/D}}$ Upward/downward reserve of CHP unit *j* deployed in scenario ω of the operating stage [MW]
$Q_{k,t}^{\mathrm{P2G}}$ Gas supply from P2G unit *k* [MW]
$QR_{k,\omega,t}^{\mathrm{P2G,U/D}}$ Upward/downward reserve of P2G unit *k* deployed in scenario ω of the operating stage [MW]
$Q_{w,t}^{\mathrm{GW}}$ Gas supply from gas source *w* [MW]
$Q_{s,t}^{\mathrm{GS,in/out}}$ Gas input/output of gas storage *s* [MW]
$Q_{l,t}^{\mathrm{LP,in/out}}$ Gas input/output of linepack pipeline *l* [MW]
$S_{mn,t}$ Gas flow rate in pipeline *m*-*n* [MW]
$S_{g,t}^{\mathrm{GC}}$ Gas flow rate through gas compressor *g* [MW]
$W_{f,t}^{\mathrm{S}}$ Power schedule for wind unit *f* [MW]
$W_{f,\omega,t}^{\mathrm{spill}}$ Wind spill for balancing in scenario ω of the operating stage [MW]

$\delta_{n,t}$ Phase angle of bus n [rad]

Note that subscripts t *and* ω indicate time period t and scenario ω, respectively.

B. Optimization Model

In this section, a two-stage stochastic programming model is formulated to represent the interaction between the scheduling stage and the real-time operation of the multi-energy systems. This problem is formulated below:

$$\begin{aligned}\min_{\Xi}\ &\sum_{t=1}^{n^{\mathrm{T}}}\Bigg\{\sum_{j=1}^{n^{\mathrm{CHP}}}\left(c_j^{\mathrm{CHP,P}}P_{j,t}^{\mathrm{CHP}}+c_j^{\mathrm{CHP,H}}H_{j,t}^{\mathrm{CHP}}\right)+\sum_{i=1}^{n^{\mathrm{CFP}}}c_i^{\mathrm{CFP}}P_{i,t}^{\mathrm{CFP}}\\&+\sum_{f=1}^{n^{\mathrm{WF}}}c_f^{\mathrm{WF}}W_{f,t}^{\mathrm{S}}+\sum_{w=1}^{n^{\mathrm{GW}}}c_w^{\mathrm{GW}}Q_{w,t}^{\mathrm{GW}}+\sum_{k=1}^{n^{\mathrm{P2G}}}\left(c_k^{\mathrm{P2G,Q}}Q_{k,t}^{\mathrm{P2G}}+c_k^{\mathrm{P2G,H}}H_{k,t}^{\mathrm{P2G}}\right)\\&+\sum_{s=1}^{n^{\mathrm{GS}}}\left(c_s^{\mathrm{GS,in}}Q_{s,t}^{\mathrm{GS,in}}+c_s^{\mathrm{GS,out}}Q_{s,t}^{\mathrm{GS,out}}\right)+\sum_{h=1}^{n^{\mathrm{HS}}}\left(c_h^{\mathrm{HS,in}}H_{h,t}^{\mathrm{HS,in}}+c_h^{\mathrm{HS,out}}H_{h,t}^{\mathrm{HS,out}}\right)\Bigg\}\\&+\sum_{\omega\in\Phi}\pi_\omega\sum_{t=1}^{n^{\mathrm{T}}}\Bigg\{\sum_{j=1}^{n^{\mathrm{CHP}}}\left[c_j^{\mathrm{CHP,P}}\left(PR_{j,\omega,t}^{\mathrm{CHP,U}}-PR_{j,\omega,t}^{\mathrm{CHP,D}}\right)+c_j^{\mathrm{CHP,H}}\left(H_{j,\omega,t}^{\mathrm{CHP}}-H_{j,t}^{\mathrm{CHP}}\right)\right]\\&+\sum_{i=1}^{n^{\mathrm{CFP}}}c_i^{\mathrm{CFP}}\left(PR_{i,\omega,t}^{\mathrm{CFP,U}}-PR_{i,\omega,t}^{\mathrm{CFP,D}}\right)+\sum_{w=1}^{n^{\mathrm{GW}}}c_w^{\mathrm{GW}}\left(Q_{w,\omega,t}^{\mathrm{GW}}-Q_{w,t}^{\mathrm{GW}}\right)\\&+\sum_{k=1}^{n^{\mathrm{P2G}}}\left[c_k^{\mathrm{P2G,Q}}\left(QR_{k,\omega,t}^{\mathrm{P2G,U}}-QR_{k,\omega,t}^{\mathrm{P2G,D}}\right)+c_k^{\mathrm{P2G,H}}\left(H_{k,\omega,t}^{\mathrm{P2G}}-H_{k,t}^{\mathrm{P2G}}\right)\right]\\&+\sum_{s=1}^{n^{\mathrm{GS}}}\left[c_s^{\mathrm{GS,in}}\left(Q_{s,\omega,t}^{\mathrm{GS,in}}-Q_{s,t}^{\mathrm{GS,in}}\right)+c_s^{\mathrm{GS,with}}\left(Q_{s,\omega,t}^{\mathrm{GS,out}}-Q_{s,t}^{\mathrm{GS,out}}\right)\right]\\&+\sum_{h=1}^{n^{\mathrm{HS}}}\left[c_h^{\mathrm{HS,in}}\left(H_{h,\omega,t}^{\mathrm{HS,in}}-H_{h,t}^{\mathrm{HS,in}}\right)+c_h^{\mathrm{HS,out}}\left(H_{h,\omega,t}^{\mathrm{HS,out}}-H_{h,t}^{\mathrm{HS,out}}\right)\right]\\&+\sum_{f=1}^{n^{\mathrm{WF}}}c_f^{\mathrm{WF}}\left(W_{f,\omega,t}-W_{f,\omega,t}^{\mathrm{spill}}-W_{f,t}^{\mathrm{S}}\right)+\sum_{d=1}^{n^{\mathrm{ED}}}V_d^{\mathrm{LOL}}D_{d,\omega,t}^{\mathrm{ED,shed}}\Bigg\}\end{aligned}\tag{1}$$

Subject to:

1) Electric power scheduling:

$$P_i^{\mathrm{CFP,min}}\le P_{i,t}^{\mathrm{CFP}}\le P_i^{\mathrm{CFP,max}},\quad \forall i\in\Omega^{\mathrm{CFP}},\forall t\in T \tag{2}$$

$$P_j^{\mathrm{CHP,min}}\le P_{j,t}^{\mathrm{CHP}}\le P_j^{\mathrm{CHP,max}},\quad \forall j\in\Omega^{\mathrm{CHP}},\forall t\in T \tag{3}$$

$$W_{f,t}^{\mathrm{S}}\le W_f^{\max},\qquad \forall f\in\Omega^{\mathrm{WF}},\forall t\in T \tag{4}$$

$$P_{i,t}^{\mathrm{CFP}}-P_{i,t-1}^{\mathrm{CFP}}\le RU_i^{\mathrm{CFP}},\quad \forall i\in\Omega^{\mathrm{CFP}},\forall t\in T \tag{5}$$

$$P_{i,t-1}^{\mathrm{CFP}}-P_{i,t}^{\mathrm{CFP}}\le RD_i^{\mathrm{CFP}},\quad \forall i\in\Omega^{\mathrm{CFP}},\forall t\in T \tag{6}$$

$$P_{j,t}^{\mathrm{CHP}}-P_{j,t-1}^{\mathrm{CHP}}\le RU_j^{\mathrm{CHP}},\quad \forall j\in\Omega^{\mathrm{CHP}},\forall t\in T \tag{7}$$

$$P_{j,t-1}^{\mathrm{CHP}}-P_{j,t}^{\mathrm{CHP}}\le RD_j^{\mathrm{CHP}},\quad \forall j\in\Omega^{\mathrm{CHP}},\forall t\in T \tag{8}$$

$$\begin{aligned}&\sum_{i\in\Omega_n^{\mathrm{CPG}}}P_{i,t}^{\mathrm{CFP}}+\sum_{j\in\Omega_n^{\mathrm{CHP}}}P_{j,t}^{\mathrm{CHP}}+\sum_{f\in\Omega_n^{\mathrm{WF}}}W_{f,t}^{\mathrm{S}}-\sum_{k\in\Omega_n^{\mathrm{P2G}}}D_{k,t}^{\mathrm{P2G}}-\\&\sum_{d\in\Omega_n^{\mathrm{ED}}}D_{d,t}^{\mathrm{ED}}=\sum_{m\in\Lambda_n}B_{nm}\left(\delta_{n,t}-\delta_{m,t}\right),\quad \forall t\in T,\forall n\in\Lambda^{\mathrm{EPS}}\end{aligned}\tag{9}$$

$$-P_{nm}^{\max}\le B_{nm}\left(\delta_{n,t}-\delta_{m,t}\right)\le P_{nm}^{\max},\quad \forall n,m\in\Lambda^{\mathrm{EPS}},\forall t\in T \tag{10}$$

2) Natural gas scheduling:

$$Q_w^{\mathrm{GW,min}}\le Q_{w,t}^{\mathrm{GW}}\le Q_w^{\mathrm{GW,max}},\quad \forall w\in\Omega^{\mathrm{GW}},\forall t\in T \tag{11}$$

$$Q_k^{\mathrm{P2G,min}}\le Q_{k,t}^{\mathrm{P2G}}\le Q_k^{\mathrm{P2G,max}},\quad \forall k\in\Omega^{\mathrm{P2G}},\forall t\in T \tag{12}$$

$$GS_{s,t}=GS_{s,0}+\sum_{t=1}^{t}\left(Q_{s,t}^{\mathrm{GS,in}}-Q_{s,t}^{\mathrm{GS,out}}\right),\forall s\in\Omega^{\mathrm{GS}},\forall t\in T \tag{13}$$

$$0\le Q_{s,t}^{\mathrm{GS,in}}\le Q_s^{\mathrm{GS,in,max}},\quad \forall s\in\Omega^{\mathrm{GS}},\forall t\in T \tag{14}$$

$$0\le Q_{s,t}^{\mathrm{GS,out}}\le Q_s^{\mathrm{GS,out,max}},\quad \forall s\in\Omega^{\mathrm{GS}},\forall t\in T \tag{15}$$

$$GS_s^{\min}\le GS_{s,t}\le GS_s^{\max},\quad \forall s\in\Omega^{\mathrm{GS}},\forall t\in T \tag{16}$$

$$LP_{l,t}=LP_{l,0}+\sum_{t=1}^{t}\left(Q_{l,t}^{\mathrm{LP,in}}-Q_{l,t}^{\mathrm{LP,out}}\right),\ \forall l\in\Omega^{\mathrm{LP}},\forall t\in T \tag{17}$$

$$LP_l^{\min}\le LP_{l,t}\le LP_l^{\max},\quad \forall l\in\Omega^{\mathrm{LP}},\forall t\in T \tag{18}$$

$$\left|LP_{l,n^{\mathrm{T}}}-LP_{l,1}\right|\le\varepsilon,\quad \forall l\in\Omega^{\mathrm{LP}} \tag{19}$$

$$D_{g,t}^{\mathrm{GC}}=\lambda_g^{\mathrm{GC}}S_{g,t}^{\mathrm{GC}},\quad \forall g\in\Omega^{\mathrm{GC}},\forall t\in T \tag{20}$$

$$\begin{aligned}&\sum_{w\in\Omega_n^{\mathrm{GW}}}Q_{w,t}^{\mathrm{GW}}+\sum_{s\in\Omega_n^{\mathrm{GS}}}\left(Q_{s,t}^{\mathrm{GS,out}}-Q_{s,t}^{\mathrm{GS,in}}\right)+\sum_{k\in\Omega_n^{\mathrm{P2G}}}Q_{k,t}^{\mathrm{P2G}}\\&+\sum_{l\in\Omega_n^{\mathrm{LP}}}\left(Q_{l,t}^{\mathrm{LP,out}}-Q_{l,t}^{\mathrm{LP,in}}\right)-\sum_{d\in\Omega_n^{\mathrm{GD}}}D_{d,t}^{\mathrm{GD}}-\sum_{g\in\Omega_n^{\mathrm{GC}}}D_{g,t}^{\mathrm{GC}}\\&-\sum_{j\in\Omega_n^{\mathrm{CHP}}}D_{j,t}^{\mathrm{CHP}}=\sum_{m\in\Lambda_n}S_{nm,t},\quad \forall m,n\in\Lambda^{\mathrm{NGS}},\forall t\in T\end{aligned}\tag{21}$$

$$-S_{nm}^{\max}\le S_{nm,t}\le S_{nm}^{\max},\quad \forall m,n\in\Lambda^{\mathrm{NGS}},\forall t\in T \tag{22}$$

3) District heating scheduling:

$$H_j^{\mathrm{CHP,min}}\le H_{j,t}^{\mathrm{CHP}}\le H_j^{\mathrm{CHP,max}},\quad \forall j\in\Omega^{\mathrm{CHP}},\forall t\in T \tag{23}$$

$$H_k^{\mathrm{P2G,min}}\le H_{k,t}^{\mathrm{P2G}}\le H_k^{\mathrm{P2G,max}},\quad \forall k\in\Omega^{\mathrm{P2G}},\forall t\in T \tag{24}$$

$$HS_{h,t+1}=HS_{h,t}+\left(H_{h,t}^{\mathrm{HS,in}}-H_{h,t}^{\mathrm{HS,out}}\right),\quad \forall h\in\Omega^{\mathrm{HS}},\forall t\in T \tag{25}$$

$$0\le H_{h,t}^{\mathrm{HS,in}}\le H_h^{\mathrm{HS,in,max}},\quad \forall h\in\Omega^{\mathrm{HS}},\forall t\in T \tag{26}$$

$$0\le H_{h,t}^{\mathrm{HS,out}}\le H_h^{\mathrm{HS,out,max}},\quad \forall h\in\Omega^{\mathrm{HS}},\forall t\in T \tag{27}$$

$$HS_h^{\min}\le HS_{h,t}\le HS_h^{\max},\quad \forall h\in\Omega^{\mathrm{HS}},\forall t\in T \tag{28}$$

$$\begin{aligned}&\sum_{j\in\Omega_n^{\mathrm{CHP}}}H_{j,t}^{\mathrm{CHP}}+\sum_{k\in\Omega_n^{\mathrm{P2G}}}H_{k,t}^{\mathrm{P2G}}+\sum_{h\in\Omega_n^{\mathrm{HS}}}\left(H_{h,t}^{\mathrm{HS,out}}-H_{h,t}^{\mathrm{HS,in}}\right)\\&-\sum_{d\in\Omega_n^{\mathrm{HD}}}H_{d,t}^{\mathrm{HD}}=\sum_{m\in\Lambda_n}H_{nm,t},\quad \forall n\in\Lambda^{\mathrm{DHS}},\forall t\in T\end{aligned}\tag{29}$$

$$-H_{nm}^{\max}\le H_{nm,t}\le H_{nm}^{\max},\quad \forall m,n\in\Lambda^{\mathrm{DHS}},\forall t\in T \tag{30}$$

4) Scheduling linking constraints:

$$H_{j,t}^{\mathrm{CHP}}=P_{j,t}^{\mathrm{CHP}}\cdot\left(1-\eta_j^{\mathrm{e}}-\eta_j^{l}\right)/\eta_j^{\mathrm{e}}\times K^{e},\quad \forall j\in\Omega^{\mathrm{CHP}},\forall t\in T \tag{31}$$

$$D_{j,t}^{\mathrm{CHP}}=P_{j,t}^{\mathrm{CHP}}/\eta_j^{\mathrm{e}},\quad \forall j\in\Omega^{\mathrm{CHP}},\forall t\in T \tag{32}$$

$$H_{k,t}^{\mathrm{P2G}}=\eta_k^{\mathrm{P2G,H}}\left(D_{k,t}^{\mathrm{P2G}}-Q_{k,t}^{\mathrm{P2G}}\right),\quad \forall k\in\Omega^{\mathrm{P2G}},\forall t\in T \tag{33}$$

$$Q_{k,t}^{\mathrm{P2G}}\le\eta_k^{\mathrm{P2G,G}}D_{k,t}^{\mathrm{P2G}},\quad \forall k\in\Omega^{\mathrm{P2G}},\forall t\in T \tag{34}$$

5) Electric power operation per scenario:

$$\begin{aligned}&P_{i,t}^{\mathrm{CFP}}+\left(PR_{i,\omega,t}^{\mathrm{CFP,U}}-PR_{i,\omega,t}^{\mathrm{CFP,D}}\right)-P_{i,t-1}^{\mathrm{CFP}}-\left(PR_{i,\omega,t-1}^{\mathrm{CFP,U}}-PR_{i,\omega,t-1}^{\mathrm{CFP,D}}\right)\\&\le RU_i^{\mathrm{CFP}},\forall i\in\Omega^{\mathrm{CFP}},\forall t\in T,\forall\omega\in\Phi\end{aligned}\tag{36}$$

$$\begin{aligned}&P_{i,t-1}^{\mathrm{CFP}}-\left(PR_{i,\omega,t-1}^{\mathrm{CFP,U}}-PR_{i,\omega,t-1}^{\mathrm{CFP,D}}\right)-P_{i,t}^{\mathrm{CFP}}-\left(PR_{i,\omega,t}^{\mathrm{CFP,U}}-PR_{i,\omega,t}^{\mathrm{CFP,D}}\right)\\&\le RD_i^{\mathrm{CFP}},\quad \forall i\in\Omega^{\mathrm{CFP}},\forall t\in T,\forall\omega\in\Phi\end{aligned}\tag{37}$$

$$P_{j,t}^{\mathrm{CHP}}+\left(PR_{j\omega,t}^{\mathrm{CHP,U}}-PR_{j\omega,t}^{\mathrm{CHP,D}}\right)-P_{j,t-1}^{\mathrm{CHP}}-\left(PR_{j,\omega,t-1}^{\mathrm{CHP,U}}-PR_{j,\omega,t-1}^{\mathrm{CHP,D}}\right)$$

$$\le RU_j^{\mathrm{CHP}}, \quad \forall j \in \Omega^{\mathrm{CHP}}, \forall t \in T, \forall \omega \in \Phi \tag{38}$$

$$P_{j,t-1}^{\mathrm{CHP}} + \left(PR_{j,\omega,t-1}^{\mathrm{CHP,U}} - PR_{j,\omega,t-1}^{\mathrm{CHP,D}}\right) - P_{j,t}^{\mathrm{CHP}} - \left(PR_{j,\omega,t}^{\mathrm{CHP,U}} - PR_{j,\omega,t}^{\mathrm{CHP,D}}\right)$$
$$\le RD_j^{\mathrm{CHP}}, \quad \forall j \in \Omega^{\mathrm{CHP}}, \forall t \in T, \forall \omega \in \Phi \tag{39}$$

$$\sum_{i \in \Omega_n^{\mathrm{CPG}}} \left(PR_{i\omega,t}^{\mathrm{CFP,U}} - PR_{i\omega,t}^{\mathrm{CFP,D}}\right) + \sum_{j \in \Omega_n^{\mathrm{CHP}}} \left(PR_{j\omega,t}^{\mathrm{CHP,U}} - PR_{j\omega,t}^{\mathrm{CHP,D}}\right)$$
$$+ \sum_{f \in \Omega_n^{\mathrm{WF}}} \left(W_{f,\omega,t} - W_{f,\omega,t}^{\mathrm{spill}} - W_{f,t}^{\mathrm{S}}\right) - \sum_{k \in \Omega_n^{\mathrm{P2G}}} \left(D_{k\omega,t}^{\mathrm{P2G}} - D_{k,t}^{\mathrm{P2G}}\right)$$
$$- \sum_{d \in \Omega_n^{\mathrm{ED}}} D_{d\omega,t}^{\mathrm{ED,shed}} = \sum_{m \in \Lambda_n} B_{nm}\left(\delta_{n\omega,t} - \delta_{m\omega,t} - \delta_{n,t} + \delta_{m,t}\right),$$
$$\forall t \in T, \forall n \in \Lambda^{\mathrm{EPS}}, \forall \omega \in \Phi \tag{40}$$

6) Natural gas operation per scenario:

$$Q_k^{\mathrm{P2G,min}} \le Q_{k,t}^{\mathrm{P2G}} + \left(QR_{k,\omega,t}^{\mathrm{P2G,U}} - QR_{k,\omega,t}^{\mathrm{P2G,D}}\right) \le Q_k^{\mathrm{P2G,max}},$$
$$\forall k \in \Omega^{\mathrm{P2G}}, \forall t \in T, \forall \omega \in \Phi \tag{41}$$

$$Q_w^{\mathrm{GW,min}} \le Q_{w,\omega,t}^{\mathrm{GW}} \le Q_w^{\mathrm{GW,max}}, \quad \forall w \in \Omega^{\mathrm{GW}}, \forall t \in T, \forall \omega \in \Phi \tag{42}$$

$$GS_{s,\omega,t+1} = GS_{s,\omega,t} + \left(Q_{s,\omega,t}^{\mathrm{GS,in}} - Q_{s,\omega,t}^{\mathrm{GS,out}}\right),$$
$$\forall s \in \Omega^{\mathrm{GS}}, \forall t \in T, \forall \omega \in \Phi \tag{43}$$

$$0 \le Q_{s,\omega,t}^{\mathrm{GS,in}} \le Q_s^{\mathrm{GS,in,max}}, \quad \forall s \in \Omega^{\mathrm{GS}}, \forall t \in T, \forall \omega \in \Phi \tag{44}$$

$$0 \le Q_{s,\omega,t}^{\mathrm{GS,out}} \le Q_s^{\mathrm{GS,out,max}}, \quad \forall s \in \Omega^{\mathrm{GS}}, \forall t \in T, \forall \omega \in \Phi \tag{45}$$

$$GS_s^{\min} \le GS_{s,\omega,t} \le GS_s^{\max}, \quad \forall s \in \Omega^{\mathrm{GS}}, \forall t \in T, \forall \omega \in \Phi \tag{46}$$

$$LP_{l,\omega,t+1} = LP_{l,\omega,t} + \left(Q_{l,\omega,t}^{\mathrm{LP,in}} - Q_{l,\omega,t}^{\mathrm{LP,out}}\right),$$
$$\forall l \in \Omega^{\mathrm{LP}}, \forall t \in T, \forall \omega \in \Phi \tag{47}$$

$$\sum_{w \in \Omega_n^{\mathrm{GW}}} \left(Q_{w,\omega,t}^{\mathrm{GW}} - Q_{w,t}^{\mathrm{GW}}\right) + \sum_{s \in \Omega_n^{\mathrm{GS}}} \left(Q_{s,\omega,t}^{\mathrm{GS,in}} - Q_{s,\omega,t}^{\mathrm{GS,out}} - Q_{s,t}^{\mathrm{GS,in}} + Q_{s,t}^{\mathrm{GS,out}}\right) +$$
$$\sum_{l \in \Omega_n^{\mathrm{LP}}} \left(Q_{l,\omega,t}^{\mathrm{LP,out}} - Q_{l,\omega,t}^{\mathrm{LP,in}} - Q_{l,t}^{\mathrm{LP,out}} + Q_{l,t}^{\mathrm{LP,in}}\right) + \sum_{k \in \Omega_n^{\mathrm{P2G}}} \left(QR_{k,\omega,t}^{\mathrm{P2G,U}} - QR_{k,\omega,t}^{\mathrm{P2G,D}}\right)$$
$$- \sum_{d \in \Omega_n^{\mathrm{GD}}} \left(D_{d,\omega,t}^{\mathrm{GD}} - D_{d,t}^{\mathrm{GD}}\right) - \sum_{g \in \Omega_n^{\mathrm{GC}}} \left(D_{g,\omega,t}^{\mathrm{GC}} - D_{g,t}^{\mathrm{GC}}\right) = \sum_{m \in \Lambda_n} \left(S_{nm,\omega,t} - S_{nm,t}\right),$$
$$\forall t \in T, \forall n \in \Lambda, \forall \omega \in \Phi \tag{48}$$

7) District heating operation per scenario:

$$H_j^{\mathrm{CHP,min}} \le H_{j,\omega,t}^{\mathrm{CHP}} \le H_j^{\mathrm{CHP,max}}, \quad \forall j \in \Omega^{\mathrm{CHP}}, \forall t \in T, \forall \omega \in \Phi \tag{49}$$

$$H_k^{\mathrm{P2G,min}} \le H_{k,\omega,t}^{\mathrm{P2G}} \le H_k^{\mathrm{P2G,max}}, \quad \forall k \in \Omega^{\mathrm{P2G}}, \forall t \in T, \forall \omega \in \Phi \tag{50}$$

$$HS_{h,\omega,t+1} = HS_{h,\omega,t} + \left(H_{h,\omega,t}^{\mathrm{HS,in}} - H_{h,\omega,t}^{\mathrm{HS,with}}\right),$$
$$\forall h \in \Omega^{\mathrm{HS}}, \forall t \in T, \forall \omega \in \Phi \tag{51}$$

$$0 \le H_{h,\omega,t}^{\mathrm{HS,in}} \le H_h^{\mathrm{HS,in,max}}, \quad \forall h \in \Omega^{\mathrm{HS}}, \forall t \in T, \forall \omega \in \Phi \tag{52}$$

$$0 \le H_{h,\omega,t}^{\mathrm{HS,out}} \le H_h^{\mathrm{HS,out,max}}, \quad \forall h \in \Omega^{\mathrm{HS}}, \forall t \in T, \forall \omega \in \Phi \tag{53}$$

$$HS_h^{\min} \le HS_{h,\omega,t} \le HS_h^{\max}, \quad \forall h \in \Omega^{\mathrm{HS}}, \forall t \in T, \forall \omega \in \Phi \tag{54}$$

$$\sum_{j \in \Omega_n^{\mathrm{CHP}}} \left(H_{j,\omega,t}^{\mathrm{CHP}} - H_{j,t}^{\mathrm{CHP}}\right) + \sum_{k \in \Omega_n^{\mathrm{P2G}}} \left(H_{k,\omega,t}^{\mathrm{P2G}} - H_{k,t}^{\mathrm{P2G}}\right) +$$
$$\sum_{h \in \Omega_n^{\mathrm{HS}}} \left(H_{h,\omega,t}^{\mathrm{HS,out}} - H_{h,\omega,t}^{\mathrm{HS,in}} - H_{h,t}^{\mathrm{HS,out}} + H_{h,t}^{\mathrm{HS,in}}\right)$$
$$= \sum_{m \in \Lambda_n} \left(H_{nm,\omega,t} - H_{nm,t}\right), \ \forall n \in \Lambda^{\mathrm{DHS}}, \forall t \in T, \forall \omega \in \Phi \tag{55}$$

$$-H_{nm,t}^{\max} \le H_{nm,\omega,t} \le H_{nm,t}^{\max}, \quad \forall m,n \in \Lambda^{\mathrm{DHS}}, \forall t \in T, \forall \omega \in \Phi \tag{56}$$

8) Operation linking constraints:

$$H_{j,\omega,t}^{\mathrm{CHP}} - H_{j,t}^{\mathrm{CHP}} = \frac{\left(PR_{j,\omega,t}^{\mathrm{CHP,U}} - PR_{j,\omega,t}^{\mathrm{CHP,D}}\right)\left(1 - \eta_j^{\mathrm{e}} - \eta_j^{l}\right)K^{e}}{\eta_j^{\mathrm{e}}},$$
$$\forall j \in \Omega^{\mathrm{CHP}}, \forall t \in T, \forall \omega \in \Phi \tag{57}$$

$$D_{j,\omega,t}^{\mathrm{CHP}} - D_{j,t}^{\mathrm{CHP}} = \left(PR_{j,\omega,t}^{\mathrm{CHP,U}} - PR_{j,\omega,t}^{\mathrm{CHP,D}}\right) / \eta_j^{\mathrm{e}},$$
$$\forall j \in \Omega^{\mathrm{CHP}}, \forall t \in T, \forall \omega \in \Phi \tag{58}$$

$$H_{k,\omega,t}^{\mathrm{P2G}} - H_{k,t}^{\mathrm{P2G}} = \eta_k^{\mathrm{P2G,H}} \left\lfloor D_{k,\omega,t}^{\mathrm{P2G}} - D_{k,t}^{\mathrm{P2G}} - \left(QR_{k,\omega,t}^{\mathrm{P2G,U}} - QR_{k,\omega,t}^{\mathrm{P2G,D}}\right) \right\rfloor,$$
$$\forall k \in \Omega^{\mathrm{P2G}}, \forall t \in T, \forall \omega \in \Phi \tag{59}$$

$$Q_{k,t}^{\mathrm{P2G}} + \left(QR_{k,\omega,t}^{\mathrm{P2G,U}} - QR_{k,\omega,t}^{\mathrm{P2G,D}}\right) \le \eta_k^{\mathrm{P2G,Q}} D_{k,\omega,t}^{\mathrm{P2G}},$$
$$\forall k \in \Omega^{\mathrm{P2G}}, \forall t \in T, \forall \omega \in \Phi \tag{60}$$

The objective function (1) to minimize the total expected system operation costs, including the costs of day-ahead scheduling and the costs of real-time operation in the multi-energy systems. The objective function is subject to two different sets of constraints, namely, the day-ahead scheduling constraints, (2)-(35); the real-time operation constraints, (36)-(60).

This objective function (1) consists of several terms: the operation cost of scheduling CHP units to produce electricity and heat; the operation cost of scheduling coal-fired power (CFP) units and wind farms (WF) to produce electricity, respectively; the cost of gas supply scheduling from gas sources (GW); the operation cost of scheduling P2G units to produce gas and heat; the operational cost of gas output and gas input of the gas storage; the operational cost of heat output and heat input in the heat storage; the expected balancing cost of operating the CHP, coal-fired power enreration (CFP), gas source, P2G, gas storage, heat storage and wind farms of the integrated system in real-time operation; the cost of any load that must be shed in real-time operation.

As mentioned previously, there are two different sets of constraints: the scheduling constraints and the real-time operation constraints. Each set of constraint is divided into four types of constraints, which are the electricity, gas, district heating, and the linking constraints. Also, we build the general formulation on the following assumptions to simplify the two-stage stochastic programming model:

1) For the gas network, we assume that all nodal gas pressures are within normal ranges.

2) For the district heating network, we assume that the water temperature and the water pressure are within normal ranges.

3) For simplicity, the gas flow rates and heat flow rates are converted to power units, and the per-unit system used.

Regarding the day-ahead scheduling constraints, (2)-(11) enforce the operational constraints from the power system side, which consist of the facility capacities of CFP (2), CHP (3) and wind farm (4); the ramping limits of CFP with

(5)-(6) and CHP with (7)-(8); the nodal power balance equations (9); the power transmission capacities (10); and reference constraints (11) at the scheduling stage. Similarly, equations (12)-(23) enforce the scheduling constraints in the natural gas network. Constrains (24)-(31) represent the scheduling constraints of the district heating network, which consist of the heat production capacities of the CHP (24) and P2G units (25); the operational constraints of the heat storage (26)-(29); the nodal heat balance equations (30); and the heat transmission capacities (31).

Finally, besides the network constraints and the operational limits for the facilities in the individual electricity, gas and heating systems, the interfaces among the electricity, natural gas and district heating systems are constrained by the energy conversion relationships of the CHP (32)-(33) and P2G units (34)-(35). The gas-fired CHP unit can generate electricity and heat simultaneously by consuming natural gas. The relationship between the output of electricity and heat is given by (32), and the gas consumption is given by (33).

P2G is an emerging technology that consumes electricity to produce gas. In practice, part of the electric energy is dissipated in forms of heat during the process of gas production. Some of the dissipated heat can be used as heating supply in the district heating system, which is stated in (34). Equation (35) shows that the gas generation should not exceed the maximum energy conversion efficiency of P2G when converting electricity to natural gas.

The remaining constraints (36)-(60) impose real-time operating restrictions. Note that some real-time operating constraints are not listed here due to limited space. But the abridged constraints do not affect the understanding of the model, as they are similar to those constraints in the scheduling stage. Equations (36)-(40) enforce real-time operational constraints in the electricity network. Equations (41)-(48) enforce the real-time operational constraints in the natural gas network. Equations (49)-(56) enforce the real-time balancing constraints in the district heating network. Finally, constraints (57)-(58) impose the energy conversion relationships of CHP units for balancing in each scenario. Constraints (59)-(60) impose the energy conversion relationships of P2G units for balancing in each scenario.

III. Case Study

A. Description of the simulation system

The test case considered in this work is shown in Fig. 1. The 4-node gas network is composed of 3 pipelines, four nodes. The 4-bus electricity system includes a CFP unit, a CHP unit, and a wind farm. The heating system includes one heat storage, two pipes, and three nodes. Finally, there are two links. One is the CHP unit, another one is the P2G unit. We have run problems with 50 scenarios using CPLEX under GAMS. The CPU core used for the simulations clocks at 2.7 GHz. Available RAM is 8 GB. The solution time is 1.64 seconds for this case with 50 wind power scenarios.

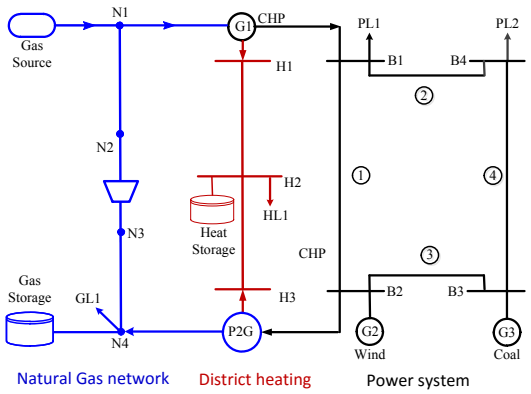

Fig. 1. The Structure of an integrated electricity, natural gas and district heating system.

It is important to note that scheduling reserve is required to cope with the uncertain wind power production, which is represented via two scenarios, namely high and low, with probability 0.6 and 0.4, respectively.

B. Day-ahead scheduling of the energy sources

In this section, the optimal scheduling strategy of the integrated energy system is analyzed over the whole 24 hour time horizon. Fig. 3 shows the optimal schedule of sources in the electrical system. It should be noted that the total power consumption includes both the power demand and the electricity consumption in the P2G unit. As you can see in Fig. 2, the generation of the CFP unit is flat. In contrast, the gas-fired CHP unit plays a critical role regarding peak regulation to accommodate the fluctuated wind power. On the gas system side, Fig. 3 shows the gas injections and consumptions. Because of the surplus wind power during in the scheduling stage, the P2G unit turns excess power into gas and heat, thereby reducing wind power curtailment. Note that the gas supply from the gas source is flat. The difference between gas supply and consumption is balanced by the gas storage and linepack. In the gas system, there are not as many regulation facilities as in the power system. So, the linepack plays an important role in balancing gas production and consumption. At the district heating system side, Fig. 4 illustrates the heat supplies and consumptions. The difference between heat supply and heat consumption is balanced by the heat storage. Note that the heat dissipation in the P2G unit is supposed to supply heating in the district heating system, to reduce the energy loss in the process of gas production.

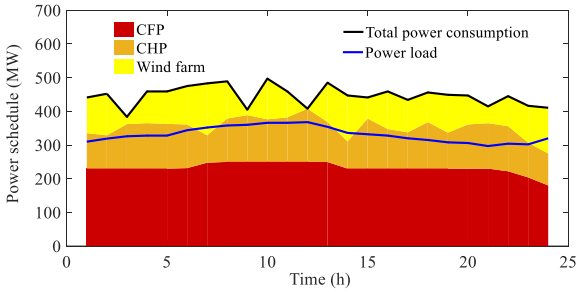

Fig. 2. Optimal schedule of sources in the electrical system.

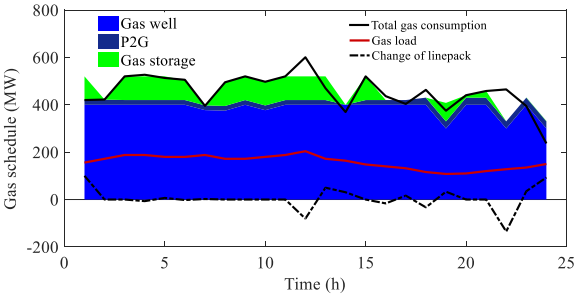

Fig. 3. Optimal schedule of sources in the gas system.

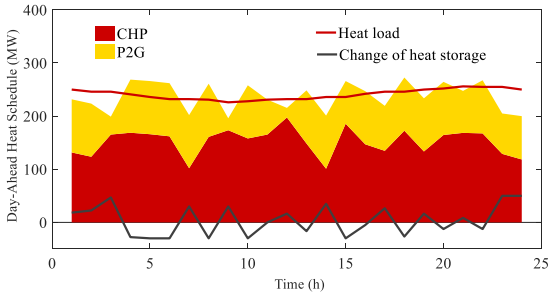

Fig. 4. Optimal schedule of sources in the district heating system.

C. *Real-time adjustment of the energy sources*

Fig. 5 provides the actual deployment of downward and upward reserve adjustment per scenario and period in the electrical system to account for wind variability. A positive value represents an upward reserve adjustment and a negative value represents a downward reserve adjustment. For scenario "high wind", the actual downward adjustment for unit CFP and CHP is deployed to compensate high wind power production in most of the periods. For scenario "low wind", the upward adjustment for unit CFP is deployed in most of the periods.

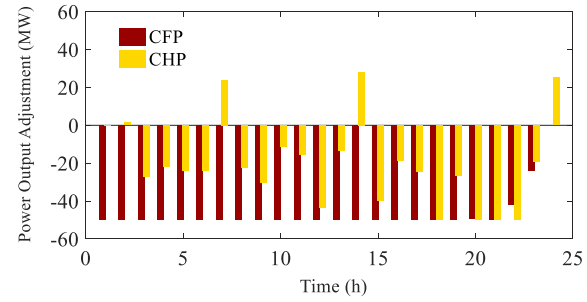

(a) High wind

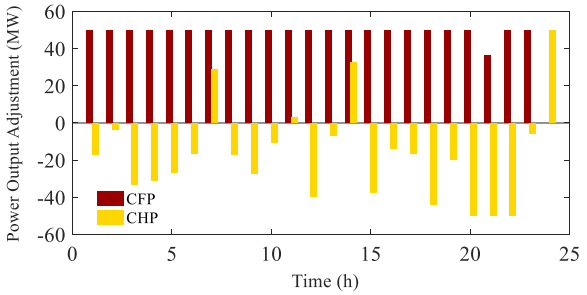

(b) Low wind

Fig. 5. Optimal adjustment of sources in the electricity system.

IV. Conclusion

This paper develops a coordinated model for jointly operating the electricity, gas, and district heating systems. The objective is to minimize the total operational costs. As wind uncertainty is considered, a two-stage stochastic formulation is developed to model the optimal scheduling of reserves to facilitate real-time adjustment decisions. The model is illustrated using a test energy system. The required computational time is small and compatible with operational requirements.

Acknowledgment

This study is a part of the research project supported by the ForskEL project Harmonized Integration of Gas, District Heating and Electric Systems (HIGHE2014-1-12220).

References

[1] C. Liu, M. Shahidehpour, Y. Fu, and Z. Li, "Security-Constrained Unit Commitment With Natural Gas Transmission Constraints," *IEEE Trans. Power Syst.*, vol. 24, no. 3, pp. 1523–1536, Aug. 2009.

[2] S. Clegg and P. Mancarella, "Integrated Electrical and Gas Network Flexibility Assessment in Low-Carbon Multi-Energy Systems," *IEEE Trans. Sustain. Energy*, vol. 7, no. 2, pp. 718–731, Apr. 2016.

[3] G. Guandalini, S. Campanari, and M. C. Romano, "Power-to-gas plants and gas turbines for improved wind energy dispatchability: Energy and economic assessment," *Appl. Energy*, vol. 147, pp. 117–130, Jun. 2015.

[4] Q. Zeng, J. Fang, J. Li, and Z. Chen, "Steady-state analysis of the integrated natural gas and electric power system with bi-directional energy conversion," *Appl. Energy*, vol. 184, pp. 1483–1492, Dec. 2016.

[5] J. Fang, Q. Zeng, X. Ai, Z. Chen, and J. Wen, "Dynamic Optimal Energy Flow in the Integrated Natural Gas and Electrical Power Systems," *IEEE Trans. Sustain. Energy*, vol. PP, no. 99, pp. 1–1, 2017.

[6] A. Adam, E. S. Fraga, and D. J. L. Brett, "Options for residential building services design using fuel cell based micro-CHP and the potential for heat integration," *Appl. Energy*, vol. 138, pp. 685–694, Jan. 2015.

[7] J. Li, J. Fang, Q. Zeng, and Z. Chen, "Optimal operation of the integrated electrical and heating systems to accommodate the intermittent renewable sources," *Appl. Energy*, vol. 167, pp. 244–254, Apr. 2016.

[8] L. Miró, J. Gasia, and L. F. Cabeza, "Thermal energy storage (TES) for industrial waste heat (IWH) recovery: A review," *Appl. Energy*, vol. 179, pp. 284–301, Oct. 2016.

[9] G. Papaefthymiou, B. Hasche, and C. Nabe, "Potential of Heat Pumps for Demand Side Management and Wind Power Integration in the German Electricity Market," *IEEE Trans. Sustain. Energy*, vol. 3, no. 4, pp. 636–642, Oct. 2012.

[10] Y. Wang, S. Zhao, Z. Zhou, A. Botterud, Y. Xu, and R. Chen, "Risk Adjustable Day-Ahead Unit Commitment With Wind Power Based on Chance Constrained Goal Programming," *IEEE Trans. Sustain. Energy*, vol. 8, no. 2, pp. 530–541, Apr. 2017.

[11] C. Yuan, M. Illindala, and A. Khalsa, "Co-Optimization Scheme for Distributed Energy Resource Planning in Community Microgrids," *IEEE Trans. Sustain. Energy*, vol. PP, no. 99, pp. 1–1, 2017.

[12] H. Ding, P. Pinson, Z. Hu, and Y. Song, "Integrated Bidding and Operating Strategies for Wind-Storage Systems," *IEEE Trans. Sustain. Energy*, vol. 7, no. 1, pp. 163–172, Jan. 2016.

[13] A. T. Al-Awami and M. A. El-Sharkawi, "Coordinated Trading of Wind and Thermal Energy," *IEEE Trans. Sustain. Energy*, vol. 2, no. 3, pp. 277–287, Jul. 2011.

Publication **C2**

Paper title:

The coordinated operation of electricity, gas and district heating systems

Publication outlet:

Applied Energy Symposium and Forum, REM2017: Renewable Energy Integration with Mini/Microgrid. In press

List of authors:

Qing Zeng, Baohua Zhang, Jiakun Fang, Zhe Chen

Available online at www.sciencedirect.com

ScienceDirect

Energy Procedia 00 (2018) 000–000

Energy Procedia

www.elsevier.com/locate/procedia

Applied Energy Symposium and Forum, Renewable Energy Integration with Mini/Microgrids, REM 2017, 18–20 October 2017, Tianjin, China

The coordinated operation of electricity, gas and district heating systems

Qing Zeng[a]*, Jiakun Fang[a], Baohua Zhang [a], Zhe Chen[a]

[a]*Department of Energy Technology, Aalborg University, Aalborg 9220, Denmark*

Abstract

This paper focuses on the coordinated operation of the electricity, gas and district heating systems in urban areas where multi-energy systems belong to a single entity. The energy conversions among these three systems are scheduled simultaneously so that the demands of the three systems could be met at the least operation cost and maximum social welfare. A nonlinear optimization problem is formulated considering the detailed network constraints in the integrated system. A case study is carried out to show the effectiveness and feasibility of the proposed approach.

Copyright © 2018 Elsevier Ltd. All rights reserved.
Selection and peer-review under responsibility of the scientific committee of the Applied Energy Symposium and Forum, Renewable Energy Integration with Mini/Microgrids, REM 2017.

Keywords: Power system, natural gas system, district heating system, coordinated operation.

Nomenclature

Indices:

CFP	coal-fired power unit
GC	gas compressor
GS	gas storage
GW	gas well
HS	heat storage

* Corresponding author. Tel.: +45 41116906.
E-mail address: qiz@et.aau.dk.

1876-6102 Copyright © 2018 Elsevier Ltd. All rights reserved.
Selection and peer-review under responsibility of the scientific committee of the Applied Energy Symposium and Forum, Renewable Energy Integration with Mini/Microgrids, REM 2017.

H, P, G heat, power, gas
LP linepack
WF wind farm

Parameters:

B	susceptance of the transmission line, p.u.
c	operational cost, \$/MWh
D	gas demand, power demand, heat demand, MW
m	water flow rate, m^3/h
Z	the resistance coefficient of the pipeline, $kPa^2/(MW)^2$
λ	energy consumption coefficient
η	energy conversion efficiency
K	heat exchange coefficient
Ξ	Set of decision variables

Variables:

P, H, Q	power flow, heat flow, gas flow, MW
δ, p, τ	the angle of voltage, gas pressure, water temperature
W	wind power, MW
S	gas flow rate, MW

1. Introduction

In recent years, research investigations have demonstrated that the integration of energy systems can balance the energy production and consumption in a broader scope, and hence improve the efficiency and sustainability of the energy utilization [1]. Therefore, the investigations of multi-energy systems (MES) are currently receiving increasing attention.

Since electricity and natural gas are two of the common options for bulk energy transmission, extensive studies have been carried out to investigate the coordinated operation of the gas and power system. [2] develops a steady-state model for the integrated gas and power systems, while [3] develops a dynamic energy flow model which considers the different response times of the gas and power systems. [4] proposes a coordinated scheduling strategy to optimize conflicting benefits of the electricity and gas networks. [5] proposes a bi-level dispatch model to minimize the total operation costs of both natural gas and electricity systems.

Several works have also been conducted in the coordination of electrical system and heating system, due to the extensive use of CHP units, heat pumps and electric boilers. [6] proposes an optimization model to coordinate the electrical and heating systems to accommodate the renewable sources. [7] proposes a combined heat and power dispatch model to operate the electric power system and district heating system. [8] develops a transmission constrained unit commitment model on the combined electricity and district heating networks. These studies suggest that the coordinated operation can enhance the flexibility of the power system and accommodate high penetration level of renewable energy generation.

Although the coordination of the gas and power systems and the coordination of electrical and heating system have been studied well, there is few work on the joint operation of electricity, gas, and district heating systems. [9] presents a steady state power flow model for combined optimization of electricity, gas, and district heating systems based on the concept of energy hubs. However, it ignores the detailed network constraints of the electricity, gas and district heating system.

This paper focuses on the coordination of electricity, gas, and district heating systems with network constraints considered. The major contribution is providing an optimization problem for joint operation of electricity, gas, and district heating systems. The objective is to minimize the operational costs of the integrated systems while maximises the renewable energy consumed.

The remainder of the paper is organized as follows. Section 2 presents a model to describe the optimization problem for joint operation of the electricity, gas and heating systems. Section 3 analyzes a case study. Finally, Section 4 gives conclusions.

2. Optimization Model

In this section, an optimal cooperation model is formulated to represent the scheduling of the integrated electricity, gas and heating system. This problem is formulated below.

$$\min_{\Xi} \sum_{t=1}^{n^{\mathrm{T}}} \left\{ \sum_{j=1}^{n^{\mathrm{CHP}}} \left(c_j^{\mathrm{CHP,P}} P_{j,t}^{\mathrm{CHP}} + c_j^{\mathrm{CHP,H}} H_{j,t}^{\mathrm{CHP}} \right) + \sum_{i=1}^{n^{\mathrm{CFP}}} c_i^{\mathrm{CFP}} P_{i,t}^{\mathrm{CFP}} + \sum_{f=1}^{n^{\mathrm{WF}}} c_f^{\mathrm{WF}} W_{f,t}^{\mathrm{S}} + \sum_{w=1}^{n^{\mathrm{GW}}} c_w^{\mathrm{GW}} Q_{w,t}^{\mathrm{GW}} \right.$$
$$\left. + \sum_{k=1}^{n^{\mathrm{P2G}}} \left(c_k^{\mathrm{P2G,Q}} Q_{k,t}^{\mathrm{P2G}} + c_k^{\mathrm{P2G,H}} H_{k,t}^{\mathrm{P2G}} \right) + \sum_{s=1}^{n^{\mathrm{GS}}} \left(c_s^{\mathrm{GS,in}} Q_{s,t}^{\mathrm{GS,in}} + c_s^{\mathrm{GS,out}} Q_{s,t}^{\mathrm{GS,out}} \right) + \sum_{h=1}^{n^{\mathrm{HS}}} \left(c_h^{\mathrm{HS,in}} H_{h,t}^{\mathrm{HS,in}} + c_h^{\mathrm{HS,out}} H_{h,t}^{\mathrm{HS,out}} \right) \right\} \tag{1}$$

The objective function (1) minimizes the total system operation cost, which consists of several terms: the operation cost of CHP units to produce electricity and heat, the operation cost of coal-fired power (CFP) units and wind farms (WF) to produce electricity, the cost of gas supply from gas wells (GW), the operation cost of P2G units to produce gas and heat, the operational cost of gas output and gas input of the gas storage, the operational cost of heat output and heat input in the heat storage.

The optimization is subjected to electric power constraints, natural gas constraints, district heating constraints and energy conversion limits.

1) Electric power constraints:

$$\sum_{j \in \Omega_n^{\mathrm{CHP}}} P_{j,t}^{\mathrm{CHP}} + \sum_{i \in \Omega_n^{\mathrm{CPG}}} P_{i,t}^{\mathrm{CFP}} + \sum_{f \in \Omega_n^{\mathrm{WF}}} \left(W_{f,t} - W_{f,t}^{\mathrm{spill}} \right) - \sum_{k \in \Omega_n^{\mathrm{P2G}}} D_{k,t}^{\mathrm{P2G}} - \sum_{d \in \Omega_n^{\mathrm{ED}}} D_{d,t}^{\mathrm{ED}} = \sum_{m \in \Lambda_n} B_{nm} \left(\delta_{n,t} - \delta_{m,t} \right),$$
$$\forall m, n \in \Lambda^{\mathrm{EPS}}, \forall t \in T \tag{2}$$

DC power flow model is used in the network constraint. The electric power constraints consist of the nodal power balance equations (2). The constraints also include the generator capacities, the ramping limits, and the power transmission capacities, which are not listed here due to page limits.

2) Natural gas constraints:

$$\sum_{w \in \Omega_n^{\mathrm{GW}}} Q_{w,t}^{\mathrm{GW}} + \sum_{s \in \Omega_n^{\mathrm{GS}}} \left(Q_{s,t}^{\mathrm{GS,out}} - Q_{s,t}^{\mathrm{GS,in}} \right) + \sum_{k \in \Omega_n^{\mathrm{P2G}}} Q_{k,t}^{\mathrm{P2G}} + \sum_{l \in \Omega_n^{\mathrm{LP}}} \left(Q_{l,t}^{\mathrm{LP,out}} - Q_{l,t}^{\mathrm{LP,in}} \right) - \sum_{d \in \Omega_n^{\mathrm{GD}}} D_{d,t}^{\mathrm{GD}} - \sum_{g \in \Omega_n^{\mathrm{GC}}} D_{g,t}^{\mathrm{GC}}$$
$$- \sum_{j \in \Omega_n^{\mathrm{CHP}}} D_{j,t}^{\mathrm{CHP}} = \sum_{m \in \Lambda_n} S_{nm,t}, \quad \forall m, n \in \Lambda^{\mathrm{NGS}}, \forall t \in T \tag{3}$$

$$p_{n,t}^2 - p_{m,t}^2 = Z_{nm} \left(S_{nm,t} \right)^2, \quad \forall n, m \in \Lambda^{\mathrm{NGS}}, \forall t \in T \tag{4}$$

Equations (3)-(4) state the steady-state model of the natural gas system. In addition, the natural gas constraints also include the gas production capacities of the GW and P2G units, the operational constraints of the gas storage and gas linepack, which are not listed here due to page limits. Finally, the model of the compressor is adapted from [2].

3) District heating constraints:

$$\sum_{j\in\Omega_n^{\mathrm{CHP}}} H_{j,t}^{\mathrm{CHP}} + \sum_{k\in\Omega_n^{\mathrm{P2G}}} H_{k,t}^{\mathrm{P2G}} + \sum_{h\in\Omega_n^{\mathrm{HS}}} \left(H_{h,t}^{\mathrm{HS,out}} - H_{h,t}^{\mathrm{HS,in}}\right) - \sum_{d\in\Omega_n^{\mathrm{HD}}} H_{d,t}^{\mathrm{HD}} = c\cdot m_{n,t}\cdot\left(\tau_{n,t}^{\mathrm{out}} - \tau_{n,t}^{\mathrm{in}}\right), \quad \forall n\in\Lambda^{\mathrm{DHS}}, \forall t\in T \tag{5}$$

$$\tau_{mn,t}^{\mathrm{out}} - \tau_{mn,t}^{\mathrm{am}} = \lambda_{mn,t}\left(\tau_{mn,t}^{\mathrm{in}} - \tau_{mn,t}^{\mathrm{am}}\right), \forall m,n\in\Lambda^{\mathrm{DHS}}, \forall t\in T \tag{6}$$

$$\tau_{n,t}\sum_{m\in\Lambda_n} m_{mn,t} = \sum_{m\in\Lambda_n}\left(m_{mn,t}\cdot\tau_{mn,t}^{\mathrm{out}}\right), \forall m,n\in\Lambda^{\mathrm{DHS}}, \forall t\in T \tag{7}$$

Equations (5)-(7) represent the model of the district heating network, which consist of the nodal heat balance equation, the temperature drop equations, and the nodal mixed temperature equation. It also consists of production capacities of the CHP and P2G units, the operational constraints of the heat storage and the heat transmission capacities.

4) Energy conversion among subsystems:

$$H_{j,t}^{\mathrm{CHP}} = P_{j,t}^{\mathrm{CHP}}\cdot\left(1-\eta_j^{\mathrm{E}}-\eta_j^{\mathrm{L}}\right)\Big/\eta_j^{\mathrm{E}}\times K^{\mathrm{E}}, \quad \forall j\in\Omega^{\mathrm{CHP}}, \forall t\in T \tag{8}$$

$$D_{j,t}^{\mathrm{CHP}} = P_{j,t}^{\mathrm{CHP}}\Big/\eta_j^{\mathrm{E}}, \quad \forall j\in\Omega^{\mathrm{CHP}}, \forall t\in T \tag{9}$$

$$H_{k,t}^{\mathrm{P2G}} = \eta_k^{\mathrm{P2G,H}}\left(D_{k,t}^{\mathrm{P2G}} - Q_{k,t}^{\mathrm{P2G}}\right), \quad \forall k\in\Omega^{\mathrm{P2G}}, \forall t\in T \tag{10}$$

$$Q_{k,t}^{\mathrm{P2G,Q}} \le \eta_k^{\mathrm{P2G}} D_{k,t}^{\mathrm{P2G}}, \quad \forall k\in\Omega^{\mathrm{P2G}}, \forall t\in T \tag{11}$$

Finally, the interfaces among the electricity, natural gas and district heating systems are constrained by the energy conversion relationships of the CHP (8)-(9) and P2G units (10)-(11).

3. Case study

3.1. System description

Fig. 1 shows a test system considered in this work. This test system includes a 4-bus electricity system, a 3-node heating system and a 4-node gas network. The electricity system is composed of a CHP unit, a CFP unit, and a wind farm. The gas network includes a gas source, a gas storage and a gas compressor. The heating system includes heat storage and three nodes. There are two links: CHP and P2G units. The coordinated operation model presented above is solved by using IPOPT [10] under GAMS [11]. The laptop used has an Intel(R) Core (TM) i7 CPU clocking at 2.70 GHz and 8 GB of RAM. The iteration number is 45; the computational time is 1.2 seconds.

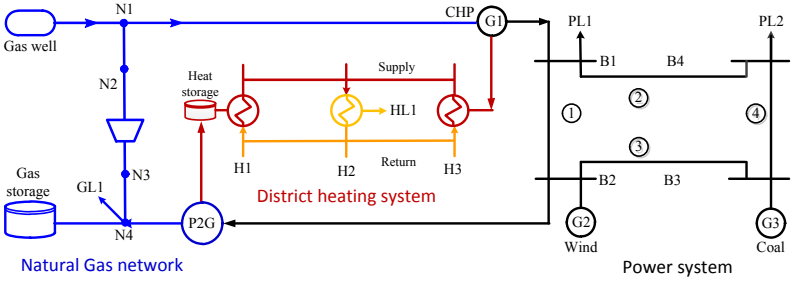

Fig. 1. The structure of an integrated electricity, natural gas and district heating system.

3.2. Network operational parameters

Just as the voltage stability, which plays a major role in the electrical power system, the gas pressure and water temperature are critical factors for the security operation of natural gas system and district heating system, respectively.

Fig. 2 demonstrates the comparison of the simulation results with P2G and without P2G. Fig. 2 (a) shows the water temperature at the inlet and outlet of node 2, which is a load node. The reference temperature is fixed to 100 ℃. As there are heat losses generated during the process of heat transmission, the water temperatures at the inlet of node 2 are lower than the reference node. Besides, there is a lot of heat exchange happen at the load node. Thus the water temperature at the outlet of node 2 will be further declined. The level of temperature drop at load node mainly depends on the amount of heat load. It shows that the temperature drop is larger during the night hours when there is higher heat demand. Finally, due to heat supply from P2G unit, the inlet and outlet temperatures of integrated system with P2G are higher than that without P2G. A higher outlet temperature helps to guarantee safety operation of heating network. Fig. 2 (b) shows the variability of nodal gas pressure. The reference pressure is fixed to 1 bar. It shows that the variability of nodal gas pressure can be dampened by assembling P2G in the multi-energy systems. Further, the nodal gas pressure varies in a narrow range, which indicates that the gas system can play a stabilizing role in multi-energy systems as there is gas linepack in the operational process. It is illustrated that both the district heating system and the natural gas system can provide flexibility to accommodate the fluctuation of the electrical power system.

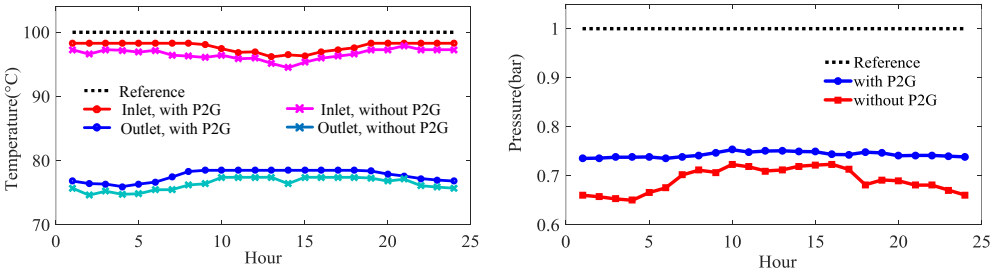

Fig. 2. Network operational parameters: (a) node 2 at the district heating system, (b) node 4 at the natural gas system.

3.3. Scheduling of the energy sources

This subsection analyzes the scheduling strategy throughout a 24-hour time horizon. Fig. 3 (a) illustrates the optimal schedule of the electrical system. The total electricity consumption is composed of the power load and the electricity consumption at the P2G unit. In this case, there is a high wind power output, but only a small amount of surplus wind power is curtailed in the night. Most of the excess electricity is converted into gas and heat by the P2G unit, which helps to reduce the wind curtailment. Fig. 3 (b) illustrates the optimal schedule of the gas system. The total gas consumption includes both the gas demand and the gas consumption at CHP unit. The difference between gas production and consumption is balanced by linepack storage, which provides the flexibility to gas networks. Fig. 3 (c) illustrates the optimal schedule of district heating system. The total heat consumption includes the heat load and the heat loss. The heat loss comes from the heat dissipation of the high-temperature water. There is about 12.4% of heat loss in this study.

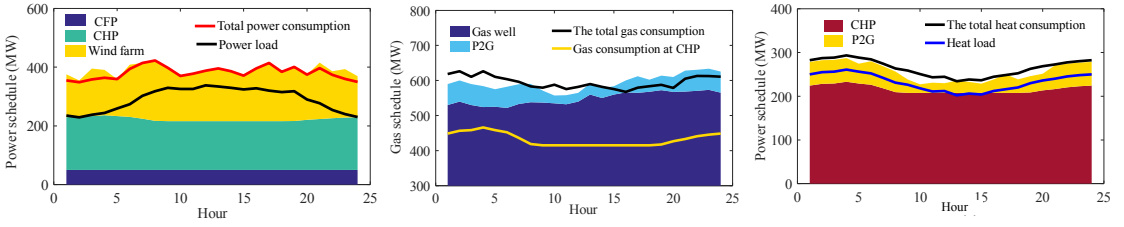

Fig. 3. Optimal schedule of sources: (a) the electrical system, (b) the natural gas system, (c) the district heating system.

4. Conclusion

This paper proposes a coordinated optimization model for the joint operation of the electricity, gas and district

heating systems of an urban area. A nonlinear programming is formulated by considering the network constraints in the integrated systems. This model is solved using IPOPT under GAMS. Simulation results demonstrate the effectiveness of the proposed approach. The required computational time is acceptable with operational requirements. It shows that most of the surplus wind power can be converted into gas and heat by the P2G unit, which helps to reduce wind curtailment. Further, both the district heating system and the natural gas system can provide flexibility to accommodate the fluctuation of the electrical power system.

Acknowledgements

This work was supported in part by the ForskEL project of Harmonized Integration of Gas, District Heating and Electric Systems (HIGHE2014-1-12220).

References

[1] Lee DH, Park SY, Hong JC, Choi SJ, Kim JW. Analysis of the energy and environmental effects of green car deployment by an integrating energy system model with a forecasting model. Appl Energy 2013;103:306–16. doi:10.1016/j.apenergy.2012.09.046.
[2] Zeng Q, Fang J, Li J, Chen Z. Steady-state analysis of the integrated natural gas and electric power system with bi-directional energy conversion. Appl Energy 2016;184:1483–92. doi:10.1016/j.apenergy.2016.05.060.
[3] Jiakun F, Qing Z, Xiaomeng Ai X, Chen Z, Wen J. Dynamic Optimal Energy Flow in the Integrated Natural Gas and Electrical Power Systems. IEEE Trans Sustain Energy 2017.
[4] Zheng JH, Wu QH, Jing ZX. Coordinated scheduling strategy to optimize conflicting benefits for daily operation of integrated electricity and gas networks. Appl Energy n.d. doi:10.1016/j.apenergy.2016.08.146.
[5] Li G, Zhang R, Jiang T, Chen H, Bai L, Li X. Security-constrained bi-level economic dispatch model for integrated natural gas and electricity systems considering wind power and power-to-gas process. Appl Energy 2017;194:696–704. doi:10.1016/j.apenergy.2016.07.077.
[6] Li J, Fang J, Zeng Q, Chen Z. Optimal operation of the integrated electrical and heating systems to accommodate the intermittent renewable sources. Appl Energy 2016;167:244–54. doi:10.1016/j.apenergy.2015.10.054.
[7] Li Z, Wu W, Shahidehpour M, Wang J, Zhang B. Combined Heat and Power Dispatch Considering Pipeline Energy Storage of District Heating Network. IEEE Trans Sustain Energy 2016;7:12–22. doi:10.1109/TSTE.2015.2467383.
[8] Li Z, Wu W, Wang J, Zhang B, Zheng T. Transmission-Constrained Unit Commitment Considering Combined Electricity and District Heating Networks. IEEE Trans Sustain Energy 2016;7:480–92. doi:10.1109/TSTE.2015.2500571.
[9] Geidl M, Andersson G. Optimal Power Flow of Multiple Energy Carriers. IEEE Trans Power Syst 2007;22:145–55. doi:10.1109/TPWRS.2006.888988.
[10] Wächter A. Short tutorial: getting started with ipopt in 90 minutes. Dagstuhl Semin. Proc., Schloss Dagstuhl-Leibniz-Zentrum für Informatik; 2009.
[11] Brook A, Kendrick D, Meeraus A. GAMS, a User's Guide. SIGNUM Newsl 1988;23:10–11. doi:10.1145/58859.58863.

Publication **C3**

Paper title:

Coordinated Operation of the Electricity and Natural Gas Systems with Bi-directional Energy Conversion

Publication outlet:

Energy Procedia

List of authors:

Qing Zeng, Baohua Zhang, Jiakun Fang, Zhe Chen

DOI: 10.1016/j.egypro.2017.03.346
Copyright © 2017 Copyright Clearance Center, Inc. All Rights Reserved. Privacy statement. Terms and Conditions.

Available online at www.sciencedirect.com

ScienceDirect

Energy Procedia 105 (2017) 492 – 497

Energy Procedia

The 8th International Conference on Applied Energy – ICAE2016

Coordinated operation of the electricity and natural gas systems with bi-directional energy conversion

Qing Zeng[a], Baohua Zhang[a], Jiakun Fang[a,]*, Zhe Chen[a]

[a]*Department of Energy Technology, Aalborg University, Aalborg 9220, Denmark*

Abstract

A coordinated operation of the natural gas and electricity network with bi-directional energy conversion is expected to accommodate high penetration levels of renewables. This work focuses on the unified optimal operation of the integrated natural gas and electricity system considering the network constraints in both systems. An iterative method is proposed to deal with the nonlinearity in the proposed model. The models of the natural gas and power system are linearized in every iterative step. Simulation results demonstrate the effectiveness of the approach. Applicability of the proposed method is tested in the sample case. Finally, the effect of Power to Gas (P2G) on the daily economic dispatch is also investigated.

© 2017 The Authors. Published by Elsevier Ltd. This is an open access article under the CC BY-NC-ND license (http://creativecommons.org/licenses/by-nc-nd/4.0/).
Peer-review under responsibility of the scientific committee of the 8th International Conference on Applied Energy.

Keywords: Integrated electricity and gas network, coordinated operation, successive linearization, Power to Gas, economic dispatch

1. Introduction

The rapid development of the renewable energy brings sustainability of the energy supply [1], while challenging the power system operators with the intermittent and unpredictable features at the same time. In recent years, research investigations have demonstrated that the integration of energy systems can balance the energy production and consumption in a broader scope, thereby improve the overall efficiency and sustainability of the energy utilization [2].

Among different energy systems such as power, gas, heating, transportation, etc., the natural gas and electrical power systems are the most common options for bulk energy transmission over thousands of kilometers. Moreover, the emerging power-to-gas technology enabling the bi-directional energy conversion further enhances the interaction

* Corresponding author. Tel.: +45 9940 3821.
E-mail address: jfa@et.aau.dk.

1876-6102 © 2017 The Authors. Published by Elsevier Ltd. This is an open access article under the CC BY-NC-ND license (http://creativecommons.org/licenses/by-nc-nd/4.0/).
Peer-review under responsibility of the scientific committee of the 8th International Conference on Applied Energy.
doi:10.1016/j.egypro.2017.03.346

between the gas and power systems [3]. More recent researches are carried out from the market perspective, illustrating that neglecting the gas supply limitations may lead to the energy cost distortion [4] and coordination can help to reduce energy supply cost [5].

The optimal operation of integrated gas and power systems can be formulated as an optimization problem. However, network constraints for both gas and electricity systems are usually presented in nonlinear forms which challenge the tractability of the global optimality. Existing work [6] decouples the optimization into two subproblems representing gas and electricity. However, it may not work for the loop-locked system with bi-directional energy conversion.

To achieve the optimal operation of the integrated gas and electricity system synchronously, this work focuses on the coordinated operation of the integrated gas and power system with bi-directional energy conversion. The objective is to minimize the operation cost for both electricity and gas systems while maximizing the renewable energy accommodation. It is mathematically formulated as a scaled nonlinear optimization problem. An iterative method is proposed to handle its scale and nonlinearity.

2. Integration of the electricity and natural gas systems

The integrated natural gas and power system is composed of a natural gas network and an electricity network as shown Fig. 1. It is a test system which has been used in the steady-state analysis of the combined gas and power system, and the details can be found in [7].

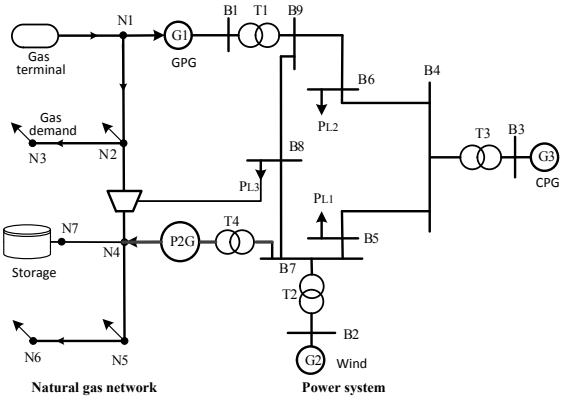

Fig. 1. The test system of a 7-node gas network coupled with IEEE-9 system

The bi-direction energy conversion between the natural gas and electric power systems primarily takes place in the GPG units and P2G. So the integrated natural gas and power system is a loop-locked system. The production and consumption in both networks need to be balanced simultaneously.

To simplify the analysis, the unit of the gas flow rate is converted to power unit as MW and then the per-unit system is used in this paper. The base value of voltage is set as 110kV. The base value of gas pressure is 1MPa. The base value of power is 100MW. Finally, all the related coefficients are adjusted to meet the per-unit system accordingly.

3. Mathematical formulations of the optimization problem

3.1. Objective function

The aim of the optimal operation is to minimize the total operational cost of the integrated electricity and gas systems.

$$F=\sum_{h=1}^{H} C_{\text{gas production}}(h)+C_{\text{power production}}(h)+C_{\text{compressor}}(h)+C_{\text{wind curtailment}}(h) \tag{1}$$

The first term is the cost of gas production. The second term represents the cost of power supply. The third term represents the operational cost of the gas compressor. The fourth term is the penalty cost of a wind farm which is proportional to the square of wind power curtailment.

3.2. Constraints

The steady-state load flow in the electrical system is well-documented as shown in (2) and (3). For the natural gas system, the natural gas flow formulated by the pipeline flow equation (4), nodal balance equation (5), gas compressor equation (6), linepack constraints (7) and (8). The energy conversions between the gas and power system primarily take place in the GPG units and P2G are shown in (9) and (10).

$$\Delta P_i = P_{\text{g},i} - P_{\text{d},i} - |V_i| \sum_{j=1}^{N} |V_j| \left(G_{ij} \cos\theta_{ij} + B_{ij} \sin\theta_{ij} \right) = 0 \tag{2}$$

$$\Delta Q_i = Q_{\text{g},i} - Q_{\text{d},i} - |V_i| \sum_{j=1}^{N} |V_j| \left(G_{ij} \sin\theta_{ij} - B_{ij} \cos\theta_{ij} \right) = 0 \tag{3}$$

$$\prod_i - \prod_j = Z_{ij} S_{ij}^2 \tag{4}$$

$$S_{\text{sup},i} - S_{\text{load},i} = \sum_{j \in i} S_{ij}, (\forall i, j \in N) \tag{5}$$

$$P_{\text{GC},ij} = K_{\text{GC}} S_{\text{GC},ij} \left[\frac{c_k}{c_k - 1} \right] \left[\left(\prod_j / \prod_i \right)^{\frac{c_k - 1}{c_k}} - 1 \right] \tag{6}$$

$$LP(t) = LP_0 + \int_0^t \left[S_{\text{sup}}(t) - S_{\text{con}}(t) \right] dt \tag{7}$$

$$LP_{\text{end}} = LP_0 \tag{8}$$

$$P_{\text{GPG}} = \eta_{\text{GPG}} S_{\text{GPG}} \tag{9}$$

$$S_{\text{P2G}} = \eta_{\text{P2G}} P_{\text{P2G}} \tag{10}$$

Those mentioned above are the equality constraints. Besides, there are various inequality constraints related to the transmission capacities of the gas pipeline and power line, the available capacities of the gas storage, gas linepack, gas terminal and electricity generator. Moreover, nodal pressures and bus voltages are also required to meet the operation limits.

4. Optimization algorithm for solving the problem

Since the objective function and most of the equality constraints are nonlinear equations, it is a large-scale nonlinear programming. Finding a globally optimal solution is difficult. To achieve the global optimal solution efficiently, this work proposes an iterative method to handle its scale and nonlinearity. The models of the natural gas and power system are linearized in every iterative step.

The nonlinear objective function can be approximated by piecewise linear curves. Then by using DC power flow, nonlinear model of the AC system is simplified to a linear form.

$$P_{ij} = B_{ij}(\theta_i - \theta_j) \tag{11}$$

$$\Delta P_i = P_{g,i} - P_{d,i} - \sum_{j \in i} P_{ij} = 0 \tag{12}$$

The nonlinear equations of the natural gas model can be linearized based on the following simplifications. Given the initial values of gas flow rate in pipelines, (4) can be linearized as (13). The compressor works with a constant compression ratio of *CR* that the compressor calculation can be rewritten as (14) and (15).

$$\prod_k - \prod_m = Z_{km} S_{0,km} \cdot S_{\text{gas},km} \tag{13}$$

$$P_{GC,km} = K' \cdot S_{\text{gas},km} \tag{14}$$

$$K' = K_{GC} \left[\frac{T_s}{E_c \eta_c} \right] \left[\frac{c_k}{c_k - 1} \right] \left[(CR)^{\frac{c_k - 1}{2c_k}} - 1 \right] Z_a \tag{15}$$

Now this problem is a linear convex optimization, which can easily be solved using commercial software such as CPLEX. As the calculated value depends on the given value $S_{0,km}$, it is an iterative process: at the beginning, given the initial value of $x(0)=[S_{0,km}(0)]$; then solve the linearized optimization problem; update the value of x(t+1) by $x(t+1) = \lambda_1 x(t-1) + \lambda_2 x(t)$, $\lambda_1 + \lambda_2 = 1$; solve the linearized optimization problem based on the updated value. Calculate $\Delta x = x(t+1) - x(t)$, if $\Delta x \cdot (\Delta x)^T \le \varepsilon$, end. Otherwise, proceed to the next iteration.

5. Case studies

The test case is shown in Fig. 1 which is used to verify the feasibility of the proposed approach. The iteration process of the calculation is shown in Fig. 2 that the value of $\Delta x \cdot (\Delta x)^T$ is under the pre-set tolerance of 10^{-4} after 7 iterations.

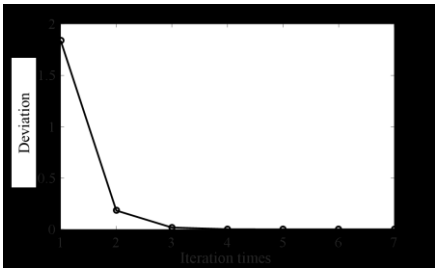

Fig. 2. The iteration of the linearized program

Fig. 3 shows the optimal output of electricity network throughout the 24 time periods. The power outputs from both of the GPG and CPG in the integrated system with P2G agree well with that in the integrated system without P2G. During the peak load periods (1:00 PM~7:00 PM), all the available wind power is used to supply the electrical load, and both the GPG and CPG increase their unit outputs to balance the power demand. However, due to the limitation of the available capacities of the generators, load curtailment happens at 6:00 PM. When the valley load occurs in the midnight (12:00 PM~6:00 AM), the excess wind power is converted into gas fuel by P2G, which decreases the wind power curtailment compared to the case without P2G. It should be mentioned that the total power load includes both the nodal power demand and electricity consumed by P2G. So the total power demand in the case with P2G is higher than that without P2G in the midnight.

Fig. 4 shows the optimal output of gas network throughout the 24 time periods. Due to the gas production from P2G, the daily gas supply from the gas terminal in the integrated

energy system with P2G is lower than that without P2G. It should be noted that the gas supply from the gas terminal is assumed to be flat. Linepack plays a major role in providing flexibility to meet the load fluctuation. In Fig. 4, the linepack is consumed when the value is positive, and the linepack is replenished when the value is negative. It can be seen that the linepack is consumed in the day and restored in the midnight. In the peak-demand hour, the increased gas demand from GPG will lead to a rapid linepack consumption, which brings challenges to the reliability of gas supply. Therefore, it is important to maintain a sufficient linepack and the linepack at the end of the day should be equal to the beginning of the day.

Fig. 5 shows the linepack variation. The linepack reaches its trough at around 9:00 PM and then starts to replenish. The linepack is growing faster in the case with P2G after 9:00 PM. The reason is that the surplus wind power can be converted to gas fuel by using P2G, which helps to replenish the linepack faster.

Compared to the case without P2G, the case with P2G can reduce the wind curtailment and natural gas consumption. Thereby, its daily operational cost can be reduced. In this case study, the daily operational costs are 355.5 thousand Euro and 368.8 thousand Euro for the integrated energy system with and without P2G, respectively. 3.6% operational cost is reduced by introducing the P2G.

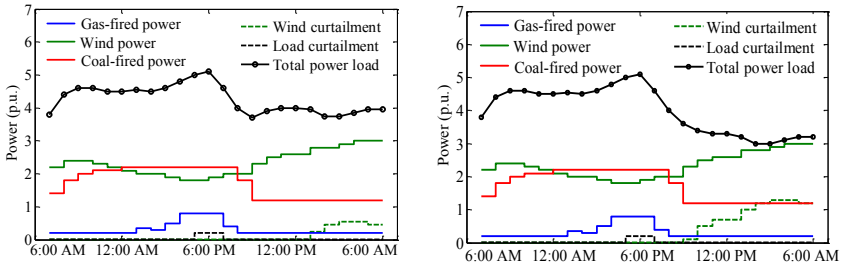

Fig. 3. (a) Daily economic dispatch of power units with P2G (b) Daily economic dispatch of power units without P2G

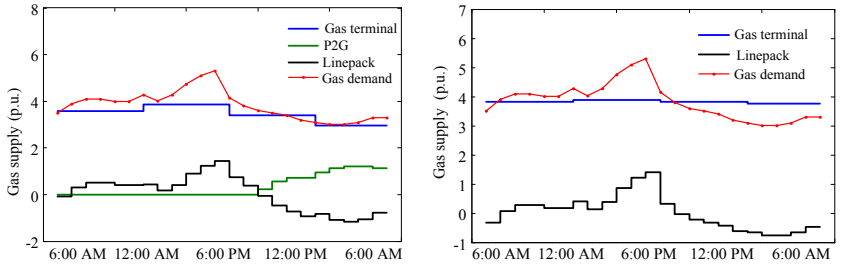

Fig. 4. (a) Daily economic dispatch of gas supply with P2G (b) Daily economic dispatch of gas supply without P2G

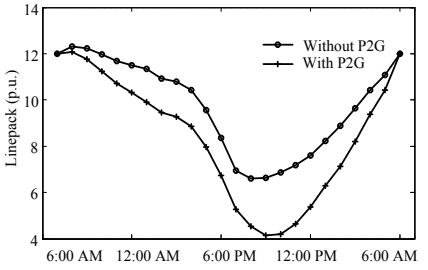

Fig. 5. The simulation results of daily linepack variation

6. Conclusion

This paper investigates the unified optimal operation of the electricity and natural gas systems with bi-directional energy conversion. It is mathematically formulated as a large-scale nonlinear program considering the network constraints in both systems. This work proposes an iterative method to handle its scale and nonlinearity. The models of the natural gas and power system are linearized in every iterative step. Simulation result demonstrates the effectiveness of the proposed method. The effect of P2G on the daily economic dispatch of the integrated energy system is also investigated. It can help to reduce the wind curtailment and natural gas consumption, thereby cut the operational cost. This model and method can provide the system operators with decision support in the integrated energy systems.

Acknowledgements

This study is a part of the research project supported by the ForskEL project Harmonized Integration of Gas, District Heating and Electric Systems (HIGHE2014-1-12220).

References

[1] Krause T, Andersson G, Fröhlich K, Vaccaro A. Multiple-Energy Carriers: Modeling of Production, Delivery, and Consumption. *Proc IEEE* 2011;99:15–27.
[2] Lee DH, Park SY, Hong JC, Choi SJ, Kim JW. Analysis of the energy and environmental effects of green car deployment by an integrating energy system model with a forecasting model. *Appl Energy* 2013;103:306–16.
[3] Gahleitner G. Hydrogen from renewable electricity: An international review of power-to-gas pilot plants for stationary applications. *Int J Hydrog Energy* 2013;38:2039–61.
[4] Toledo F, Sauma E, Jerardino S. Energy Cost Distortion Due to Ignoring Natural Gas Network Limitations in the Scheduling of Hydrothermal Power Systems. *IEEE Trans Power Syst* 2015; PP:1–9.
[5] Adamek F, Arnold M, Andersson G. On Decisive Storage Parameters for Minimizing Energy Supply Costs in Multicarrier Energy Systems. *IEEE Trans Sustain Energy* 2014;5:102–9.
[6] Qadrdan M, Wu J, Jenkins N, Ekanayake J. Operating Strategies for a GB Integrated Gas and Electricity Network Considering the Uncertainty in Wind Power Forecasts. *IEEE Trans Sustain Energy* 2014;5:128–38.
[7] Zeng Q, Fang J, Li J, Chen Z. Steady-state analysis of the integrated natural gas and electric power system with bi-directional energy conversion. *Appl Energy* n.d. doi:10.1016/j.apenergy.2016.05.060.

Qing Zeng obtained his M.S. degree in Department of Engineering Mechanics from Tsinghua University, B.S. degree in Thermal Energy and Power Engineering from Huazhong University of Science and Technology.

He is now a Ph.D. fellow in the Department of Energy Technology at Aalborg University, focus on the Integrated Energy System.

Publication **C4**

Paper title:

A multistage coordinative optimization for sitting and sizing P2G plants in an integrated electricity and natural gas system

Publication outlet:

2016 IEEE International Energy Conference (ENERGYCON)

List of authors:

Qing Zeng, Jiakun Fang, Jinghua Li, Zhe Chen, B. Zhang

DOI: 10.1109/ENERGYCON.2016.7514061
0885-8993© 2016 IEEE. Personal use is permitted, but republication/redistribution requires IEEE permission.

A Multistage Coordinative Optimization for Siting and Sizing P2G Plants in an Integrated Electricity and Natural Gas System

Q. Zeng, J. Fang, Z. Chen
Department of Energy Technology
Aalborg University, Aalborg, Denmark

J. Li
College of Electrical Engineering
Guangxi University, Nanning, China

B. Zhang.
Shenzhen Academy of Aerospace
Technology, Shenzhen, China

***Abstract*—Power-to-Gas (P2G) allows for the large scale energy storage which provides a big potential to accommodate the rapid growth of the renewables. In this paper, a long-term optimization model for the co-planning of the electricity and natural gas systems is presented. The P2G Plants are optimally sited and sized in the integrated energy system. The problem model is formulated as a multi-stage integer nonlinear optimization. The objective is to minimize the investment plus operation costs by determining the optimal location, capacity, and installation time of P2G. Case studies are simulated to illustrate the proposed approach.**

***Index Terms*--Power to gas; integrated gas and electricity system; natural gas network; electric power system; optimal planning.**

I. INTRODUCTION

The social awareness in term of sustainability has promoted the deployment of the renewable energy generations. However, the intermittent and unpredictable features of the renewable energy raise the challenge to the power system operators to balance energy production and consumption [1]. The coordination of natural gas and electricity systems receives increasing interest to accommodate the high penetration level of renewables.

Recently, some works have been conducted on the integrated gas and power system expansion planning to meet the future load growth [2]–[4]. A long-term, multi-area and multi-stage model has been proposed for the expansion planning of integrated electricity and natural gas system [2]; the result shows that the coordinated expansion planning has more advantages than the separate planning. But when considering both of the two systems in planning, there are many challenges, such as increased system complexity and risk, market timeline mismatch, overall system reliability evaluation, etc. The authors of [3], [4] proposed a novel expansion co-planning framework to tackle these problems. This approach can effectively identify the weakness of the energy infrastructure, and thus to enable safe and reliable energy supply in a long-term while meeting the planning requirements. The co-optimizations mentioned above have been carried out to determine the optimal location or installation times of new facilities to meet the future load growth. But there are few reports focus on the expansion co-planning of the integrated energy system to meet the rapid growth of renewable energy.

Today, for some developed countries, the average annual increase in electricity consumption is nearly zero, but the energy mix is changed rapidly that renewable energy gradually replaces the traditional fossil fuel. Taking Denmark for example, on the one hand, the increase in Danish electricity consumption will decrease to approximate 0 percent from 2020 to 2035 [5]. On the other hand, the wind power produced the equivalent of 39% of Denmark's electricity consumption in 2014 [6]. Further, an energy policy was adopted to increase the share of electricity production from wind to 50% by 2020, and to 84% in 2035 [6]. And a long-term goal has been put forwarded in Denmark that a 100% renewable energy should be implemented in 2050 [7]. Thus, the energy mix of Denmark is dramatically transferring from fossil energy to renewable energy. With the extensive development of the intermittent renewable energy, a large scale and long duration energy storage technology is needed to store the surplus renewable energy for later reuse. Power to gas (P2G) is such a promising technique that works by using the surplus wind power or other renewable sources to produce gas fuel, and the produced gas fuel can be stored in the natural gas networks[8], [9]. A multi-criteria optimization has been carried out to select the installation locations for P2G [10]. It shows that P2G implementation makes it possible to increase the security of the chosen region. However, there are still few reports focus on the medium or long term planning of P2G for determining the optimal capacity or installation times to accommodate the increasingly high penetration level of renewable energy.

This paper focuses on a multi-stage coordinative optimization for siting and sizing P2G Plants in the integrated natural gas and electric power system. These two networks are mainly coupled by using Power to gas (P2G) and Gas-fired power generation (GPG). The objective is to minimize the total investment plus annual operation costs. This optimization is subject to the energy flow equations in both systems as well

Research supported by the Forskel project Harmonized integration of gas, district heating and electric systems (HIGHE).

978-1-4673-8463-6/16/$31.00 ©2016 IEEE

P2G and GPG. Thus, this co-planning problem is bounded by a set of nonlinear constraints. Besides, the siting of the P2G plants is set as binary variables, make it a mixed integer optimization. Therefore, the co-optimization is a multi-stage and mixed integer nonlinear programming.

The paper is organized as follows: Section II presents the model of the integrated gas and power system. The formulation of the co-planning model is described in Sections III. Section IV presents the numerical results corresponding to the application of these proposed models to an integrated system. Finally, Section V gives the conclusion of this work.

II. Modeling of the Integrated Gas and Power System

The integrated gas and power system is mainly composed of gas network, power system, and the links between the gas network and power system, such as GPG, P2G, gas compressors, etc. In order to analyze the steady state energy distribution in the integrated energy system, the integrated energy flow is formed by gathering the stated flow models of both natural gas and electricity system. In this paper, gas flow and gas load are measured by MW for the unification of the units. And the widely used per-unit system is exploited to describe the integration of gas and power system. In this paper, we consider that the base value of voltage is 110kV, the base value of gas pressure is 10 bar, the base values of power is 100MW. Then the rest of the units can be derived from the independent base values. Finally, all the related coefficients are adjusted to meet the per-unit system accordingly.

A. Power flow in the electrical system

Power flow studies are of great importance in planning and operation of power systems. The goal of a power-flow study is to obtain voltage angle and magnitude information for each bus in a power system for specified load and generator power and voltage conditions [31]. The problem can be formulated as follows

$$\Delta P_i = P_{i,g} - P_{i,d} - |V_i| \sum_{j=1}^{N} |V_j| \left(G_{ij} \cos\theta_{ij} + B_{ij} \sin\theta_{ij} \right) = 0 \quad (1)$$

$$\Delta Q_i = Q_{i,g} - Q_{i,d} - |V_i| \sum_{j=1}^{N} |V_j| \left(G_{ij} \sin\theta_{ij} - B_{ij} \cos\theta_{ij} \right) = 0 \quad (2)$$

B. Preliminary on the energy flow in the natural gas system

The load flow in the power system is well-documented for steady-state analysis, focusing on the voltage, voltage angel, active and reactive power. Similarly in the natural gas system, the steady-state analysis focuses on the pressure, gas density and mass flow. For the steady-state isothermal flow in a gas pipeline, the flow rate is determined by the pressure drop [11]:

$$p_i^2 - p_j^2 = S_{ij} \left(P_{ij}^{\text{gas}} \right)^2 \quad (3)$$

where p_i and p_j are the nodal gas pressure. P_{ij}^{gas} is the gas flow from node i to j. S_{ij} represents the hydraulic resistance coefficient of the pipeline, similar to the line impedance of the power system.

The nodal gas balance equations simply indicate that the sum of the inflows and outflows at the node should be zero:

$$P_{\text{sup},i}^{\text{gas}} - P_{\text{con},i}^{\text{gas}} - \sum_{j \in i} P_{ij}^{\text{gas}} = 0 \quad (4)$$

where $P_{\text{sup},i}^{\text{gas}}, P_{\text{con},i}^{\text{gas}}$ are gas supply and gas demand at node i respectively.

C. Energy Conversion between the gas and power systems

The energy can convert between the gas and power systems via the GPG, P2G and gas compressors. GPG is gas-fired power generation. It burns natural gas to produce electricity. P2G is the emerging technology in recent years, which provides an opportunity to convert surplus electrical power to a gas fuel. Gas compressors consume electricity to increase the pressures at the specific bus in the gas system.

The relationship between the electricity consumed by the gas compressor and the gas pressure can be defined as [12].

$$P_{\text{GC},i} = K_{\text{GC}} Z_{\text{a}} P_{\text{C},i}^{\text{gas}} \left[\frac{T_i}{E_{\text{c}} \eta_{\text{c}}} \right] \left[\frac{c_k}{c_k - 1} \right] \left[\left(\frac{p_i^{\text{out}}}{p_i^{\text{in}}} \right)^{\frac{c_k - 1}{c_k}} - 1 \right] \quad (5)$$

where $P_{\text{GC},i}$ is power consumption of the gas compressor i; K_{GC} represents the unit conversion factor; Z_{a} is average compressibility factor; $P_{\text{C},i}^{\text{gas}}$ represents natural gas flow in the compressor, p.u.; η_{c} is compression efficiency; T_i is suction temperature, °R; E_{c} is compressors parasitic efficiency; c_k is specific heat ratio for natural gas; p_i^{in} and p_i^{out} are pressures at suction and discharge flanges, respectively, p.u..

The energy conversion relationship between the gas generation rate $P_{\text{P2G},i}$ and the consumed power $P_{\text{D},i}^{\text{elec}}$ is related to the energy conversion efficient [11], which can be given as

$$P_{\text{P2G},i} = \eta_{\text{P2G}} P_{\text{D},i}^{\text{elec}} \quad (6)$$

where η_{P2G} denotes the energy conversion efficiency in P2G system. Note that the efficiency of the P2G plant is around 55%-80% according to the state-of-the-art technology.

D. Linepack Storage

In the natural gas system, linepack plays an important role in providing system flexibility. Linepack is proportional to the average pressure in a pipe [13]. In dynamic situations, based on the law of conservation of mass, linepack can be determined by the changes in the initial gas stored in the pipe and the net consumption [4], [14]

$$LP(t) = LP_0 + \int_0^t \left[P_{\text{sup}}^{\text{gas}}(t) - P_{\text{con}}^{\text{gas}}(t) \right] dt \quad (7)$$

Where LP is the current quantity of the linepack, LP_0 is the initial gas stored in pipes, $P_{\text{sup}}^{\text{gas}}$ is the supplied gas, and $P_{\text{con}}^{\text{gas}}$ is the consumed gas. It should be noted that the system linepack is equal at the beginning of each day in this study.

III. CO-PLANNING OF NATURAL GAS AND ELECTRICITY

In this section, the optimization problem for the integrated gas and power systems is formulated. This co-planning problem is bounded by a set of nonlinear constraints. Besides, the siting of the P2G plants are set as binary variables, make it a mixed integer optimization. Thus, this co-optimization is a multistage and mixed integer nonlinear programming.

A. Objective Function

The objective function consists of the annualized investment and operation cost.

$$\text{Objective} = \sum_{t=1}^{T} \frac{1}{(1+r)^{t-1}} \left(C_{\text{investment}}(t) + C_{\text{operation}}(t) \right) \tag{8}$$

where r is risk-free rate, $C_{\text{investment}}(t)$ represents investment cost and $C_{\text{operation}}(t)$ represents the operation cost.

The investment cost $C_{\text{investment}}(t)$ includes the investment to build new plants. In this work, three kinds of installations including P2G, GPG and gas compressor are considered. The operational costs are composed of the following parts： the production cost of P2G, GPG, coal-fired power plant and gas compressor; the cost of gas production; the penalty cost of a wind farm which is proportional to the square of wind power curtailment [15], [16]; as well as the power deficit cost [2].

B. Constraints

Following constraints are considered in the optimization.

1) Nodal gas flow constraints

$$P_{\text{sup},i}^{\text{gas}} - P_{\text{con},i}^{\text{gas}} = \sum_{j \in i} P_{ij}^{\text{gas}}, (\forall i, j \in N) \tag{9}$$

2) The pipeline flow constraints

$$\underline{P_{ij}^{\text{gas}}} \le P_{ij}^{\text{gas}} \le \overline{P_{ij}^{\text{gas}}}, (\forall i, j \in N) \tag{10}$$

3) Gas nodal pressure constraints:

$$\underline{p_i} \le p_i \le \overline{p_i}, (\forall i \in N) \tag{11}$$

4) Compressor station constraints:

$$1 < \frac{p_i^{\text{out}}}{p_i^{\text{in}}} < \overline{\xi_i}, (\forall i \in N_{\text{GC}}) \tag{12}$$

$$\underline{p_i^{\text{in}}} \le p_i^{\text{in}}, (\forall i \in N_{\text{GC}}) \tag{13}$$

$$p_i^{\text{out}} \le \overline{p_i^{\text{out}}}, (\forall i \in N_{\text{GC}}) \tag{14}$$

$$P_{\text{GC},i} \le \overline{P_{\text{GC},i}}, (\forall i \in N_{\text{GC}}) \tag{15}$$

5) Gas output at gas producer:

$$\underline{P_{\text{GP},i}} \le P_{\text{GP},i} \le \overline{P_{\text{GP},i}}, \left(\forall i \in N_{\text{GP}}\right) \tag{16}$$

6) The generation capacity of P2G: It might be affected by Power availability.

$$\underline{P_{\text{P2G},i}} \le P_{\text{P2G},i} \le \overline{P_{\text{P2G},i}}, \left(\forall i \in N_{\text{P2G}}\right) \tag{17}$$

$$\underline{P_{\text{P2G},i}} \le P_{\text{P2G},i} \le \eta_{\text{P2G}} \overline{P_{\text{D},i}^{\text{elec}}}, \left(\forall i \in N_{\text{P2G}}\right) \tag{20}$$

7) The power flow constraints:

$$P_{\text{G},i} - P_{\text{D},i}^{\text{elec}} = \sum_{j=1}^{N} P_{ij}, \ \left(\forall i, j \in N\right) \tag{21}$$

$$P_{ij} = B_{ij} \theta_{ij}, \ \left(\forall i, j \in N\right) \tag{22}$$

8) The electricity branch flow constraints:

$$\left|P_{ij}\right| \le \overline{P_{ij}}, \ \left(\forall i, j \in N\right) \tag{23}$$

9) Power limit of coal-fired power generators:

$$\underline{P_{\text{C},i}} \le P_{\text{C},i} \le \overline{P_{\text{C},i}}, \ \left(\forall i \in N_{\text{C}}\right) \tag{24}$$

10) Power limit of gas-fired power generators: The generation capacity of GPGs who might be affected by gas availability.

$$\underline{P_{\text{G},i}} \le P_{\text{G},i} \le \overline{P_{\text{G},i}}, \ \left(\forall i \in N_{\text{G}}\right) \tag{25}$$

$$\underline{P_{\text{G},i}} \le P_{\text{G},i} \le \eta_{\text{G},i} \overline{P_{\text{D},i}^{\text{gas}}}, \ \left(\forall i \in N_{\text{G}}\right) \tag{26}$$

where $P_{\text{D},i}^{\text{gas}}$ is the gas load of GPGs at i.

11) Available wind power output constraints:

$$0 \le \hat{P}_{\text{W},i} \le \overline{P_{\text{W},i}}, \left(\forall i \in N_{\text{W}}\right) \tag{27}$$

12) Allowable electricity deficit constraints: The electricity deficit is the load shedding due to inadequate power supply. It is used to measure the reliability of the combined energy network.

$$0 \le P'_{\text{D},i} \le \overline{P'_{\text{D},i}}, \left(\forall i \in N_{\text{D}}\right) \tag{28}$$

13) Linepack constraints: The system linepack is equal at the beginning of each day. The linepack should be limited in the safe operational region.

$$LP_{\text{end}} = LP_0 \tag{29}$$

$$\underline{LP} \le LP \le \overline{LP} \tag{30}$$

C. The proposed methodology for coordinated expansion planning

The co-planning problem is divided into two levels of the investment plan and the optimal operation. A series of candidate expansion plans are created at the planning level, which provides network topology and operational requirement for the operation optimization. And then the operation optimization is carried out by considering the daily optimal economic dispatch of the integrated gas and power system. Both levels are mutually embedded to form an integrated process that can display a better system expansion planning.

The major steps of the proposed optimization method to solve the optimal co-planning problem are given in the following. Firstly, a series of initial expansion plans will be created based on the current situation and the future scenario forecasting. Secondly, once the novel network topology is formed, daily optimal economic dispatch will be carried out in the integrated gas and power system within the operating constraints. Thirdly, verify if the optimization satisfies objectives within constraints. If it is not satisfied, possible augmentations will be done based on the simulation results.

Fourthly, if no violations occur, multi-stage optimization will be carried out on the operational cost plus capital investment cost. In order to improve the computational efficiency, the Monte Carlo (MC) simulation is applied to randomly pick out daily scenarios over a given planning horizon. Finally, if the iteration converges, select a preferred plan by economic analysis. Otherwise, creates another series of novel candidate expansion plans.

IV. CASE STUDY

Case studies are presented to validate the performance of the proposed approach. The co-planning model is proposed to analyze the location and the optimal dispatch of the different generation capacities. The variation of P2G planning with the penetration of wind power is investigated to determine a suitable installation time and to study potential benefits of installation of P2G. The reduction of primary energy consumption, such as coal, is also investigated to achieve higher environment efficiency. All nonlinear programming problems are solved by using YALMIP [17], a free toolbox for modeling and optimization in MATLAB [18].

An IEEE-9 test system combined with a 7-node natural gas network is applied to illustrate the proposed approach as shown in Fig. 1. The natural gas network is composed of a gas source, gas storage, gas compressor and pipes. On the other hand, the electricity infrastructure has three generators at B1, B2, and B3. Moreover, the gas-fired generator is installed at B1 in the power system and connected with N1 in the gas system. B2 and B3 are wind farm and coal-fired power plant, respectively. Scheduling mismatch between the gas network and electricity system is also considered in this study. Specifically, power plants can be scheduled to operate for hourly intervals. In contrast, normal gas scheduling of gas source is performed on a daily basis. So it is essential to consider the daily linepack variations. In this paper, the balancing interval in the power system is considered as 60 minutes; for the natural gas network, we consider that there are four supply reschedules at 6.00 AM, 12.00 PM, 6.00 PM and 12.00 PM. The pipeline parameters of the gas network are shown in Table I.

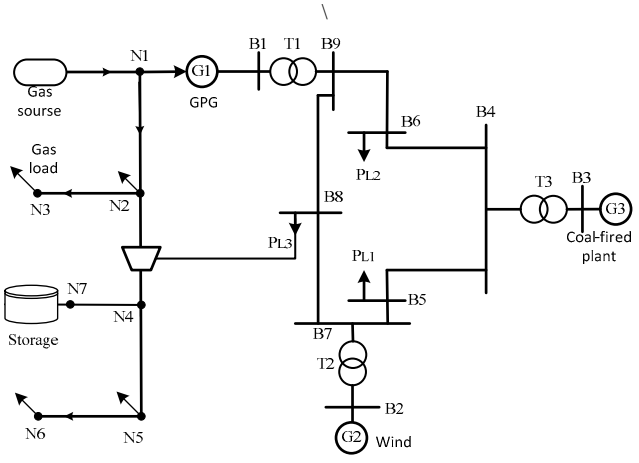

Figure 1. The 7-node gas network coupled with IEEE-9 systems

TABLE I. THE PIPELINE PARAMETERS OF THE GAS NETWORK

Pipeline	From	To	S_{km} (p.u.)	Capacity (p.u.)
1	1	2	0.028	12
2	2	3	0.037	12
3	2	4	0.019	12
4	4	7	0.028	12
5	4	5	0	12
6	5	6	0.029	12

A. Experiment Setting

The system planning horizon is nine years consisting of 3 stages. Take 2014 as the initial year of the planning horizon, the data of the initial year is obtained from Energinet.dk [19]. In the initial year of the planning horizon, the wind power produced 39% of the electricity consumption. Assuming that the average annual increase in electricity consumption is zero, but the fossil fuel is gradually replaced by wind power that the annual growth rate of wind power is assumed as 6%.

For the gas network, the transmission capacity, diameter, and pressure obligation are 500MW, 500 mm, and 20 bar respectively. The calorific value of the natural gas is set as 37.26 MJ/m^3. Each gas compressor has a compression ratio of 2. For the electricity system, the electricity transmission line candidates are 110 kV with the capacity of 300 MW. The investment cost of P2G is 2 million Euro/MW, the investment cost for the gas-fired power plant is about 0.8 million Euro/MW and is 1.5 million Euro/MW for coal power plant. As mentioned above, a per-unit system is proposed to describe the integrated gas and power system. We consider that the base value of voltage is 110kV, the base value of gas pressure is 10 bar, the base values of power is 100MW. Then the rest of the units can be derived from the based values.

B. The multistage evolution of the power capacity of P2G, GPG and coal-fired power plant

The purpose of this expansion co-planning is to get both the location and the optimal dispatch of the different generation capacities by considering the increase in wind penetration. The detailed expansion planning of the integrated system is illustrated in Fig. 2. According to the optimization results, the first P2G must be implemented in stage one with a capacity of 80MW. The P2G2 and GPG2 must be implemented in stage two with a capacity of 50MW and 45MW, respectively. The capacity of the GPG2 is then doubled to compensate the forecasted wind power expansion in stage three. And the capacity of P2G2 is expanded to 95 MW in the third stage. It can also be observed that GPG and P2G play a critical role in balancing energy production and consumption on the growing supplies of intermittent renewable energy. Fig. 3 shows the multistage evolution of the total power capacity of the P2G, GPG, and coal-fired power plant. As the penetration level of the wind power increases, the annual coal consumption is decreased in coal-fired power plant. Meanwhile, the annual generations of both GPG and P2G are increased with wind penetration. Accordingly, the capacity of the coal-fired power plant is shrank from 310MW to 220MW, while the total generation capacity of GPG increased from 115MW to 205MW and the total capacity of P2G increases from 80MW to 175MW.

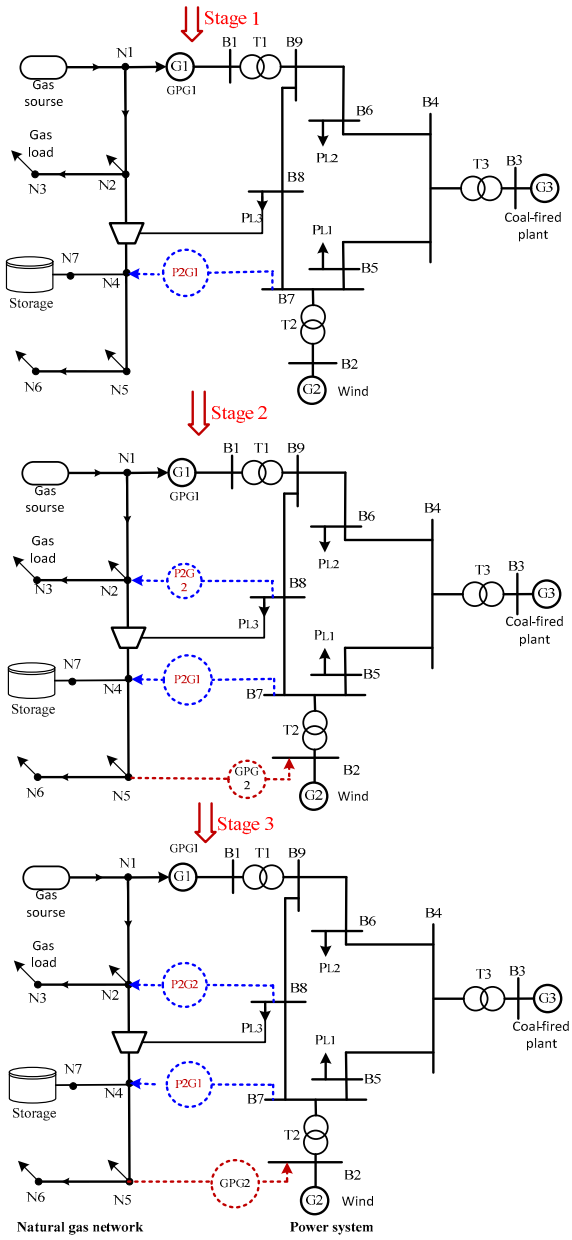

Figure 2. Co-planning scheme of the integrated gas and power system

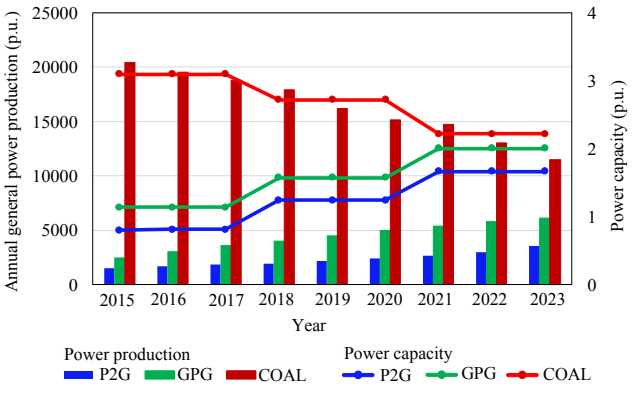

Figure 3. The multistage evolution of the total power capacity

C. *Comparison of the daily operation between two schemes*

In order to investigate the effect of P2G on the daily operation of the integrated gas and power system, we compared the daily operation result in the first stage between two schemes: a P2G with the capacity of 80 MW has been installed at B7 and put into operation in Scheme 1; the integrated system works without P2G in Scheme 2.

Scheduling mismatch between the gas system and electricity system is also considered in this paper. The change of gas load will result in linepack variation. Especially, during the peak hours, the increased gas demand from GPG will lead to a rapid linepack reduction, which brings a great challenge to the daily linepack management. Thus, a sufficient linepack is critical for the reliability of gas supply. It should be noted that the linepack at the end of the day should be equal to the beginning of the day. Fig. 4 shows the linepack variation in a given day when the wind is strong, the total gas demand reaches its peak around 6:00 PM and then decline. Accordingly, the linepack will reach its troughs at around 9:00 PM. Both of the linepack variations show some comparability, whereas also show some differences. First, the linepack is growing faster in the integrated system with P2G after 9:00 PM. The reason is that the surplus wind power can be converted to gas fuel in the night, which can increase the replenishing speed of the linepack. Besides, there is a lower gas supply in the integrated system with P2G, and the decrement is indicated by the area surrounded by those two contours.

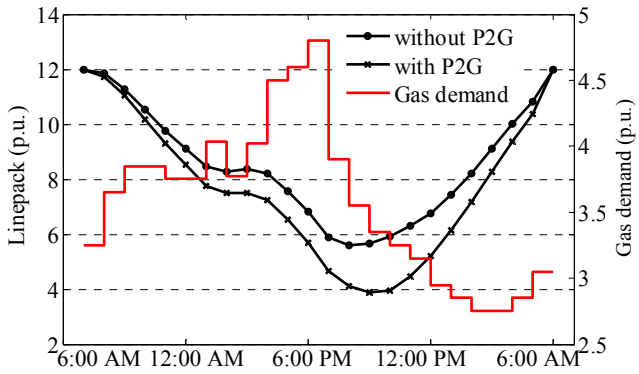

Figure 4. The simulation results of daily linepack variation

The comparison of the integrated energy system with P2G and without P2G is carried out in the context of operational cost, gas supply, and wind curtailment, as shown in Fig. 5. All the comparisons are carried out in a given week when the wind is strong. Simulation result shows that the operational cost is higher when there is a larger power demand and lower wind power. Furthermore, compared with the integrated system without P2G, the integrated system with P2G has much lower operational cost. This benefits from the lower gas supply cost from the gas source and lower wind curtailment cost, as shown in Fig. 5. As a part of surplus wind power can be converted to gas fuel by using P2G, the gas supply is decreased, and the wind curtailment can also be reduced by the using of P2G. This indicates that P2G can help to accommodate the rapid growth of renewable energy.

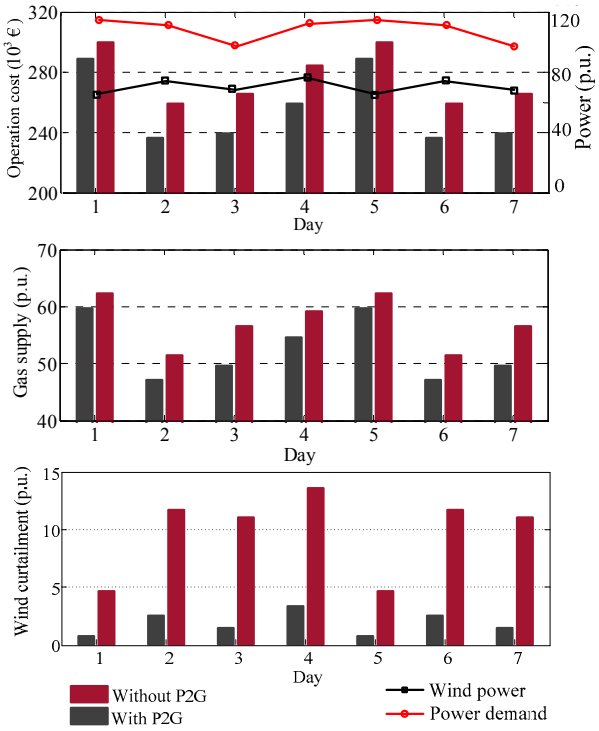

Figure 5. Comparison of the integrated system with and without P2G

V. CONCLUSION

This paper proposes a multi-stage expansion co-planning model in the integrated natural gas and electricity system. The proposed model is formulated as a mixed-integer nonlinear multi-stage optimization problem that minimizes the costs of investments plus operation. The timeline mismatch between gas and power system is also considered by introducing the daily linepack variation. Case studies on a test gas network and IEEE9 system are presented to verify the applicability of the proposed approach. The effect of the installation of P2G on the daily operation in the integrated gas and power system is also investigated by comparing the daily operations between two schemes. Simulation results show that the integrated system with P2G has much lower operational cost, gas supply, and wind curtailment than that without P2G. Further, it shows that more generation capacities of P2G are required to accommodate the increasingly high penetration levels of wind power in the power system while GPG gradually replaces the coal-fired power plant because of its fast-ramping feature.

ACKNOWLEDGEMENT

This study is a part of the research project supported by the ForskEL project Harmonized Integration of Gas, District Heating and Electric Systems (HIGHE).

REFERENCES

[1] J. Li, J. Fang, Q. Zeng, and Z. Chen, "Optimal operation of the integrated electrical and heating systems to accommodate the intermittent renewable sources," *Appl. Energy*.

[2] C. Unsihuay-Vila, J. W. Marangon-Lima, A. C. Z. de Souza, I. J. Perez-Arriaga, and P. P. Balestrassi, "A Model to Long-Term, Multiarea, Multistage, and Integrated Expansion Planning of Electricity and Natural Gas Systems," *IEEE Trans. Power Syst.*, vol. 25, no. 2, pp. 1154–1168, May 2010.

[3] J. Qiu, Z. Y. Dong, J. H. Zhao, Y. Xu, Y. Zheng, C. X. Li, and K. P. Wong, "Multi-Stage Flexible Expansion Co-Planning Under Uncertainties in a Combined Electricity and Gas Market," *IEEE Trans. Power Syst.*, vol. PP, no. 99, pp. 1–11, 2014.

[4] J. Qiu, Z. Y. Dong, J. H. Zhao, K. Meng, Y. Zheng, and D. J. Hill, "Low Carbon Oriented Expansion Planning of Integrated Gas and Power Systems," *IEEE Trans. Power Syst.*, vol. 30, no. 2, pp. 1035–1046, Mar. 2015.

[5] Energinet.dk, "Energinet dk's analysis assumptions 2014-2035," Sep-2014. [Online]. Available: http://www.energinet.dk/SiteCollectionDocuments/Engelske%20dokumenter/El/Energinet%20dk's%20analysis%20assumptions%202014-2035%20-%20September%202014.pdf.

[6] J. N. Rasmussen, "Vindmøller slog rekord i 2014," *Energinet.dk*, 06-Jan-2015.

[7] B. V. Mathiesen, H. Lund, and D. Connolly, "Limiting biomass consumption for heating in 100% renewable energy systems," *Energy*, vol. 48, no. 1, pp. 160–168, Dec. 2012.

[8] G. Gahleitner, "Hydrogen from renewable electricity: An international review of power-to-gas pilot plants for stationary applications," *Int. J. Hydrog. Energy*, vol. 38, no. 5, pp. 2039–2061, Feb. 2013.

[9] M. Jentsch, T. Trost, and M. Sterner, "Optimal Use of Power-to-Gas Energy Storage Systems in an 85% Renewable Energy Scenario," *Energy Procedia*, vol. 46, pp. 254–261, 2014.

[10] N. Moskalenko, P. Lombardi, and P. Komarnicki, "Multi-criteria optimization for determining installation locations for the power-to-gas technologies," in *2014 IEEE PES General Meeting,* pp.1–5, 2014.

[11] Q. Zeng, J. Fang, J. Li, and Z. Chen, "Integrated Energy Flow Analysis in a Harmonized Natural Gas and Electricity Network with Bi-directional Energy Conversion," presented at the Proceedings of the 10th Conference on Sustainable Development of Energy, Water and Environment Systems, SDEWES2015.0639,1-17, 2015.

[12] S. Mokhatab, W. A. Poe, and J. G. Speight, *Handbook of Natural Gas Transmission and Processing*. Burlington, MA, USA: Gulf Publishing Company, 2006.

[13] A. Kabirian and M. R. Hemmati, "A strategic planning model for natural gas transmission networks," *Energy Policy*, vol. 35, no. 11, pp. 5656–5670, Nov. 2007.

[14] M. Chaudry, N. Jenkins, and G. Strbac, "Multi-time period combined gas and electricity network optimisation," *Electr. Power Syst. Res.*, vol. 78, no. 7, pp. 1265–1279, Jul. 2008.

[15] W. Wu, J. Chen, B. Zhang, and H. Sun, "A Robust Wind Power Optimization Method for Look-Ahead Power Dispatch," *IEEE Trans. Sustain. Energy*, vol. 5, no. 2, pp. 507–515, Apr. 2014.

[16] Z. Li, W. Wu, B. Zhang, and B. Wang, "Adjustable Robust Real-Time Power Dispatch With Large-Scale Wind Power Integration," *IEEE Trans. Sustain. Energy*, vol. 6, no. 2, pp. 357–368, Apr. 2015.

[17] J. Löfberg, "Modeling and solving uncertain optimization problems in YALMIP," in *Proceedings of the 17th IFAC World Congress*, 2008, pp. 1337–1341.

[18] J. Lofberg, "YALMIP : a toolbox for modeling and optimization in MATLAB," in *2004 IEEE International Symposium on Computer Aided Control Systems Design*, 2004, pp. 284–289.

ISSN (online): 2446-1636
ISBN (online): 978-87-7210-175-0

AALBORG UNIVERSITY PRESS